DETERMINANTS OF TEMPERATURE AND SALINITY IN THE LEVANTINE SEA USING IN-SITU DATA

A THESIS SUBMITTED TO
THE BOARD OF GRADUATE PROGRAMS
OF
MIDDLE EAST TECHNICAL UNIVERSITY, NORTHERN CYPRUS CAMPUS

BY

CEM SERİMÖZÜ

IN PARTIAL FULFILLMENT OF THE REQUIREMENTS FOR THE DEGREE
OF
MASTER OF SCIENCE
IN
SUSTAINABLE ENVIRONMENT AND ENERGY SYSTEMS

AUGUST 2019

Approval of the Board of Graduate Programs _____

Prof Dr. Gürkan Karakaş,
Chair Person

I certify that this thesis satisfies all the requirements as a thesis for the degree of Master of Science

_____

Assist. Prof. Dr. Ceren İnce Derogar,
Program Coordinator

This is to certify that I have read this thesis and that in my opinion it is fully adequate, in scope and quality, as a thesis for the degree of Master of Science.

_____

Prof. Dr. Ali Cevat Taşıran,
Supervisor

Examining Committee Members

Assist. Prof. Dr. Bertuğ Akıntuğ, Jury Chair,
METU NCC/Civil Engineering Prog. _____

Prof. Dr. Ali Cevat Taşıran, Jury Member,
METU NCC, Economics Prog. _____

Prof. Dr. İlkay Salihoğlu, Jury Member,
University of Kyrenia, Oceanography Prog. _____

Date: August 27,2019

I hereby declare that all information in this document has been obtained and presented in accordance with academic rules and ethical conduct. I also declare that, as required by these rules and conduct, I have fully cited and referenced all material and results that are not original to this work.

Name, Last name: Cem Serimözü

Signature : _____

ABSTRACT

DETERMINANTS OF TEMPERATURE AND SALINITY IN THE LEVANTINE SEA USING IN-SITU DATA

Serimözü, Cem

MSc., Department of Sustainable Environment and Energy Systems

Supervisor: Prof. Dr. Ali Cevat Taşıran

August 2019, 211 pages

The Levantine Sea, part of the Eastern Mediterranean where international interests collide and exposed to rising anthropogenic pressure, is our focus in this study. Additionally, four of its sub-regions: Cilician and Levantine Basins, Coastal Nile Delta and Rhodes Gyre are chosen. On account of the relative scarcity of scientific studies of these regions, we aimed to contribute to the investigation of Sea Water Temperature and Salinity, two critical oceanographic parameters in the context of climate change. To this end, we selected a dataset demonstrating sparse observations and erratic distribution for this pioneering in-depth analysis. We begin by presenting a comprehensive spatial definition and introduce conventional data collection tools and sharing infrastructures. An in-situ aggregated dataset, "Mediterranean Sea - Temperature and Salinity Historical Data Collection SeaDataCloud V1" covering the area between 1960 and 2017 is retrieved to conduct a descriptive analysis for multiple depth layers and seasons. Climatological and isothermal maps are used to sketch the boundaries of the sub-regions. Meanwhile, cluster analysis is employed to define the limits and further identify the existence of distinct regional properties. Moreover, we replace missing observations with approximations using chained equations to increase the robustness of our analysis, and the resulting datasets are

analysed on a yearly and monthly basis to determine variability. Furthermore, empirical and theoretical cumulative distribution functions of the data supported by classical statistical methods are used to establish optimal theoretic models. Finally, regression analyses are performed to measure the significance of spatiotemporal parameters using predicted values.

Keywords: Sea Water Temperature, Sea Water Salinity, In-Situ Data, Oceanography, Levantine Sea.

ÖZ

YERİNDE TOPLANAN VERİLERİ KULLANARAK LEVANTİN DENİZİNDE SICAKLIK VE TUZLULUK BELİRLENMESİ

Serimözü, Cem

Yüksek Lisans, Sürdürülebilir Çevre ve Enerji Sistemleri

Tez Yöneticisi: Prof. Dr. Ali Cevat Taşıran

Ağustos 2019, 211 sayfa

Çarpışan uluslarası çıkarlar ve yükselen antropojenik baskılar altındaki Doğu Akdeniz'in bir parçası olan Levanten Denizi bu araştırmaki odak noktamız. Buna ek olarak, bilimsel çalışmaların göreceli olarak daha az olması nedeniyle alt bölgelerinden dördü: Kilikya ve Levanten Havzaları, Kıyı Nil Deltası ve Rodos Döngüsü seçildi. Seyrek gözlemler ve düzensiz dağılımı gösteren bir veri seti seçtik ve öncü bir çalışma ile, oşinografinin iki önemli parametresi, Deniz Suyu Sıcaklığının ve Tuzluluğunun araştırılmasına, iklim değişikliği bağlamında katkıda bulunmak istedik. Bu amaçla kapsamlı bir saha tanımının ardından, geleneksel veri toplama araçları ve mevcut veri paylaşım altyapılarını sunarak başladık. 1960 ve 2017 yılları arasındaki dönemi kapsayan yerinde toplanmış veri seti "Akdeniz - Sıcaklık ve Tuzluluk Tarihsel Veri Toplama SeaDataCloud V1", birden fazla derinlik katmanı ve mevsimin tanımlayıcı analizini yapmak üzere ele alındı. Alt bölgelerin sınırlarını çizmek için klimatolojik ve izotermal haritalar değerlendirildi. Bu arada, farklı bölgesel özellikleri konumlandırmak amacıyla küme analizi uygulandı. Ayrıca, analizin sağlamlığını arttırmak için eksik değerler, zincirleme denklemler gerçekleştirilerek tamamlandı, ve elde edilen yeni veri setleri değişkenliği yıllık ve aylık olarak analiz edildi. Ayrıca, klasik istatistiksel yöntemlerle desteklenen verilerin ampirik ve teorik kümülatif dağılım fonksiyonları optimal teorik modeller

oluşturmak için kullanıldı. Son olarak, tahmini değerler kullanılarak spatiotemporal parametrelerin önemini ölçmek için regresyon analizleri yapıldı.

Anahtar Sözcükler: Deniz Suyu Sıcaklığı, Deniz Suyu Tuzluluğu, Yerinde Toplanan Veri, Oşinografi, Levant Denizi

To My Family & Friends

ACKNOWLEDGEMENTS

I want to express my gratitude towards my advisor Prof. Dr. Ali Cevat Taşıran, for his mentorship, encouragement and guidance throughout the research process. His constant support for the last two years we have been working together has been crucial in creating this work.

Besides my supervisor, I would like to thank Prof. Dr. İlkay Salihoğlu and Assoc. Prof. Dr. Bertuğ Akıntuğ for being my examining committee members.

I would also like to give my thanks to Asst. Prof. Dr. Ceren İnce Derogar for her directions during the thesis submission process. I would also like to acknowledge Asst. Prof. Dr. Yeliz Yeşilada for her trust and the Computer Engineering Department staff I have had the pleasure to work with during my master studies. I would also like to recognise the help provided by Aslı Ökten from the Graduate Studies Office, who always welcomed me with a smile.

Another group that I would like to thank are my fellow master students who would always give me new ideas on how to tackle issues and have broadened my perspective. Amongst them, I would like to especially thank Ahmet Faruk, Burak Kızılkaya, Mustafa Safa Kırlı, Hakan Yatbaz and Mohammad Abujubbeh.

Finally, I would like to thank my family for their constant support, without them none of this would have been possible.

TABLE OF CONTENTS

LIST OF TABLES

LIST OF FIGURES

LIST OF ABBREVIATIONS

AD	Anderson Darling Test
AIC	Akaike's Information Criterion
AUV	Autonomous Underwater Vehicle
AVHRR	Advanced Very High Resolution Radiometer
AW	Atlantic Water
CB	Cilician Basin
CDF	Cumulative Distribution Function
CIESM	Mediterranean Science Commission
CLARA	Clustering Large Application
CMIP5	Coupled Model Intercomparison Project 5
CND	Coastal Nile Delta
CTD	Conductivity, Temperature, and Depth
DIVA	Data-Interpolating Variational Analysis
DOI	Digital Object Identifier
EC	European Commission
EDMO	European Directory of Marine Organisations
EM	Eastern Mediterranean
EMDW	Eastern Mediterranean Deep Water
EMT	Eastern Mediterranean Transient
EU	European Union
GERD	Grand Ethiopian Renaissance Dam
GHG	Greenhouse Gas
GHRSST	Group for High Resolution Sea Surface Temperature
GODAR	Global Oceanographic Data Archaeology and Rescue
GOING	Soviet State Oceanographic Program
HyMeX	Hydrological cycle in the Mediterranean Experiment
IFREMER	L'Institut Français de Recherche pour l'Exploitation de la Mer
IOC	Intergovernmental Oceanographic Commission

IPCC	Intergovernmental Panel on Climate Change
LB	Levantine Basin
LIW	Levantine Intermediate Water
LS	Levantine Sea
LSW	Levantine Surface Water
MAW	Modified Atlantic Water
MBT	Mechanical Bathythermograph
MDW	Mediterranean Deep Water
MEDAR	Mediterranean Data Archaeology and Rescue
NOAA	National Oceanic and Atmospheric Administration
OA	Objective Analysis
ODV	Ocean Data View
OI	Optimal Interpolation
POEM	Physical Oceanography of the Eastern Meditteranean
QC	Quality Check
QF	Quality Flag
RCP	Representative Concentration Pathways
RG	Rhodes Gyre
SDC	SeaDataCloud
SDN	SeaDataNet
SST	Sea Surface Temperature
SWS	Sea Water Salinity
SWT	Sea Water Temperature
VIM	Variational Inverse Method
WM	Western Mediterranean
WMDW	Western Mediterranean Deep Water
WOA	World Ocean Atlas
WOD	World Ocean Database
XBT	Expendable Bathythermograph

(*This page is intentionally left blank*)

(*This page is intentionally left blank*)

CHAPTER 1

INTRODUCTION

Global sea surface temperatures have significantly warmed during the past 30 years alongside more than 70% of the world's coastlines, with highly heterogeneous rates of change both spatially and seasonally (Lima et al., 2012) [1]. The average rate was 0.18°C ± 0.16°C per decade and the average change in seasonal timing was -3.3 ± 4.4 days per decade. These values are more significant in coastal waters than in the global ocean where the average change has been 0.11°C per decade in the upper 75m of the ocean during the 1971-2010 period, and the seasonal shift was -2.3 days per decade (Lima et al., 2012) [1]. The already heightened anthropogenic greenhouse gases (GHG) are expected to intensify further, causing more significant climate change according to the predictions made by the Intergovernmental Panel on Climate Change (IPCC) in 2014 [2].

Representative Concentration Pathways (RCPs) are predicted outcomes for GHG concentrations published by the IPCC. RCPs indicate a definite increase in global temperatures, ranging from 1°C for the RCP26 model optimistically, to a staggering 5°C at the end of the 21st century in case anthropogenic GHG emissions follow the RCP85 model and GHG accumulation in the atmosphere continue to increase at the current rate. While the global temperatures rise, it is a fact that Ocean warming makes up the majority of the increase in contained energy in the climate system, accounting for more than 90% of the energy accumulated between 1971 and 2010. The upper layers, defined as 0 to 700m, account for approximately 60% of the total heat stored according to the Physical Science Basis [3] section of the Fifth

Assessment Report of the IPCC, published in 2013. The global ocean will most likely continue to warm during the 21st century, and the heat will penetrate from the sea surface to the deep oceans and affect global ocean circulation. With higher mean temperature values, there is also evidence of significant increases in the frequency of marine heatwaves in the observational record (Oliver et al., 2018) [4].

The Mediterranean Sea, due to its quasi-enclosed nature with most of its waters coming from the strait of Gibraltar (Robinson et al., 2001) [5] and the relatively few avenues of freshwater input (Rohling et al., 1992) [6] is considered to be one of the most affected regions by climate change (Giorgi, 2006) [7]. It is by its nature an evaporative basin with an estimated freshwater loss of 50 to 100 cm $year^{-1}$ (Bethoux, 1979; Bryden et al., 1991) [8][9]. Furthermore, the Mediterranean Sea loses heat to the atmosphere at about 4 ± 7 Wm^{-2} (Bunker et al., 1982) [10]. These two factors translate into higher Sea Water Salinity (SWS) than most bodies of water while the quick turnover rate makes it a miniature laboratory for studying the effects of global warming on the world oceans at a human scale. (Lejeusne et al., 2010) [11]. Additionally, the Mediterranean Sea influences the global thermohaline circulation and by extension plays an important role in the regulation of the global climate (Lozier et al., 1995; Bethoux et al., 1998; Rahmstorf, 1998) [12][13][14].

The acquired knowledge of the Mediterranean Sea by researchers is still insufficient to forecast the impact global warming will have on the complex natural balance at work in the area and the results of climate change on the ecological, hydrological and human systems. The information available is doubly so lacking for the Levantine Sea (LS), being at the easternmost part of the Mediterranean where the majority of studies conducted are focused on the western regions. The LS plays a critical role in the oceanic circulation while also having the highest overall Sea Water Temperature (SWT) and SWS in the Mediterranean Sea. A variation in water chemistry will most likely lead to a change in the oceanic circulation system affecting both the local ecology and the human populations depending on the sea locally and at large.

Another primordial issue arising from a warmer Mediterranean Sea is the intrusions of tropical species, such as the case of the Lessepsian migration. Introduced either through the Suez Canal or, to a lesser extent through the Strait of Gibraltar, the so-called exotic species are increasing as the Eastern Mediterranean (EM) is warming (Raitsos et al., 2010; Schmidt et al., 2015)[15][16]. Thus knowledge of the spatiotemporal variability of SWT and SWS is of vital interest to grasp the extent of the change in the marine ecosystem.

The selected spatial scope of this thesis is the LS in the EM, a major sub-basin that exchanges water with the Ionian Sea, Aegean Sea and the Red Sea and four of its sub-regions selected for evaluation: the Cilician Basin (CB), the Levantine Basin (LB), the Coastal Nile Delta (CND) and the Rhodes Gyre (RG). We will use in-situ data in this thesis to conduct a localised study of the area. Although satellite data are the most abundant source of observation available to oceanographers, however, the modern instruments at the service of the scientific community are limited to the surface layers making the use of scarcer in-situ data mandatory for analysing deeper layers below the surface.

The purpose of this study is to explain in detail the in-situ data available for LS SWT and SWS between 1960 and 2017. In order to so, this thesis focuses on two main objectives. The first objective is to conduct a descriptive analysis of the area and the sub-regions. The second objective is to determine the theoretical distribution of SWT and SWS to identify the data distribution and conduct a regression analysis.

For the rest of the thesis, the breakdown of the chapters is as follows:

- The second chapter defines this dissertation from a spatial and physical perspective. Furthermore, its strategic importance for both its energy potential and the current political instability that are shaping the region should not be ignored and taken into consideration when attempting to describe the area. Relevant information within the scope of our study about the EM and its sub-regions are presented, the LS is more accurately identified.

- The third chapter examines the data collection methods in oceanography. The SeaDataCloud (SDC) infrastructure, from where our dataset originates, is detailed from a historical and architectural perspective. The dataset used in this thesis, "Mediterranean Sea - Temperature and salinity Historical Data Collection SeaDataCloud V1"'s format and content are inspected, followed by an explanation of quality control systems. Additionally, this chapter sets the spatio-temporal range selected in this investigation and the methodology behind how our dataset is prepared for analysis.

- The fourth chapter reviews the previous scientific studies related to this thesis's objectives. At this point, a warning should be made regarding the different appellations of "The Levantine Sea" and "The Levantine Basin" throughout the literature review. Since the investigations and results of other publications are discussed, the spatial definition might differ from one work to the next.

- The fifth chapter, the core of this work, presents the tools and methodologies applied for seasonal and monthly climatological maps and descriptive statistical analysis at different depth levels employing Data-Interpolating Variational Analysis (DIVA) and classical statistical methods. Clustering is applied to showcase the amorphous nature of the sub-regions, and yearly data sampling patterns are scrutinised. Plots and histograms of our data are created to obtain a general picture of the evolution of SWT and SWS in the region.

- The sixth chapter deals with an exploratory analysis of SWT and SWS. Optimal theoretical distribution models for SWT and SWS are determined for the LS seasonally, and at all depth levels, using cumulative distribution functions and conventional statistical fitness tests. Furthermore, we present the results of our exogenous regression analysis using predicted SWT and SWS, laying out the weaknesses and strengths of our dataset.

- In the seventh and final chapter, we conclude this dissertation by revisiting our methodologies, findings, contributions and some pointers for future works.

CHAPTER 2

SPATIAL DEFINITION

When it comes to the sea as a subject of study, a system always in motion, it is almost a given that the spatial definition of the boundaries needs to be determined precisely. There is often ample confusion around this subject among the scientific community and the interested parties of the names and the range of areas and regions. In this chapter, we aim to clarify the areas that are of concern to this work, starting from the definition of the Mediterranean Sea (Section 2.1) both vertically and horizontally. The focus of this thesis, the LS and the four selected sub-regions, are further detailed in Section 2.2. Additionally, the selection criteria are presented for the CB (Section 2.2.1), the LB (Section 2.2.2), the CND (Section 2.2.3) and the RG (Section 2.2.4) with all relevant details.

2.1 MEDITERRANEAN SEA

The Mediterranean is an intercontinental sea and spans from the Atlantic Ocean on the west to Asia on the east, separating Europe from Africa. It occupies a deep, elongated, and almost landlocked irregular depression with spatial boundaries lying between latitudes 30° and 46° N and longitudes 5.50° W and 36° E. The Mediterranean Sea, including the Sea of Marmara, occupies an area of approximately 2,510,000km^2.

Even though representing only 0.8% of the surface area and 0.3% of the volume of the world oceans, the Mediterranean is a hot-spot of biodiversity (Myers et al., 2000) [17], and despite its limited geographical dimensions, it is the focus of a vast range of process and interactions, such as the global circulation. Although it is considered one of the most sophisticated marine environment, there is insufficient knowledge of its circulation mechanics, biogeochemistry and biological activity; not enough is known (Tanhua et al., 2013) [18].

The Mediterranean Sea is comprised of a series of connected sub-basins with connections to the Atlantic Ocean through Gibraltar and the Black Sea through the Dardanelles. Furthermore, there is a division into two distinct western and eastern sub-basins by the boundary line set at the Strait of Sicily. It is not only a geographic or conventional distinction as the two sub-basins show different physical and hydrological properties regarding temperature, salinity and circulation.

Figure 1 Map of the Mediterranean Sea and its sub-basins, Source:
https://en.wikipedia.org/wiki/Mediterranean_Sea

Figure 1 displays the Mediterranean Sea and its sub-basins labelled in white. The Western Mediterranean (WM) region includes the Alboran Sea between the northern Moroccan and the southern Spanish coasts with the Strait of Gibraltar allowing the exchange of water with the Atlantic Ocean; the Balearic Sea located between the Spanish and French coastline to the west, the Algerian coast to the south and Sardinia and Corsica to the east. The Ligurian Sea covers an area between the Italian coast in the Liguria region and Corsica and finally the Tyrrhenian Sea on the western coast of Italy.

The EM region includes the Adriatic Sea between the eastern coast of Italy and the Balkans; the Ionian Sea delimited by the Otranto Strait in the north and the Libyan Sea in the south which in turn extends to the island of Crete in the east. The Aegean Sea is located between Turkey and Greece and finally the LS, the focus area of this work nested in the easternmost part of the Mediterranean. The definition of the LS is presented in detail in Section 2.2.

The circulation of the Mediterranean is forced by water exchange through the interaction of various straits, wind stress and buoyancy flux at the sea surface due to freshwater and heat fluxes (Robinson et al., 2001) [H]. In order to describe the circulation of the Mediterranean Sea, the water masses must be identified and described. The three main Mediterranean water masses (Figure 2) and the Levantine Surface Water (LSW) are detailed as follows:

- The Modified Atlantic Water (MAW), which forms the upper layer between the surface and 100m and enters from the Strait of Gibraltar flowing westward starting from the Alboran Sea and ending its course in the LS.

- The Levantine Intermediate Water (LIW), formed during the winter months in LB with the cooling and sinking of the MAW and in RG and LSW in LS. It flows from east to west between 200m and 300m and is spread across the entire Mediterranean basin. The LIW is identifiable from its slightly higher salt concentration compared to the MAW.

- The Mediterranean Deep Water (MDW) is divided into two distinct water masses by the Strait of Sicily acting the role of a dam in the middle. The Western Mediterranean Deep Water (WMDW) forms during the winter in the Gulf of Lions and the Eastern Mediterranean Deep Water (EMDW) which in turn forms in the Adriatic Sea and the Aegean Sea during the winter and in extreme winter conditions in the RG. The EMDW is significantly saltier and warmer than the WMDW.

- LSW forms during summer and boasts the highest salinity in the Mediterranean due to excessive heating induced evaporation in the region due to the warm summer months (Gertman et al., 2002) [19]. It sinks during the fall and winter months caused by the cooling and its higher salt content to form the LIW.

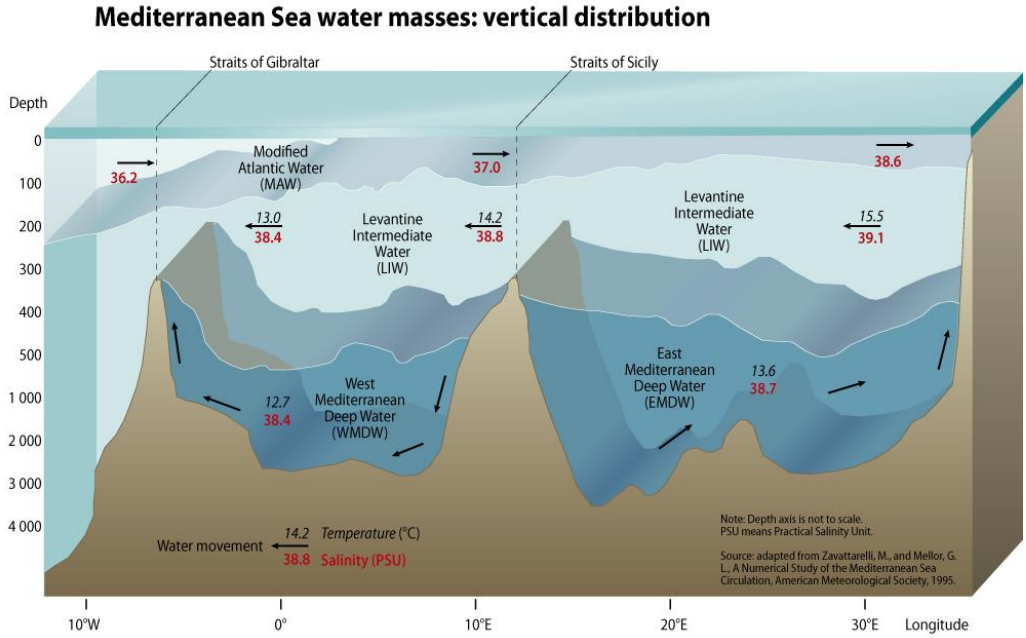

Figure 2 Mediterranean Sea water masses: vertical distribution, Source:

http://www.grida.no/resources/5885

2.2 THE LEVANTINE SEA

LS is bordered by Turkey in the north, Syria, Lebanon, Israel and the Gaza Strip in the East, Egypt and Libya in the south, and the Aegean Sea in the north-west with the island nation of Cyprus in the middle. The western border to the open Mediterranean is delimited by a line from the cape Ra's al-Hilal in Libya to the island of Gavdos, south of Crete [20]. It stretches across over an area of 320,000km^2 and has a maximum depth of 4,384m in the Pliny Trench. Except for the Suez Canal in Egypt, it has no external connection with other bodies of water. Moreover, the Red Sea's higher sea level compared to the Mediterranean Sea makes the canal act like a tidal strait that pours the saltier water of its southern counterpart. Its main natural inflow of freshwater comes from the Nile, Ceyhan and Seyhan rivers.

The four sub-regions of LS selected for evaluation in this thesis work, are the CB, LB, CND and RG. They are chosen according to different factors, which are detailed below in their respective sections and are illustrated in Figure 3.

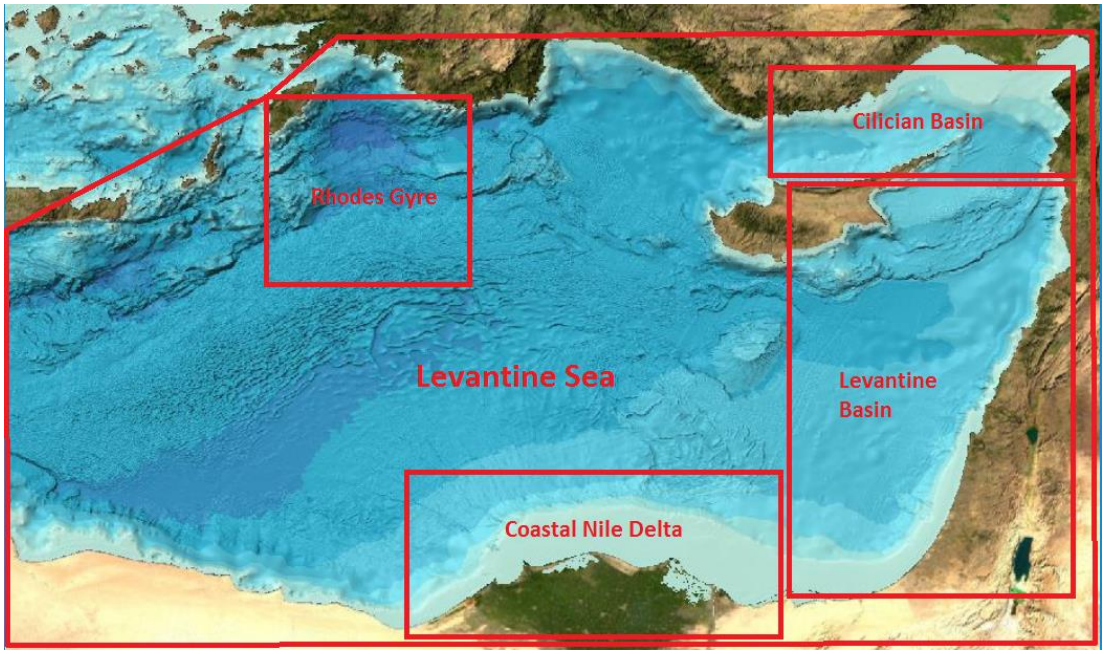

Figure 3 Map of the Levantine Sea and the sub-regions of interest, base taken from GEBCO

2.2.1 CILICIAN BASIN

The area is frequently neglected as a separate entity in the majority of studies and is often included in the wider Levantine Sea or one of its sub-basins. This lack of attention is one of the main reasons for our selection. The name was applied variously to regions at different periods but came ultimately to designate the eastern half of the south coast. The region was home for successive Armenian Kingdoms over the centuries where the basin takes its name [21].

CB is situated the north-eastern part of LS between Cyprus and Turkey, and it also contains the Gulf of Iskenderun in its mist and includes the shallow continental shelf areas of Mersin and Iskenderun Bay. The continental shelf of Mersin Bay forms the north-western margin of the Adana-CB; it extends from the Göksu delta in the southwest to the Seyhan-Tarsus-Ceyhan delta in the northeast and is narrower and steeper in the southwest than in the northeast. The continental shelf adjoining Mersin and Iskenderun Bays are one of the widest in the entire Levantine Sea, excluding the Nile Cone where the coastal bathymetry is often very steep (Özsoy & Sözer, 2006) [22].

Two main types of circulation can be observed within the Iskenderun Bay: in summer, two counter-rotating eddies driven by surface currents entering west of the Bay were inferred, while in winter it was supposed that the currents following the eastern coast could enter east of the Bay. Less saline and cooler waters were observed in the inner part of the Bay (Özsoy & Sözer, 2006) [22]. Eddies and meanders, wind-driven currents, topographic/continental shelf waves, inertial/internal oscillations add significant variability to the primary cyclonic circulation while the bifurcating mid-basin jet and the Asia-Minor current along the Turkish coast, interspersed with quasi-permanent anticyclonic eddies in the EM (Robinson et al., 1992; Özsoy et al., 1993) [23][24].

The Seyhan-Sarus is the longest river (560km) that flows southeast from its headwaters in the Anti-Taurus Mountains into the Mediterranean Sea via a broad

delta, Cape Deli. The river is currently under extensive development for hydroelectric power and irrigation and Seyhan Dam upstream of Adana serves for irrigation, hydroelectric power, and flood control. The Ceyhan-Pyramus River has a length of 509km and takes its source from the Eastern Taurus Mountains range. The amount of water flowing on the Ceyhan River changes significantly seasonally. From the end of summer to the last month of fall, the river is at its lowest flow meanwhile from November to December, and the fall rains raise the flow rate temporarily from $50m^3/s$ to $380m^3/s$. The flow increases during spring and early summer months as the snow in the Taurus Mountains melt, leading to floods before its damming. Other contributing rivers are the Göksu-Calycadnus (260km) and the Berdan-Cydnus (124km), with their main headwaters in the Taurus Mountains. Although the river is quite short (124km) it has a discharge average of $42m^3/s$, much higher than most short rivers in the area. The drainage basin covers $1,592km^2$, and there are four dams on the Berdan River. The dams are used for flood control and electricity production.

The Asi-Orontes River is the only river in the region flowing in the northern direction, draining from west to the Levant coastline of the Mediterranean sea. As a transboundary basin with a total area of $24,660km^2$ divided between three countries, 69% of the river is located in the Syria, 23% in Turkey and the remaining 8% in Lebanon (Lehner et al., 2008)[25]. The river takes its source in the mountains of Lebanon initially flowing 40km within the country, then traverses Syria for 325km to reach Turkish frontier and another 88km to the Mediterranean Sea (Bonacci, 2002) [26] before draining from the west. Its flow volume shows typical winter peak flows due to increased precipitation, and summer low flows maintained exclusively by groundwater discharge. In 2002 the dams built in the Syrian part of the basin numbered 41, with a total reservoir capacity of $741m^3/s$, all built on tributaries of the Asi-Orontes River. At the present times, Syria is using roughly 90% of the total flow, and only an annual average of $12m^3/s$ flow cross the Turkish-Syrian border. Although building a shared dam on the Asi-Orontes River has always been discussed albeit fruitlessly over the decades between Turkey and Syria, under the current political circumstance, this utopian idea seems far off.

Nowadays the Turkish rivers and the other perennial streams account for a total freshwater flux of 870m^3/s (Özsoy & Sözer, 2006) [22] contributing for about half of their discharge along the northern Mediterranean and Aegean coasts, much higher than the discharge of the Nile River, (Hamza et al., 2003; Pinardi et al., 2005) [27][28] estimated to be 540m^3/s, with the Nile itself representing 110m^3/s and the overall Nile Delta runoff at 430m^3/s. These values are expected to decrease even further in the near future. Struglia et al., 2003 [29], state that river discharge is one of the five components of the Mediterranean Sea water budget, together with the net inflow of Atlantic water through the Strait of Gibraltar that from the Black Sea at the Dardanelles Strait, evaporation, and precipitation. Nevertheless, due to the significant input of these rivers, CB has all the characteristics of costal or near-shore coastal area under river runoff influence (Pinardi et al., 2005) [28]. Although in terms of absolute values, river discharge represents only the smallest contribution and the evaporation largely dominates the Mediterranean water budget resulting in a general freshwater deficit, no other major river systems are feeding the EM. Devoid of almost 95% of its discharge, runoff of the Nile being regulated by the Aswan dam is now lower than other river runoffs (Pinardi et al., 2005) [28]. Figure 4 displays the most important inflow of freshwater into the Mediterranean Sea.

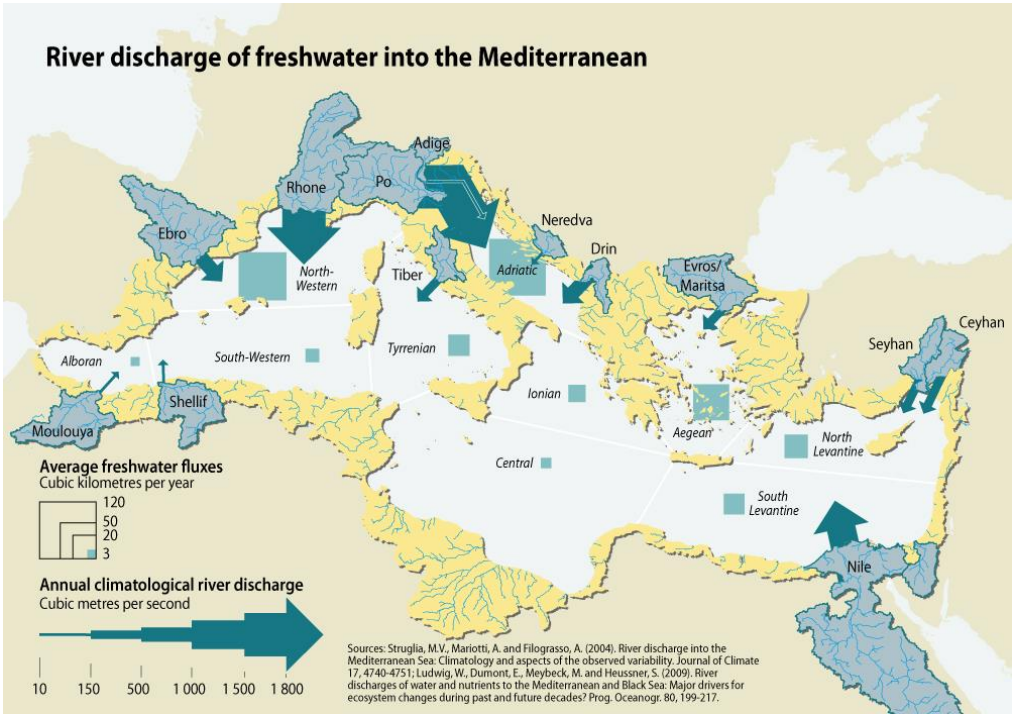

Figure 4 River Discharge of freshwater into the Mediterranean, Source:

http://www.grida.no/resources/5897

Moreover, the CB is severely affected by a range of anthropogenic stresses and is further projected to suffer from the harmful social, environmental and economic impact of coastal litter (Aydın et al., 2016) [30]. Additionally, the controversial Baku-Tbilisi-Ceyhan pipeline operated by British Petroleum transporting oil and gas from the Caspian Sea, commercial and military marine transports linked to the harbours of Mersin, Iskenderun and Taşucu, crude oil storage tanks, pipeline and terminals are the most significant potential threats of the region. On the other hand, the Akkuyu Nuclear Power Plant, the country's first nuclear power plant is under development since April 2018 in Mersin Province comes on top of it. Admittedly Russia takes a leading role in offering to finance, moreover, the aim is to complete the first reactor in 2023, the same year the Republic of Turkey celebrates its 100th anniversary. To crown it all, the deployment of a nuclear power plant is perceived as irritating in Cyprus, as one might expect, due to its proximity to the island.

2.2.2 LEVANTINE BASIN

LB is located in the easternmost region of the Mediterranean Sea between Cyprus and the Nile Delta Cone and Sinai in Egypt. It is constrained to the east by the Israel and Lebanon coastlines and the Dead Sea rift. Levantine countries surround the basin, Syria, Lebanon, The Palestinian Territories and Israel, respectively.

As one of the world's significantly under-explored region, LB existed since the Late Palaeozoic era, is a deep marine basin with water depths of 1,500 – 2,000m. LB is the area with the highest temperature and salinity values in the entire Mediterranean Sea. It is also the formation point of LIW during the winter months, making it an indispensable area of study for having a better comprehension of the changes the complex Mediterranean Sea circulation patterns and ecological balance.

There are eight energy basins in the eastern Mediterranean region; Cyprus Basin, Eratosthenes High, Latakia Basin, LB, Judea basin, Nile Delta Basin, Western Arabian province and Zagros province. Historically most of the hydrocarbon

production occurred mainly the Western Arabian, and the Zagros Provinces and in the Nile Delta Basin. According to a U.S. Geological Survey published in 2010, the Levant Basin Province is a geological structure. It covers 83,000km^2 of the eastern Mediterranean, and it is estimated to hold undiscovered reserves of 1.7 billion barrels of oil and around 3,420bcm of gas (Schenk et al., 2010) [31]. Moreover, these estimates were given before the discovery of significant volumes of gas fields in Israeli and Egyptian off-shores. On the other hand, the Eastern Mediterranean probably contains even more reserves other than LB. Figure 5 shows known gas and oil fields in the LB and the surrounding region.

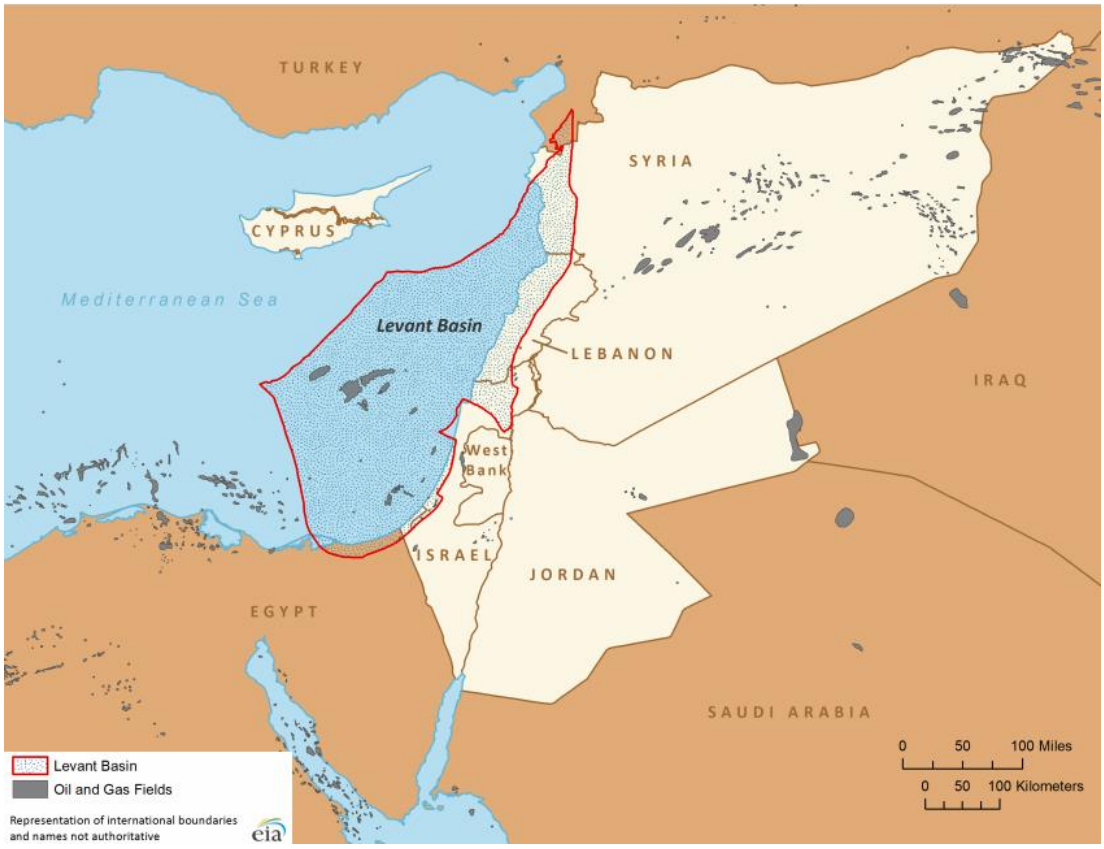

Figure 5 Oil and gas reserves in the Levantine Basin, Source: U.S. Energy Information Administration, IHS EDIN

EM region is currently undergoing changes to its energy landscape and is subject to exploratory missions for natural gas extraction, and the detection of gas fields in the Mediterranean Sea, specifically Tamar (2009), Aphrodite (2010) Leviathan (2011)

and recently Egyptian off-shore Zohr (2015) in the Nile Delta Basin brings a new energy portrait of the EM on the world agenda. Nevertheless, the exploitation of the gas fields raises also new challenges. Undoubtedly this reserve tug-of-war will add another layer to prevalent conflicts (Bornstein, 2018) [32], and will intensify the rivalry over the rights to pre-empt those resources combined with existing tensions over supremacy and maritime borders (Zhukov, 2013) [33].

2.2.3 COASTAL NILE DELTA

The Nile River, one of the primary inflows of freshwater to the Mediterranean, forms an arcuate shape delta covering 240km in the northern coastline of Egypt where it disembogues into the Mediterranean Sea. One of the world's largest river deltas, CND, is also an essential source of nutrients for LS, playing a vital role in the regulation of the local marine ecosystem due to inputs by the Nile River. The Mediterranean Seas circulation patterns keep nutrients from flowing to the east, therefore, creating an extremely hostile environment for ecological system, raising the importance of the nutrients brought by the Nile River into the EM.

The longest river in the world, the Nile River has a total length of 6.695km from Lake Victoria, confined by Uganda, Kenya and Tanzania, where it takes its source and runs through eleven countries eliminating 94% of fresh Nile water that once reached the EM. Ethiopia contributes 85% of the total flow of the Nile, with its two main tributaries, the White Nile and the Blue Nile. The vast majority of the 97 million Egyptians who live along the Nile Valley and have depended on the river as a vital resource and any threat to this lifeline would devastate the country. Meanwhile, Ethiopia's Grand Renaissance Dam (GERD), which is under construction and reportedly financed by Chinese banks, seems to be a tremendous threat not only for the future of the Nile River's flow but also a great source of political pressure on Egypt's national survival.

The Nile River flowed for ages from Aswan, in the south of Egypt and 600 km from Cairo to its Mediterranean border for more than 1200km with no bar or cataract.

From the 1950s the name of the city commonly refers to the High Dam, constructed between 1960s and 1970s following Egypt's independence from the United Kingdom in 1953, replacing the Aswan Low Dam first completed in 1902. Financed by then the Soviet Union (USSR) at the pinnacle of the Cold War, more than thirty thousand people worked round the clock to build the Aswan High which was completed in 1964, and since that time all the Nile discharge, including sediments, has been impounded in Lake Nasser. (El Din, 1977) [34] Control of flooding is carried out from the dam to Lake Nasser, the largest artificial lake in the world. The construction of the dam aimed to increase economic production by preventing, further regulating the annual flood and generating electrical power. The post-dam era had a significant impact on Egypt's economy, culture and sense of identity.

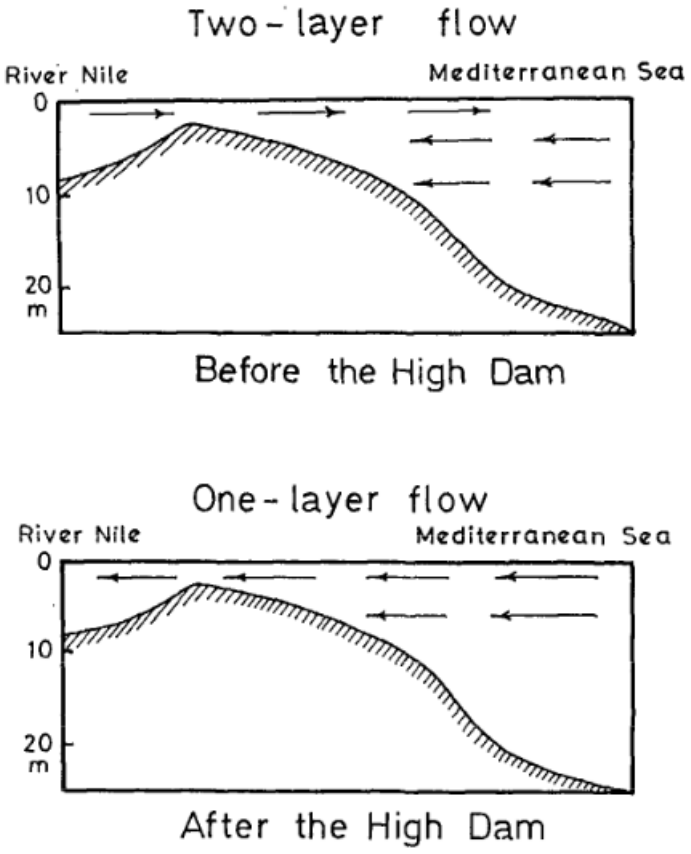

Figure 6 Flow of the Nile before and after the Aswan High Dam, Source: El Din, 1977 [34]

Construction of the Aswan High Dam brought an end to the historic flooding of the Nile which had taken place undisturbed since ancient times changing the local natural balance and leading to the collapse of the fisheries on the coast. The freshwater discharge was reduced nearly into half, but oceanographic conditions in the offshore region past the continental shelf did not showcase a noticeable change. Nevertheless, hydrographical conditions over the continental shelf in front of the Delta considerably changed (Figure 6) upon the closing of the High Aswan Dam in 1964 (El Din, 1977) [34]. Darwish et al., 2017 [35], studied geomorphologic changes along the Nile Delta coastline between 1945 and 2015 using topographic maps produced by the Egyptian Geological Survey in 1945 and Landsat satellite imagery between 1973 and 2015. They found that the delta coastline was highly eroded after the construction of the Aswan High Dam.

Although the presence of the Aswan High Dam tends to increase the salinity of the Mediterranean Sea, which in turn affects the Mediterranean's outflow current into the Atlantic Ocean, Egyptian Mediterranean fishing declined after the dam was completed because nutrients that used to flow the Nile River to the Mediterranean Sea were trapped behind the dam. On the other hand and in an unexpected turn of events, the fisheries were restored in the 1980s to the surprise of scientists, coinciding with increasing artificial fertilizer use, expanded agricultural drainage, growing human population, in parallel with significant extension of sewage installations, therefore more wastewater and even more sanitary discharges (Nixon, 2004)[36]. Even if quite different from the past the Nile River and by extension, the Nile Delta still play a crucial role in providing nutrient to the EM, although in a different form (Nixon, 2003) [37]. The Nile Delta is also one of the most at-risk areas to be affected by the rising of the sea level and the salinization of its soils, rendering agricultural work harder.

There is a relative scarcity of data in the region compared to the risks brought by climate change that will affect both the Mediterranean as a whole and the people living in the Delta. These factors make the area an essential study subject for ecological, hydrological and socioeconomic reasons. Moreover, when completed,

The GERD will be the new reality of the Nile. It will further reduce the discharge of the river waters into the Mediterranean in the limelight of having a capacity of about half of the Aswan Dam and will take between eight to ten years to fill the new dam [38].

2.2.4 RHODES GYRE

There are four primary sub-basin eddies within the LS, which interact dynamically being the two anti-cyclonic Mersa Matruh gyre in the south-western LB, the Shikmona gyre in the south-eastern LS, the cyclonic West Cyprus gyre in the north-western LS and the RG east of Crete.

The RG is a persistent cyclonic feature of the general circulation of the EM and has been the subject of multiple investigations. According to the oceanographic studies, it is approximately centred at around 36 °N and 28.5 °E and has a radius of 300km (Milliff & Robinson, 1991) [39]. In the LS known humorously as the Blue Desert, the RG with its overall cooler yearlong waters, it stands as an area where late-winter pulses of high primary productivity are likely to create suitable feeding conditions for various marine life (Notarbartolo di Sciara & Bearzi, 2010) [40]. It is also a point of formation for the LIW (Lascaratos et al., 1993) [41] and also occasionally becomes a point of formation for the EMDW when the winter conditions are severe (Lascaratos & Nittis, 1998) [42] as demonstrated during the Eastern Mediterranean Transient (EMT).

Even if the area covered by the RG is known, there is a certain degree of variability as demonstrated by Marullo et al. [43], but using the estimated central coordinate and the radius previously mentioned when working in the area seems unproductive. This conclusion is due to the analysis conducted during the preliminary work for the selection and localisation of the sub-regions using the data available on the World Ocean Atlas 2018 (WOA18, https://www.nodc.noaa.gov/OC5/woa18/) yielding a different area than the definition given by the previous literature presented at the opening of this section. The geospatial analysis of the temperature maps obtained by

treating the WOA18 data with the System for Automated Geoscientific Analysis (SAGA GIS) software, we obtain isothermal maps with the visible pocket of colder water locating the RG further south than expected (e.g., Figure 7). Additional temperature isotherm maps are available in Appendix B.

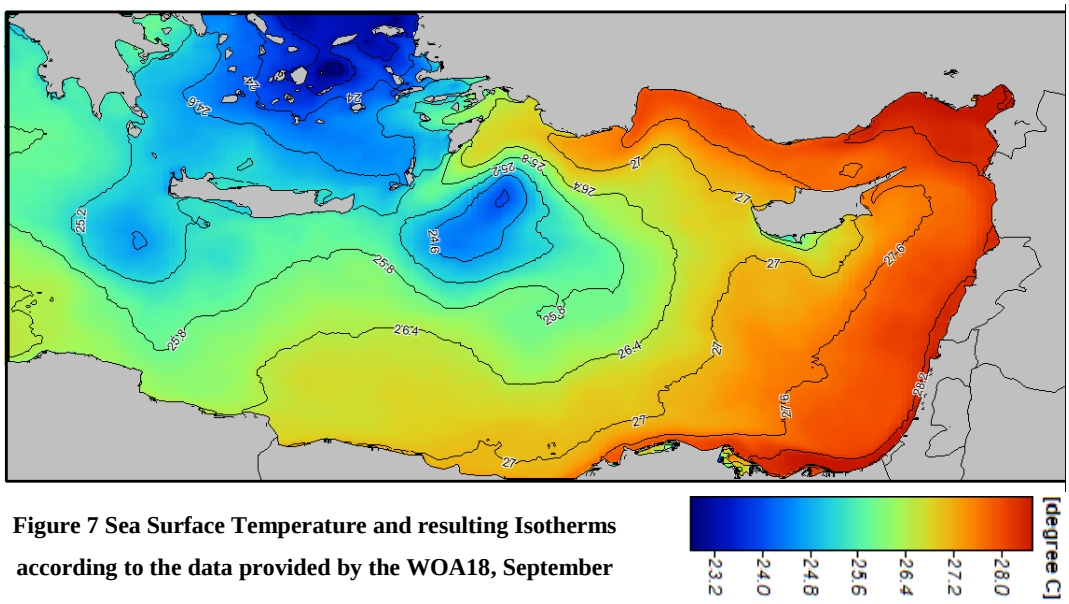

Figure 7 Sea Surface Temperature and resulting Isotherms according to the data provided by the WOA18, September

From the results of the preliminary analysis and the tendency of the RG to shift, it is vital to select a wider spatial area compared to the given coordinates to get the best coverage even with the changing location of the cyclonic feature while proceeding with calculations.

CHAPTER 3

DATA INFORMATION & INFRASTRUCTURE

The basic working principle of satellite and in-situ data collection (Section 3.1) and an overview of the SDC infrastructure from an architectural and historical perspective (Section 3.2) are given followed by an introduction to the in-situ aggregated dataset used in our analysis (Section 3.3). The details of the quality check procedures applied to the dataset (Section 3.4) and the available variables in the dataset of concern to our study are explained (Section 3.5). In this chapter, we further provide information about the data sources and the content detailed of the dataset (Section 3.6). The spatial scope for the LS and its sub-regions and the temporal range of our analysis are presented respectively in Section 3.7 and Section 3.8. The Ocean Data View (ODV, https://odv.awi.de/) [44] software developed with the explicit purpose of working with marine data interpretation is introduced in Section 3.8. Finally, the methodology (Section 3.9) used to reduce the aggregated data to conform to the limits of this thesis is explained step by step.

3.1 DATA COLLECTION METHODS

Ocean observations originate from a variety of sources and change the way ocean science evolves. The ocean observation systems currently in operation can be categorised as in-situ observations and satellite observations. Standardised Sea Surface Temperature (SST) in-situ observations, mainly from trading ships, began in the second half of the 19th century according to the rules set at the Brussels Maritime Conferences of 1853 (Rayner et al. 2006) [45].

Surface and sub-surface buoys, floats and volunteer observing ships are some of the in-situ observation instruments for capturing and tracking changes in time and depth at specific points. The most commonly used platforms are: moored and drifting buoys, bathythermographs deployed from research vessels to measure the temperature along with its route and conductivity-temperature-depth sensor launched from ships and Niskin bottles. Since the middle of the twentieth-century data from ocean profilers and drifting buoys were incorporated to the global observation of SST.

Satellite remote sensing systems are aerial systems to capture the spatial and temporal variations of surface parameters. With the advent of remote satellite data gathering technology in the 1980s, satellite data became a staple tool of the oceanographic community and revolutionised the field. Compared to in-situ data gathering, which often has sparse space-time resolution, it allows for high-resolution data collection. However, it is mostly limited to sea-surface observations, and the collected data are mainly for sea level height, temperature, salinity and chlorophyll analysis purposes.

The Advanced Very High Resolution Radiometer (AVHRR) is the most commonly encountered satellite sensor in oceanographic data collected by satellites. Relevant to our work, the satellite has a maximum resolution of 1.1 km2 and provided data precisely are excellent sources of uninterrupted data series starting from 1981 to the present. AVHHRs are present on both the National Oceanic and Atmospheric Administration (NOAA, https://www.noaa.gov/) Polar-orbiting Operational Environmental Satellite (POES) and the MetOp Satellites (Figure 8) of the European Space Agency (ESA, https://www.esa.int/ESA). Recently, the Group for High Resolution Sea Surface Temperature (GHRSST, https://www.ghrsst.org/) has established a framework and set rules for best practices of processing and sharing SST data in an organised and standardised way handy for scientists and data users. GHRSST is an international science group that promotes the monitoring of SST. Satellite data providers involved in the collaborative effort deliver their accumulated

data to the GHRSST Data Assembly Centre (GDAC, online at http://ghrsst.jpl.nasa.gov) which in turn distributes data to users in near-real-time. Furthermore, 30 days after their submission data, are stored at the Long Term Stewardship and Reanalysis Facility (LTSRF, online at http://ghrsst.nodc.noaa.gov) for long-term archive.

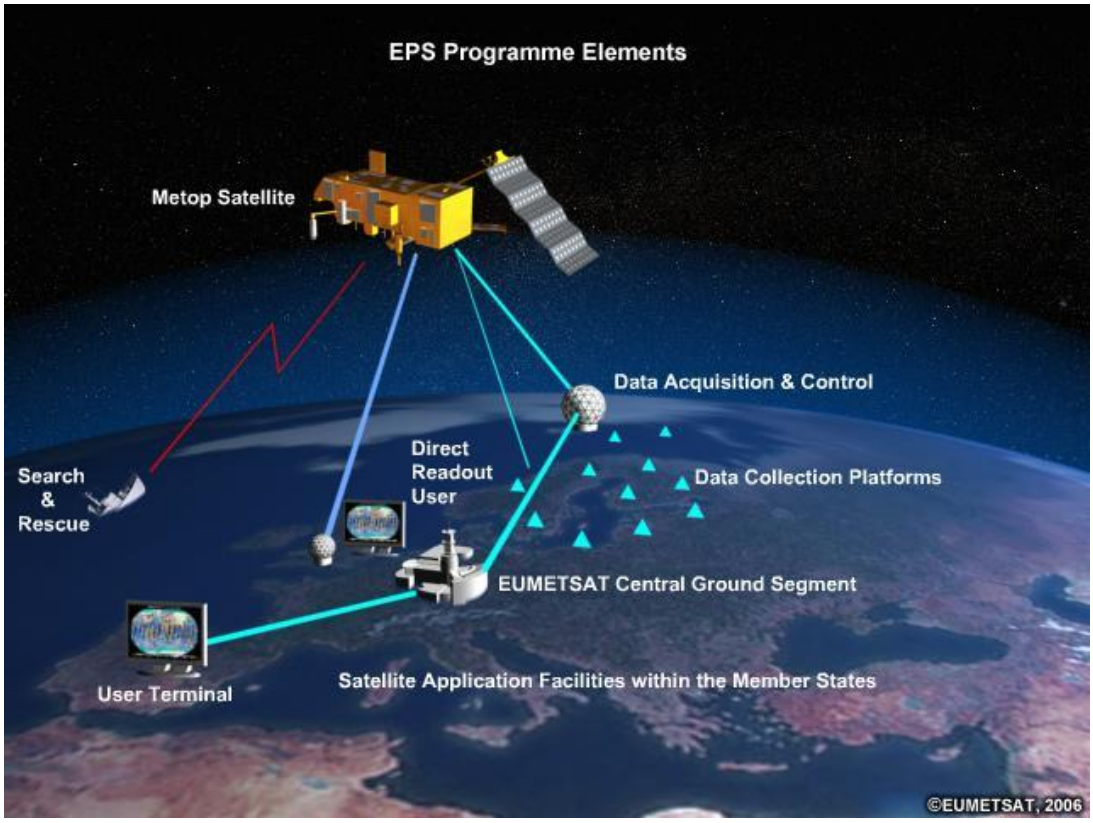

Figure 8 MetOp satellite system, Source: https://www.eumetsat.int/eps_webcast/eps/print.htm

Even though the oceanographic community has been using it for a long time, in-situ data collection still preserves its importance as a reference point and complement to the satellite-based observations. Reciprocally in-situ observation systems use satellite data to relay from remote areas. Meanwhile, the high cost of in-situ instruments and the limited availability of in-situ data with high spatial and temporal resolutions, deploying and maintaining the observational platforms in place, together with the degradation of sensor performance and their short lifespan in the harsh marine environment are the downsides of in-situ observations. Traditional sub-surface observations and satellite-derived observations of the sea surface and the potential

models developed from those observations might allow the oceanographic community in the future to attain observational capability similar to what meteorologists use daily.

Researchers interested in oceanography used in-situ data collection platforms for decades. Classical in-situ platforms include moorings, profiling floats, gliders, ships volunteering for observation and research vessels are incorporated with highly specialised equipment. The most routine variables measured by in-situ installations are temperature, salinity, currents, dissolved oxygen, hydrogen sulphur, alkalinity, phosphate, ammonium, nitrite, silicate, chlorophyll and PH. The first two variables, salinity and temperature, are our primary involvement in this thesis. The descriptions of the most usual tools and conventional methods of in-situ collection are listed and described as follows:

Moorings, capable of being employed for more extended data collection periods, are fixed in position with a wire anchored to the seafloor and a platform on the surface. Specialised sensory equipment can be attached to a wire to go up and down different depth levels along a vertical line. The data collected by the sensors are transmitted back by the agency via the use of satellites or radio waves. Figure 9 exhibits a standard mooring setup.

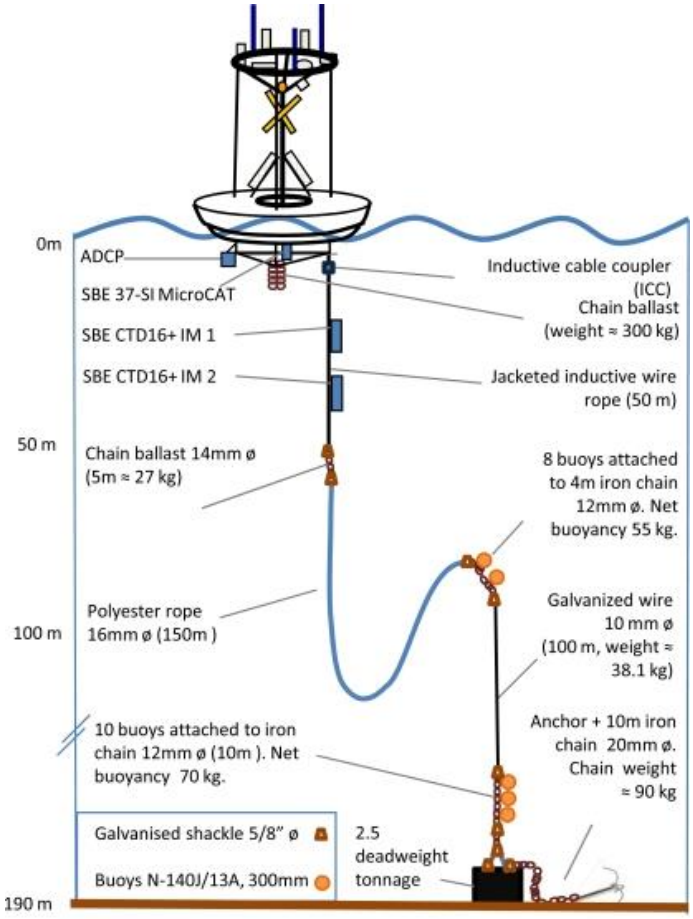

Figure 9 A mooring system example, Source: Bahamon et al, 2011 [46]

Profiling floats (Figure 10) used by the ARGO program are often called "ARGO floats" and deployed worldwide. The program is a collaborative effort by more than 30 nations and consists of a 3,800 unit fleet. The free-drifting profiling floats that measure the temperature and salinity of the upper 2000 m of the ocean. Each float weighs 20-30 kg and equipped to descend into thousands of meters in depth by regulating their buoyancy. Every ten days they move to the sea-surface, measuring conductivity and temperature profiles as well as pressure. This instrument will go as far as possible until it ends up on the ocean floor when its battery fails, the so-called parking depth happens in most cases when probes drift at a depth of 1000m. They are widely utilised due to their disposable pattern qualification and prohibitive costs. The collected data are sent back for analysis through the agency of satellites when they resurface. This program allows for the continuous monitoring of the physical

properties of the upper ocean, with all data obtained being relayed and made available publicly within hours after collection (http://www.argo.ucsd.edu/).

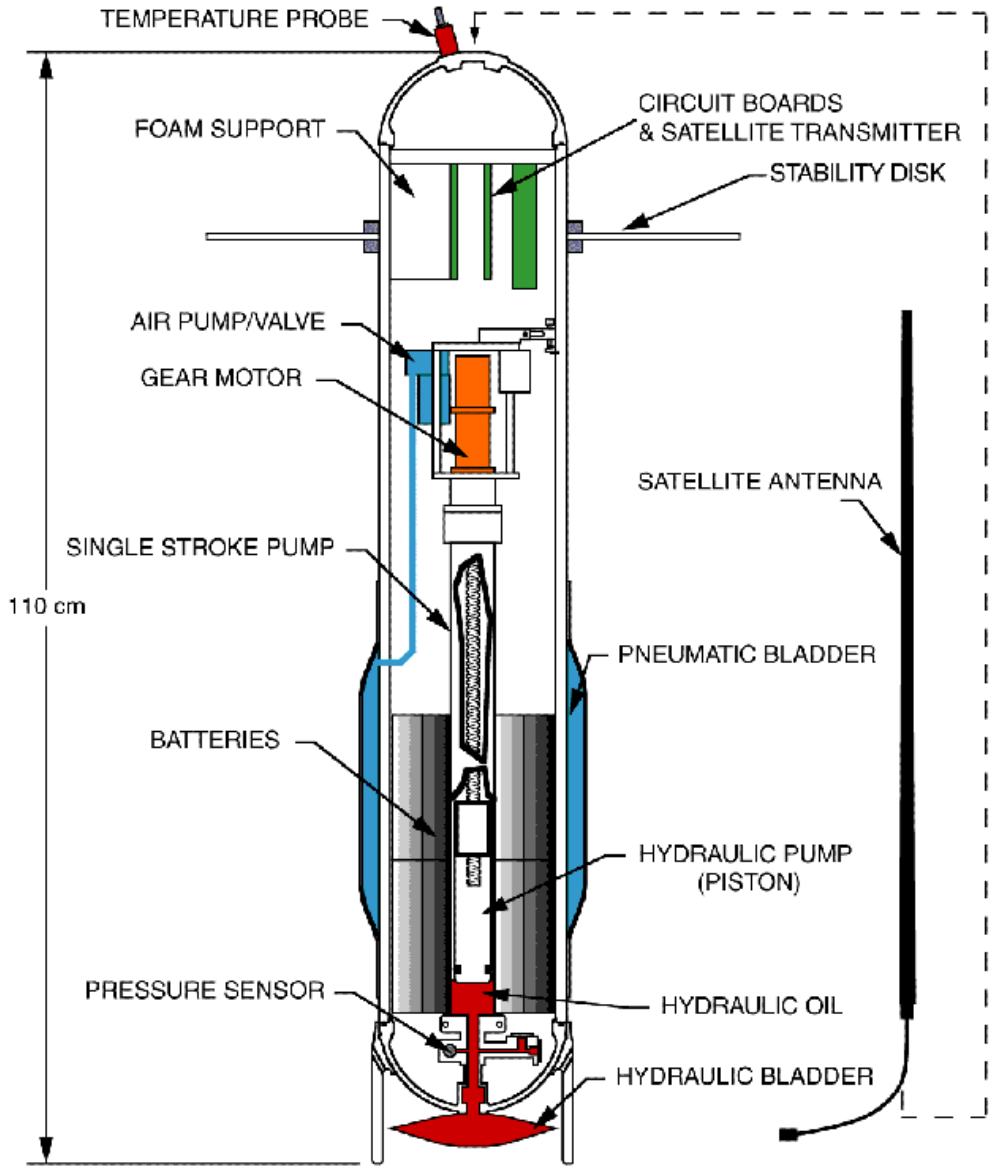

Figure 10 ARGO Float Schematic, Source: http://www.argo.ucsd.edu/

Gliders are autonomous underwater vehicles (AUV) that can move both horizontally with their internal battery to propel themselves and vertically through control of their buoyancy. Meanwhile, an underwater glider is a type of AUV that employs variable-buoyancy propulsion instead of traditional propellers or thrusters. Many glider designs are using different techniques to move through the water, but all gliders

share the common ability to travel long distances over extended periods, without maintenance. They will transmit their findings through satellite or be collected when their mission is complete (Figure 11).

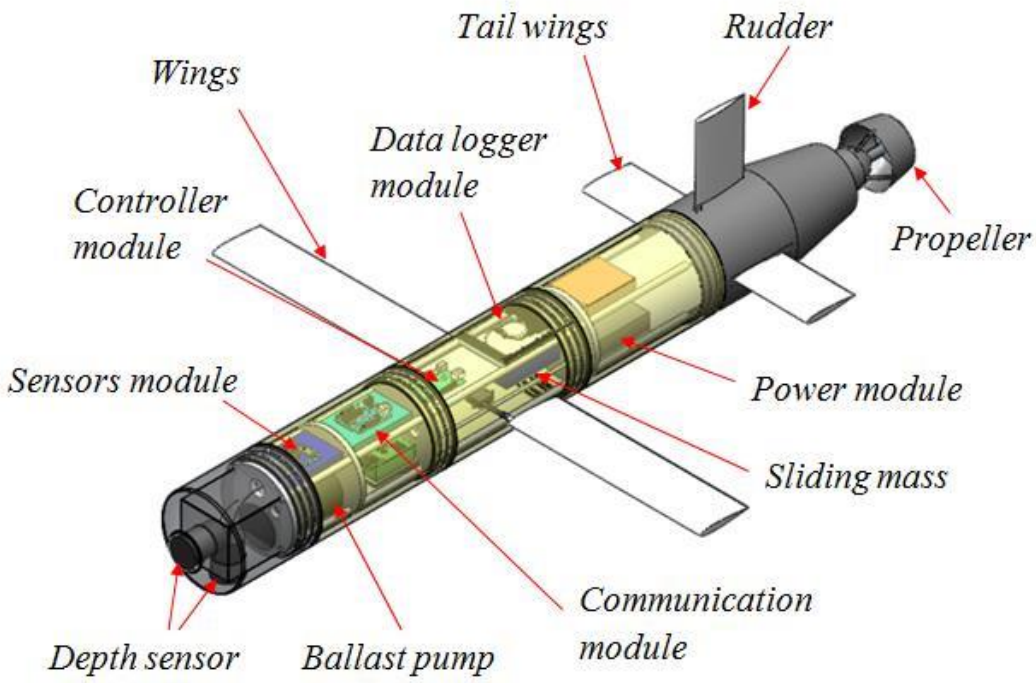

Figure 11 3-D Model of an Underwater Glider, Source: Isa et al, 2015 [47]

Research vessels are employed to deliver and conduct accurate and highly specialised data collection from the surface to the deepest reaches of the seafloor. The main drawback is the intermittent spatial coverage and the high cost of running such an operation for long periods. The main instruments handled on these kinds of vessels are the Niskin bottle, the mechanical bathythermograph (MBT), expendable bathythermograph (XBT) and CTD (Conductivity, Temperature, and Depth):

MBT is a small cylindrical device used to detect changes in water temperature to depth down to approximately 300m. Lowered by a winch on the ship into the water, the MBT records pressure and temperature as it is dropped freely through the water. When the instrument drops, the wire unfurls until it reaches a predetermined depth, then a brake is applied, and the operator draws the MBT back to the surface. Initially

a military technology, it has been phased out in the 1980s for the operational danger it posed. Figure 12 is the schematic of a classical MBT. Although obsolete, some of our data are provided by MBTs requiring their presentation.

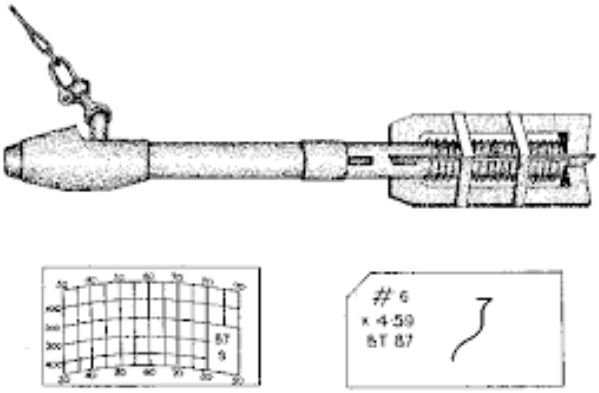

Figure 12 MBT Schema, Source: Measuring the Ocean - Coastal Oceanography, modb.oce.ulg.ac.be/mediawiki/upload/Aida/OCEA0011/MeasuringOcean.pdf

XBT is a probe deployed from the ship and not meant to for recovery. As it does not interfere with the vessels normal operations, it is launched from volunteer vessels such as cargo ships or ferries rather than scientific vessels. The probe falls freely and provides a temperature-depth which is connected electronically to a chart recorder through a wire where readings are displayed. Eventually, the wire reaches its maximum length and snaps, resulting in the XBT to sink to the ocean floor. Figure 13 is a rendering of an XBT with its copper wire visible.

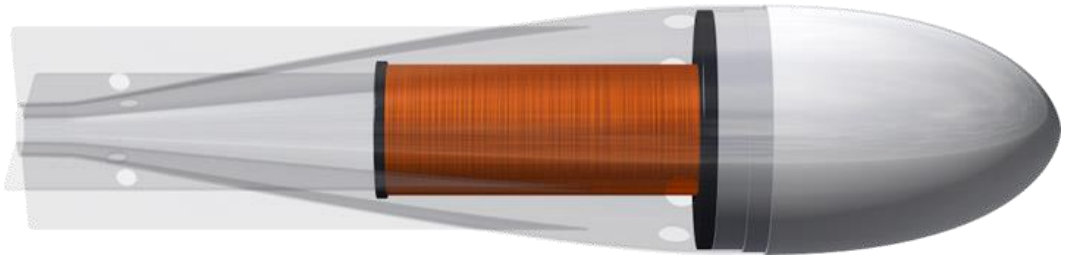

Figure 13 Rendering of an XBT, Source: https://en.wikipedia.org/wiki/Bathythermograph

CTD indicates a package of electronic instruments in order to assess the three variables of its namesake. It derives depth measurement from the measurement of hydrostatic pressure and measures salinity from electrical conductivity. It is possible to obtain for seawater density, which is a significant component of ocean circulation by doing further calculations using SWT and SWS values. With proper casing material, such as titanium, depths over 10,000m are reachable. It is the preferred method for conducting sampling of the water column for scientific vessels. If necessary, the installation of additional sensors on the apparatus is possible for additional measurements of chemical and physical properties. Often CTD and other equipment are attached to a rosette before being lowered into the water from research vessels with any additional equipment for the collection of more specific data. Figure 14 shows the electronic components, sensors and casing of a CTD.

Figure 14 CTD Source: https://en.wikipedia.org/w9iki/CTD_(instrument)

Niskin bottles are plastic cylinders with stoppers at both ends to seal the bottle entirely and employed to take water samples at the desired depth without risking contamination from other depth levels. They are relatively simple to handle for taking samples of the water column at different depths. When used alone, a weight is attached to a separate line to the bottle. It is released from the surface when the desired depth is deemed reached and slides down until hitting a button that under the

shock will close the apparatus. In the case a CTD and Niskin bottles are mounted together onto a carousel and used concurrently, an electronic system takes charge of the sealing of the bottles. In Figure 15, a Niskin bottle is being lowered into the sea for individual sampling, and Figure 16 shows a CTD with Niskin Bottles arranged into a carousel, a so-called Rosette in action.

Figure 15 Niskin Bottle, Courtesy of NIOZ

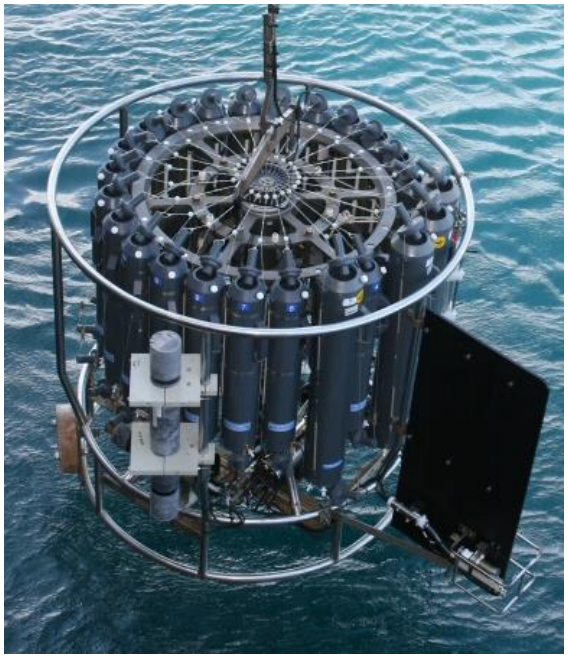

Figure 16 Rosette with CTD and Niskin Bottles, Source: http://intothecaymanabyss.noc.ac.uk/p/equipment.html

3.2 SEADATACLOUD

SDC (https://www.seadatanet.org/) is a Pan-European infrastructure for ocean and marine data management [48] currently coordinated by "L'Institut Français de Recherche pour l'Exploitation de la Mer" (IFREMER, https://wwz.ifremer.fr/). SDC goals are to address the problem of the fragmentation of the marine scientific community. The infrastructure facilitates the management and data sharing, originating from several scientific and research institutes along the coastlines of the European seas, introducing common standards for metadata format, quality control of data format methods, and Quality Flags (QF). Furthermore, the system allows users to retrieve data, metadata, and products coming from different data centres through a unique integrated portal.

SDC initially started its existence as the SeaDataNet (SDN, 2006) initiative with funding in the scope of the EU Sixth Framework and coordinated by IFREMER. The first phase was deemed successful and an effort to create an operationally robust and state-of-the-art Pan-European infrastructure and ended in 2011. The second round of

funding was granted for four additional years starting from 2011 to 2015, changing its name to SeaDataNet2 (SDN2) in the scope of the second phase with much of its original goals intact with the addition of two main objectives, promoting common data management standards and realizing technical and semantic interoperability with other relevant data management systems and initiatives.

Currently in its third phase, SDC with a funding period starting in 2016 and continuing until 2020 in the scope of EU Horizon2020 programme, intending to considerably advance SDN Services and increasing their usage, adopting cloud and High-Performance Computing technology for better performance and creating a virtual research environment. The network intends to enhance the currently existing infrastructures, which are the national oceanographic data centres or data focal points of 34 European, coastal Mediterranean countries and Australia active in data collection shown in Figure 17 [48].

Figure 17 SeaDataCloud Partners Map, Source: https://www.seadatanet.org/About-us/SeaDataCloud/Partners

SDC metadata catalogue contains the following sections allowing users to access and find information about marine data, cruise reports and research projects:

- European Directory of Marine Organisations (EDMO)
- European Directory of Marine Environment Data sets (EDMED)
- European Directory of Marine Environmental Research Projects (EDMERP)
- Cruise Summary Reports (CSR)
- European Directory of the Initial Ocean-Observing Systems (EDIOS)
- Common Data Index (CDI)

The components of the SDC project are succinctly summarised as follows:

- Networking Activities (NA)'s purposes are to improve the services while providing research infrastructure in order to foster co-operation between the project participants and the scientific communities. NA includes project coordination, training of data providers and users, communication and distribution, and management of SDN metadata catalogues.

- Virtual Access Activities (VAA) provide continuous access to the national marine data and information services including: SDN portal, SDC metadata catalogue (EDMED, EDMERP, EDMO, EDIOS and CSR), product catalogue such as aggregated datasets, vocabulary, monitoring, authentication and authorisation, help desk, cloud replication, online SWE, Virtual Research Environment (VRE) and MySeaDataCloud.

- Joint Research Activities (JRA) aims to contribute further to quantitative and qualitative advances of the current standards, tools and services provided by the infrastructure in the cloud environment. Furthermore, new scientific marine data products are developed under JRA activities.

SDN metadata catalogue, not to be confused with the old SDN platform, is a standardized infrastructure for managing the broad and diverse data gathered by the research vessels and making use of automatic land-based or oceangoing observation systems providing a virtual data management system for integrated data sets of standardized quality on-line.

The underlying architecture of SDC is summarised in Figure 18, showing the Sextant portal (https://sextant.ifremer.fr/eng), where our dataset is located as a different entity separated from the general data products of SDN. Sextant goal is to document, spread and promote a catalogue of data related to the marine environment. Sextant services are exclusively for laboratories and partners of IFREMER as well as other European national entities working in the marine and coastal domain.

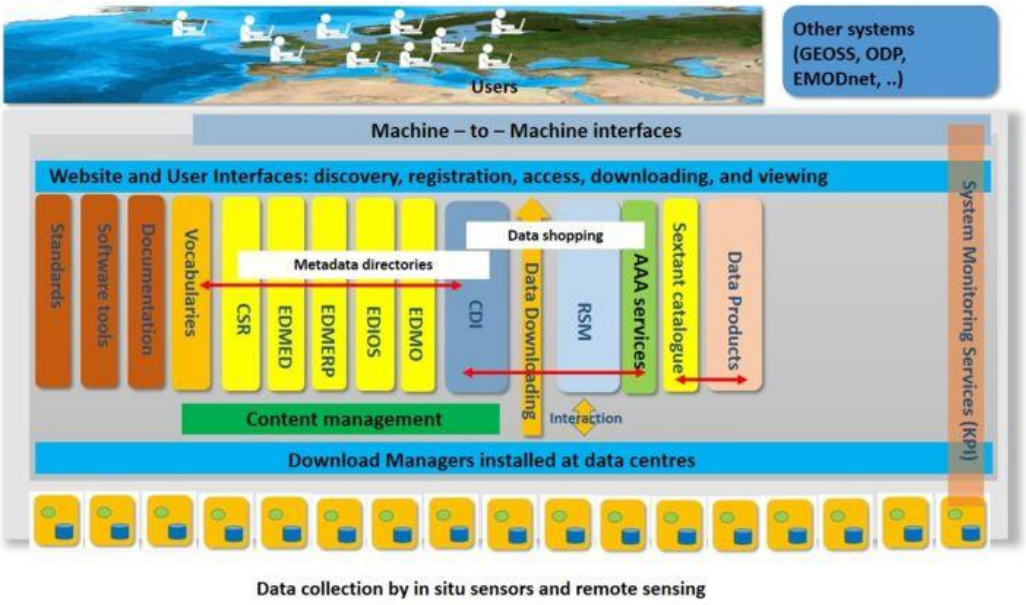

Figure 18 SeaDataCloud Architecture, Source: https://www.seadatanet.org/About-us/SeaDataCloud

3.3 DATA GATHERING

The data used in this work are taken from the SDN infrastructure and the dataset selected for the analysis is "Mediterranean Sea - Temperature and salinity Historical Data Collection SeaDataCloud V1", [49] is available on the Sextant portal. The data

covers a temporal range between 1900 and 2017 and possess a spatial coverage between 9.25° W and 37° E, encompassing the whole Mediterranean basin. It also includes an Atlantic box and the Marmara Sea. According to those coordinates, a more substantial part of the Atlantic Ocean should be included but left out of the dataset on purpose.

The data set contains all open access in-situ temperature and in-situ salinity data retrieved from the SDN infrastructure until the end of October 2017, collected by autonomous underwater gliders, profiling floats, and research vessels using CTD, MBT, XBT and Niskin bottles. The dataset is visually represented using ODV in Figure 19.

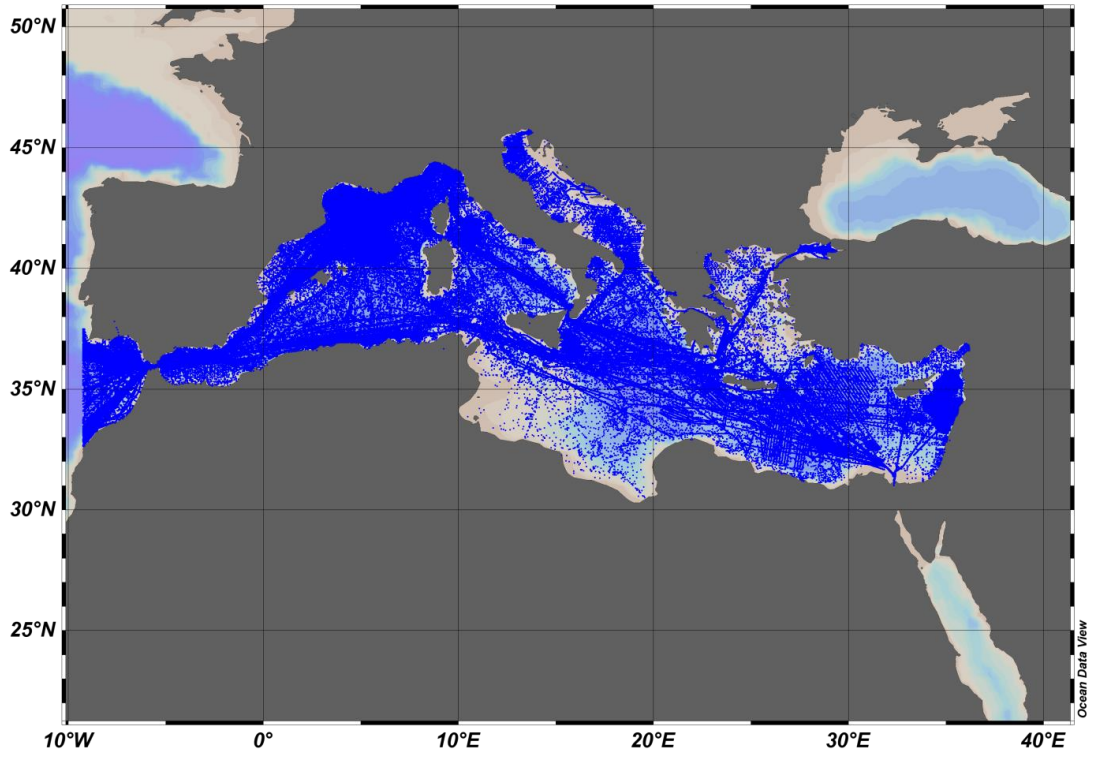

Figure 19 Mediterranean Sea - Temperature and salinity Historical Data Collection SeaDataCloud V1

3.4 DATA QUALITY

SDN members conduct Quality Control (QC) of the collected data before submission. The QC process is made in accordance with the Intergovernmental Oceanographic Commission (IOC) and the International Council for the Exploration of the Seas (ICES) baselines and employs human and standard automatic monitoring test of instruments and parameters.

The three primary QC checks are:

- Format checks flag missing mandatory information such as cruise, sensor type and observation system. Alerts to wrong variable names and incorrect platform codes and names.

- Location and date checks, which can be further detailed as:
  - Duplicate Test for eliminating multiple entries of the same data twice or more.
  - Date and Time Test to confirm that the temporal format is respected.
  - Longitude and Latitude Test to ascertain that the range of the coordinates falls between -180° and 180° for the former and 90° and 90° for the latter.
  - Position Test to ensure that the data points are not on land.

- Measurement checks are different according to the parameters and instrument employed, but three general tests apply to all of them.
  - Global Range Test confirms if the measurements are in the proper range of the ocean.
  - Regional Range Test checks if the values fall within the usual limits of each particular region.
  - Deepest Pressure Test to confirm whether the pressure values do not exceed the bathymetry values.

The data are quality checked using ODV 5.0 software presented in Section 3.9 and treated to conform to the temporal and spatial range we define in Section 3.7 and Section 3.8. QFs of anomalous data are revised according to the necessary quality control procedures; only data entries that are given a QF value of 1 or 2 according to Table 1 rating QFs are included in our calculations.

Key	Entry Term	Abbreviated term	Term definition
0	no quality control	none	No quality control procedures have been applied to the data value. This is the initial status for all data values entering the working archive.
1	good value	good	Good quality data value that is not part of any identified malfunction and has been verified as consistent with real phenomena during the quality control process.
2	probably good value	probably_good	Data value that is probably consistent with real phenomena but this is unconfirmed or data value forming part of a malfunction that is considered too small to affect the overall quality of the data object of which it is a part.
3	probably bad value	probably_bad	Data value recognised as unusual during quality control that forms part of a feature that is probably inconsistent with real phenomena.
4	bad value	bad	An obviously erroneous data value.
5	changed value	changed	Data value adjusted during quality control. Best practice strongly recommends that the value before the change be preserved in the data or its accompanying metadata.
6	value below detection	BD	The level of the measured phenomenon was too small to be quantified by the technique employed to measure it. The accompanying value is the detection limit for the technique or zero if that value is unknown.
7	value in excess	excess	The level of the measured phenomenon was too large to be quantified by the technique employed to measure it. The accompanying value is the measurement limit for the technique.
8	interpolated value	interpolated	This value has been derived by interpolation from other values in the data object.
9	missing value	missing	The data value is missing. Any accompanying value will be a magic number representing absent data.
A	value phenomenon uncertain	ID_uncertain	There is uncertainty in the description of the measured phenomenon associated with the value such as chemical species or biological entity.

Table 1 List of SeaDataNet Quality Flags. Quality flags are used to describe the data value. Source: SeaDataNet DATA QUALITY CONTROL PROCEDURES Version 2.0 [50]

MBT and XBT are known to have incorrect fall rates often and results in warm bias in measurement (Wijffels et al., 2008) [51], and there is no possible bias correction for them in the Mediterranean Sea unlike the one available by NOAA for the global

oceans [52]. In our study, MBT and XBT data entries were not discarded for two main reasons, the first being that the data provided by MBT and XBT significantly improve the amount of geographical coverage, especially for the 1960 to 1985 range. The second is the resulting bias being relatively small, outweighing the disadvantages of their inclusion compared to the slight bias that might arise from their use (Iona et al., 2018) [53].

3.5 VARIABLES

The essential variables for this study in the aggregated dataset entries are Date, Latitude, Longitude, Depth, Temperature and Salinity. A short a brief definition of each variable and its corresponding unit is presented in Table 2 for ease of reference. Angular distance north or south from the equator of a point on the earth's surface, measured on the meridian of the point.

Variable	Definition	Unit
Date	Moth, Day and Year of the in-situ measurement as recorded in the entry.	MM/DD/YYYY
Latitude	Angular distance north or south from the equator of a point on the earth's surface, measured on the meridian of the point.	Decimal Degrees (N°/S°)
Longitude	Angular distance east or west on the earth's surface, by the angle contained between the meridian, in this case Greenwich	Decimal Degrees (E°/W°)
Depth	Vertical distance from the sea surface during the measurement.	Meter (m)
Temperature	In-situ Sea Water Temperature measured using equipment in section 4.2.1.	Degree Celsius (C°)
Salinity	In-situ Sea Water Salinity measured using equipment in section 4.2.1. It is referred to as the Practical Salinity.	Practical Salinity Unit (PSU)

Table 2 List of Variables in the Dataset

Temperature is not a foreign idea and is easy to understand, but non-specialist might get confused with the concept of Practical Salinity. This issue arises due to a technical mismatch that prevents an absolute definition since the convention was established. As a crutch, the PSU is used, but doing so is formally discouraged and incorrect. Practical Salinities are numerically smaller by about 0.5% than the mass fraction of dissolved solid when this fraction is expressed as grams of solute per kilogram of seawater. For ease of comprehension, the values are expressed in PSU in this work, but we concluded that informing our readers on this subject was relevant.

3.6 DATA SAMPLING

In the original dataset used in this work contains SWS and SWT measurement obtained during the 20th century and the first two decades of the 21st century by research institutes of different origins as noted in Section 3.3. It contains precisely 739,784 stations and 41,001,444 individual data entries from various devices. The entries are from CTD, MBT, XBT, floats, gliders, moorings and Niskin bottles. The vertical distribution of the data entries per instrument differs due to the actual physical limits of the hardware. Moreover, the spatial coverage depends on the countries resources and their priorities. Some entries are sampled by commercial or trading vessels while some others are the result of dedicated scientific cruises.

3.7 TEMPORAL RANGE

Despite the historical in-situ dataset having a temporal range between 1900 and 2017, the nature of the data's distribution makes it unfeasible to take into account the totality of the available data for two reasons. The first issue arises from the many yearlong gaps in the data collection, especially in the EM compared to the WM, precluding a significant interpretation of the entirety of the dataset.

The second important factor is the considerable amount of error and uncertainty in the quality of the data available before 1960, mainly due to the quality and reliability

of equipment available and the scant resources devoted to the region. Technological advances of the hardware and methodological improvements assure a higher degree of quality in collected data after that year, which in turn sets the reliable limit while determining the temporal range of the analysis presented in Chapter 5.

In this study, LS is investigated over the period 1960-2017, utilising all available products from 1960 onwards in order to cover a maximum amount of possible time intervals. The statistical method is applied to the datasets with three different temporal ranges, respectively 1960-1980 (20 years), 1960-2017 (57 years) and 1980-2017 (37 years).

The selection of three distinct temporal ranges may seem exuberant. However, our primary purpose is to be of service to other studies on the subject area and are useful when comparing our findings — Moreover, very few studies discussed in Chapter 4 adopted ranges going as far back as our initial start date. Most studies in the area are post-1980 be it due to the previous lack of in-situ data or due to the abundance of available satellite data with the launch of AVHRR equipped platform in the 80s. There is also a visible trend upward both in SWT, and SWS values in studies performed past the 1980 mark making results produced after that period consequently a more accurate representation of the current conditions of the physical properties of the sea caused by climate change.

Some depth ranges in our first dataset lack the necessary amount of data points or/and continuity, especially at lower depth levels to allow for an inferential statistical analysis to support a yearly analysis. In such a case, the selected starting year is the minimum possible date for allowing the most extensive coverage. Let us bear in mind that the second dataset does not contain enough entries to interpret the sub-regional areas, limiting its versatility statistically.

3.8. SPATIAL LIMITS

LS, due to its shape, cannot be depicted as a single box for analysis. In order to achieve maximum coverage, three segments of the data are defined to encompass the whole area. The latitudinal and longitudinal coordinates of the three rectangular sectors are selected as follows:

- [36.80 °N; 36.01 °N; 28.00°E; 39.00 °E]
- [36.00 °N; 34.51 °N; 26.00°E; 39.00 °E]
- [34.50 °N; 30.00 °N; 22.10°E; 39.00 °E]

The resulting area is a non-rectangular shape and contains CB, LB, CND and RG. In order to focus on the four sub-regions included in our work, further division of the dataset is required. For LB, CB, and CND, the process is straightforward as they correspond to actual geographical features resulting in a simple spatial delimitation. The dataset is cut into appropriate rectangular shapes in order to accommodate the basins and CND according to the spatial definitions to obtain the following spatial limits:

- CB: [36.80 °N; 35.51 °N; 32.40°E; 39.00 °E]
- LB:[35.50 °N; 30.00 °N; 33.00°E; 39.00 °E]
- CND: [33.00 °N; 30.00 °N; 29.00°E; 32.99 °E]

RG is a particular case, as demonstrated in Section 2.2.4 due to its shifting nature. From the observation of the WOA18 data in Appendix B and the climatological maps produced in Section 5.1.2, RG is delimited to encompass the region showing a distinctly different SWT and SWS compared to the local average which in theory corresponds to the area mentioned above resulting in the following rectangular box with the following latitudinal and longitudinal coordinates.

- RG: [36.50 °N; 34.00 °N; 27.00°E; 29.5.00 °E]

The eight vertical depth ranges selected for this study are surface (0m-10m), 25m, 50m, 100m, 200m, 500m, 1000m and 2000m. The high density of the first four layers is due to the more significant seasonal variability ensuing from their interaction with the atmosphere leading to more significant changes in SWT and SWS, especially at the surface where the SST is greatly affected by atmospheric trends and events. Lower layers are thus much more spread out relative to the upper layer as they do not show much seasonal variability at first glance. The surface is referred to as 10m in the analysis section.

As the water masses are not well defined vertically, a 5% margin is given for each depth level to increase the amount of data available at that range. As an example, 50m corresponds to 50m ± 2.5m, while 100m corresponds to 100m ± 5m. Thus when we refer to a depth range during analysis, unless specified otherwise, it should be assumed that the actual range is an interval of the stated number ± 5%. Also, the surface layer is a particular case (as depth cannot be negative), leading to the surface layer to refer to a corresponding interval between 0m and 10m.

3.9. OCEAN DATA VIEW

ODV is a software package developed by the Alfred Wegener Institute for Polar and Marine Research (AWI, https://www.awi.de/en.html) for the interactive exploration, analysis and visualization of oceanographic and other geo-referenced profile, time-series, trajectory, and sequence data. It can display original data points or a gridded field based on the original data and includes two fast weighted-averaging gridding algorithms as well as the highly efficient DIVA algorithm (Section 5.1).

The unique data format of the software allows compact storage and high-speed data access where extensive data collections containing millions of stations can adequately be maintained and explored on personal computers with relative ease. This feature allows for easy data manipulation and visualization without access to powerful computing facilities — the base data for the EM is shown in Figure 20 using the ODV software.

In order to obtain the selected spatial range for the datasets required for our calculations, the station selection criteria are set to three different latitudes and longitudes limit for accepted station positions for the LS as defined previously. The resulting parts are recombined and then exported into a single file from which further generation of datasets as needed. The primary purpose of extracting the data and recombining them is the fact that station selection in ODV is limited to rectangular shapes. Meanwhile, the subject area is by default non-rectangular, allowing for some more precise control on the boundaries of the LS in order to not treat is as a block.

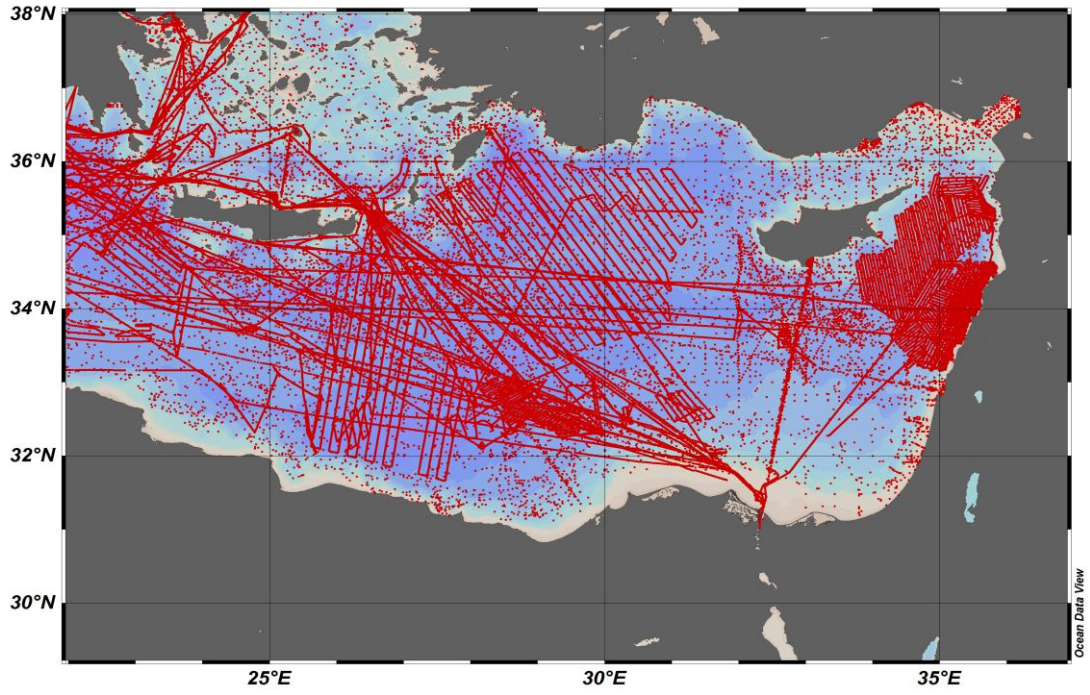

Figure 20 Map of the spatial distribution for the in-situ data available in the Eastern Mediterranean in the SeaDataNet archives

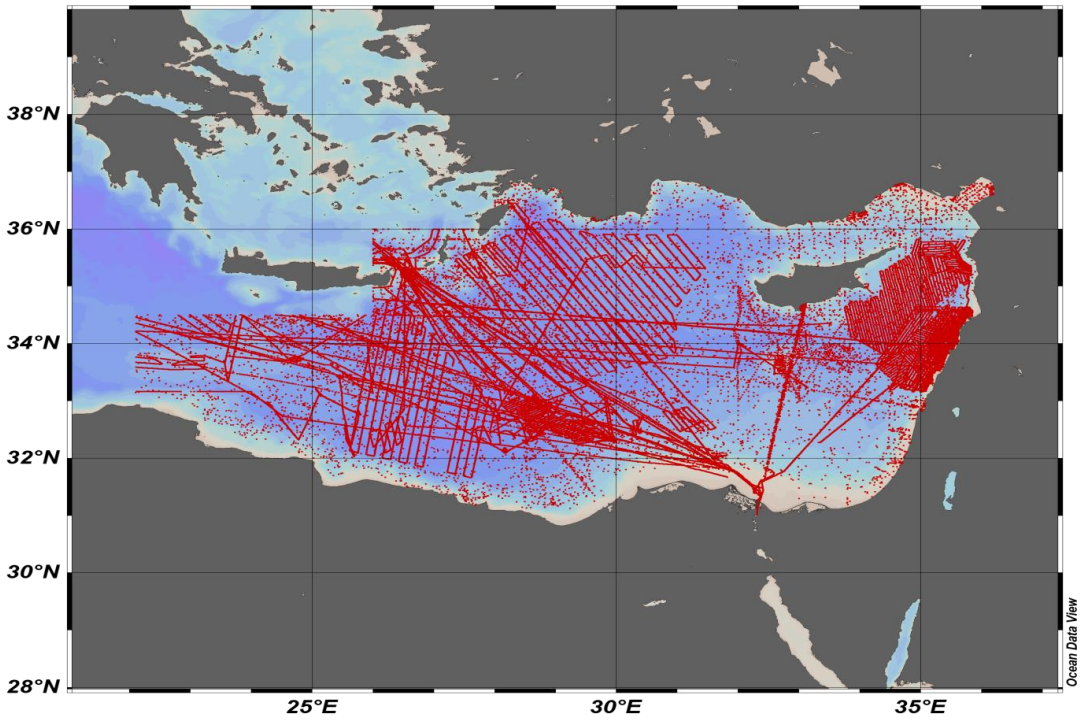

Figure 21 Map of the spatial distribution for the in-situ data available for the Levantine Sea after recombination in the SeaDataNet archives in the 1960-2017 period

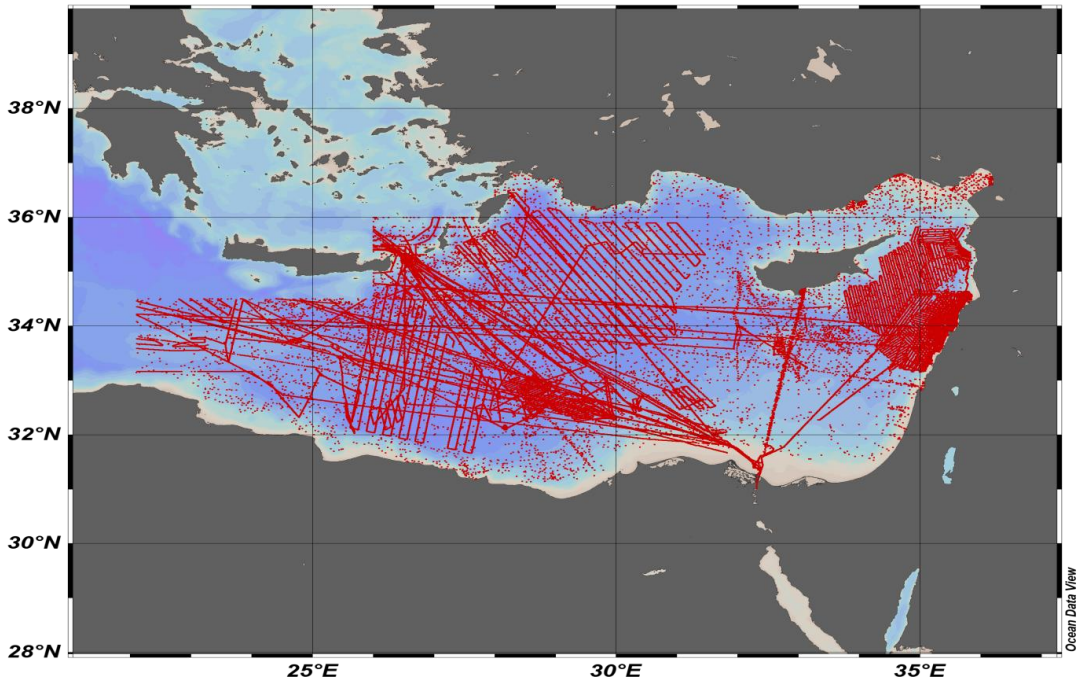

Figure 22 Map of the spatial distribution for the in-situ data available for the Levantine Sea after recombination in the SeaDataNet archives in the 1980-2017 period

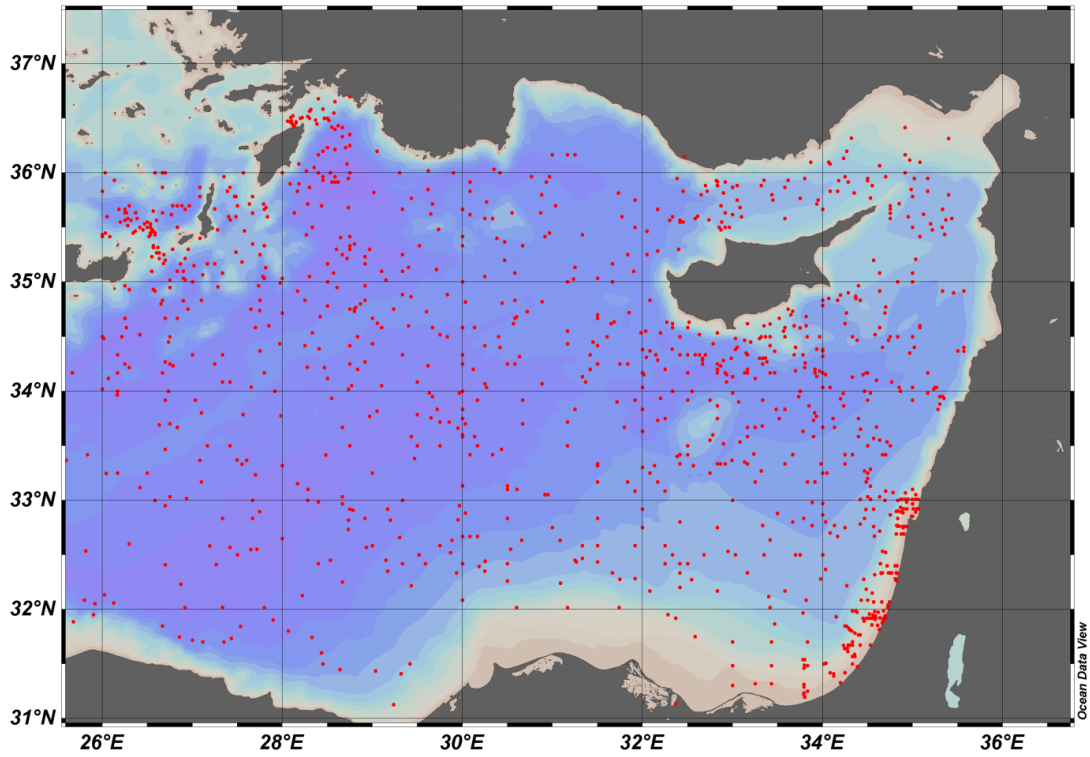

Figure 23 Map of the spatial distribution for the in-situ data available for the Levantine Sea after recombination in the SeaDataNet archives in the 1960-1980 period

The dataset with the appropriate spatial distribution is then further subdivided for LB, CB, CND and RG according to the spatial ranges (Section 3.8) of interest. The sub-regional datasets are exploited to be able to conduct a more specific regional analysis of their respective areas.

For the two required temporal ranges proposed (Section 3.7), the station selection criteria are once again changed to only accommodate data at first from 1960 to 2017, and then from 1980 to 2017 for proper statistical analysis in our desired timeframe for all previously created spatial range selections. Afterwards, the same process is repeated to get seasonal datasets by changing the station selection criteria for three month periods to create spring, summer and fall. However, the winter season requires the creation of two distinct datasets, one containing the data from stations in January and February and the second harbouring values for December of the previous year.

Figure 21 displays the dataset obtained after the spatial limits for the LS defined in Section 3.8 are applied to the aggregated 1960-2017 dataset through ODV. Meanwhile, Figure 22 is the representation of the 1980-2017 time range. Finally, Figure 23 shows the data points for 1960 to 1980. The number of stations and data entries for each area of the study are detailed in Table 3.

Region	LS	CB	LB	CND	RG
1960-2017 Station	81,317	2,690	25,925	9,556	8,401
1960-2017 Data Entries	10,590,891	481,592	2,679,179	787,890	1,686,260
1980-2017 Station	81,317	2,626	21,828	9,453	8,184
1980-2017 Data Entries	10,481,474	480,439	2,597,862	777,073	1,639,337
1960-1980 Station	101	8	46	11	14
1960-1980 Data Entries	107,466	1,153	13,528	12,629	3,079

Table 3 Regional Station and Data Entry Numbers

In Table 3, the sum of stations and entries when for the 1960-1980 and 1980-2017 do not equal to the values of the 1960-2017 period. This discrepancy is the result of overlap in the two datasets at the 1980 boundary where simply summing the numbers of both periods would give a misleading outcome.

CHAPTER 4

LITERATURE REVIEW

There are specific acknowledge facts by the scientific community in the literature when it comes to the Mediterranean Sea. The mean SST and SWS tend to increase when the observation point moves further south and east in all monthly, seasonal and annual gradients. The further south-eastwards the area is in relation to the Strait of Gibraltar as a point of reference, the higher the SST values are. The warmest observed segment is in the LS and especially the LB. The same pattern is also valid for SWS in the same manner as SST.

Meanwhile, the Aegean Sea, with its latitude and longitude, is an exception in the EM showing a lower SST as well as SWS average. This anomaly is due to the cold Black Sea outflow coming from the Strait of the Dardanelles into the Mediterranean. Figure 24 and Figure 25 illustrate the SST and SWS gradients for the Mediterranean Sea from west to east.

Russian oceanographic expeditionary research history, dating back over 300 years, is very comprehensive and loaded with a myriad of global-scale explorations of scientific importance (Mikhaĭlov et al., 2002) [54]. Previously Soviet and then from 1993 onwards Russian researchers were the pioneers showing a deep interest in the Mediterranean Sea. Climatological water masses of the Mediterranean Sea and its general circulation have been the main subject of liberal studies. The first climatological analyses of hydrographic data as a basis of geostrophic circulation in the Mediterranean has been conducted by Ovchinnikov (1966) [55] following the pioneering work of Nielsen (1912) [56].

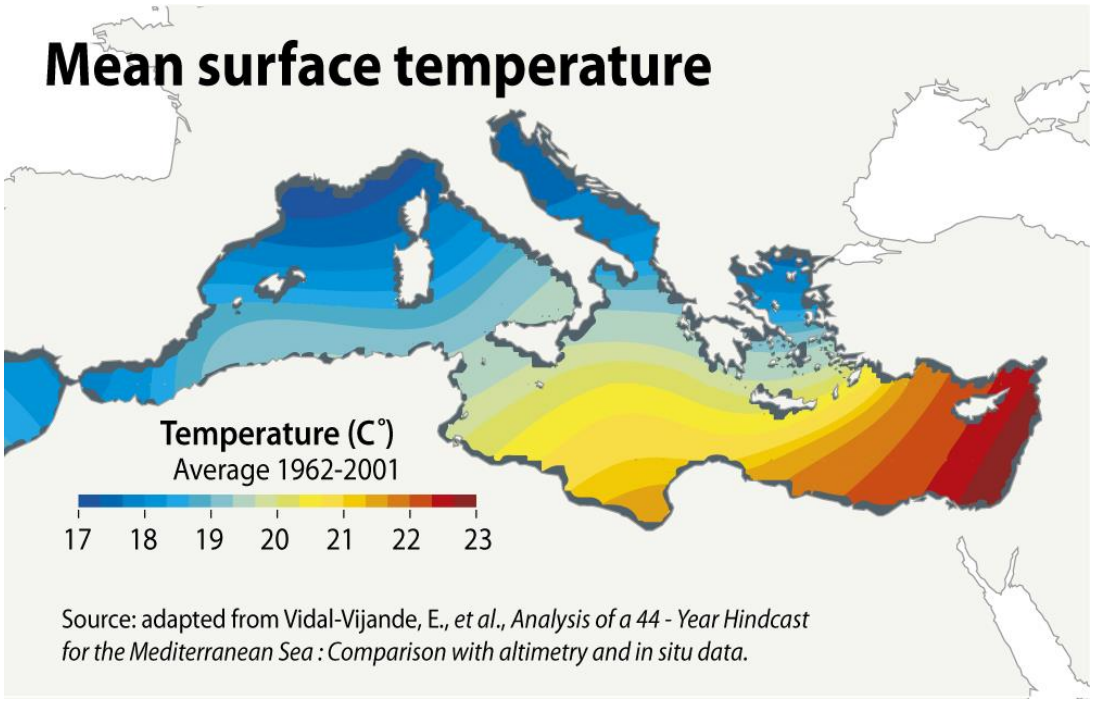

Figure 24 Mean Surface Temperature Map of the Mediterranean Sea, Source:

http://www.grida.no/resources/5919

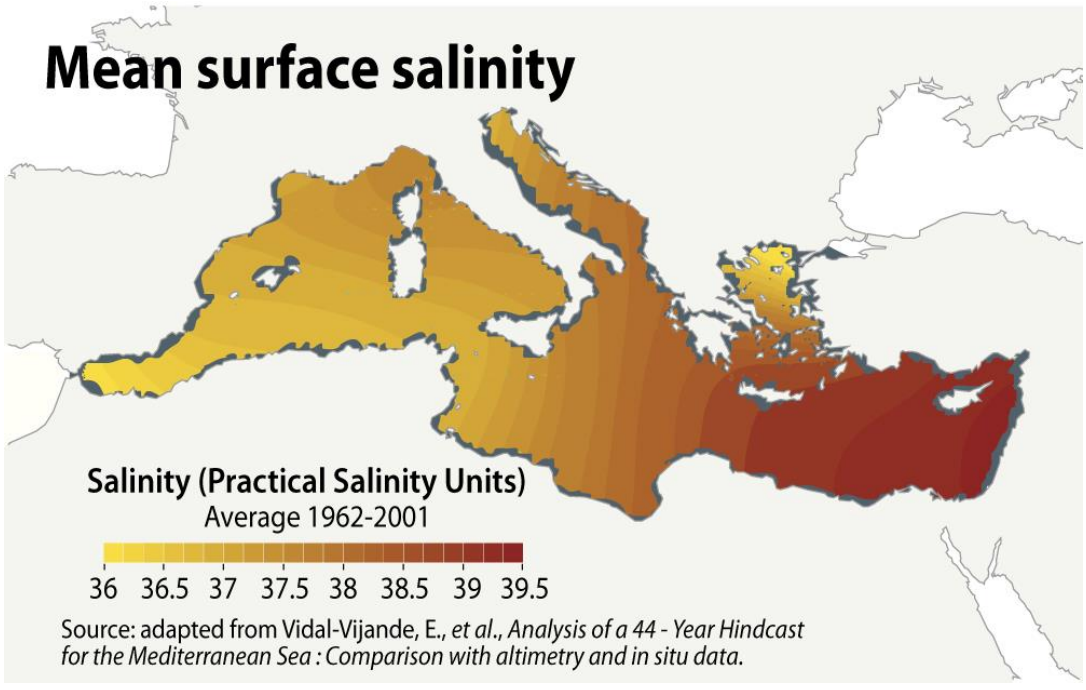

Figure 25 Mean Surface Salinity Map of the Mediterranean Sea, Source:

http://www.grida.no/resources/5889

The Soviet program led by Ovchinnikov in the Mediterranean contributed significantly to the investigation of physical processes of the region, under his supervision, a group of Russian scientists, in addition to numerous publications also created a substantial, comprehensive monograph (Ovchinnikov & Plakhin, 1976) [57] of the Mediterranean. The program was nearly a decade before the Physical Oceanography of the Eastern Mediterranean (POEM), and GOIN cruises commence.

The EM has become the subject of advanced studies towards the end of the last century, starting with two extensive expeditions of the EM, POEM, an international effort, and GOIN, an initiative of the State Oceanographic Institute of the former Soviet Union, were undertaken between 1985 and 1995. Although two projects were not related and the cruises were carried out according to the requirements of their respective programs, as a consequence intensive oceanography research has been accomplished for a better understanding of the dynamics of the EM waters masses (Hecht & Gertman, 2001) [58].

From 1987 to 1990 GOIN carried out 9 EM cruises in the EM, during which data collected at 1779 stations. Later in the nineties, Ovchinnikov initiated a brand new scientific program and targeted to investigate the circulation of the sub-basins this time, focusing on the variability of the thermohaline structure related to synoptic-scale eddies. (Ovchinnikov & Plakhin, 1976) [57]. Meanwhile, the scene of history decided otherwise on the future, and Perestroika slowed down the Soviet oceanographic research enterprise, carrying out only the initial analyses of the Mediterranean GOIN cruises. The research expeditions were put on hold during the post-Soviet period, apparently due to funding difficulties.

The circulation of the EM has been studied by POEM, a research group founded in 1982, under the auspices of IOC/UNESCO and of The Mediterranean Science Commission (CIESM), via both in-situ and modelling studies (Özsoy et al., 1989; 1991; 1993) [59][60][24]. The focus on the EM was motivated by the very little knowledge of this basin compared with other world regions (Malanotte, 1988) [61] as well as by a particular interest in some of its characteristics reproducing the global

ocean general circulation accordingly to the multiple and interactive space and time scales. POEM carried out six coordinated cruises between 1985 and 1995 with a total number of 1674 stations. As a result of the scrupulous collection and accurate measurements of the POEM data, an exhaustive description and comprehensive circulation pattern of the EM was achieved (Özsoy et al., 1989; Özsoy et al., 1991; Robinson et al., 1991; POEM Group, 1992; Malanotte-Rizzoli et al., 1997). [59][60][62][23][63]

Even though the POEM data were available to researchers publicly, the GOIN data access was given only to a very few investigators who participated in the data collection. Nevertheless, the opening permission of these data has been granted by the Ukrainian Scientific Centre of Sea Ecology, formerly Odesa branch of the State Oceanographic Institute, are presently displayed on the CIESM (http://ciesm.org) portal. Meanwhile, some selected GOIN cruises are also available for download in different formats at IFREMER (http://www.ifremer.fr/sismer/ formats).

Despite both POEM and GOIN projects explained in detail a vast range of the phenomena regarding EM, nevertheless, abundant questions require further investigations and validations. Moreover, the period of both programs coincided with the unique climatic transient of deep water formation, EMT, in the EM in the late 1980s and mid-1990s. At this point, it is worth mentioning that POEM cruises provide the observational evidence of the profound changes due to EMT. This phenomenology has been and still is investigated and debated extensively in oceanographic studies (Klein et al., 1999; Lascaratos et al., 1999; Malanotte-Rizzoli et al., 1999; Roether et al., 1996) [64][65][66][67]. Therefore the observations performed during this relevant period persist drawing the oceanographic community's attention.

The first reported research on an increase of SWS in the Mediterranean Sea is by Nof (1979) [68] evaluating the impact of the man-induced reduction of freshwater inflow from rivers, such as the Nile, for agricultural purposes. Examining the change in circulation caused by the diversion and damming of the rivers in the region he

theorised according to the results of his model a net increase in SWT and SWS due to changing circulation patterns in the entire basin. Lacombe et al. (1985) [69] examined historical hydrographic data in the WM and did not find any significant evidence for variability in SWT and SWS of deep waters between 1910 and 1970, although changes were already underway during the conduction of their studies.

The model constructed by Skliris and Lascaratos (2004) [70] evaluated that removing the flow from the Nile into the Mediterranean completely will results in an increase of 0.04 PSU over 40 years pointing at the importance of the freshwater inflow into the Mediterranean Sea in order to regulate its SWS levels, giving credence to Nof's findings (1979) [68]. The higher SWS of LIW, which courses through the entire Mediterranean Sea makes the effect global rather than localised. Knowing the fact that the discharged amount of freshwater is continually falling due to the need for irrigation resulting from a rapidly increasing population and the development of intensive agriculture on the shores of LS, this study is also a valuable supporting document for proving the existence an upward trend of SWS in the region. Understanding the evolution of SWT and SWS in the CND is an essential factor to comprehend how the changes in the seawater physical properties will affect the global circulation of the Mediterranean. During EMT between 1988 and 1992, new and more saline deepwater formation happened in the Aegean Sea according to the work of Roether et al. (1996) [67], increasing the salt content of EMDW whose generation was limited to the Adriatic Sea. The change in water mass formation patterns also affected the salt content of LS.

The Global Oceanographic Data Archaeology and Rescue (GODAR), followed by the World Ocean Database project are two crucial international ocean data management projects. GODAR was initiated in 1993 under the auspices of the UNESCO's IOC to establish and increase the volume of historical oceanographic data available to climate change studies and other research purposes. The project had the goal of first locating and then transfer to the advanced digital media pre-1992 historical oceanographic data that existed in manuscript and electronic media format under the risk of loss due to media decay (Levitus, 2007) [71]. Meanwhile, the IOC

World Ocean Database (WOD) project initiated in 2001 focused on the development of regional atlases encouraging international data exchange for the post-1991 period. All data acquired as part of the GODAR project were included in WOD 2001 and released in March 2002.

In addition to the significant programmes such as GODAR 4, we should also mention the largest multidisciplinary research project, Mass Transfer and Ecosystem Response (MATER) supported and carried out by the European Commission within the framework of the Marine Sciences and Technology (MAST) targeting an integrated and a multi-scale approach on the marine systems of regional seas, especially Mediterranean Targeted Project (MTP) [72]. Moreover, new initiatives are being taken in the Mediterranean region, where climate change is a severe physical menace. Launched by the French scientific community and released for the first time through the White Book in 2007, the Hydrological cycle in the Mediterranean Experiment (HyMeX) (http://www.hymex.org/) program targeting at a better understanding, quantification and modelling of the hydrological cycle of the Mediterranean in the context of global change. HyMeX has since been extended to the international community, producing an international science plan, and is currently working on the implementation of an international program.

Meanwhile, the most representative and comprehensive project for the Mediterranean and the Black Sea is the Mediterranean Data Archaeology and Rescue (MEDAR/MEDATLAS II, http://www.ifremer.fr/medar/) including a collection of historical data from roughly 1890 to 2002. MEDAR/MEDATLAS is the ancestor of the SDN (2006-present) which still uses the foundation set by its predecessors. Figure 26 shows the partners of the MEDAR/MEDATLAS project.

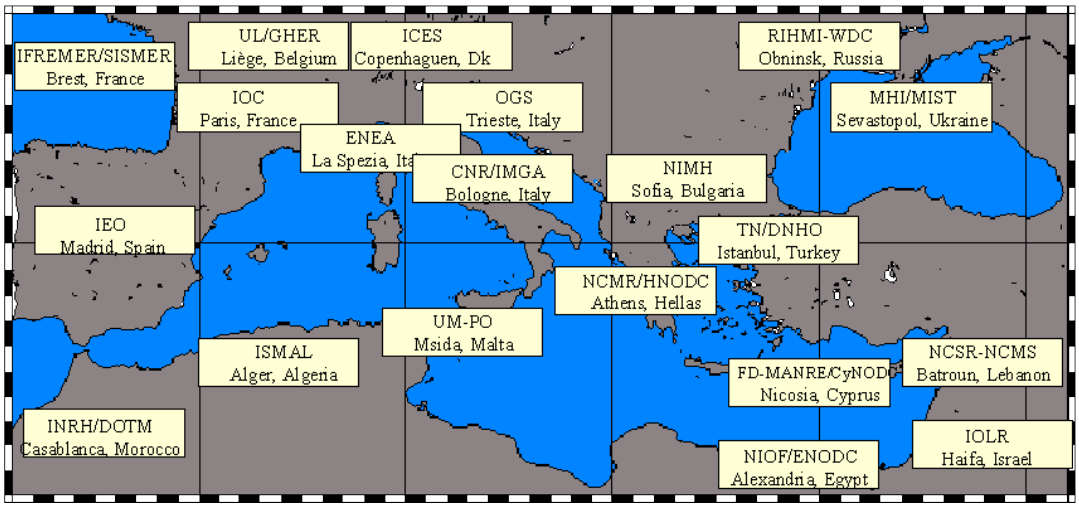

Figure 26 MEDATLAS Partners, Source: http://doga.ogs.trieste.it/medar/

The first work to use the MEDATLAS dataset is by Jourdan et al. (1998) [73]. The study treats the data to construct SWT and SWS maps for the whole Mediterranean Sea. The work itself does not extrapolate much on its findings besides confirming the degree of reliability of the MEDATLAS dataset. Gertman & Hecht (2002) [19] is the oldest investigation available for trend identification in the LB available was conducted with data from the Israel Marine Data Centre (ISRAMAR, https://isramar.ocean.org.il/), established in 2001 at the Israel Oceanographic and Limnological Research (IOLR, http://www.ocean.org.il/) at the time and found statistically significant rising trends above 50m by about 0.5 ± 1 °C between 1945 and 2001. They also uncovered a very slight increment in SWT in EMDW (0.002 ± 0.0003°C) per year but noted that if the EMT period is discarded, because the data do not satisfy statistical significance tests.

Skliris et al. (2011) [74] used satellite data and in-situ data to calculate yearly trends for the Mediterranean SST in the following particular time ranges, 1985-2008 for satellite and 1973-2008 for in-situ data. Their results are for the entire Mediterranean Sea, but their East Mediterranean results are of interest to this work. For in-situ data, they selected multiple ranges to conduct statistical evaluations. For comparison purposes, the 1985-2008 range where both satellite and in-situ results are available is of note. Both analyses show an upward trend for SST, 0.042°C/year for satellite and

0.031°C/year for in-situ data, respectively. There is an apparent increase with the results obtained from satellite data showing a more significant warming trend.

Zveryaev (2015) [75] documented the intraseasonal and interannual variability of Mediterranean SST on the rise across the whole region with a marked increase in the LS. Macias et al. (2015) [76] stated the positive trends with an increase in mean SST between 1985 and 2009 corresponding to 0.17±0.67°C for the entire Mediterranean and 0.16±0.77°C for EM.

Pastor et al. (2019) [77] led recent research concerning seasonal SST trend analysis dividing their work area into clusters and in their work two of them correspond approximately to our area of in winter and three in summer. For winter, they calculated a yearly trend of 0.0379°C/year and 0.0402°C/year for the two regions while summer clusters values are respectively 0.0377°C, 0.0373°C/year and 0.0347°C/year. The first winter trend covers an area extending away north-westward from LS, resulting in a smaller increase. Interestingly the last summer value is covering an area spanning CB and LB, which is the only example of a study in that precise area which in turn shows that the local SST increase is slower in that region.

The study by Shaltout & Omstedt (2014) [78] is a valuable source for understanding the recent SST trends and future scenarios for the LS being one of the rare work that takes an interest in the sub-basins instead of the larger EM/WM area. They demonstrated that an annual trend of 0.042°C/year for LS using a linear regression analysis conducted on a satellite dataset in the 1982-2012 time range. Their projections using RCP26, RCP45, RCP60, RCP85 scenario of the IPCC for the area is unique and descriptive of the potential future SST of LS. The outcome of their research points out that the resulting trends from satellite data and the Coupled Model Intercomparison Project 5 (CMIP5), a collaborative framework aiming to improve knowledge of climate change, is severely underestimating the rate of change in the region, with the mean SST changes found by the CMIP5 at the end of the 21st century are presented in Table 4. The paper finds from satellite data the following seasonal upward trends: 0.028°C/year winter, 0.031°C/year spring, 0.041 °C/year

summer and 0.038°C/year fall. When comparing both values for the control period between 1982 and 2012, the CMIP5 mean values demonstrate lower results ranging from -0.9°C to -1.6°C for each month.

Season	RCP26	RCP45	RCP60	RCP85
Winter	**0.5** °C	**1.1** °C	**1.3** °C	**2.3** °C
Spring	**0.5** °C	**1.1** °C	**1.4** °C	**2.5** °C
Summer	**0.4** °C	**1.2** °C	**1.5** °C	**2.8** °C
Fall	**0.4** °C	**1.1** °C	**1.4** °C	**2.5** °C

Table 4 CMIP5 Estimates for mean temperature change in the Levantine Sea by season and RCP model, Source: Shaltout & Omstedt[BD]

If the trends of mean SST values found using satellite data are correct, the consequences are alarming. According to these values, LS may experience approximately, according to some simple calculations, a 4.2°C annual mean SST increase at the end of the 21st century which can have disastrous results for both the physical and ecological balance on the region. It is highly likely that those changes will also impact the human populations in the area, although the actual severity is not evident.

Even minute changes in SWT and SWS can have long lasting impact on the environment. An example would be the freezing point of seawater at around -2°C, which can result in drastic changes in the polar icecaps even with a small warming trend. The Mediterranean warming will also impact global oceanic circulation, making it crucial to study the evolution of SWT and SWS in the region as we accomplished in Chapter 5 and Chapter 6.

CHAPTER 5

DESCRIPTIVE ANALYSIS

In each section of this chapter for each method, we first introduce the theory and methodology and then we present our results. The first part (Section 5.1) is about the DIVA gridding algorithms and the resulting seasonal SWT and SWS gridded fields at different depth levels and their corresponding climatological maps. Afterwards, we continue by introducing the R software (Section 5.2). We present the results of our cluster analysis in Section 5.3, showing the amorphous nature of the sub-regions. Next, the descriptive analysis we obtained for 1960-1980 (Section 5.4), 1980-2017 (Section 5.5) and 1960-2017 (Section 5.6) time ranges are presented and commented upon.

5.1. DATA-INTERPOLATING VARIATIONAL ANALYSIS

The inhomogeneous distribution of in-situ data compared to satellite data leads to a common problem faced by oceanographer being the gridding of the available data point in space-time to determine a field on a regular grid. To solve this issue, the GeoHydrodynamics and Environment Research (GHER, http://modb.oce.ulg.ac.be/), a working group at the University of Liège has developed the DIVA (http://modb.oce.ulg.ac.be/mediawiki/index.php/DIVA) software in the Fortran 90 compiled imperative programming language making use of the Variational Inverse Method (VIM) comparable to Optimal Interpolation (OI) while taking into account observational uncertainties.

Compared to standard OI employed in data assimilation, DIVA takes into account coastlines, sub-basins and advection because of its variational formulation on the real domain when applied to ocean data. The calculations rely on a finite element resolution and are highly optimised.

5.1.1. THEORY

In order to understand the development and working principle of DIVA, it is necessary to examine the first method in meteorological and oceanographic climatology for constructing optimal interpolation of data, Objective Analysis (OA) by Gandin [79] in 1965. VIM used in DIVA and introduced to the field of meteorology by Wahba & Wendelberger [80] was proven in 1996 to be statically equivalent to OA by Brasseur et al. [81]. VIM's main difference is the fact that it employs a method of minimization of resolution of a variational principle of a domain of interest with a finite element method denoted as *D*.

The variational principle of *D* to be minimized is:

$$J[\varphi] = \sum_{j=1}^{Nd} \mu_j \left[d_j - \varphi(x_j, y_j)\right]^2 + \|\varphi\|^2 \quad (1)$$

And the norm is defined as:

$$\|\varphi\| = \int_D \left(\alpha_2 \boldsymbol{\nabla}\boldsymbol{\nabla}\varphi : \boldsymbol{\nabla}\boldsymbol{\nabla}\varphi + \alpha_1 \boldsymbol{\nabla}\varphi \cdot \boldsymbol{\nabla}\varphi + \alpha_0 \varphi^2\right) dD \quad (2)$$

Where:

- α0 penalizes the field itself (anomalies),
- α1 penalizes gradients (no trends),
- α2 penalizes variability (regularization),
- μ penalizes data-analysis misfits (objective)

Introducing non-dimensional space coordinates using a characteristic length scale L:

- for the gradients: $\tilde{\boldsymbol{\nabla}} = L\boldsymbol{\nabla}$
- for the domain: $\Omega = L^2\tilde{\Omega}$

Replacing ||φ|| in (1) with (2) the formula takes on this final form:

$$\tilde{J}[\varphi] = \sum_{i=1}^{N} \mu_i L^2 [d_i - \varphi(x_i, y_i)]^2 + \int_{\tilde{\Omega}} \left(\tilde{\boldsymbol{\nabla}}\tilde{\boldsymbol{\nabla}}\varphi : \tilde{\boldsymbol{\nabla}}\tilde{\boldsymbol{\nabla}}\varphi + \alpha_1 L^2 \tilde{\boldsymbol{\nabla}}\varphi \cdot \tilde{\boldsymbol{\nabla}}\varphi + \alpha_0 L^4 \varphi^2 \right) d\tilde{\Omega}.$$

Notes:

- α_0 fixes the length scale L the front and the end term of the integral have a similar importance: $\alpha_0 L^4 = 1$.
- $\mu_i L^2$ fix the weights on the individual observations. If the typical misfit is represented by the observational noise standard deviation ϵ_i^2 of data point i and the integral norm representative of the background field variance σ^2, then the weights of the data are given by:

$$\mu_i L^2 = 4\pi \frac{\sigma^2}{\epsilon_i^2}.$$

- Finally α_1 fixes the influence of gradients: $\alpha_1 L^2 = 2\xi$, the default value in DIVA being $\xi = 1$.

The domain Ω, corresponding in this case to the selected oceanic area, which is bounded by the coasts, makes prevention of overland association a necessity. In order to achieve this objective, a finite element method is used hence the need for generating a finite element grid. Because the domain Ω is limited to the water, the minimization will only function on the area delimited by the perimeter generated by the coastline and defined area. In order to solve this problem, the domain is transformed into a mesh of triangles (e.g. Figure 27) where the identification of adjacent connectors assures the continuity of the elements.

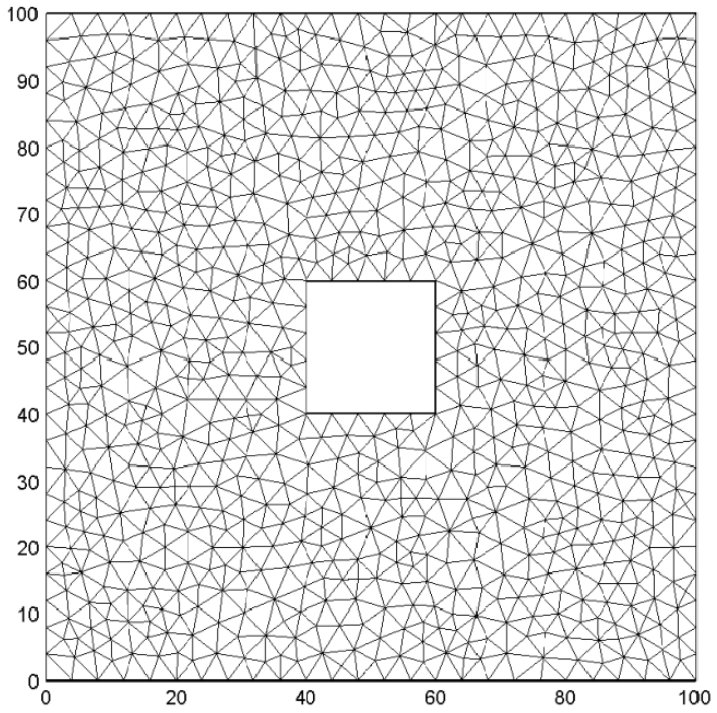

Figure 27 DIVA Example Mesh, Source: Troupin et al. (2013) [82]

The resulting gridding is optimal for solving and displaying complex problems such as the one faced by oceanographers. In oceanography, a climatological map is a set of gridded fields that describe the mean state of the oceanic properties over a given period. It is constructed by the analysis of in-situ data and has many applications such as the initialisation of numerical models and quality control of observational data. In our case, the climatological maps are useful as a baseline to understand how the oceans are changing and the identification of intriguing areas for study. The climatological maps obtained using DIVA are displayed in Section 5.1.2.

5.1.2 RESULTS

In this section, we present the seasonal climatological maps for LS constructed using the DIVA algorithm and the 1980-2017 dataset on ODV. The winter, spring, summer and fall SWT and SWS maps, grouped according to their corresponding vertical layer in the following ranges surface, 25m, 50m, 100m, 200m as defined in Section 3.7 for easier comparison. Past 200m the results did not show any significant

seasonal variation and were omitted due to not showing any definite conclusion. White spots are areas where there is not enough to create a climatological projection.

At the surface layer, there is significant seasonal variation, as shown in Figure 28. The season with the highest average SST is summer followed by fall, with the warmest spot falling in LB and CB. There is a sharp drop in SST average when going from fall to winter, but the basin remains relatively warm year-round compared to the rest of the Mediterranean. In Figure 29, we can observe pockets of extreme SWS starting in summer and intensifying in fall and ending in winter, with spring being the season with the least amount of SWS in LS. RG area stands out with lower SWT consistently except for the fall season. These results are following the existing literature reviewed in the previous chapter and our statistical findings.

The 25m layer in Figure 30 has some similarities with the surface layers with significant variation seasonal in SWT between seasons. The highest averages are recorded during the fall season followed by summer. SWT temperature difference in all seasons, more pronounced in fall and winter, makes RG conspicuous on the maps. Figure 31 shows that SWS is highest in fall, and the summer values are less significant. The CND area presents a high peak of SWS in summer.

The 50m layer also displays higher SWT temperature for the fall season with the coldest temperatures in spring, as seen in Figure 32. RG is especially visible in summer and fall, forming a discernable circular pattern of colder SWT. SWS is evenly distributed with slight seasonal variation compared to the upper layer. Of note is the highly saline water in the east of the LS during winter, the pockets in CB and CND band that stands out in the winter season of Figure 33.

In the 100m layer, there is a perceptible seasonal variation in winter when the upper water masses sink towards the bottom of LS to form LIW with for two points of interest. The first is located in the southeast of Crete in fall and the slight peak on the coast of CND, visible in Figure 34, which also shows RG with a slightly colder

average SWT across all season. The results obtained from the fall and winter SWS values of Figure 35 correlates the sinking of the denser water observed in SWT.

The 200m demonstrates no perceptible SWT seasonal variability except in CDN, discernable in the summer section of Figure 36. RG area is once again showing colder SWT values. SWS values are more uniformly distributed and there only significant pockets of higher seasonal variation in summer in LB, and the central LS observed in Figure 37. SWS stability is most likely due to LIW which course through the Mediterranean Sea east to west remaining relatively undisturbed by the other masses.

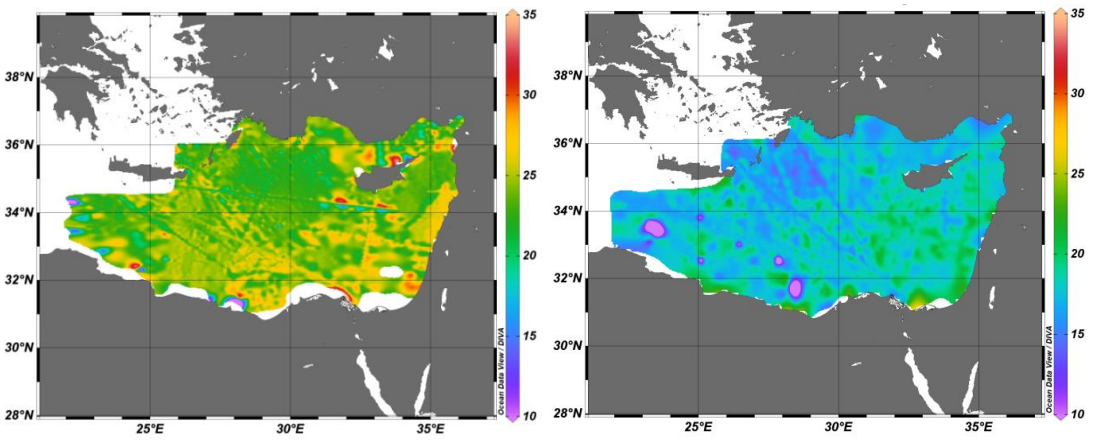

Fall **Winter**

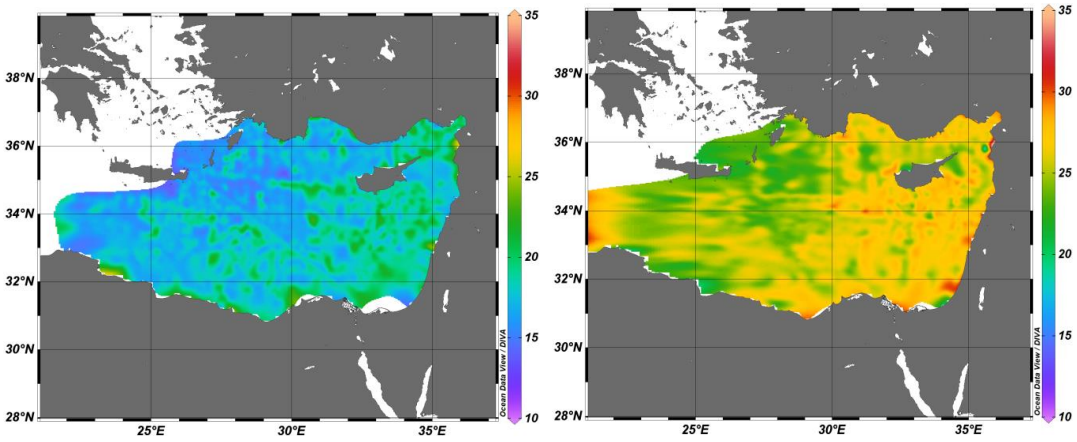

Spring **Summer**

Figure 28 Seasonal temperature climatological maps at the surface, units in (°C)

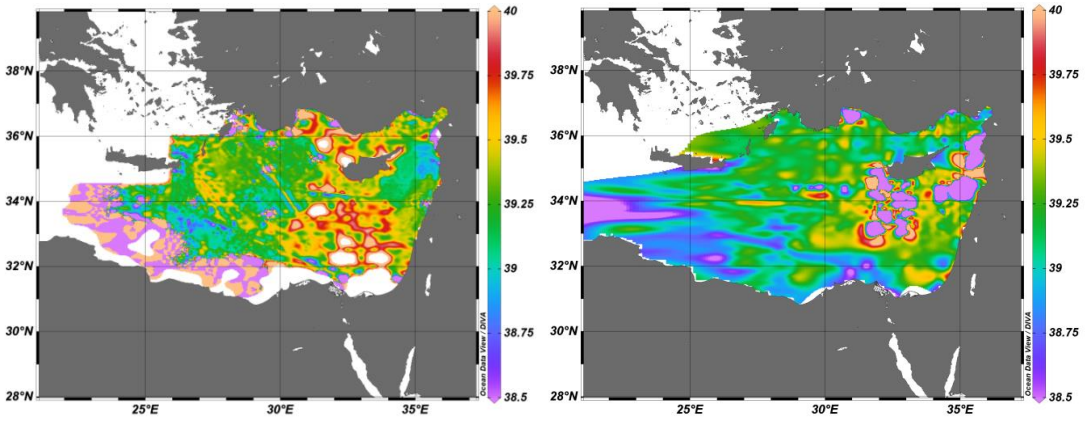

Fall **Winter**

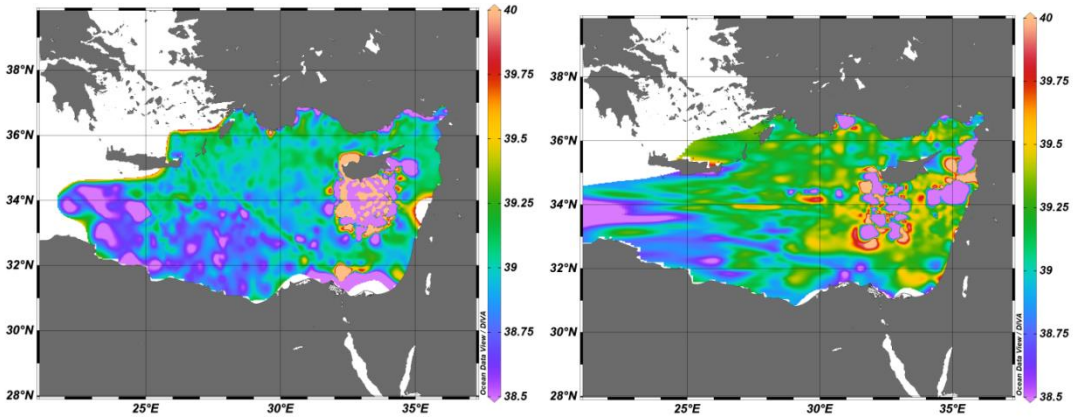

Spring **Summer**

Figure 29 Seasonal salinity climatological maps at the surface, units in (PSU)

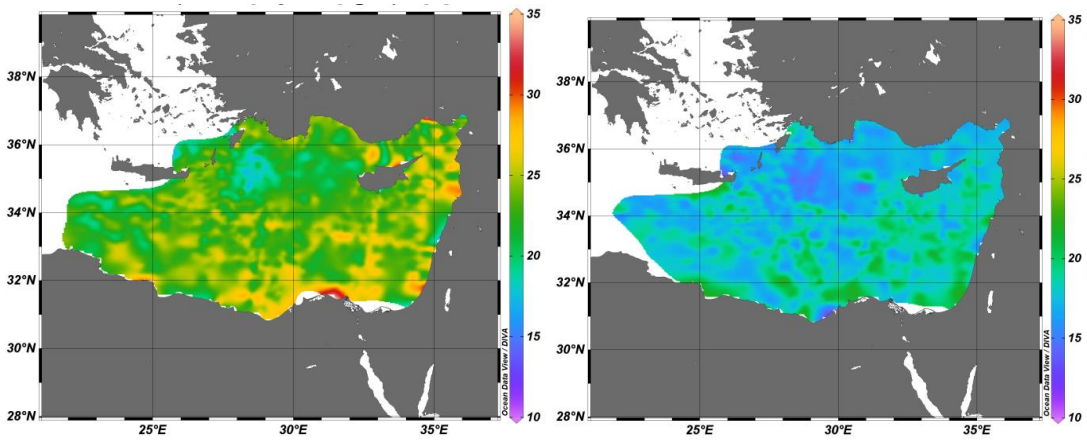

Fall **Winter**

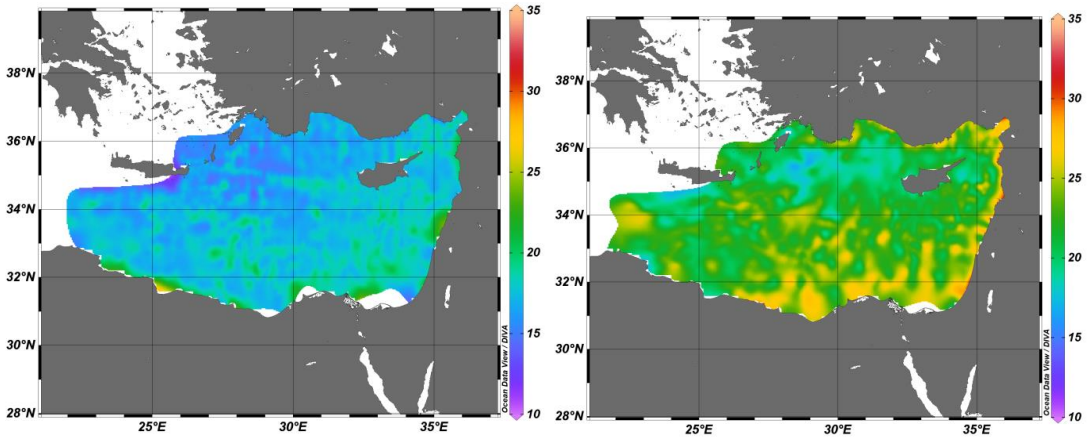

Spring **Summer**

Figure 30 Seasonal temperature climatological maps at 25m, units in (°C)

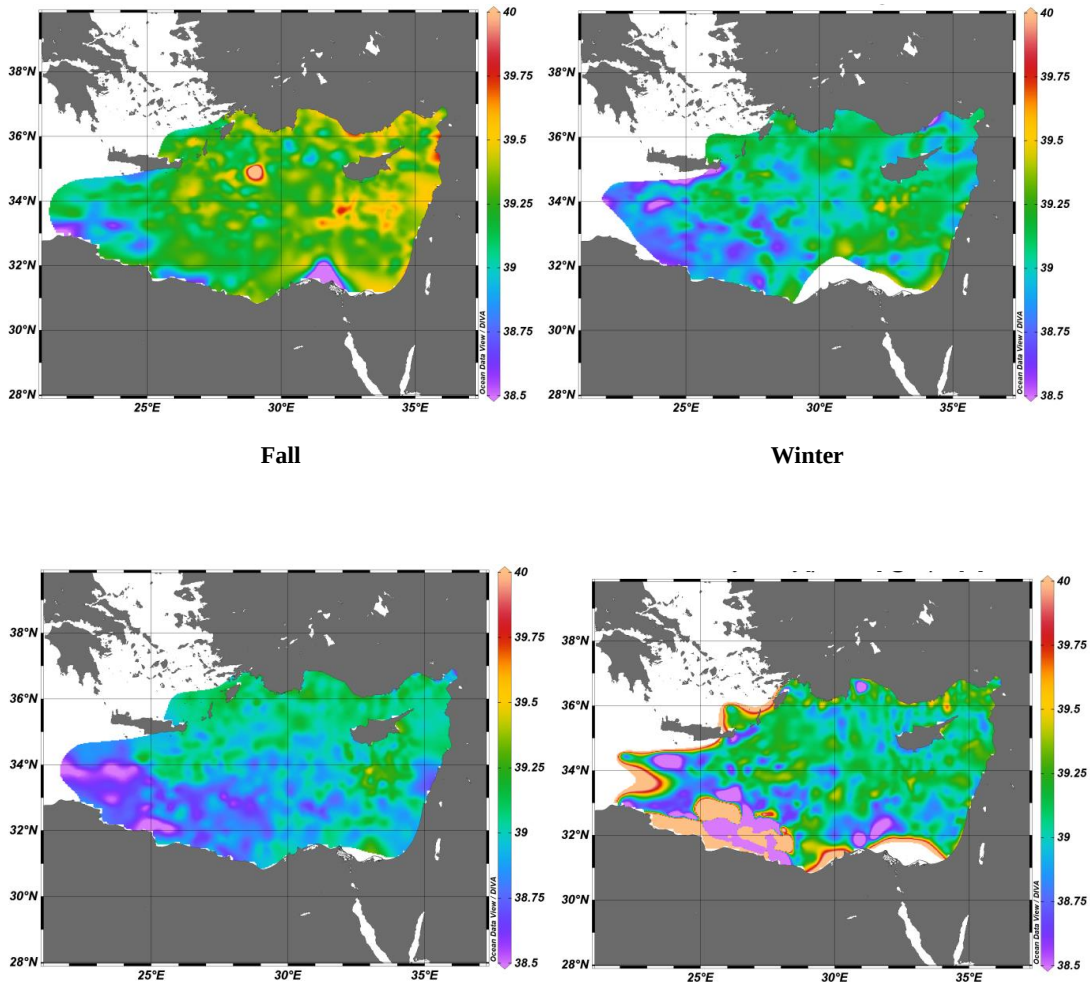

Fall **Winter**

Spring **Summer**

Figure 31 Seasonal salinity climatological maps at 25m, units in (PSU)

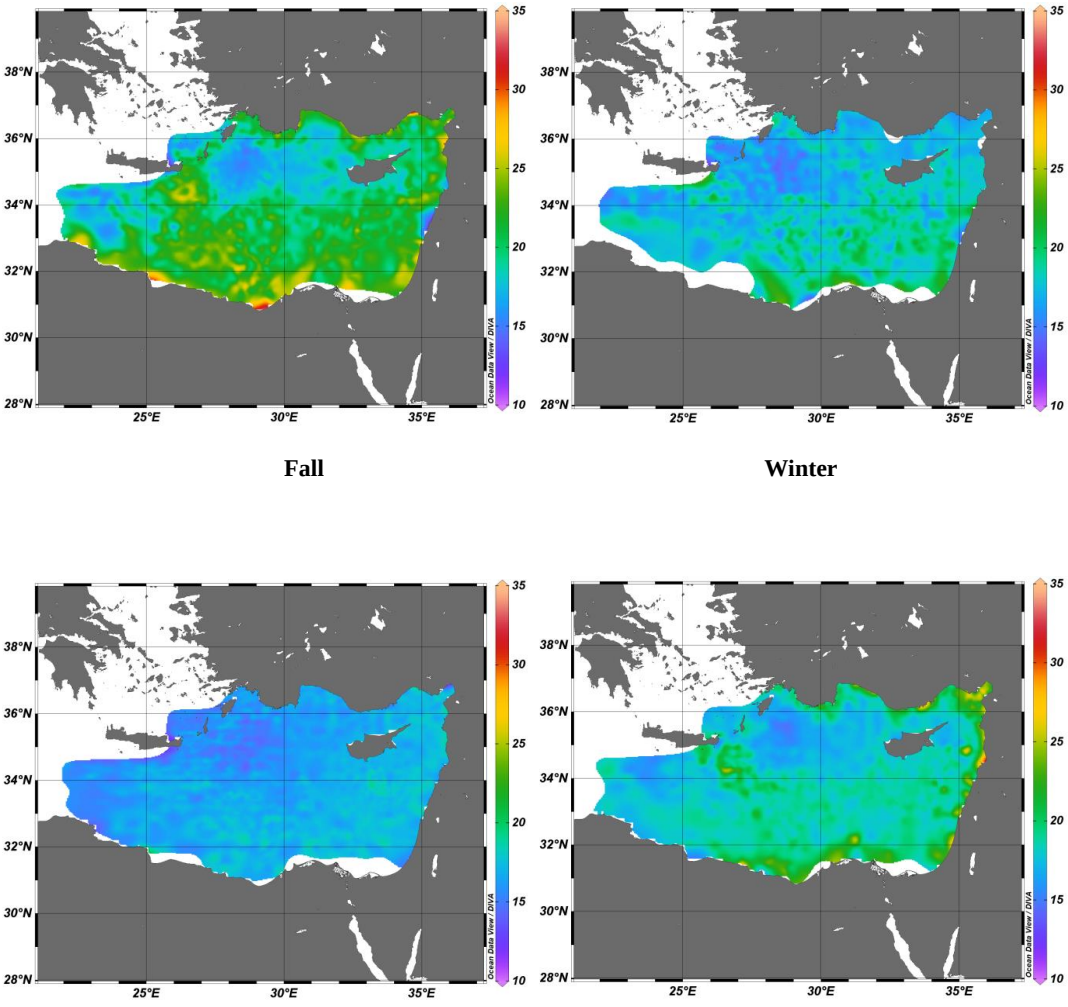

Fall **Winter**

Spring **Summer**

Figure 32 Seasonal temperature climatological maps at 50m, units in (°C)

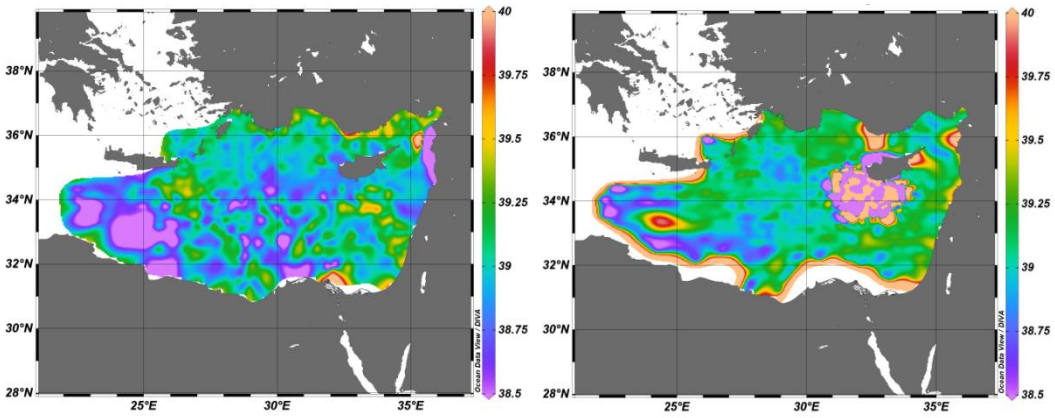

Fall **Winter**

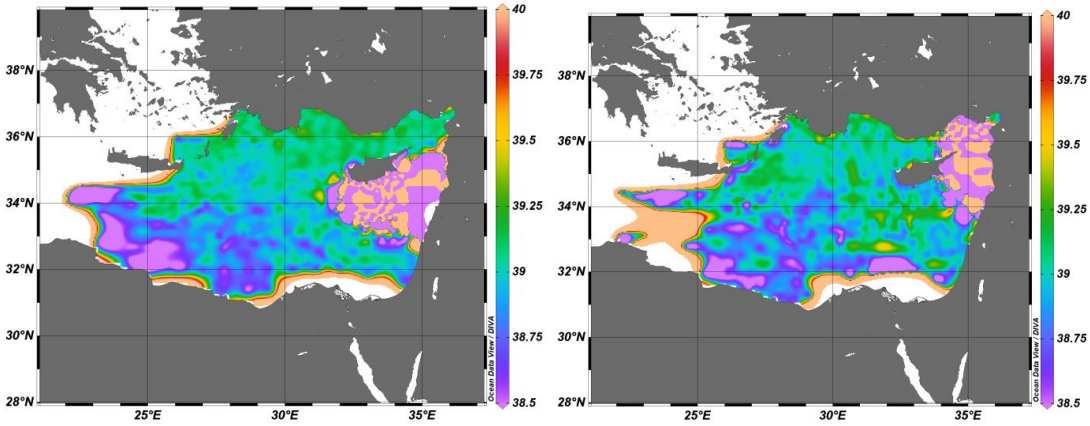

Spring **Summer**

Figure 33 Seasonal salinity climatological maps at 50m, units in (PSU)

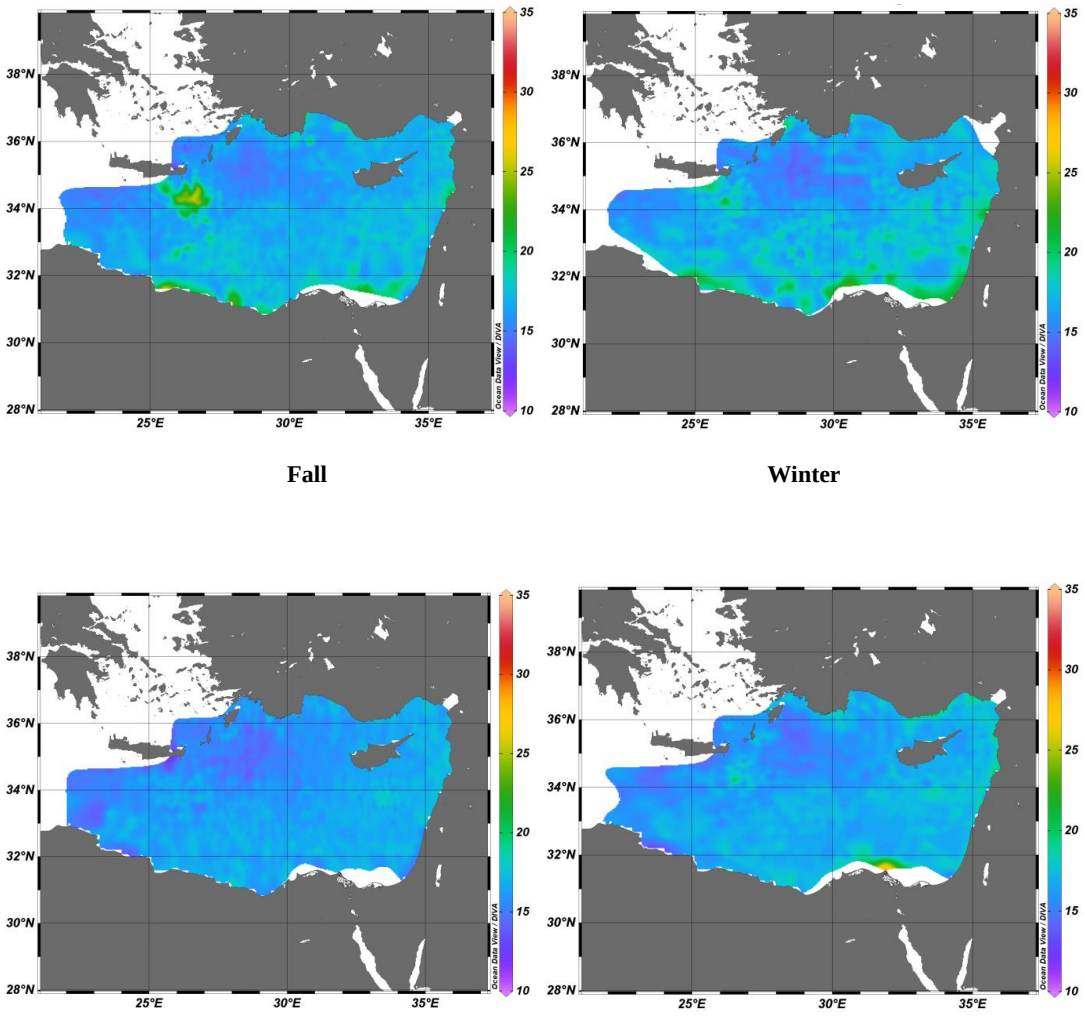

Fall **Winter**

Spring **Summer**

Figure 34 Seasonal temperature climatological maps at 100m, units in (°C)

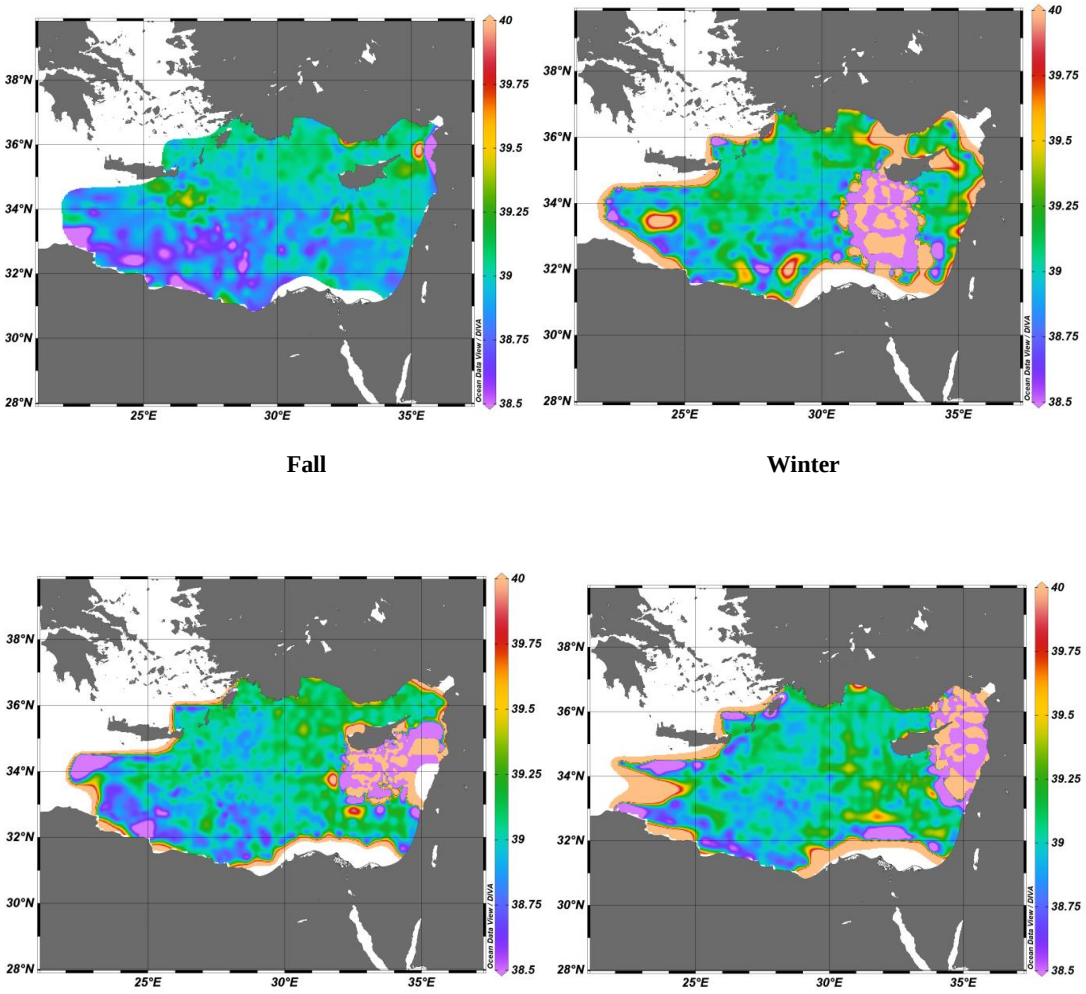

Fall **Winter**

Spring **Summer**

Figure 35 Seasonal salinity climatological maps at 100m, units in (PSU)

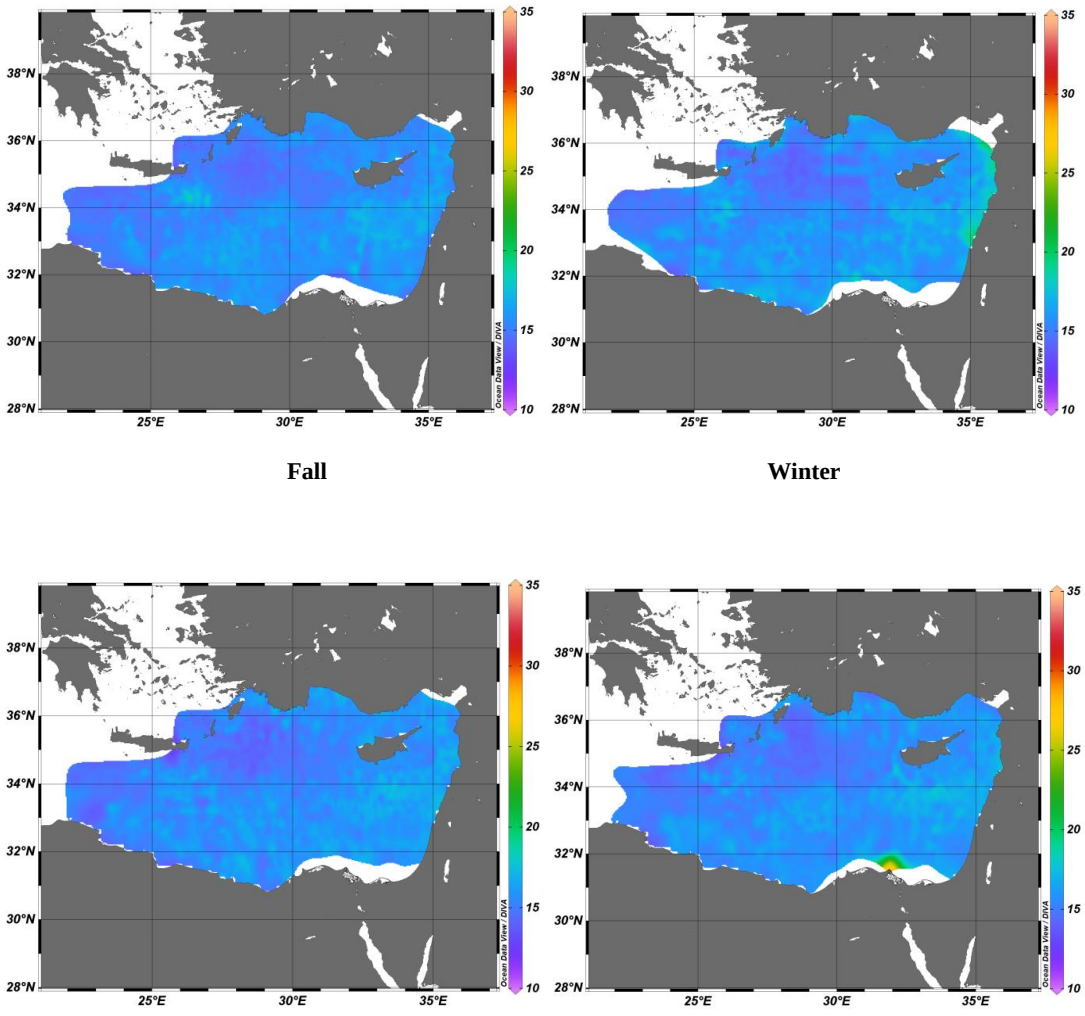

Fall **Winter**

Spring **Summer**

Figure 36 Seasonal salinity climatological maps at 200m, units in (°C)

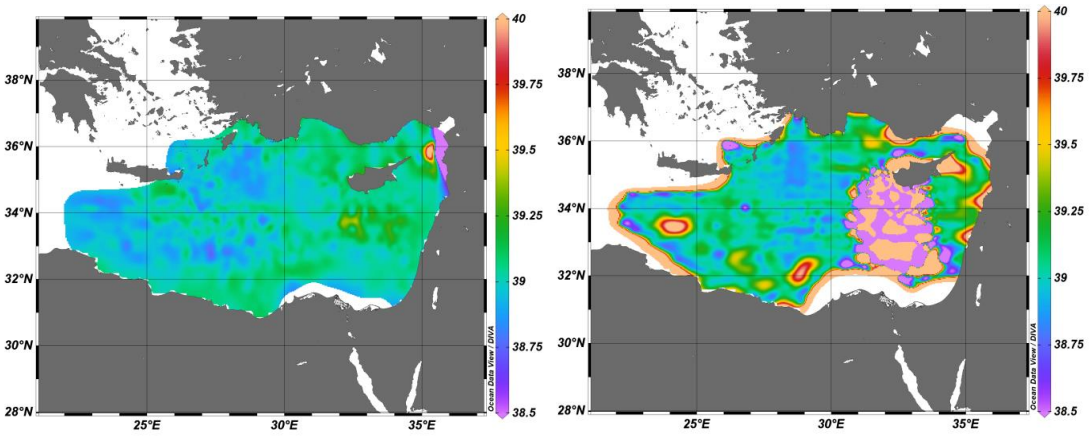

Fall **Winter**

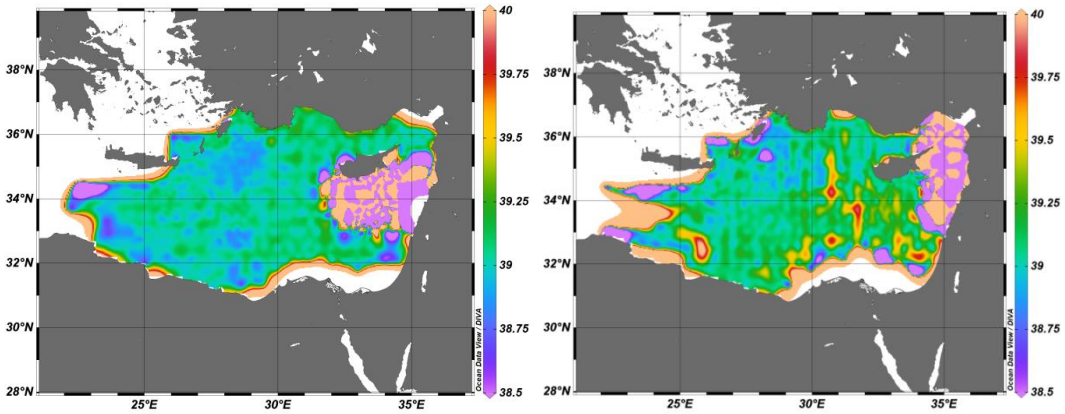

Spring **Summer**

Figure 37 Seasonal salinity climatological maps at 200m, units in (PSU)

5.2 Descriptive Statistical Analysis

The data have been subjected to descriptive statistical analysis to get a better understanding of seasonal and monthly datasets at different depth levels and in two different temporal ranges. The R software, version 3.6.0 (Planting of a Tree), detailed in Appendix D, is exclusively used for computational purposes in this study for both descriptive and exploratory analysis (Chapter 6).

Beyond classical analysis we also use clustering methods for better delimiting the spatial boundaries of our data (Section 5.3). Sub-regional analyses are conducted when feasible.

5.3 Clustering

In order to ascertain our selection of regions using a more robust method than just pointing out areas of interest, we attempted the use of clustering on our data. As the number of data points we have in our dataset is too large, conventional clustering algorithms are unable to group the data in an efficient manner properly. To accomplish our task, we decided to use the Clustering Large Application (CLARA) algorithm (Rousseeuw & Kaufman, 1990) [83], an extension of the k-medoid (PAM) method applied to data with a large number of objects to reduce RAM usage and computing time.

Instead of finding medoids for the entire data set, CLARA considers a small sample of the data with fixed size and applies the PAM algorithm to generate an optimal set of medoids for the sample. The quality of resulting medoids is measured by the average dissimilarity between every object in the entire data set and the medoid of its cluster, defined as the cost function. CLARA repeats the sampling and clustering processes a pre-specified number of times in order to minimize the sampling bias. The final clustering results correspond to the set of medoids with the minimal cost.

Due to the nature of our data, only the surface layer is subjected to the cluster analysis in order to determine the spatial fitness of our selections. The first step was the preparation of our data for cluster analysis. The rows must correspond to observations and the columns to variables, and any missing values must be removed and then the values must be scaled to make different variables comparable. Standardisation, in our case, corresponds to setting the variables to have a mean of 0 and a standard deviation of 1.

The second step was the identification of the optimal k, meaning the optimal number for cluster analysis. We applied the Elbow, Average Silhouette and Gap Statistic methods to determine *k*. From the results of the k determination, the optimal number appears to be 4 clusters at the surface resulting in the following cluster in Figure 38.

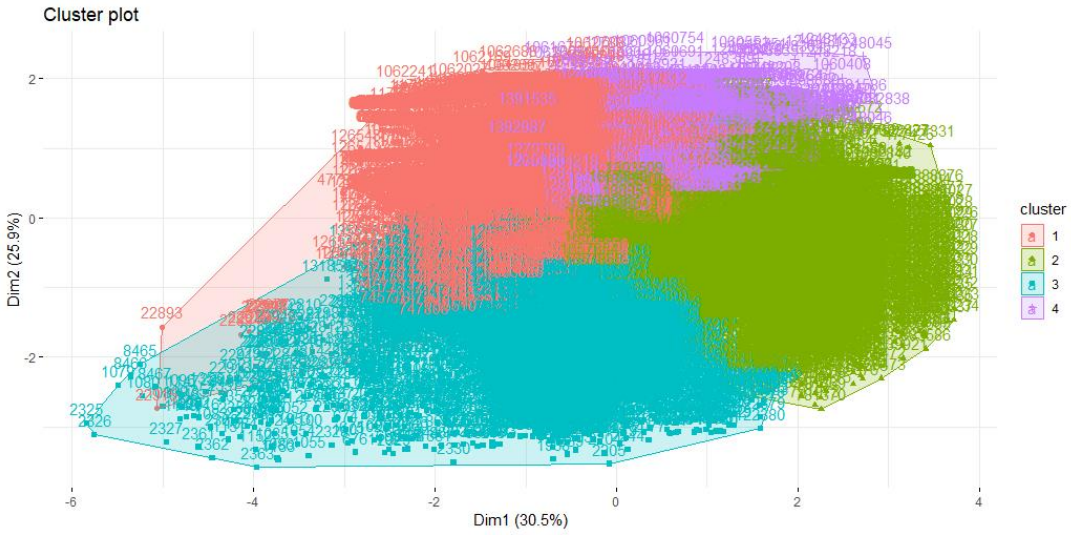

Figure 38 Clusters obtained using the CLARA algorithm at the surface layer with *k*=4

The overlap of the different clusters was an expected result, and in order to determine their exact spatial distribution, we proceed to plot them according to their latitude and longitude. The overlap of CB and LB appear quite clearly at the edges. RG is at the initial location theorised but extends very slightly further from our delimited area towards the south-east. Meanwhile, CND seems to go further west than what was thought off and shows some minute overlap with LB. Overall our regional selection seemed to be correct as the areas show distinct SWT and SWS properties.

5.4 1960-1980 DATA

The distribution of the data in the dataset between 1960 and 1980 shows a relatively higher interest in the region starting from 1967 until a drastic collapse in data collection efforts between 1973 and 1975 is observed, coinciding seemingly with the conflict on the island of Cyprus which had a significant impact in the region. Figure 39 displays the amount of collected data in LS between 1960 and 1979, as the inclusion of the values from 1980 makes it challenging to comprehend the annual observations. The year 1959 only represents the month of December as our analysis is seasonal and thus requires its inclusion.

The number of annual observations does not allow a meaningful investigation from a statistical perspective and to do any in-depth regional analysis in CB, LB, CND and RG over the 1960-2017 period.

The descriptive analysis is computed for monthly values for both SWT and SWS at the following depth ranges: Surface (0-10m), 25m, 50m, 100m, 200m, 500m, 1000m and 2000m. The results are presented in this section.

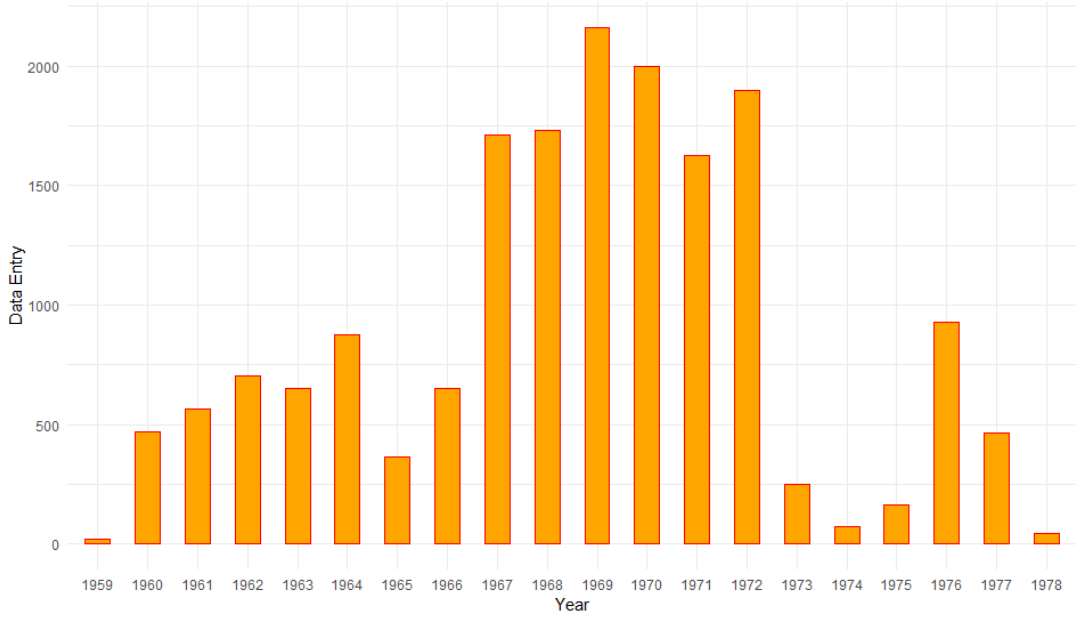

Figure 39 Number of data entries per year over the 1960-1980 period.

Table 5 and Table 6 show the exact amount of entries for SWT and SWS in LS seasonally for the 1960 to 1980 time range per depth level and the total amount of data entries for the two variables. The most sampled seasons for both SWT and SWS are spring and summer. Meanwhile, the most sampled depths for SWT are respectively 1000m layer and the surface layer and 1000m and 500m for SWS. There are extremely few entries in the 2000m layers, most likely due to the lack of the modern technological methods of data collection available to modern oceanographers. The relatively few data points at the 25m layers are consistent with the overall sampling patterns observed from a general overview of all the time ranges in LS and its sub-regions as shown in this and the following sections.

The density plots for the time range for SWT and SWS are available in Appendix A and show interesting results. At the surface level, SWT presents a bimodal plot while moving towards the deeper layers the density is evolving into a mounded shape progressively. For SWS, the density shows a definite bimodal tendency from the surface to the 200m layer before taking on a mounded appearance starting from 500 meters.

Temperature Data	Winter	Spring	Summer	Fall	Total
10m	941	1,319	1,090	992	4,342
25m	88	131	133	36	388
50m	284	382	371	263	1,300
100m	339	475	452	191	1,457
200m	451	677	644	123	1,895
500m	964	1,467	1,421	141	3,993
1000m	1,183	1,695	1,886	99	5,133
2000m	39	260	206	46	551

Table 5 Temperature data entries per season and depth, the Levantine Sea from 1960 to 1980

Salinity Data	Winter	Spring	Summer	Fall	Total
10m	817	1,093	958	164	3,775
25m	81	107	101	29	318
50m	266	348	339	229	1,182
100m	290	432	411	164	1,297
200m	1,184	640	629	115	551
500m	900	1,408	1,383	111	3,802
1000m	1,184	1,964	1,884	99	5,131
2000m	39	260	207	45	551

Table 6 Salinity data entries per season and depth, the Levantine Sea from 1960 to 1980

The amount of missing SWT and SWS in percentage is approximately 0% and 4% respectively (Figure 40 and Figure 41). These numbers are relatively low and within an acceptable margin to allow us to fill the missing values with approximations. The plot seen in Figure 42 obtained through the use of the VIM package shows that the amount of both SWT and SWS missing values do not overlap significantly and there is only a negligible amount, 0.1%, where the two variables are both missing.

The entries where SWT and SWS are missing are by default discarded as they would not be able to be filled using an educated guess. As for the other entries, we can use the chained equation method to fill the missing values with the results derived from existing variables for a more robust analysis. Additionally, regression analysis conducted on the obtained dataset does not show any significant dispersion for both SWT and SWS values.

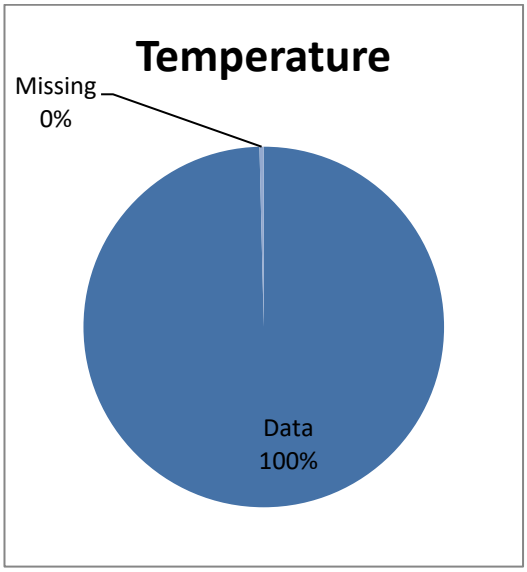

Figure 40 Missing SWT values for 1960-1980

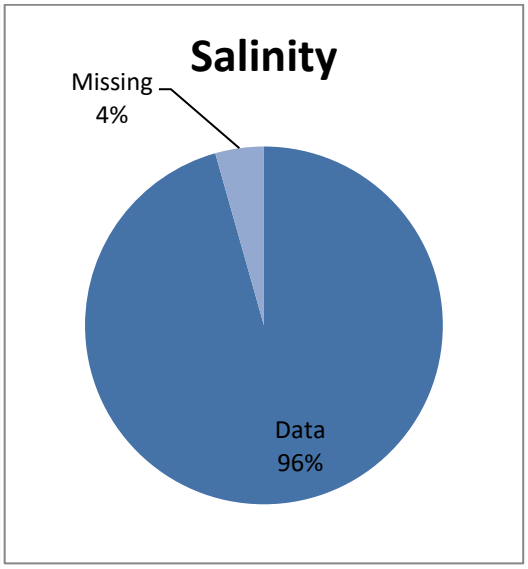

Figure 41 Missing SWS values for 1960-1980

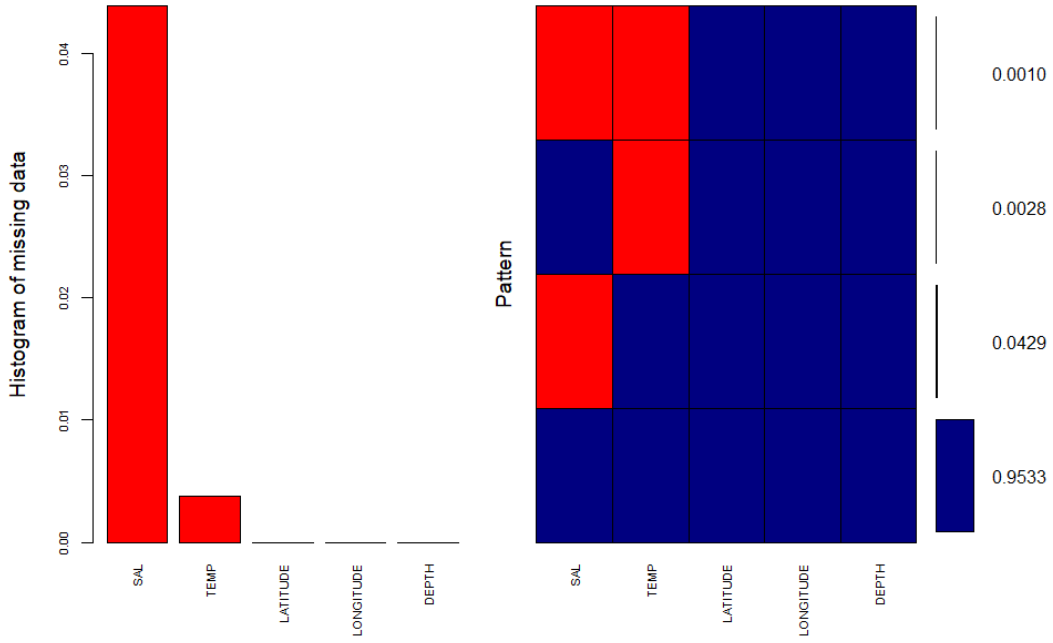

Figure 42 VIM plot for missing value combinations between 1960 and 1980, the Levantine Sea

There is a significant monthly variation in LS SWT at the surface but also the 25m and 50m layers (Figure 43). Seasonal variability is highest in SST at the surface layer with peak temperatures around 28°C in August. The 25m and 50m layers attain their respective peak of 26°C and 21°C also in August and converge in December.

As seen in Figure 44, SWT at the 100m layer displays only a very slight monthly increase peaking in December before falling back. The 200m layer showcases an erratic pattern for SWT which does not conform to seasonal influence, and are most likely due to sporadic data sampling. Figure 48 showcases that the 500m, 1000m, and 2000m ranges have almost no significant monthly variation staying at the same level year-round. The depth of the water mass between the higher and lower layers prevents any significant seasonal influence. Unfortunately, we do not aboard the potential causes and consequences of these findings in this work and can only speculate on the observed results concerning SWT values.

SWS for the surface, 25m, 50m and 100m show some seasonal variability with two peaks in August and November but seem to hover around the same level (Figure 45). The lower layers are considerably more stable and show similar numbers throughout the year (Figure 46). There is a slight indication of the formation of LIW at the start of fall with the 25m layer overtaking the surface layer in terms of SWS, but it is not very perceptible.

The overall stable picture not showcasing the formation of LIW from MAW and LSW should be attributed to the lower amount of data entries in this period compared to the 1980-2017 time range as investigated in Section 5.4 and as exhibited in the aggregated analysis for the 1960-2017 period in Section 5.5 The values for the 1960-1980 dataset do not influence significantly the results in Section 5.6 as they only make up 1.03% of the total dataset used in our calculations. This factor is the reason why they are presented separately for comparison purposes and in order to have a better understanding of this period.

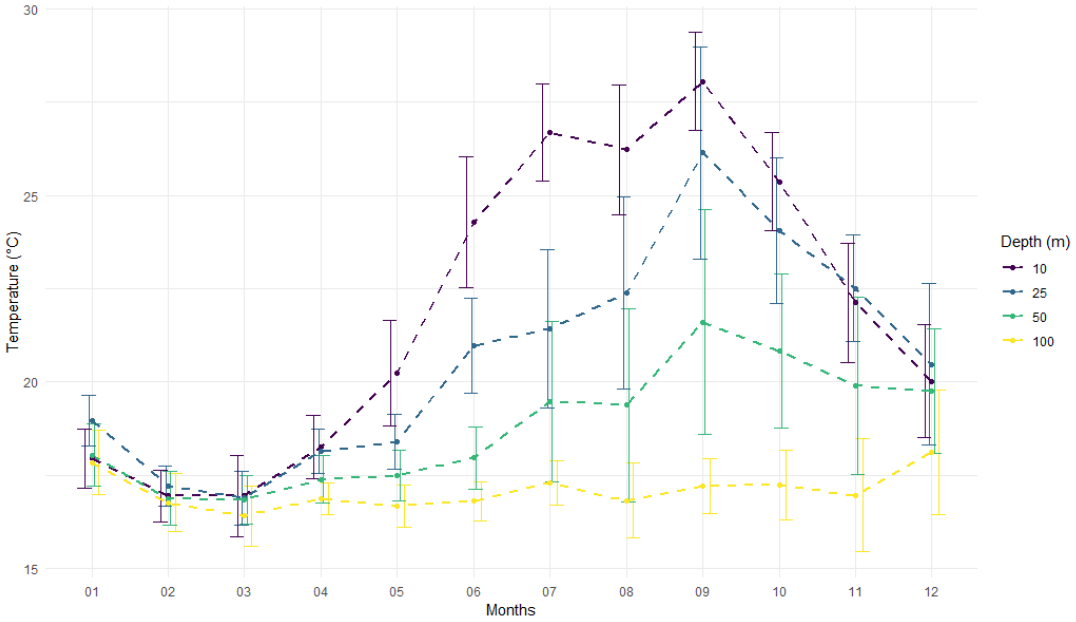

Figure 43 Monthly temperature means and standard deviations in the surface to the 100m range, the Levantine Sea from 1960 to 2017

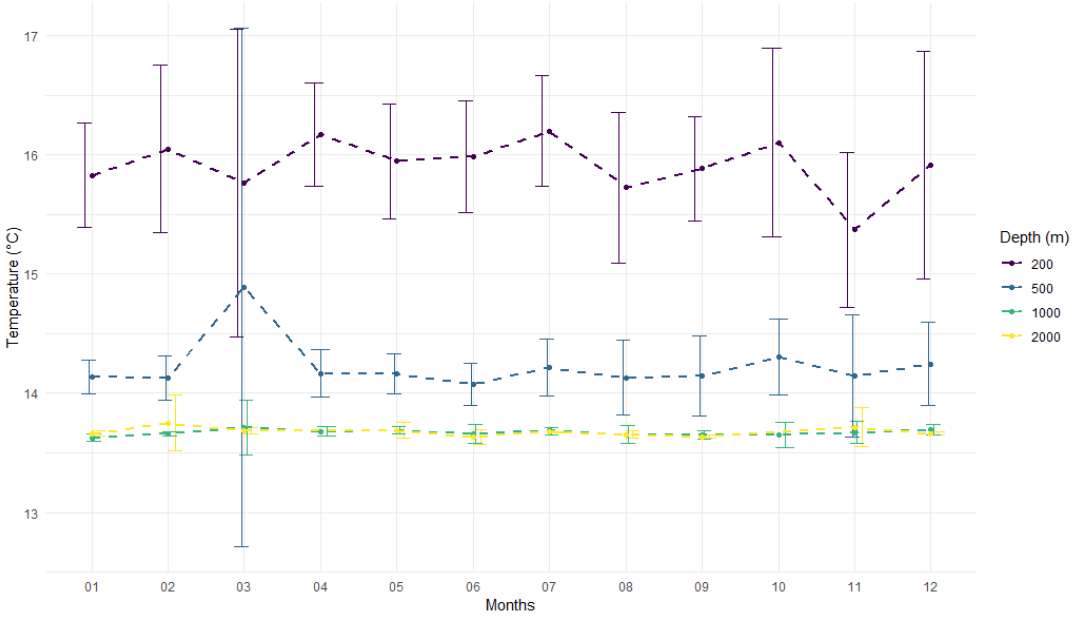

Figure 44 Monthly temperature means and standard deviations in the 200m to the 2000m range, the Levantine Sea from 1960 to 2017

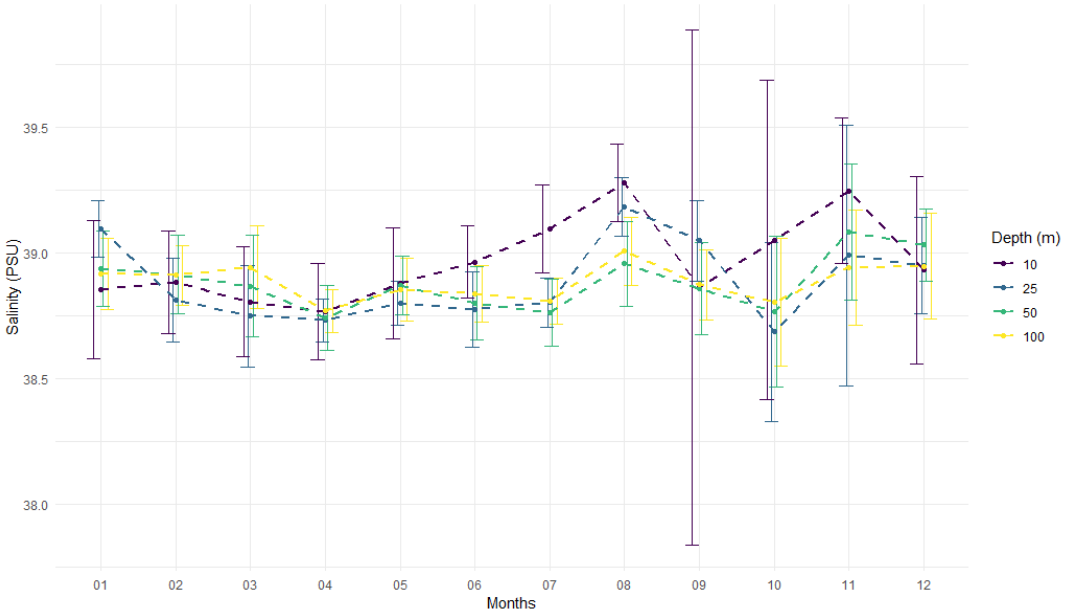

Figure 45 Monthly salinity means and standard deviation in the surface to the 100m range, the Levantine Sea from 1960 to 2017

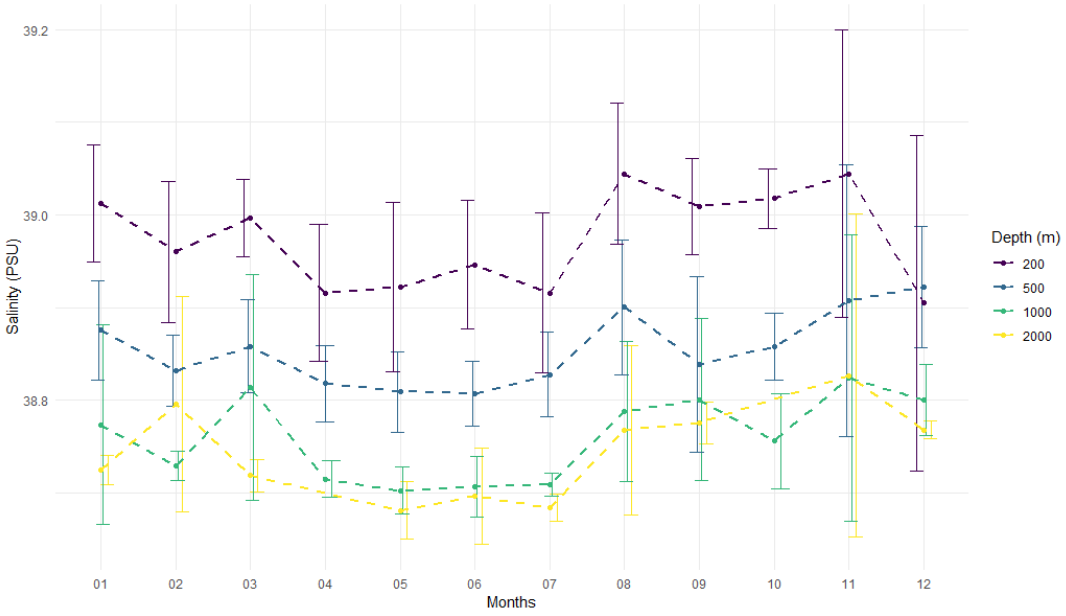

Figure 46 Monthly salinity means and standard deviations in the 200m to the 2,000m range, the Levantine Sea from 1960 to 2017

5.5 1980-2017 DATA

The distribution of the data in the dataset between 1980 and 2017 show a limited uptake in the regional data collection compared to the 1960-1980 time range, with the turning point visible in Figure 47. The influence of the POEM project in the 1980s is noticeable in the graph. Other significant data collection years which can be singled out are 1995, 1999, 2000, 2004 and 2005. This section will provide a general look at SWT and SWS data entries for LS. The sub-regional analysis for CB, LB, CND and RG are conducted in Section 5.6 as the results are not significantly different from the 1980-2017 range and would be just a repetition of our findings. The advantage of taking the 1960-2017 period allows us for a longer time to be analysed.

The descriptive analysis for the LS is very similar to those of the 1960-2017 range presented in Section 5.6 for both SWT and SWS at the following depth ranges: Surface (0-10m), 25m, 50m, 100m, 200m, 500m, 1000m and 2000m. Therefore they are not presented in this section to avoid repletion.

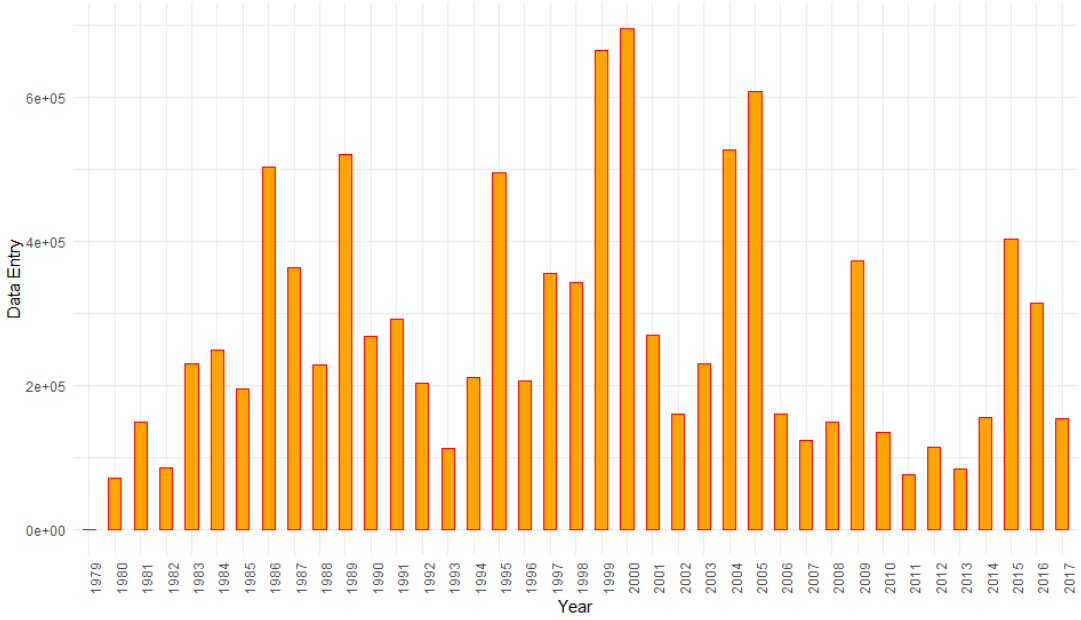

Figure 47 Number of data entries per year over the 1980-2017 period.

Table 7 and Table 8 demonstrate the exact amount of entries for SWT and SWS in the LS seasonally for the 1980 to 2017 time ranges per depth level and the total

amount of data entries for the two variables. The most sampled seasons for both SWT and SWS are spring and fall. Meanwhile, the most sampled depth for SWT and SWS is the 500m layer and the 1000m. The data collection effort seems to be focused below the 100m layer with significant interest in the lower water masses. The amount of entries still indicates a reduction in the 2000m layer. The increased interest of international research groups in the region such as POEM and GOIN, combined with the improvement of in-situ data collection technologies should be attributed to the abundance of data compared to the 1960-1980 time range. The relatively few data points at the 25m layers are consistent with the overall sampling patterns observed from a general overview of all the time ranges in LS and as seen previously in Section 5.4.

Temperature Data	Winter	Spring	Summer	Fall	Total
10m	27,365	43,674	41,066	76,194	188,299
25m	6,038	12,564	10,139	10,735	39,476
50m	10,361	20,626	16,604	18,815	66,400
100m	20,180	39,142	30,487	34,682	124,491
200m	37,031	72,169	56,072	61,608	226,880
500m	56,467	127,173	97,894	106,129	387,663
1000m	44,901	109,380	72,119	90,179	316,579
2000m	16,278	22,230	14,563	34,478	87,549

Table 7 Temperature data entries per season and depth, the Levantine Sea from 1980 to 2017

Salinity Data	Winter	Spring	Summer	Fall	Total
10m	19,924	34,752	34,255	66,858	155,789
25m	3,823	9,843	8,148	7,766	29,580
50m	6,556	15,990	13,334	12,944	48,824
100m	11,815	29,448	23,877	23,988	89,128
200m	21,321	53,954	43,876	44,079	163,230
500m	35,996	107,829	85,287	81,890	311,002
1000m	41,684	109,022	65,901	90,081	306,688
2000m	15,822	22,175	14,536	34,464	86,997

Table 8 Salinity data entries per season and depth, the Levantine Sea from 1980 to 2017

The density plots for the time range for SWT and SWS are available in Appendix A and show interesting results. Once again at the surface level, SWT presents a bimodal plot while moving towards deeper layers the density is evolving into a mounded shape progressively. One significant difference is the multimodal shape of the SWT values at the 2000m layer. The shape might be the result of the noticeably colder EMDW formed during the EMT uncovered during the POEM project in the RG region. For SWS, the density shows a definite bimodal tendency from the surface to the 200m layer before taking on a mounded appearance starting from 500m but once again showing a bimodal density, due most likely to the saltier EMDW resulting from EMT skewing the density plots.

The amount of missing SWT and SWS in percentage is approximately 7% and 27% respectively (Figure 48 and Figure 49). These numbers are relatively low for SWT and within an acceptable margin to allow us to fill the missing values with approximations. On the other hand, the amount of missing SWS value is troubling but still barely within an acceptable range for the insertion of appropriate inferred values from existing variables. After inserting SWS missing value, we tested if there was any significant variation in our results, but the only difference is slightly smoother plots and not a major change in the obtained value. The plot seen in Figure 50 obtained through the use of the VIM package indicates that the amount of both SWT and SWS missing values overlap are noticeable with 6.8% entries where the two variables are both missing.

The entries where SWT and SWS are missing are by default discarded as they would not be able to be filled in with any representative values. For the other entries, we used the chained equation method, and the missing values are filled with the results derived from existing variables for a more robust analysis going forward. Meanwhile, the regression analysis conducted on the obtained dataset does not show any significant dispersion for both SWT and SWS values.

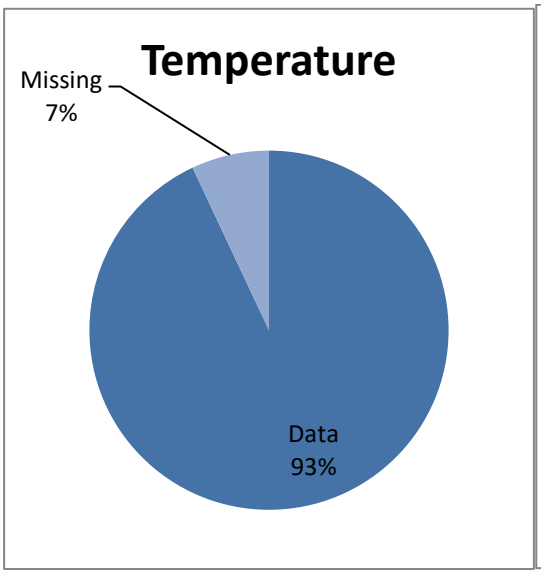

Figure 48 Missing SWT values for 1980-2017

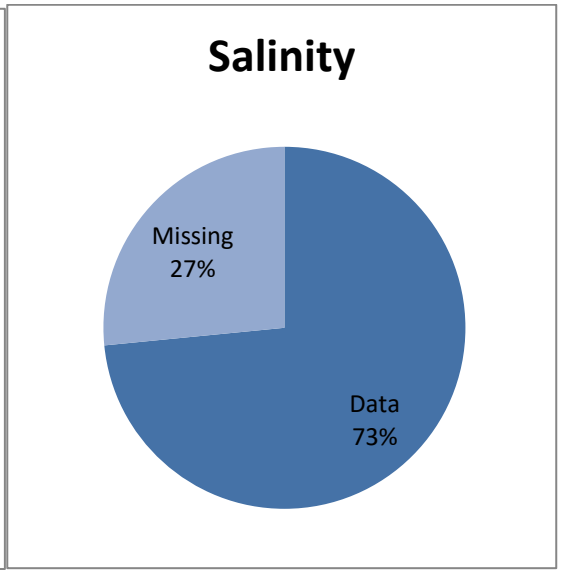

Figure 49 Missing SWS values for 1980-2017

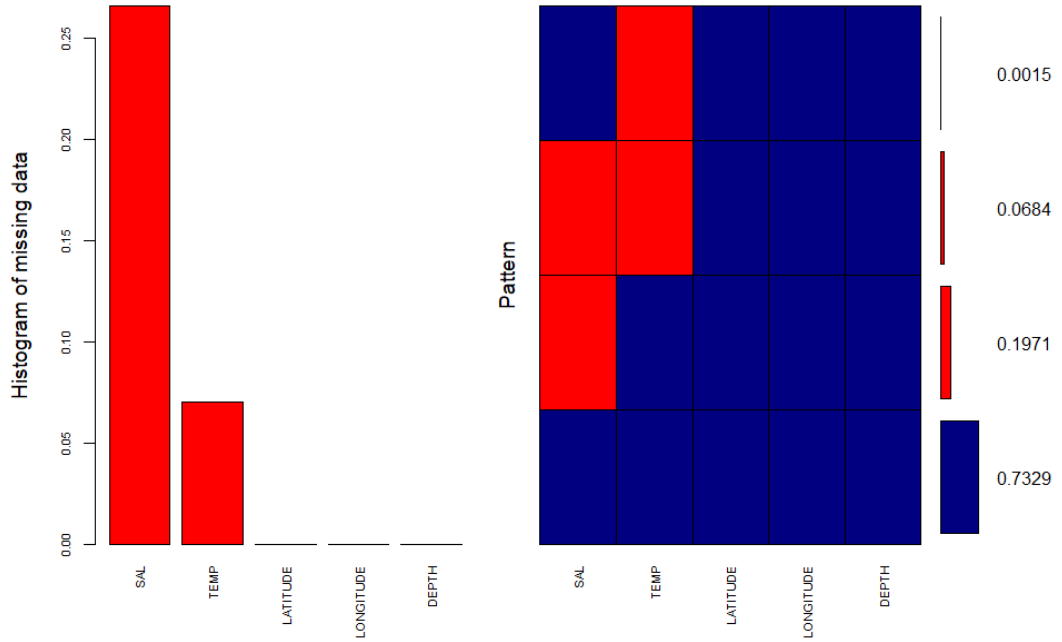

Figure 50 VIM plot for missing value combinations between 1980 and 2017, the Levantine Sea

5.6 1960-2017 DATA

The bar plot (Figure 51) demonstrates a significant increase in the amount of in-situ data collected in LS after 1979, which stands as a point of interest. There is no distinct information on the cause of this abrupt change in the amount of data and might require further study to ascertain the reason for such a drastic increase between two consecutive years. It should be noted that 1979 correspond to the second oil crisis and the increased exploration for hydrocarbon sources globally. The sub-regional analysis for CB, LB, CND and RG are conducted in Section 5.6.1, Section 5.6.2, Section 5.6.3 and Section 5.6.4, respectively. Moreover, empirical and theoretical distribution of SWT and SWS will be explored in Section 6.1.

The descriptive analysis is conducted for monthly, seasonal and yearly values for both SWT and SWS at the following depth ranges: Surface (0-10m), 25m, 50m, 100m, 200m, 500m, 1000m and 2000m.

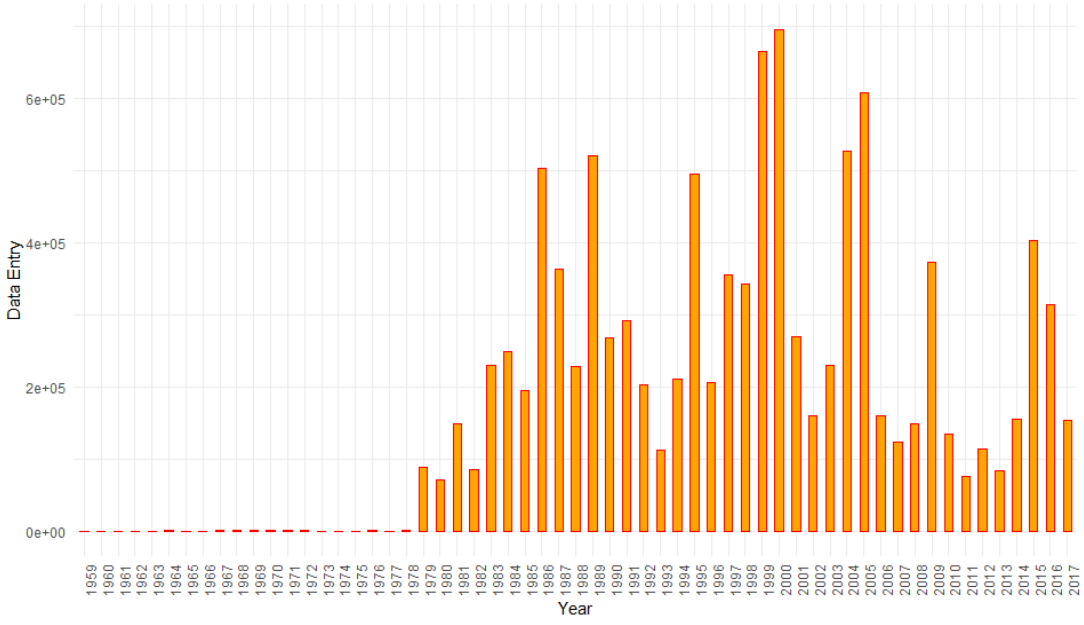

Figure 51 Number of data entries per year over the 1960-2017 period

Temperature Data	Winter	Spring	Summer	Fall	Total
10m	28,379	45,008	42,252	77,163	192,802
25m	6,129	12,696	10,283	10,773	39,881
50m	10,655	21,013	17,011	19,079	67,758
100m	20,542	39,624	30,969	34,874	126,009
200m	37,510	72,849	56,745	61,733	228,837
500m	57,461	128,646	99,341	106,272	391,720
1000m	46,084	111,346	74,026	90,278	321,734
2000m	16,318	22,491	14,777	34,524	88,110

Table 9 Temperature Data Entries per Season and Depth, the Levantine Sea from 1960 to 2017

Salinity Data	Winter	Spring	Summer	Fall	Total
10m	20,733	35,830	35,260	67,723	159,546
25m	3,906	9,950	8,246	7,794	29,896
50m	6,819	16,334	13,699	13,171	50,023
100m	12,106	29,880	24,307	24,151	90,444
200m	21,727	54,595	44,523	44,195	165,040
500m	36,895	109,237	86,684	81,996	314,812
1000m	42,867	110,984	67,799	90,172	311,822
2000m	15,861	22,435	14,749	34,504	88,110

Table 10 Salinity Data Entries per Season and Depth, the Levantine Sea from 1960 to 2017

Table 9 and Table 10 show the exact amount of entries for SWT and SWS in the LS seasonally for the 1960 to 2017 time ranges per depth level and the total amount of data entries for the two variables. The most sampled seasons for both SWT and SWS are spring and fall. Meanwhile, the most sampled depth for SWT and SWS are the 500m layer and the 1000m. The details concerning the trends in data collection, such as the POEM and GOIN initiatives are discussed in Section 5.5. As expected, the amount of data from the 1980-2017 range drowns the less numerous 1960-1980 data creating similar results to the one observed in the previous section.

Nevertheless, the inclusion of the 1960-1980 dataset allows for more prolonged yearly analysis both at the descriptive stage and inferential analysis going forward in our study. Not all sub-regions allow going as far back as 1960 due to data collection differences and the periods mentioned above results should be taken with a grain of salt.

There is a significant monthly variation in SWT at the surface, 25m and 50m layers (Figure 52). As expected, the surface demonstrates the highest variability peaking at around an average of 30°C in August. The 25m and 50m layers accumulate and dissipate heat slower attaining their respective peak in September and November. The 100m layer only displays a very slight monthly increase peaking in December before falling back. Figure 53 showcases that the 200m, 500m, 100m, 2000 ranges have almost no significant monthly variation staying at the same level year-round. There is significant water mass between the higher and lower layers for the heat to be able to reach the bottom, resulting in the stability observed. Of note is the fact that the 2000m range sometimes shows higher temperature rates than the 1000m strata. There are likely two reasons, oceanographic phenomena or data collection techniques. Our work does not cover the causes and consequences of these findings, but data collection methods might have played a part in these results, and further research might be advisable in the area.

There is an apparent increase in SWS during the winter months, and the sinking of the highly saline LSW towards lower depth ranges to form the LIW (Figure 54). The

sinking of the water masse is inferable from the rise of SWS in the 25m range even after the decline of salinity at the surface level between September and October, with the increase in the 25m range being almost equal to the falling SWS values at the surface indicating that the water mass is shifting. The shift is even more pronounced starting from October onward as the surface, and the 25m SWS declines which in turn is followed by the sharp rise at the 50m depth range. The rise of SWS during the summer months up to the end of November is an expected result, corresponding to the region's warm months and the increased rate of evaporation due to the higher SWT temperature, as shown in Figure 54. There is no significant monthly variation in SWS at the depth levels of the 200m, 500m, 1000m and 2000 ranges, and they follow an overall uniform trend. The 500m, 1000m and 2000m correspond to EMDW with few interactions with the higher layers and the nearly no discernable change in SWT (Figure 55). The 200m range is remarkably stable, falling into the scope of LIW which spans the entirety of the Mediterranean Sea from LS to the Strait of Gibraltar.

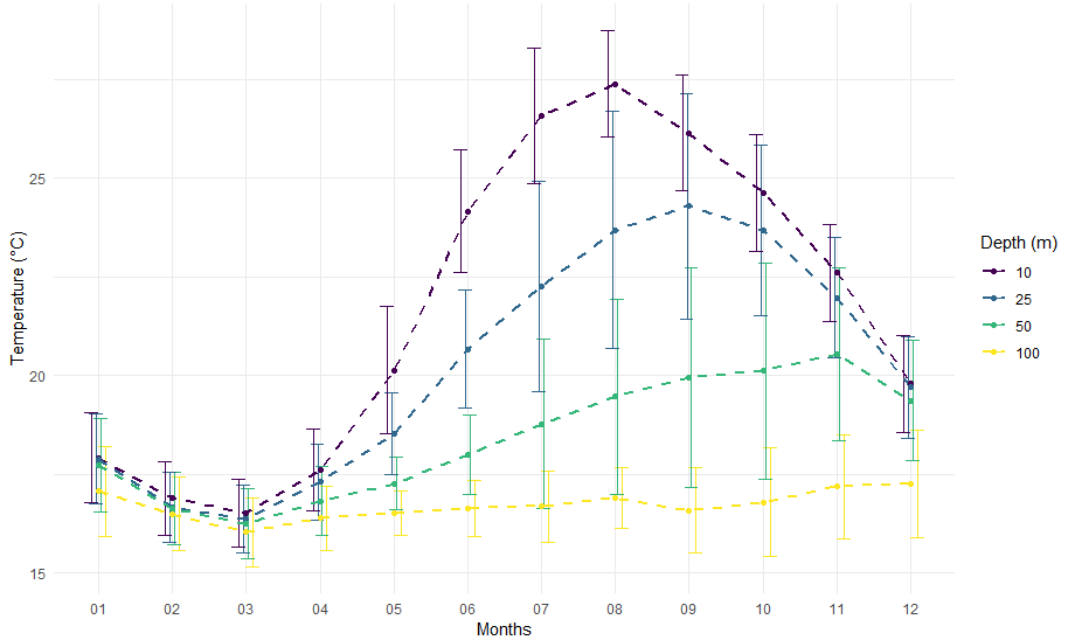

Figure 52 Monthly temperature means and standard deviations in the surface to the 100m range, the Levantine Sea from 1960 to 2017

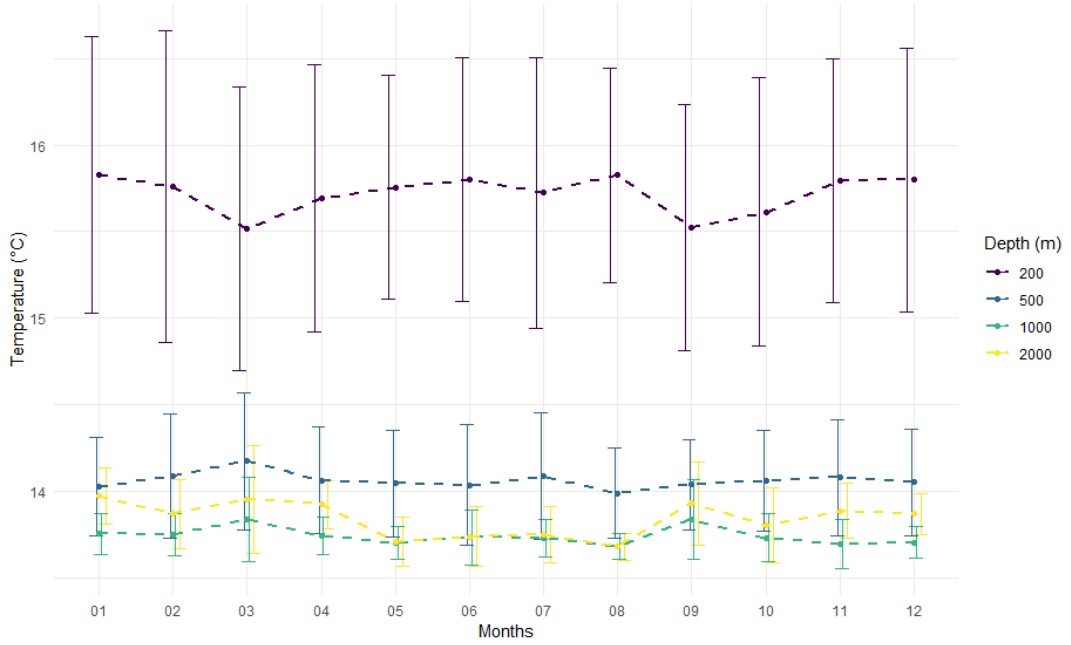

Figure 53 Monthly temperature means and standard deviations in the 200m to the 2000m range, the Levantine Sea from 1960 to 2017

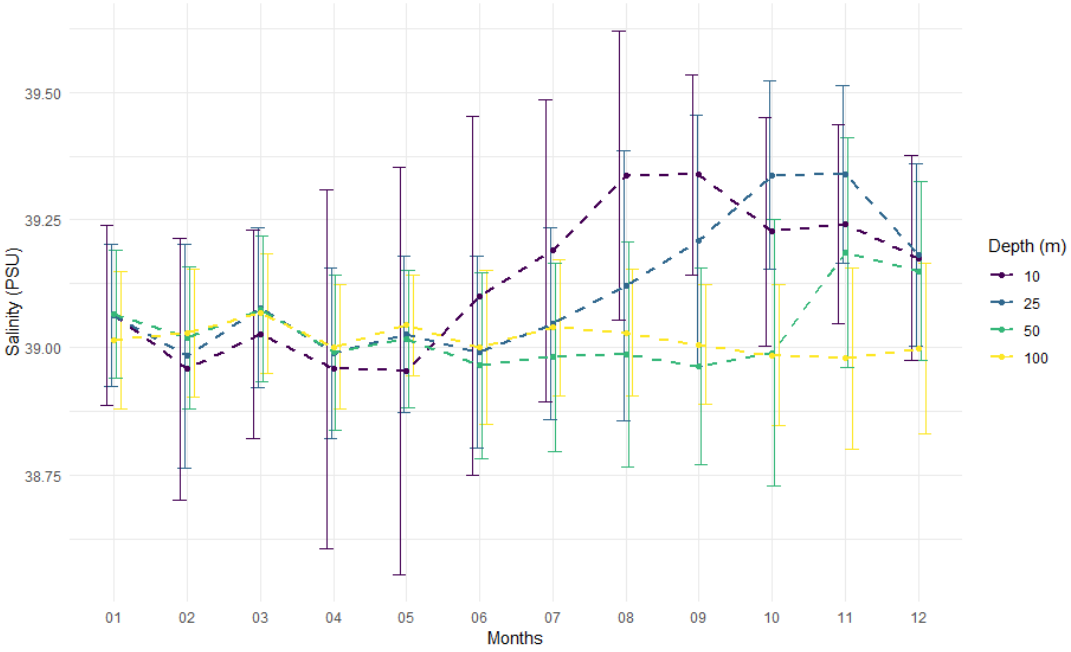

Figure 54 Monthly salinity means and standard deviation in the surface to the 100m range, the Levantine Sea from 1960 to 2017

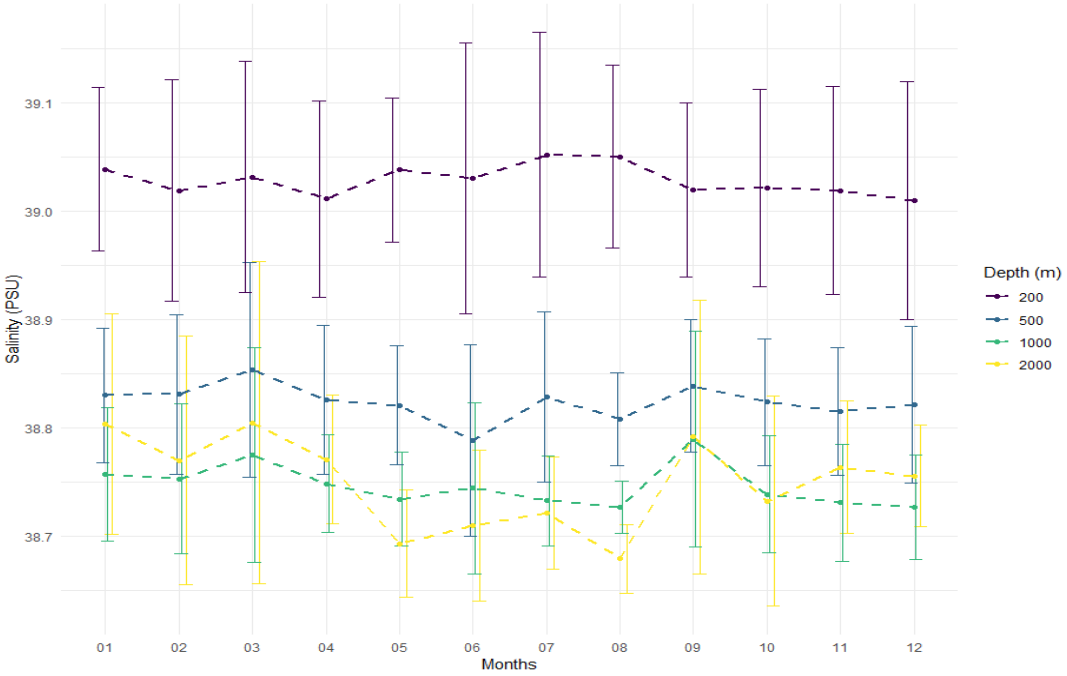

Figure 55 Monthly salinity means and standard deviation in the 200m to the 2000m range, the Levantine Sea from 1960 to 2017

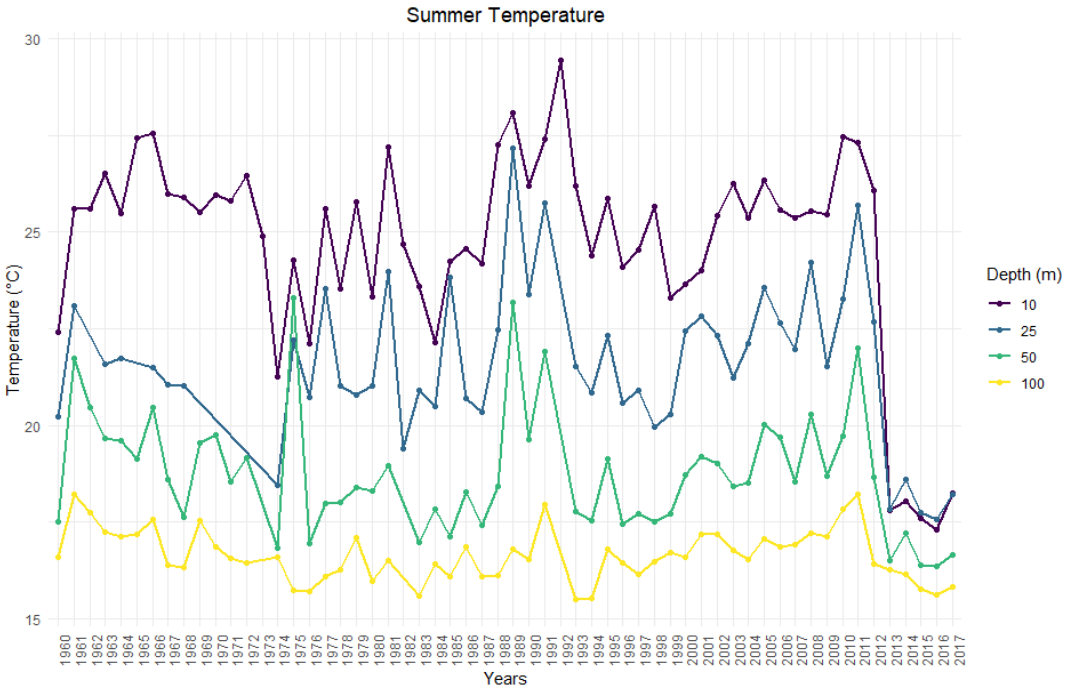

Figure 56 Annual summer temperature means in the surface to the 100m range, the Levantine Sea from 1960 to 2017

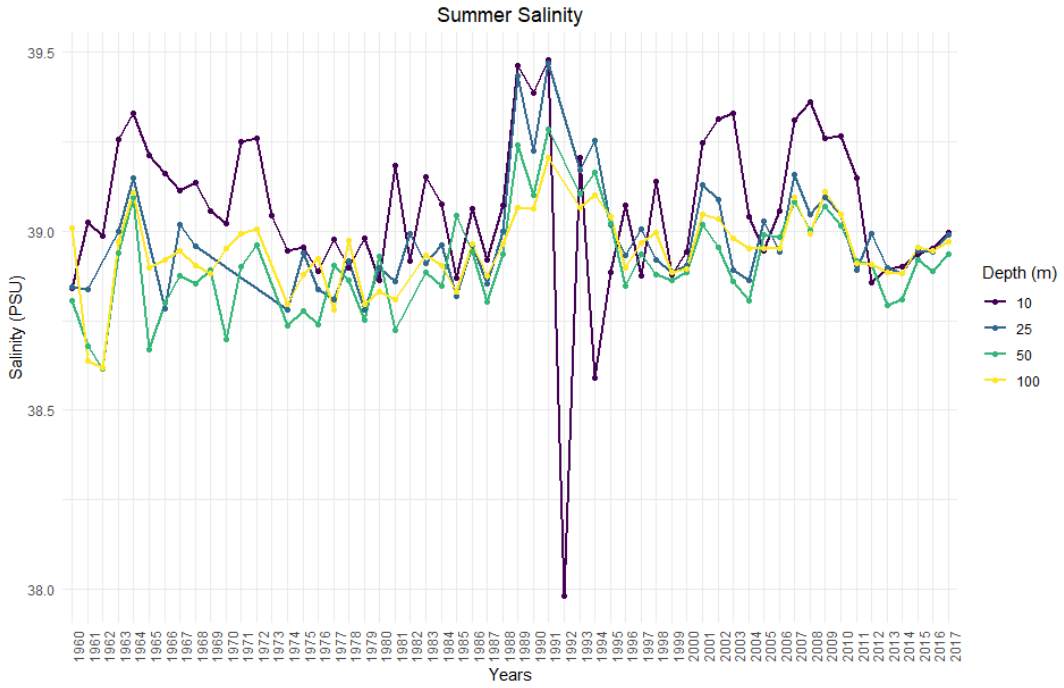

Figure 57 Annual summer salinity means in the surface to the 100m range, the Levantine Sea from 1960 to 2017

SWS values are on the rise across the board for LS like in Figure 56, but there is a sharp drop in the last couple of years concerning SWT which invariably shows higher values on average each successive year. The results for SWT in the last few years of our dataset, such as the one seen in Figure 57 are most likely due to data collection preference, rather than an actual drop of SWT. Additional plots for the global LS are available in Appendix C.

5.6.1 Cilician Basin Analysis

The following section will detail the information concerning the CB from 1960 to 2017. From Table 11 and Table 12, we can conclude some general information about the data collection pattern in the region. The number of data points both for salinity and temperature available for CB is the lowest amongst all sub-regions. Moreover, it is the only area of this study that does not have a depth that requires analysis beyond 1000m due to its relative shallowness compared to the other areas. The most significant amount of data for both SWT and SWS are available primarily during the summer and fall seasons with the most sampled depth appears to be in the 500m

layer, followed by the 10m layer. Compared to other sub-region, the measurements are relatively recent as the difference between the percentage of SWT to SWS measurements are relatively low, indicating a more modern approach with better equipment.

Temperature Data	Winter	Spring	Summer	Fall	Total
10m	1,150	4,390	6,876	7,457	19,873
25m	814	1,224	1,788	1,363	4,685
50m	349	1,599	2,385	1,690	6,023
100m	446	1,981	3,197	2,114	7,738
200m	814	3,174	5,224	3,392	12,604
500m	1,453	5,575	9,754	4,770	21,552
1000m	56	1,179	2,020	797	4,052
2000m	NA	NA	NA	NA	NA

Table 11 Temperature data entries per season and depth, the Cilician Basin from 1960 to 2017

Salinity Data	Winter	Spring	Summer	Fall	Total
10m	983	4,208	6,700	7,314	19,205
25m	272	1,185	1,742	1,318	4,517
50m	272	1,555	2,333	1,551	5,711
100m	279	5,146	3,131	1,982	7,265
200m	466	2,937	5,146	3,171	11,720
500m	884	5,195	5,195	4,453	20,198
1000m	6	1,176	1,965	795	3,942
2000m	NA	NA	NA	NA	NA

Table 12 Salinity data entries per season and depth, the Cilician Basin from 1960 to 2017

CB exhibits higher monthly SWT temperature at the surface compared to the global LS. SWT difference between the 10m, 25m and 50m is the lowest in the region during the summer and fall seasons, as seen in Figure 58. There is a noticeable drop during August for the 50m layer standing as a point of interest. The average SWT results for the 100m and 200m layers are slightly higher than the average of LS.

Figure 59 demonstrates that the 500m and 1000m are closely following the trend for LS and do not show any unexpected behaviour.

From Figure 60 we can infer that the SWS of the 10m, 25m, 50m and 100m layers are close from summer until the end of winter with a significant difference of the 10m layers observable during winter where SWS drops noticeably compared to the lower depth ranges.

There is not an as significant difference as LS when it comes to SWS during the summer and fall months, which might indicate a constant exchange of the water masses in the region. SWS for the 200m, 500m and 1000m are giving expected results with no significant change year long and do not seem to be strongly affected by seasonal variability as revealed by Figure 61.

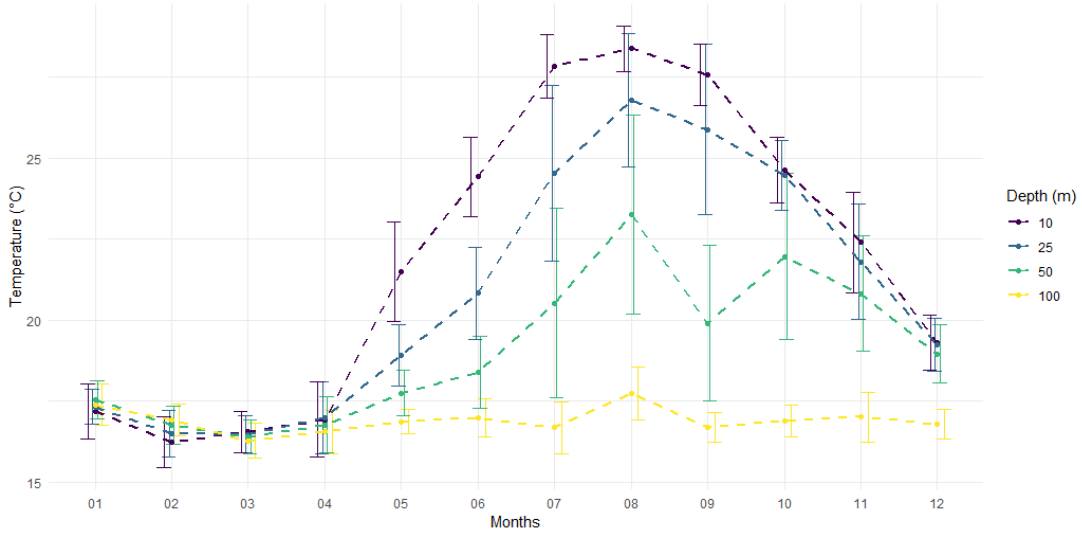

Figure 58 Monthly temperature means and standard deviations in the surface to the 100m range, the Cilician Basin from 1960 to 2017

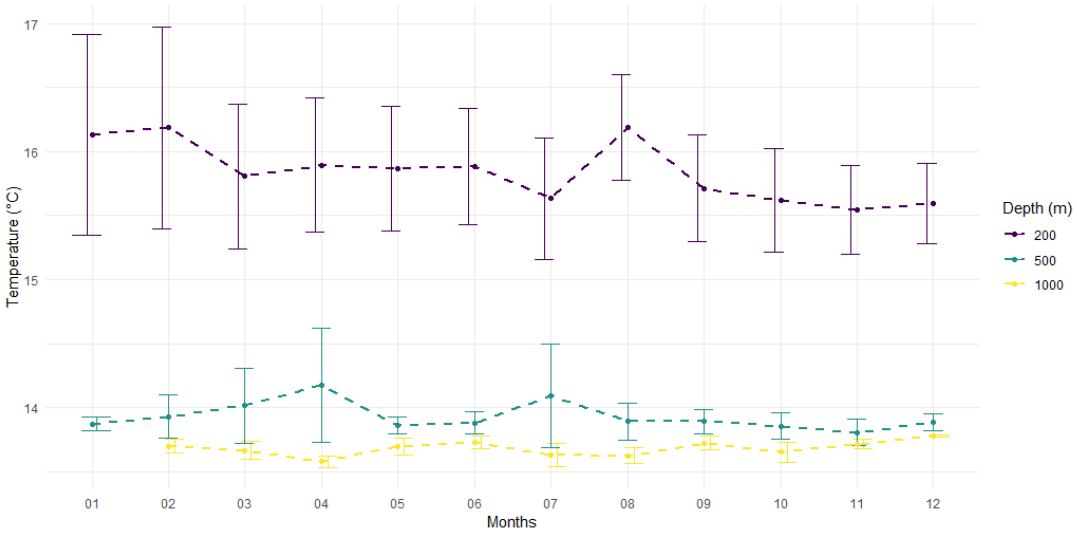

Figure 59 Monthly temperature means and standard deviation in the 200m to the 1000m range, the Cilician Basin from 1960 to 2017

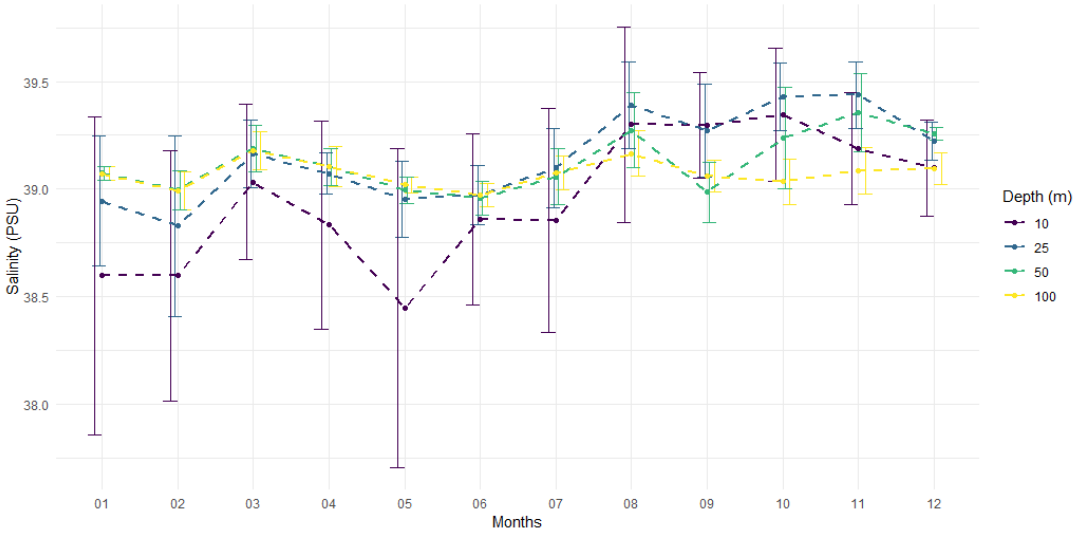

Figure 60 Monthly salinity means and standard deviations in the surface to the 100m range, the Cilician Basin from 1960 to 2017

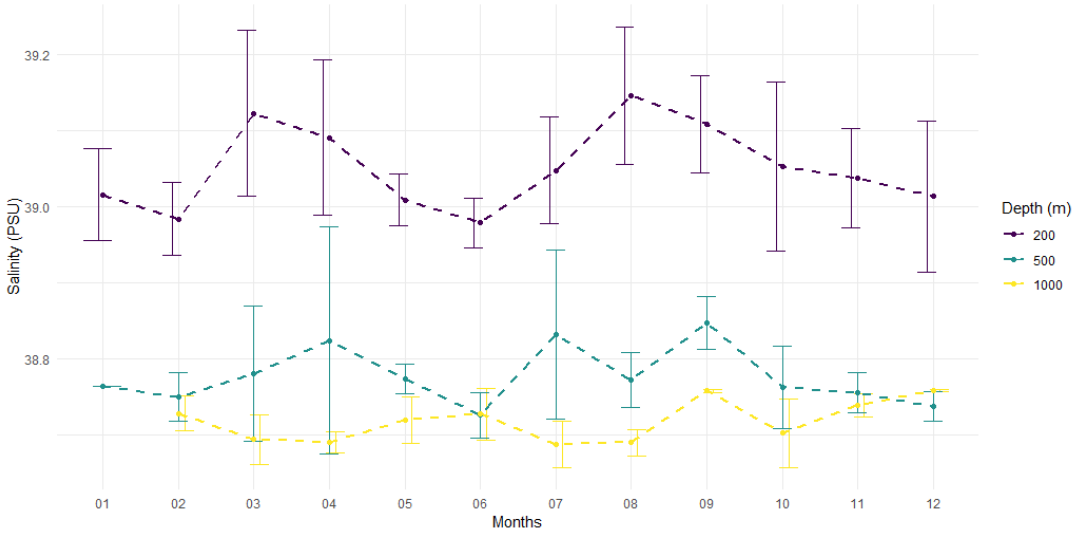

Figure 61 Monthly salinity means and standard deviation in the 200m to the 1000m range, the Cilician Basin from 1960 to 2017

There is a significant upward trend in the 200m layer SWT during spring, which is of note in CB, as Figure 62 demonstrates. Figure 63 and other seasonal plots in Appendix C display higher SWS values, indicating that there is a non-negligible mixing between LSW and LIW in the area. It should once again be noted that CB is the least sampled area.

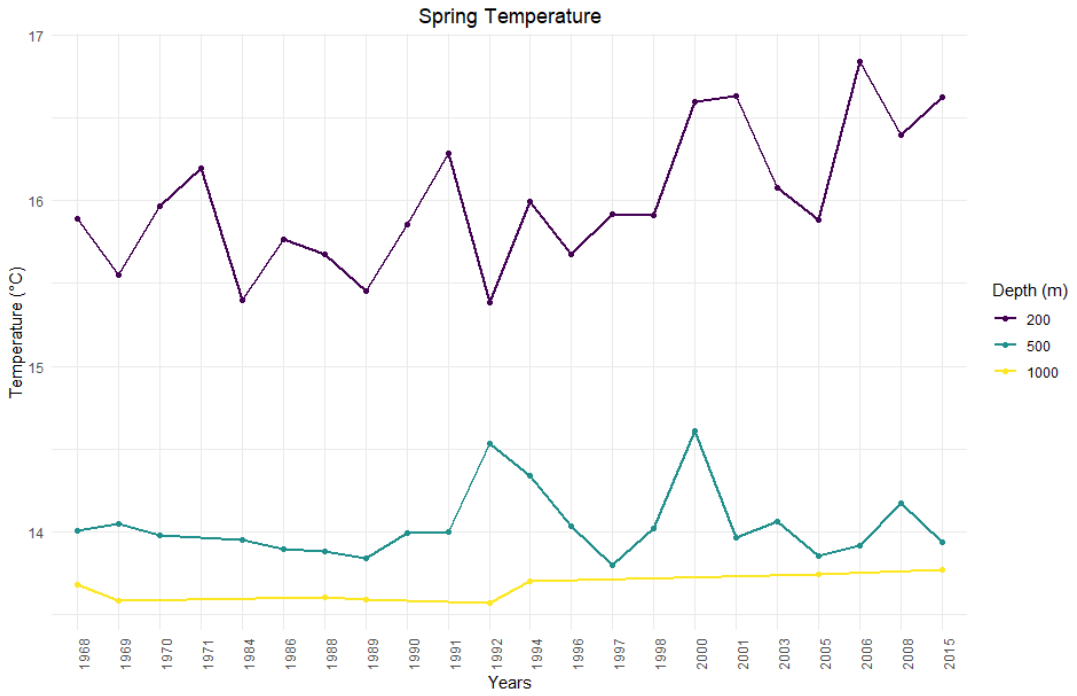

Figure 62 Annual spring temperature means in the 200m to the 1000m range, the Cilician Basin from 1960 to 2017

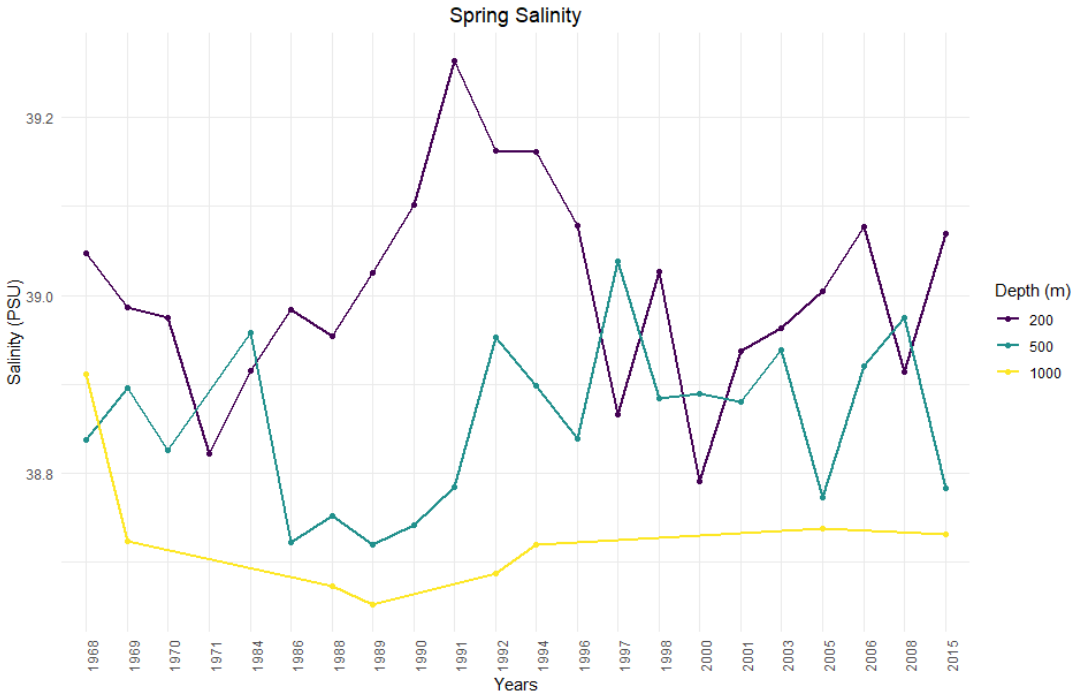

Figure 63 Annual spring salinity means in the 200m to the 1000m range, the Cilician Basin from 1960 to 2017

5.6.2 LEVANTINE BASIN ANALYSIS

The following section will detail the information concerning LB from 1960 to 2017. From Table 13 and Table 14, we can conclude that among the four selected sub-regions LB is by far the most studied area amongst our four selected regions. For SWT the greatest amount of casts have been accomplished in the summer season followed by fall and spring leaving winter the least studied seasonal period. Compared to other regions the number of casts is proportionately high in the 200m and 500m ranges, most likely due to the interest of researchers working on LIW with also high interest in the 1000m layer corresponding to EMDW. The surface is also amply sampled in a methodical fashion showing the great interest that the neighbouring countries and members of SDC networks have in the area, which in turn is an excellent opportunity to understand LSW. Unlike CB the area has points reaching to the 2000m depth.

Temperature Data	Winter	Spring	Summer	Fall	Total
10m	6,569	12,321	13,471	20,357	52,719
25m	1,500	3,476	2,721	2,098	9,795
50m	2,537	5,655	4,595	3,822	16,609
100m	4,568	10,495	8,454	7,415	30,932
200m	8,045	18,951	15,189	13,271	55,456
500m	16,679	39,923	33,644	27,775	117,021
1000m	16,121	10,495	25,993	25,774	78,383
2000m	4,013	2,410	1,780	3,468	11,671

Table 13 Temperature data entry per season and depth, the Levantine Basin from 1960 to 2017

Salinity Data	Winter	Spring	Summer	Fall	Total
10m	5,443	10,822	11,970	19,494	47,729
25m	1,248	3,162	2,365	1,824	8,599
50m	2,087	5,055	3,949	3,240	14,331
100m	3,505	9,357	7,189	6,274	26,325
200m	5,981	16,695	12,976	11,272	46,924
500m	13,386	36,928	29,874	24,373	104,561
1000m	16,066	37,523	23,062	25,784	102,435
2000m	4,013	2,380	1,759	3,468	11,620

Table 14 Salinity data entries per season and depth, the Levantine Basin from 1960 to 2017

LB demonstrates higher monthly SWT temperature at the surface compared to the global LS, which is expected from what we know of the region. There is a distinct SWT difference between the 10m, 25m and 50m are the highest in the region during the summer with an average peak temperature in August of 30°C at the surface. The peaks for 25m and 50m are delayed and occur in September and November respectively as seen in Figure 64, most likely due to the time required for the heat transfer from the surface to the lower layers to occur. SWT for the upper layers converge back to similar values in December, but the mean SWT remains higher than the global LS with less significant standard deviation yearlong. The average SWT results for the 100m and 200m layers are noticeably higher than the average of LS. Figure 65 demonstrates that the 500m to 2000m conform closely to the trend for LS and do not show any unforeseen behaviour.

Figure 66 displays SWS of the 10m, 25m and 50m layers have significant seasonal variability and also the highest salinity rating in the whole LS. The formation of LIW from LSW is observable from the plots clearer than the global LS. The sinking of LSW is clearly shown with the sharp rise of SWS at 25m starting from September with the slowing down of the rise of SWS at the surface layer. The phenomenon is followed by a continuous rise of SWS peaking in October for 25m and December for 50m. From its peak, in September the surface SWS drops below the 25m range before converging in December with the three topmost ranges SWS. From Figure 67,

we can see that the 200m SWS is slightly more elevated than the one for LS, but the lower layers are consistent with our general findings.

In general, there is a noticeable upward trend in both SWT and SWS in LB, as seen from both Figure 68 and 69 from 1960 to 2017. It is more distinctly visible than the global LS. The region having higher SWT and SWS combined with a good spatial and temporal sampling of the area is the most likely reason for such an evident picture of the evolution of the physical parameters in the region.

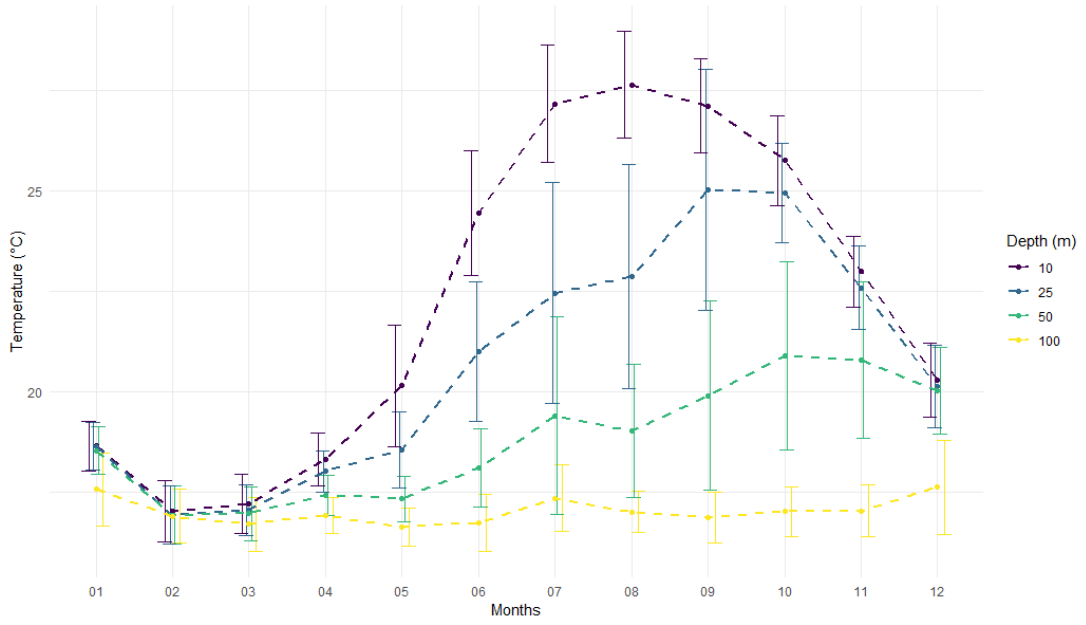

Figure 64 Monthly temperature means and standard deviations in the surface to the 100m, the Levantine Basin from 1960 to 2017

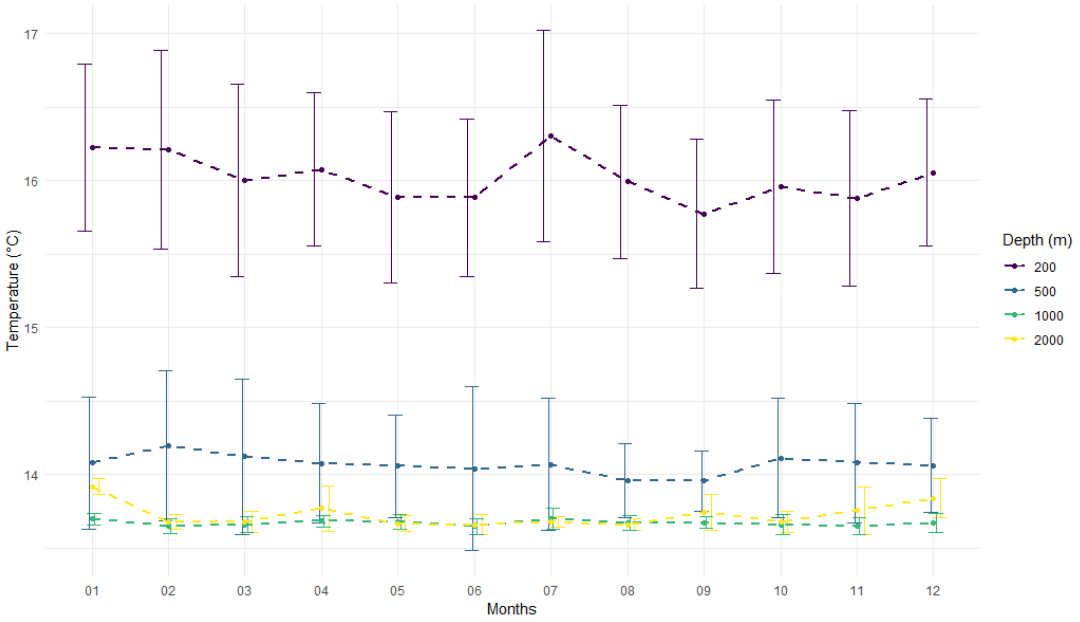

Figure 65 Monthly temperature means and standard deviation in the 200m to the 2000m range, the Levantine Basin from 1960 to 2017

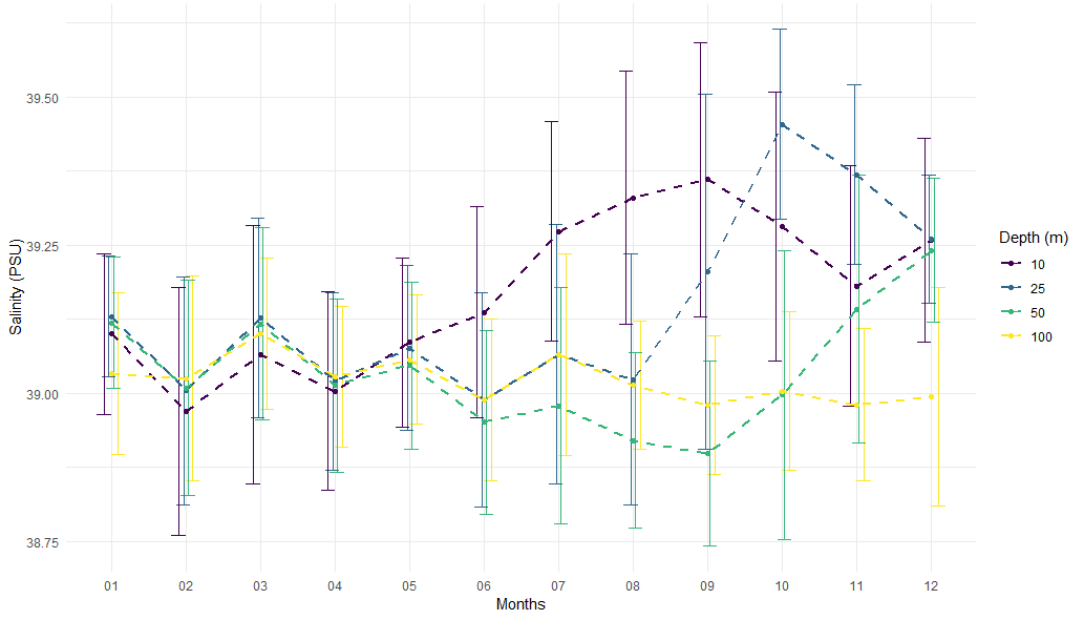

Figure 66 Monthly salinity means and standard deviations in the surface to the 100m range, the Levantine Basin from 1960 to 2017

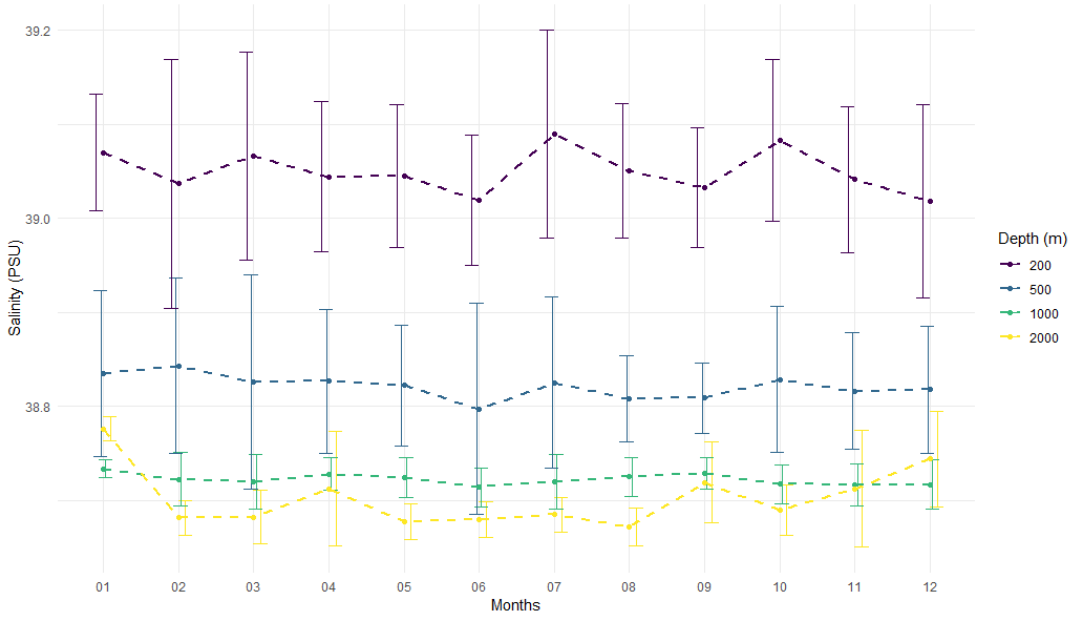

Figure 67 Monthly salinity means and standard deviations in the 200m to the 2000m range, the Levantine Basin from 1960 to 2017

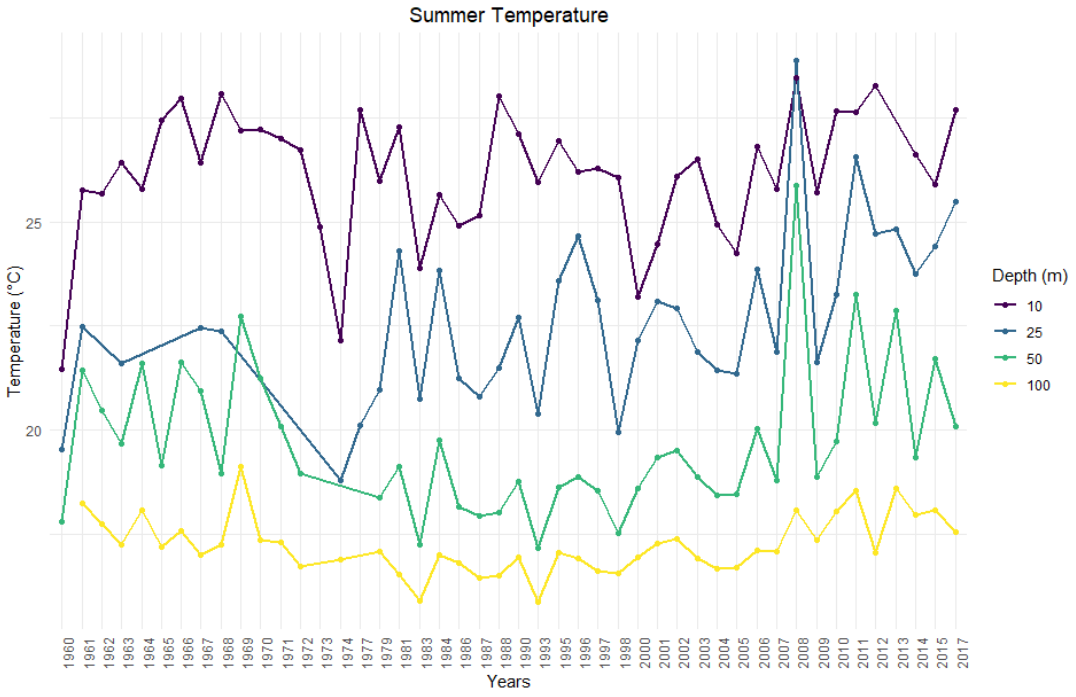

Figure 68 Annual summer temperature means in the surface to the 100m range, the Levantine Basin from 1960 to 2017

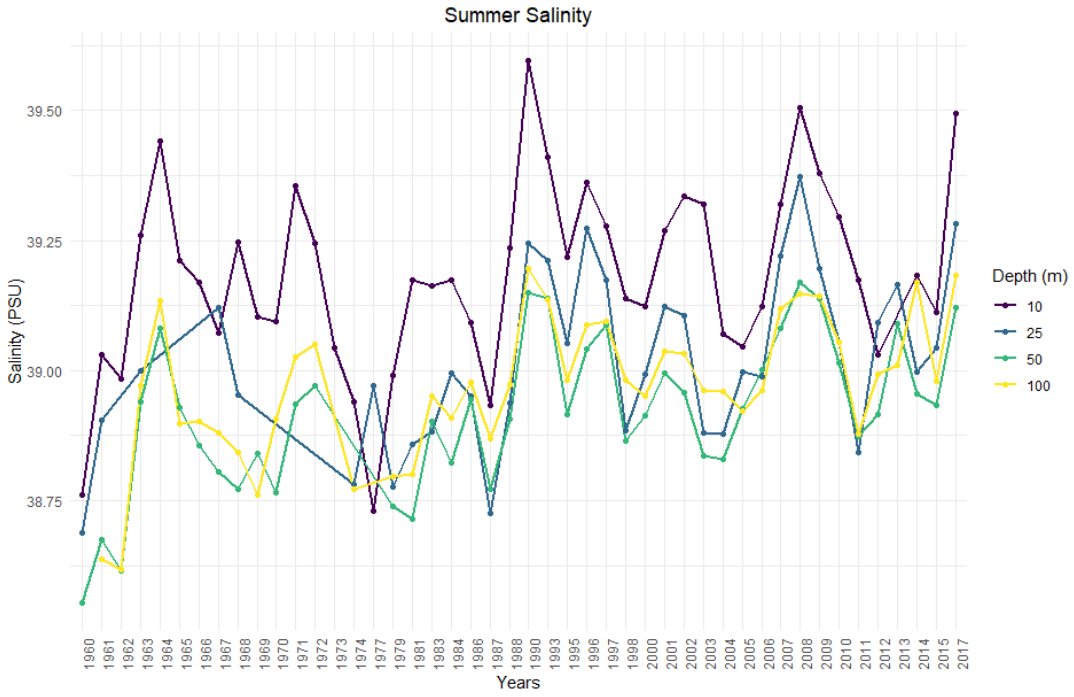

Figure 69 Annual summer salinity means in the surface to the 100m range, the Levantine Basin from 1960 to 2017

5.6.3 Coastal Nile Delta Analysis

The following section will detail the information concerning the CND from 1960 to 2017. Table 15 and Table 16 clearly show that CND is the second least studied region despite the significant number of people living in the area. For SWT the most amount of casts have been accomplished in fall. The other three seasons are equally sampled, a different distribution compared to the other regions. The number of casts is concentrated in the surface and 200m to 1000m layers.

There is a significant difference between the number of SWS values and SWT measurements in the region. At this point, it should be noted that the discrepancy is by far the highest amongst our sub-regions. The discrepancy is most likely due to the preferences of the research interests of the scientists in the area or a lack proper scientific cruises resulting in the data available originating from trade vessels, which are mostly equipped to measure SWT rather than other variables and limited to the surface. SWS measurements are the most prominent in fall followed by summer.

Temperature Data	Winter	Spring	Summer	Fall	Total
10m	4,585	3,502	2,276	7,030	17,393
25m	747	967	623	823	3,160
50m	1,315	1,672	1,071	1,526	5,584
100m	2,622	3,367	2,082	2,910	10,981
200m	4,736	895	3,888	5,399	20,399
500m	4,869	6,968	5,249	7,731	24,817
1000m	2,510	4,390	4,639	5,872	17,411
2000m	27	895	689	731	2,342

Table 15 Temperature data entries per season and depth, the Coastal Nile Delta from 1960 to 2017

Salinity Data	Winter	Spring	Summer	Fall	Total
10m	2,989	1,817	1,200	5,556	11,562
25m	194	356	231	316	1,097
50m	379	638	432	560	2,009
100m	637	1,231	817	1,044	3,729
200m	1,185	2,403	1,544	2,044	7,176
500m	1,369	4,209	3,176	4,284	13,038
1000m	1,714	4,369	4,474	5,858	16,415
2000m	25	895	689	731	2,340

Table 16 Salinity data entries per season and depth, the Coastal Nile Delta from 1960 to 2017

CND shows on average higher SWT at 50m layer when compared to the LS, but lower peak temperature for its surface water as seen in Figure 70. Of note are the nearly identical values for SWT at the surface and 25m in August showing considerable seasonal variation although this phenomenon does not seem to influence the 50m range as much as LB. The average SWT for the 100m and 200m ranges, even if not affected by seasonality has higher monthly mean values compared to LS. Lower depth ranges are within the norm for LS as can be observed in Figure 71 and which have been the case for all the previous regions so far. From their peak in August around 27°C interestingly the 10m and 25m layers remain at the same SWT until they get normalised in December with the 50m layer.

SWS values for the region are the highest for LS with mean values at the surface of 39.45 PSU without even taking into account standard deviation, as seen in Figure 72. There is distinct seasonal variability in the upper three layers and especially in the 50m range, which shows a sharp increase between September and November. Figure 73 indicates that the 100m range is higher than the global LS values, but once again, the deepest three ranges are within expected values for LS.

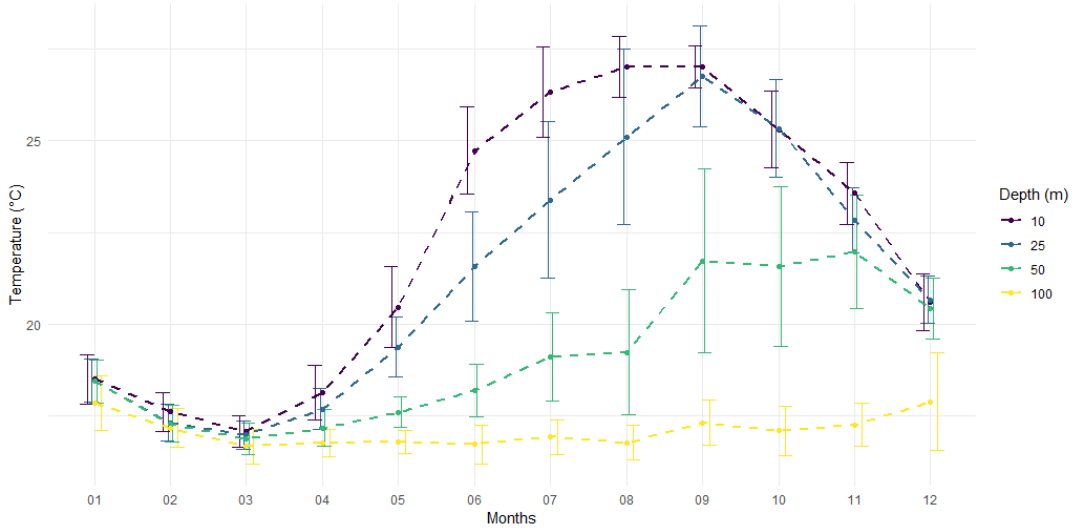

Figure 70 Monthly temperature means and standard deviations in the surface to the 100m range, the Coastal Nile Delta from 1960 to 2017

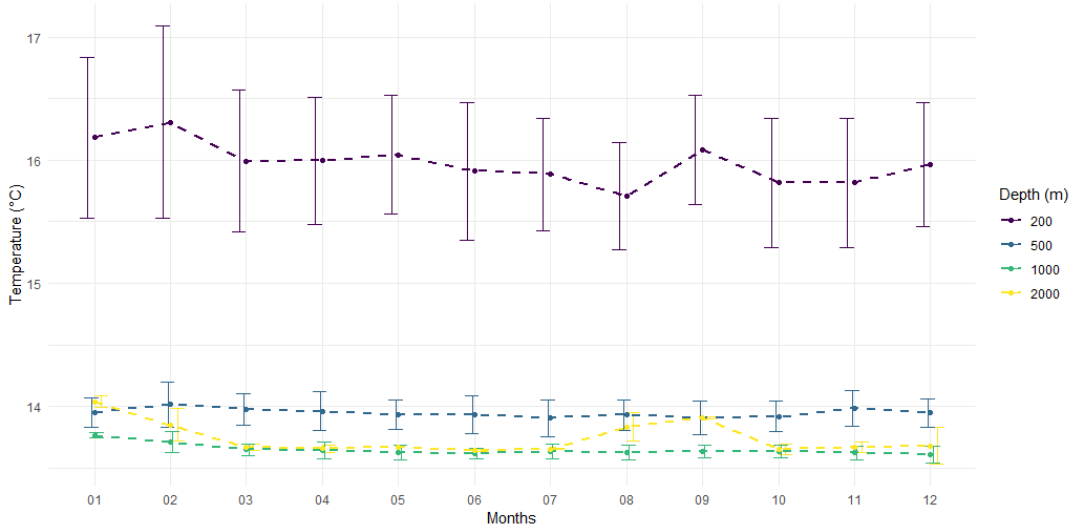

Figure 71 Monthly temperature means and standard deviations in the 200m to the 2000m range, the Coastal Nile Delta from 1960 to 2017

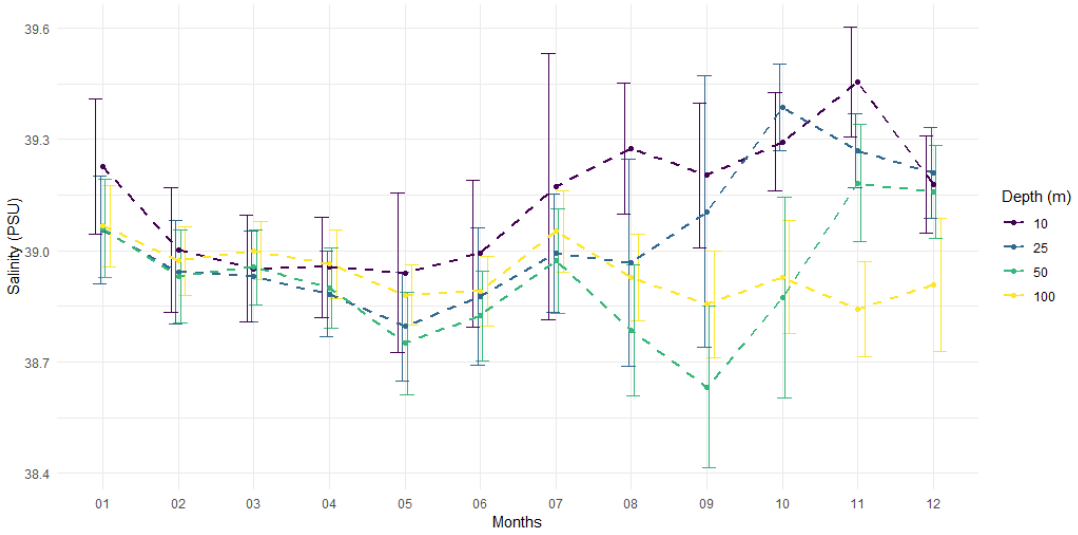

Figure 72 Monthly salinity means and standard deviation in the surface to the 100m range, the Coastal Nile Delta from 1960 to 2017

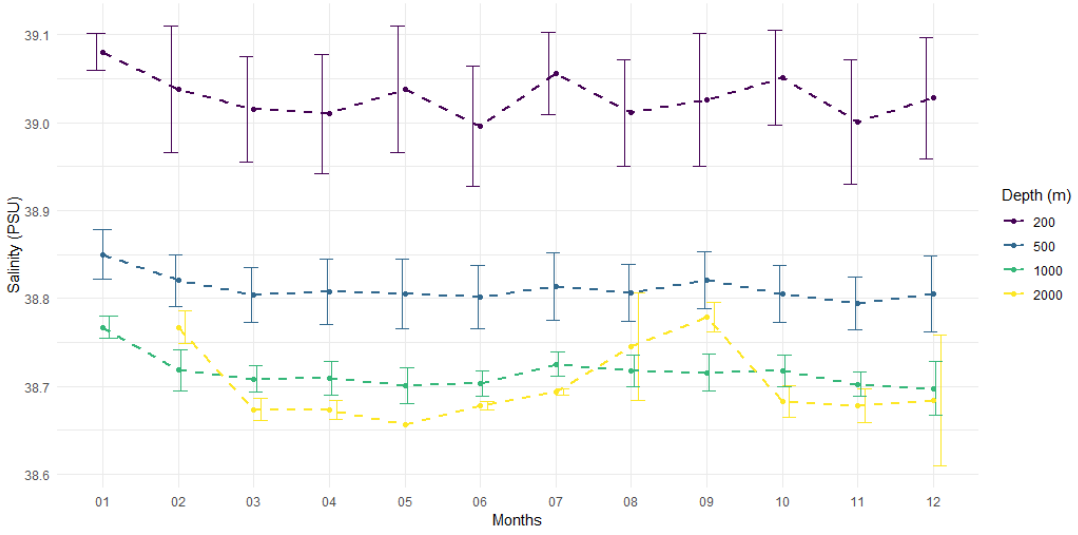

Figure 73 Monthly salinity means and standard deviations in the 200m to the 2000m range, the Coastal Nile Delta from 1960 to 2017

SWT seems to be on the rise in CND as can be seen from Figure 74, a noticeable trend may be observed across all seasons presented in Appendix C. SWS values, such as the one in Figure 75, are extremely erratic except for the lower layers, and it is not really possible to comment on them without further smoothing.

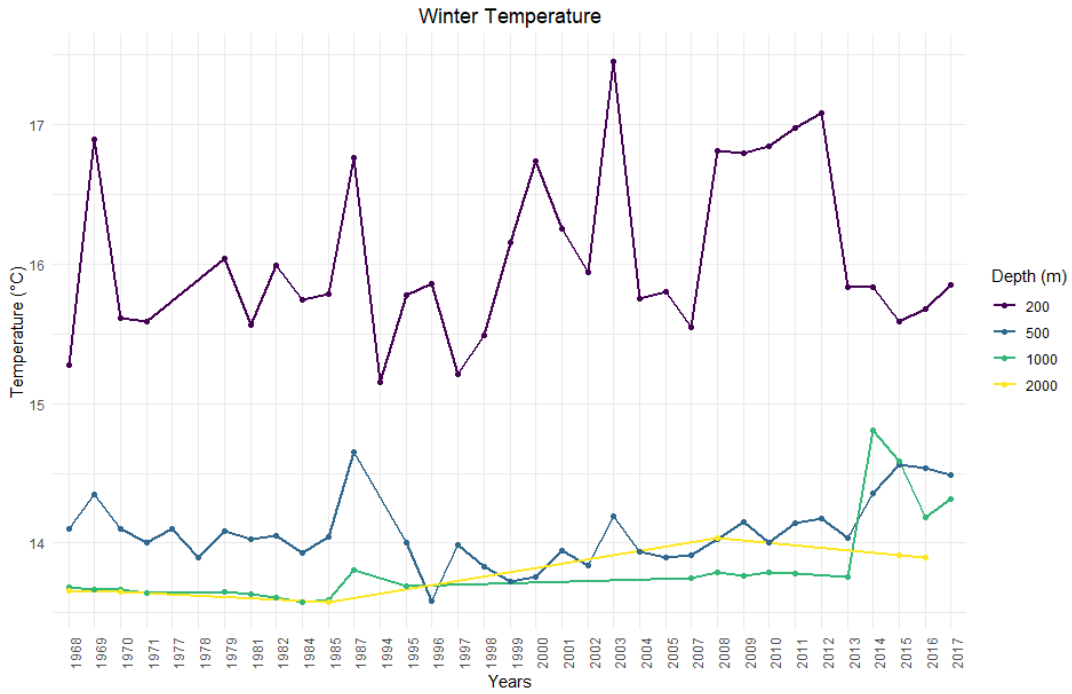

Figure 74 Annual winter temperature means in the 200m to the 2000m range, the Coastal Nile Delta from 1960 to 2017

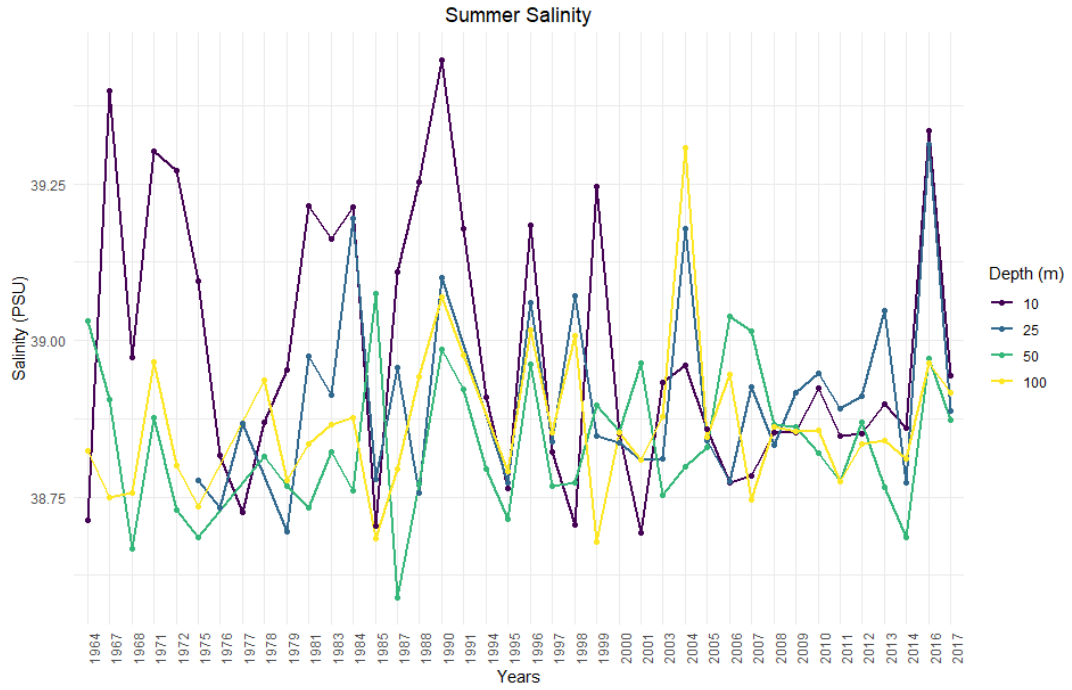

Figure 75 Annual summer salinity means in the surface to the 100m range, the Coastal Nile Delta from 1960 to 2017

5.6.4 RHODES GYRE ANALYSIS

The following section will detail the information concerning RG from 1960 to 2017. From Table 17 and Table 18, we can conclude that among the four selected sub-regions, RG is the second most studied area after LB. For SWT the most amount of casts have been accomplished in the fall season followed by spring. Distinctly from the other regions, summer is the least studied seasonal period. The winter season has a proportionally elevated number of data points. The casts are concentrated in the 200m to 1000m layers, most likely due to the interest of researchers concerning EMT and EMDW formation in the region, which would explain the higher winter sampling rate. The surface always shows a proper spread of data entries.

Meanwhile, SWS measurements are the most numerous in fall followed by spring. As it is always the case, there are less SWS samples compared to SWT measurements, but these differences are less pronounced than the other regions indicating that proper scientific cruises were conducted in the area.

Temperature Data	Winter	Spring	Summer	Fall	Total
10m	3,479	5,582	3,179	9,876	22,116
25m	791	1,545	767	1,813	4,916
50m	1,589	2,880	1,579	3,453	9,501
100m	3,112	5,505	2,937	6,252	17,806
200m	5,923	10,619	5,596	11,428	33,566
500m	9,380	19,060	6,635	17,366	52,441
1000m	8,439	19,784	6,929	17,634	52,786
2000m	3,694	4,609	1,762	10,489	20,554

Table 17 Temperature data entries per season and depth, the Rhodes Gyre from 1960 to 2017

Salinity Data	Winter	Spring	Summer	Fall	Total
10m	2,631	4,762	2,479	8,868	18,740
25m	553	1,338	603	1,497	3,991
50m	1,189	2,812	1,300	2,812	7,830
100m	2,239	4,776	2,405	5,215	14,635
200m	4,259	9,236	4,617	9,747	27,859
500m	6,627	17,119	5,726	14,855	44,327
1000m	8,327	19,773	6,128	17,619	51,847
2000m	3,482	4,607	1,762	10,482	20,333

Table 18 Salinity data entries per season and depth, the Rhodes Gyre from 1960 to 2017

RG has noticeably lower SWT than LS at all depth levels and most noticeably in the upper layers. The mean SWT for the surface is barely reaching 25°C in August compared to the 26° in LS at large. It is apparent in Figure 76 that the seasonal variability is much less drastic, yet apparent, with a more mitigated slope for the surface, 25m and 50m ranges. As demonstrated in all previous regional and sub-regional analysis, and also seen in Figure 76 and Figure 77, there is no significant seasonal variability below the 100m to 2000m depth ranges. SWT values for the upper layers converge in January and stay uniform until they bifurcate once more starting in March. These results correlate well with the literature and the preliminary exploration we conducted concerning the location of RG from the DIVA climatological maps in Section 5.1.2. These results also confirm SWT maps created using WOA18 dataset showing lower temperature isotherms with an example in Section 2.2.4 and the complete seasonal SWT and isotherm maps in Appendix B.

SWS values of RG are equivalent to the one of LS except for a slightly more pronounced peak for the surface layer in August and display the usual pattern of seasonal variability common in the region. The sinking of the saline water during the fall months is also observable in Figure 78. Compared to LS at large and the other regions in our study Figure 79 showcases that there seems to be an erratic behaviour in SWS readings in the 200m, 500m, 1000m, and 2000m layers that do not seem

linked to seasonality. We can only speculate about these findings, but they are most likely the result of the gyre in action and potential formation of EMDW.

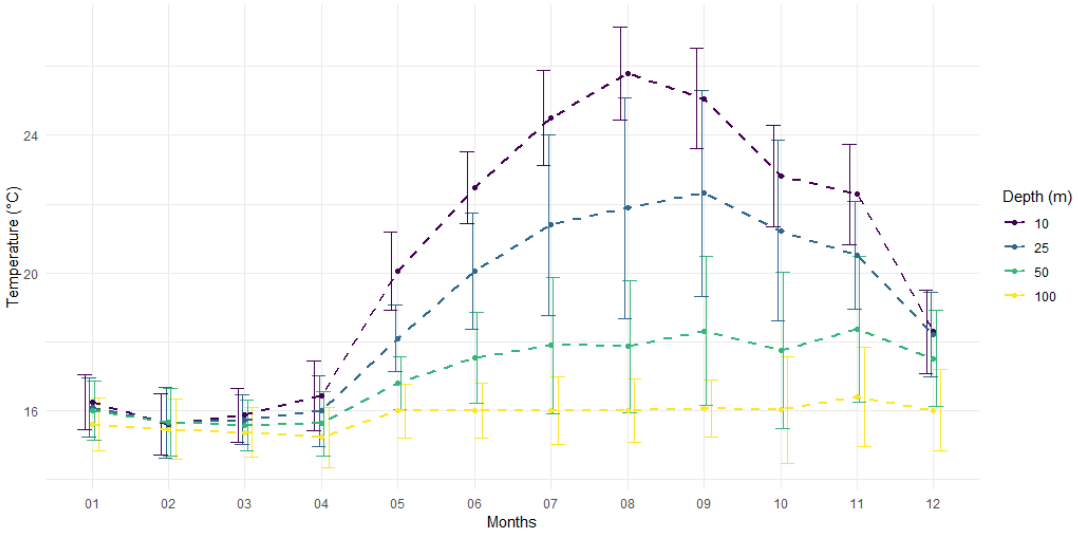

Figure 76 Monthly temperature means and standard deviations in the surface to the 100m range, the Rhodes Gyre from 1960 to 2017

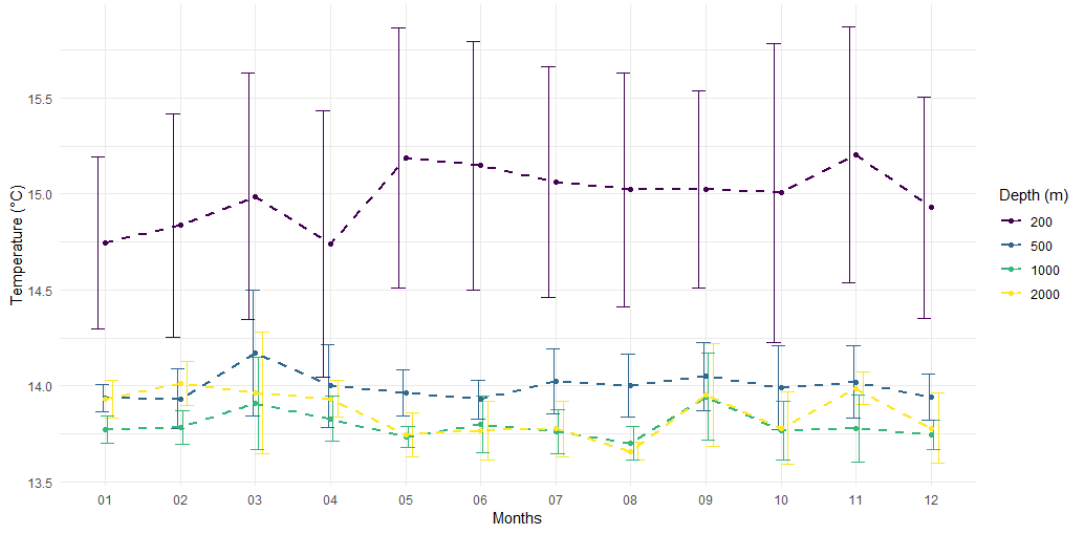

Figure 77 Monthly temperature means and standard deviations in the 200m to the 2000m range, the Rhodes Gyre from 1960 to 2017

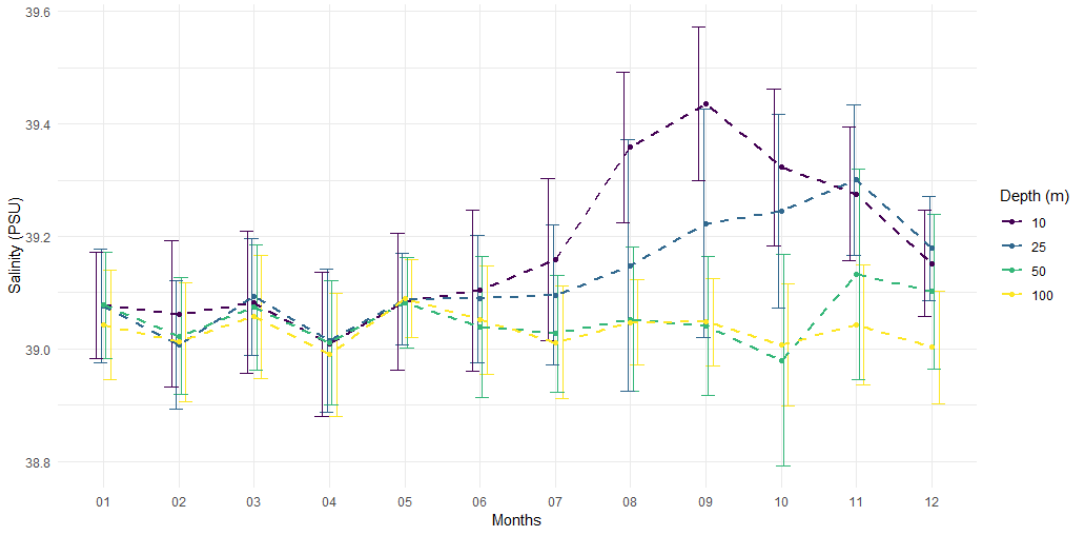

Figure 78 Monthly salinity means and standard deviations in the surface to the 100m range, the Rhodes Gyre from 1960 to 2017

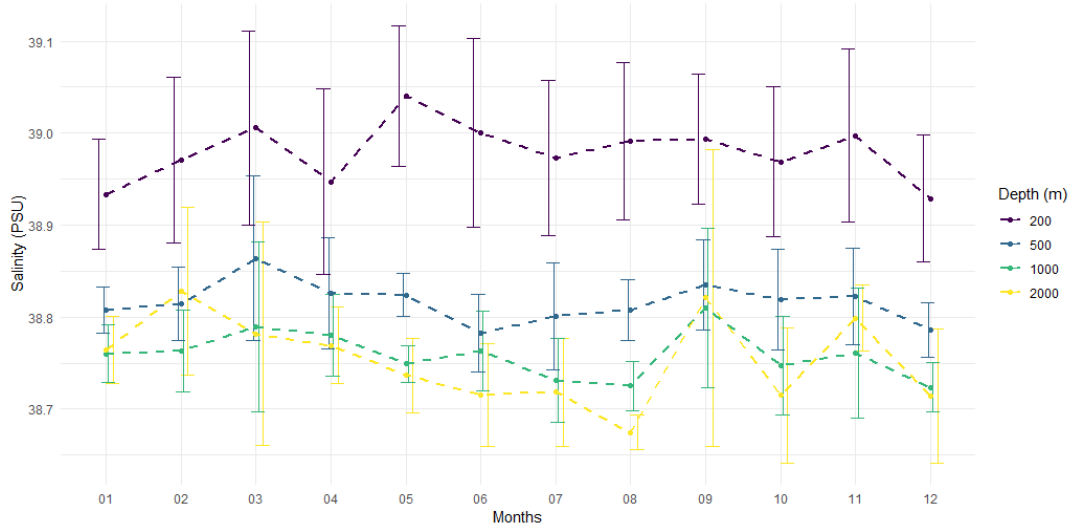

Figure 79 Monthly salinity means and standard deviations in the 200m to the 2000m range, the Rhodes Gyre from 1960 to 2017

EMT phenomenon is visible in an average yearly plot as seen in Figure 80 and 81 with the drop in SWT, creating a sudden rise in SWS in the region at lower depth ranges. The overall temperatures are consistently cooler compared to the rest of the LS, as can be seen from the detailed yearly plots in Appendix C.

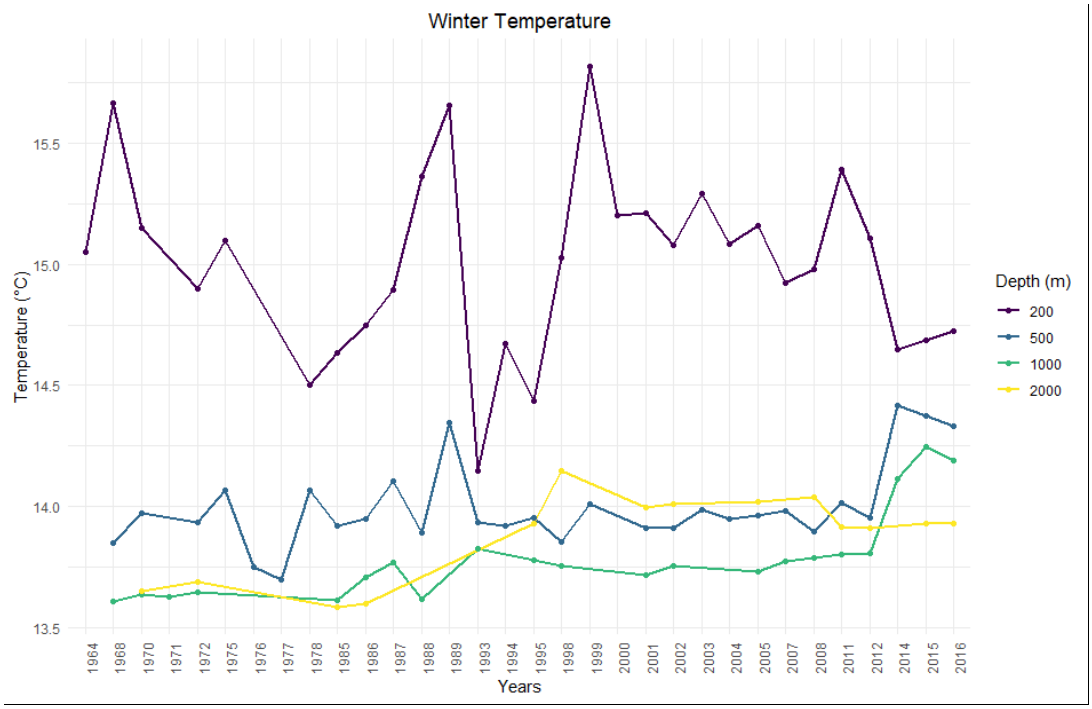

Figure 80 Annual winter temperature means in the 200m to the 2000m range, the Rhodes Gyre from 1960 to 2017

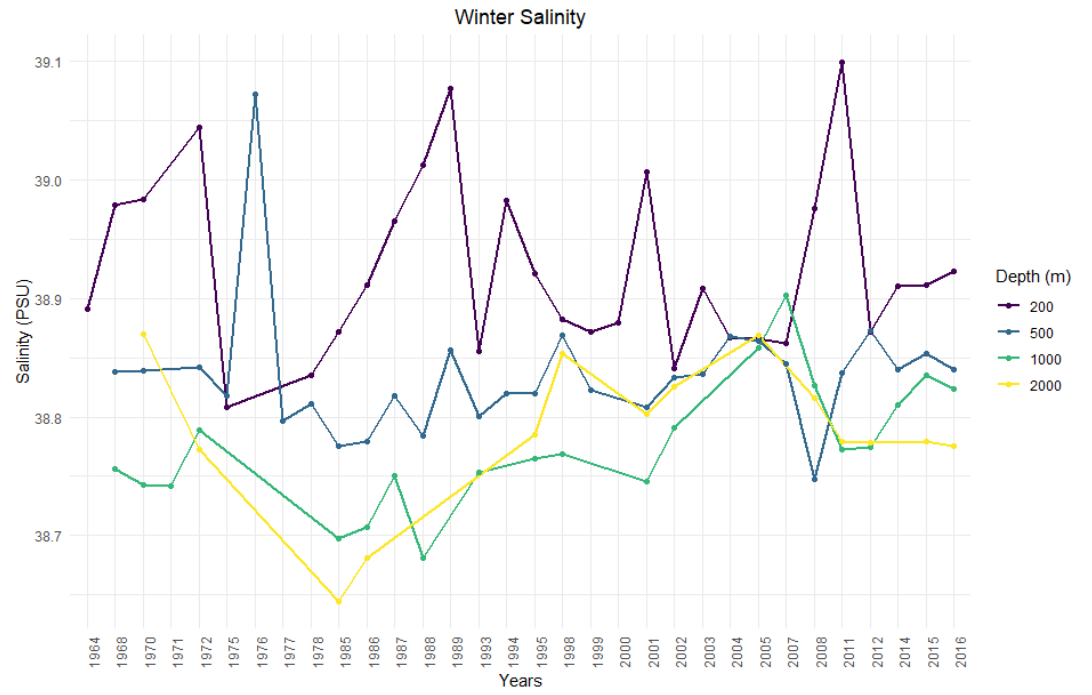

Figure 81 Annual winter salinity means for the 200m to the 2000m range, the Rhodes Gyre from 1960 to 2017

CHAPTER 6

EXPLORATORY ANALYSIS

In order to determine the distribution of the data, empirical and theoretical distribution of the seasonal observations at each depth level is determined and tested using standard statistical Cullen & Frey graphs and CDF methods in Section 6.1. Meanwhile, Section 6.2 is dedicated to the regression analysis according to the found distribution patterns conducted on our data to determine the significance of different geospatial factors on SWT and SWS and their interaction with each other.

6.1 EMPIRICAL AND THEORETICAL DISTRIBUTION

In order to determine the theoretical distribution model of SWT and SWS data points seasonally and per depth level we first started our analysis by plotting Cullen and Frey graphs such as Figure 82 at every single depth level seasonally for the LS. By comparing the square of skewness and kurtosis, we can identify potential distribution patterns of our data to narrow the tested models. From our preliminary density plots displayed in Appendix A, we expected the potential distribution to follow a lognormal, normal, beta or gamma trend. Most layers seasonally do indeed seem to correspond to our hypothesis except for normal distribution, which appears not to be compatible with any of the layers. In some rare cases, they seem to conform to a Weibull distribution which fits better than the more common lognormal or beta distribution.

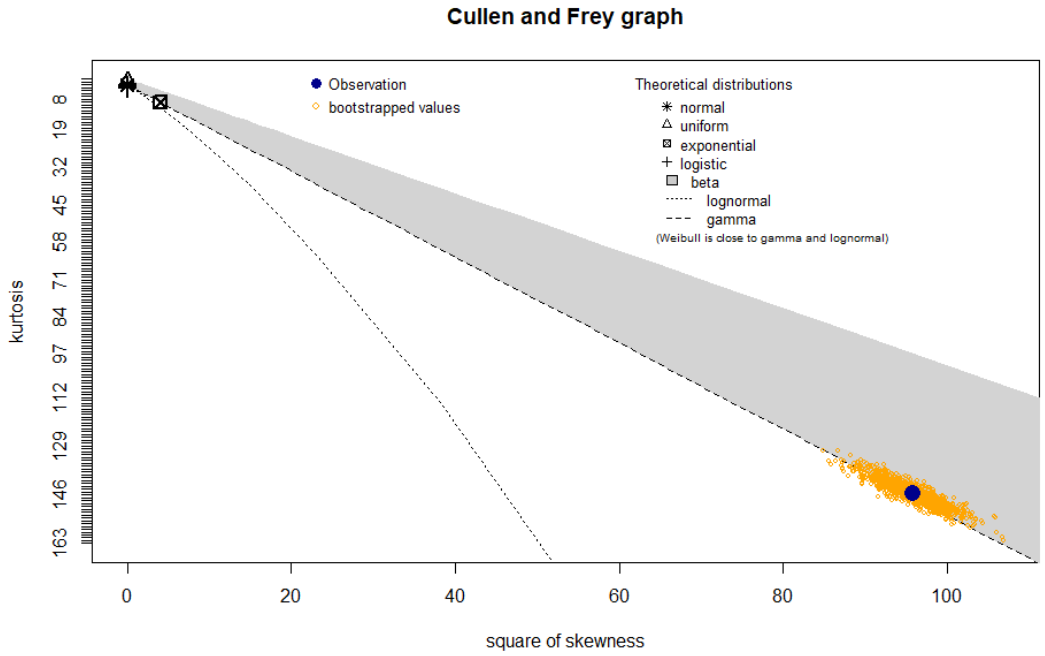

Figure 82 Cullen and Frey graph for the 500m layer in summer of the LS with the data of the 1960-2017 period

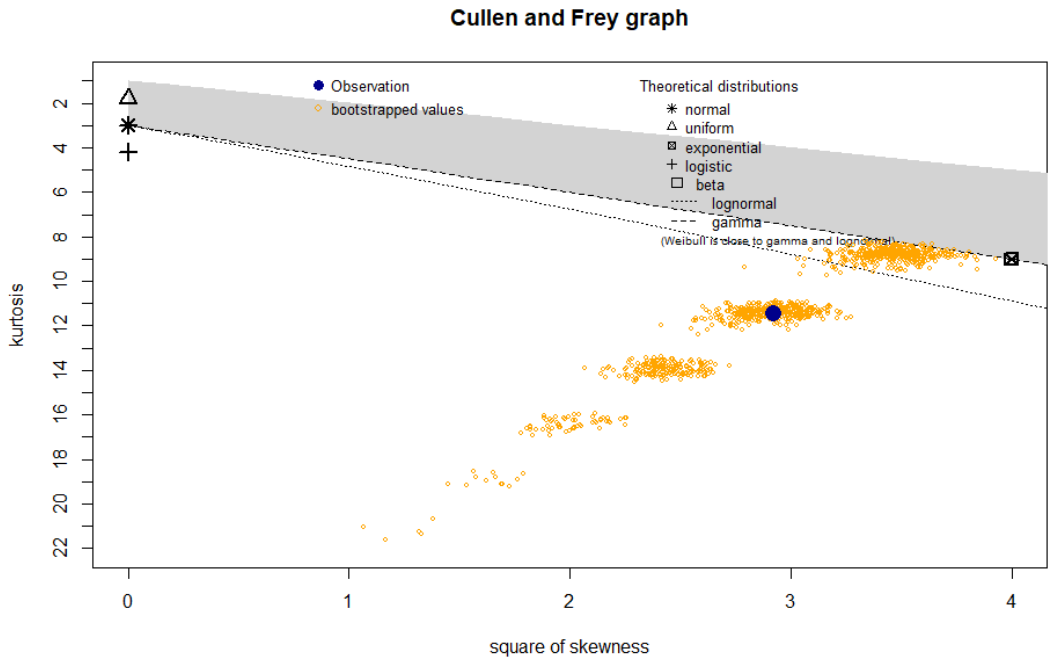

Figure 83 Cullen and Frey graph for the 500m layer in winter of the LS with the data of the 1960-2017 period

Occasionally the available data points did not conform to any easily discernable distribution being scattered unexpectedly. Further work is necessary to determine any potential distribution model they might conform too, but such a task would require a huge amount of time and human resources and is beyond the scope of this thesis.

Figure 83 is an example of a layer where the Cullen and Frey graph remains inconclusive, showing a very disparate distribution. Fortunately, these are relatively few overall, but in such cases; it is not feasible to find out a prope theoretical distribution model for those layers. They are representative of a non-parametric distribution and will be noted as such.

Before going forward with empirical and theoretical Cumulative Distribution Functions (CDF), the data must be manipulated. The beta distribution only works with data having values between 0 and 1, which is not the case for both SWT and SWS. In order to make it compatible, we divide both SWT and SWS by 1000 and create new datasets. We expected SWS to follow a beta distribution meaning that only SWS should be standardised, but to check if SWT also follows a beta distribution we also standardised the temperature values. We compared the results for non-beta distributions for the two datasets at the same layer and season and observed identical results meaning that this action did not disturb other potential theoretical known models by standardisation.

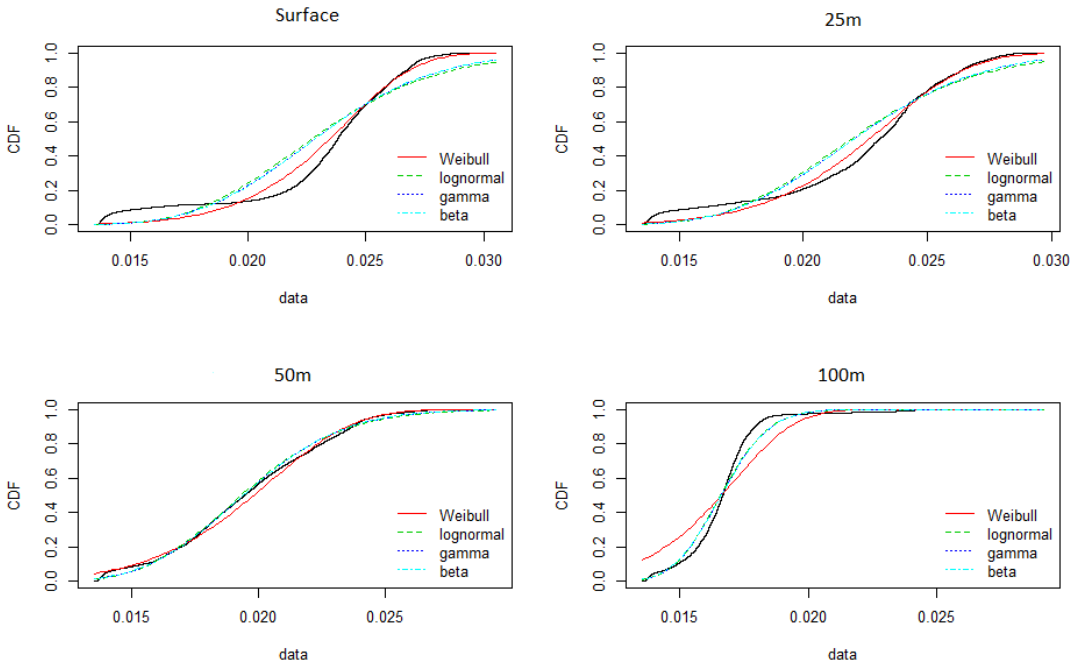

Figure 84 Temperature empirical and theoretical CDFs for fall season between 1960 and 2017

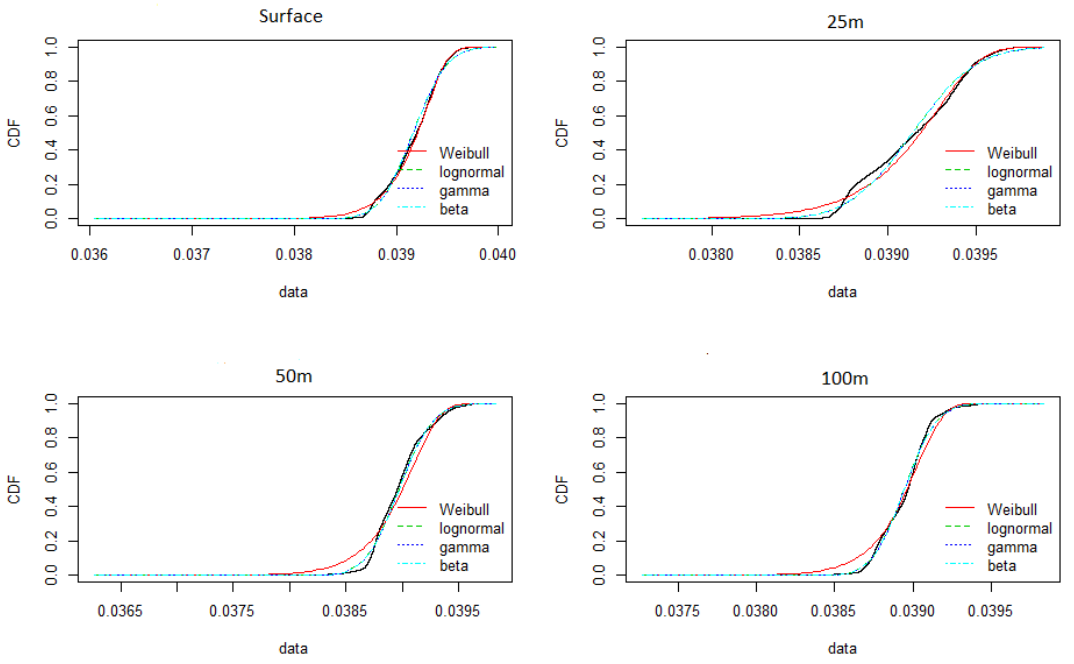

Figure 85 Salinity empirical and theoretical CDFs for fall season between 1960 and 2017

Figure 84 and Figure 85 are examples of the CDFs obtained. The black plot represents the empirical distribution of the data while the coloured plots are the theoretical distribution for Weibull, lognormal, gamma and beta distribution. This process has been applied to every single season and depth layer. When applicable, each seasonal layer is tested for lognormal, gamma, beta and Weibull distribution. In case a particular model is not fit under any circumstances due to the data structure, it is omitted from the CDFs.

Once we obtain the theoretical distribution, we proceed to look at the area between the empirical plot and the different models. We accomplish this with an Anderson Darling goodness of fit test (AD) to ascertain if the models correspond to our data and which model is the most suitable at a certain depth level and season. The results for each season and depth level are further controlled using an Akaike's goodness of fit information criterion measurement (AIC). The following tables show the results of AD test and the AIC measurement. In the case of a non-parametric result, no Akaike test is performed.

Temperature Data	Weibull	Lognormal	Gamma	Beta	NP
10m				AD	
25m				AD	
50m				AD	
100m				AD	
200m					AD
500m	AD				
1000m	AD				
2000m	AD				

Table 19 Optimal theoretical model using Anderson Darling test for SWT LS in winter from 1960 to 2017

Salinity Data	Weibull	Lognormal	Gamma	Beta	NP
10m			AD		
25m			AD		
50m				AD	
100m		AD			
200m				AD	
500m		AD			
1000m					AD
2000m					AD

Table 20 Optimal theoretical model using Anderson Darling test for SWS LS in winter from 1960 to 2017

Temperature Data	Weibull	Lognormal	Gamma	Beta	NP
10m		AD			
25m				AD	
50m		AD			
100m					AD
200m					AD
500m	AD				
1000m	AD				
2000m				AD	

Table 21 Optimal theoretical model using Anderson Darling test for SWT LS in spring from 1960 to 2017

Salinity Data	Weibull	Lognormal	Gamma	Beta	NP
10m					AD
25m			AD		
50m				AD	
100m			AD		
200m				AD	
500m					AD
1000m					AD
2000m		AD			

Table 22 Optimal theoretical model using Anderson Darling test for SWS LS in spring from 1960 to 2017

Temperature Data	Weibull	Lognormal	Gamma	Beta	NP
10m	AD				
25m	AD				
50m		AD			
100m		AD			
200m					AD
500m	AD				
1000m	AD				
2000m		AD			

Table 23 Optimal theoretical model using Anderson Darling test for SWT LS in summer from 1960 to 2017

Salinity Data	Weibull	Lognormal	Gamma	Beta	NP
10m				AD	
25m		AD			
50m		AD			
100m				AD	
200m					AD
500m					AD
1000m					AD
2000m					AD

Table 24 Optimal theoretical model using Anderson Darling test for SWS LS in summer from 1960 to 2017

Temperature Data	Weibull	Lognormal	Gamma	Beta	NP
10m	AD				
25m	AD				
50m				AD	
100m		AD			
200m					AD
500m	AD				
1000m	AD				
2000m	AD				

Table 25 Optimal theoretical model using Anderson Darling test for SWT LS in fall from 1960 to 2017

Salinity Data	Weibull	Lognormal	Gamma	Beta	NP
10m	AD				
25m	AD				
50m		AD			
100m				AD	
200m				AD	
500m					AD
1000m					AD
2000m		AD			

Table 26 Optimal theoretical model using Anderson Darling test for SWS LS in fall from 1960 to 2017

Temperature Data	Weibull	Lognormal	Gamma	Beta	NP
10m		AIC			
25m				AIC	
50m				AIC	
100m		AIC			
200m					
500m		AIC			
1000m		AIC			
2000m		AIC			

Table 27 Optimal theoretical using Akaike measurement model for SWT LS in winter from 1960 to 2017

Salinity Data	Weibull	Lognormal	Gamma	Beta	NP
10m				AIC	
25m				AIC	
50m		AIC			
100m		AIC			
200m			AIC	AIC	
500m		AIC			
1000m					
2000m					

Table 28 Optimal using Akaike measurement theoretical model for SWS LS in winter from 1960 to 2017

Temperature Data	Weibull	Lognormal	Gamma	Beta	NP
10m		AIC			
25m				AIC	
50m				AIC	
100m					
200m					
500m		AIC			
1000m		AIC			
2000m		AIC			

Table 29 Optimal theoretical using Akaike measurement model for SWT LS in spring from 1960 to 2017

Salinity Data	Weibull	Lognormal	Gamma	Beta	NP
10m					
25m				AIC	
50m				AIC	
100m				AIC	
200m				AIC	
500m					
1000m					
2000m		AIC			

Table 30 Optimal theoretical using Akaike measurement model for SWS LS in spring from 1960 to 2017

Temperature Data	Weibull	Lognormal	Gamma	Beta	NP
10m	AIC				
25m	AIC				
50m		AIC			
100m		AIC			
200m					
500m		AIC			
1000m		AIC			
2000m		AIC			

Table 31 Optimal theoretical model using Akaike measurement for SWT LS in summer from 1960 to 2017

Salinity Data	Weibull	Lognormal	Gamma	Beta	NP
10m	AIC				
25m				AIC	
50m		AIC			
100m				AIC	
200m				AIC	
500m					
1000m					
2000m		AIC			

Table 32 Optimal theoretical model using Akaike measurement for SWS LS in summer from 1960 to 2017

Temperature Data	Weibull	Lognormal	Gamma	Beta	NP
10m	AIC				
25m	AIC				
50m				AIC	
100m		AIC			
200m					
500m		AIC			
1000m		AIC			
2000m		AIC			

Table 33 Optimal theoretical model using Akaike measurement for SWT LS in fall from 1960 to 2017

Salinity Data	Weibull	Lognormal	Gamma	Beta	NP
10m	AIC				
25m				AIC	
50m		AIC			
100m				AIC	
200m				AIC	
500m					
1000m					
2000m		AIC			

Table 34 Optimal theoretical model using Akaike measurement for SWS LS in fall from 1960 to 2017

Our results indicate that approximatively 25% of the layers have non-parametric distributions for SWT and SWS which would require further analysis. Theoretical lognormal distribution has the highest ration of the goodness of fit according to the AIC, where 12 out of 13 results are confirmed. Lognormal distribution is followed closely by the beta distribution with a ratio of 11 to 15. Weibull is only ascertained for 5 out of 16 AD outcomes. Meanwhile, gamma distribution is not established for any layer with a 0 to 4 ratio, meaning that it can most likely be discarded in any further attempt.

Of note is SWS 200m layers in winter which gave identical results, with both gamma and beta showing the lowest results, ergo potentially confirming beta as the right model between the available options. SWT seems to conform majorly to a lognormal, secondly Weibull distribution and few instances of beta distribution. On the other hand, SWS is mostly compliant with beta distribution, followed by lognormal and few instances of Weibull.

SWT lognormal distribution is valid for 10m in three seasons, 50m in two seasons, 100m in two seasons and for all seasons at 500m, 1000 and 2000m layers. Meanwhile, SWS beta distribution is applicable for 10m in two seasons, 25m in three seasons, 50m for two seasons, 100m for three seasons and 200m for three seasons. The 500 and lower layers for SWS are non-parametric.

The previous results are expected as SWS is measured a ration between 0 and 1, which are expected to display a beta distribution mostly. SWT is a value theoretically unbound, and such a spread conforms to a lognormal distribution. As seen in the distribution plots in appendix A, SWT and SWT show a non-monotonic distribution. Apart from a lognormal distribution, every other model we test has monotonic variants, but in our case, they are in a non-monotonic form.

6.2 Regression Analysis

The seasonal theoretical model of the data at different depth levels have been established in Section 5.6.6. Knowing that SWT has a lognormal distribution while SWS appears to be a beta distribution, we attempted to build a regression model using those two parameters generated using predicted values to evaluate the impact of latitude, longitude and the effects of SWT on SWS and vice versa. Boxplots for SWT and SWS seasonally per depth and outlier values per season are presented from Figure 86 to Figure 93.

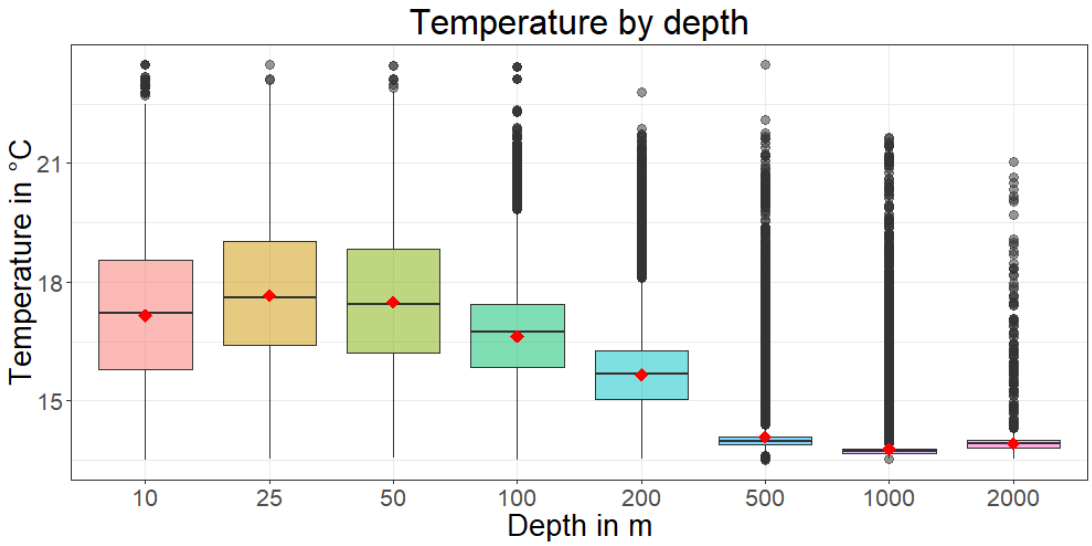

Figure 86 Winter SWT boxplot per depth

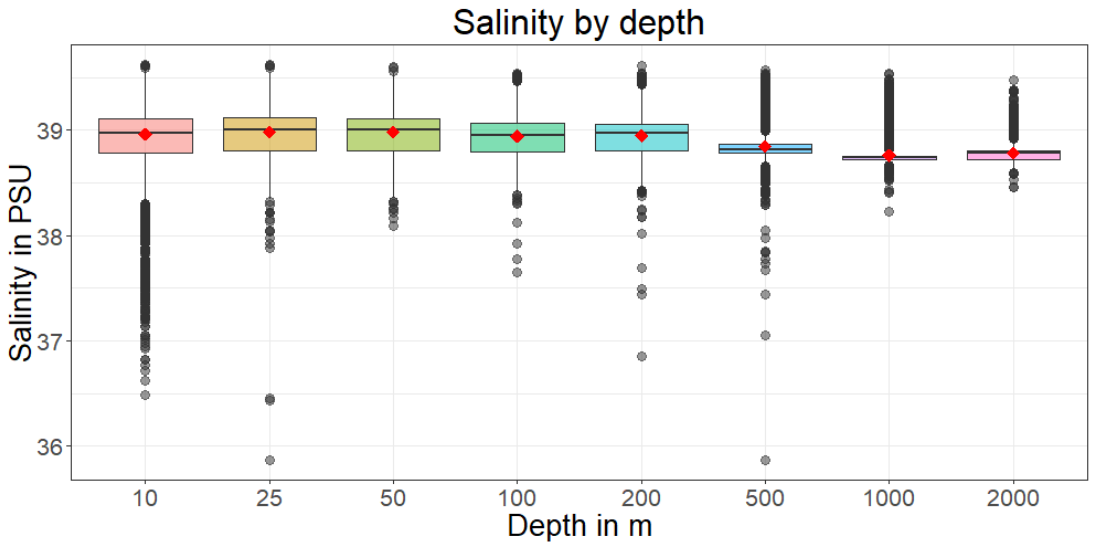

Figure 87 Winter SWS boxplot per depth

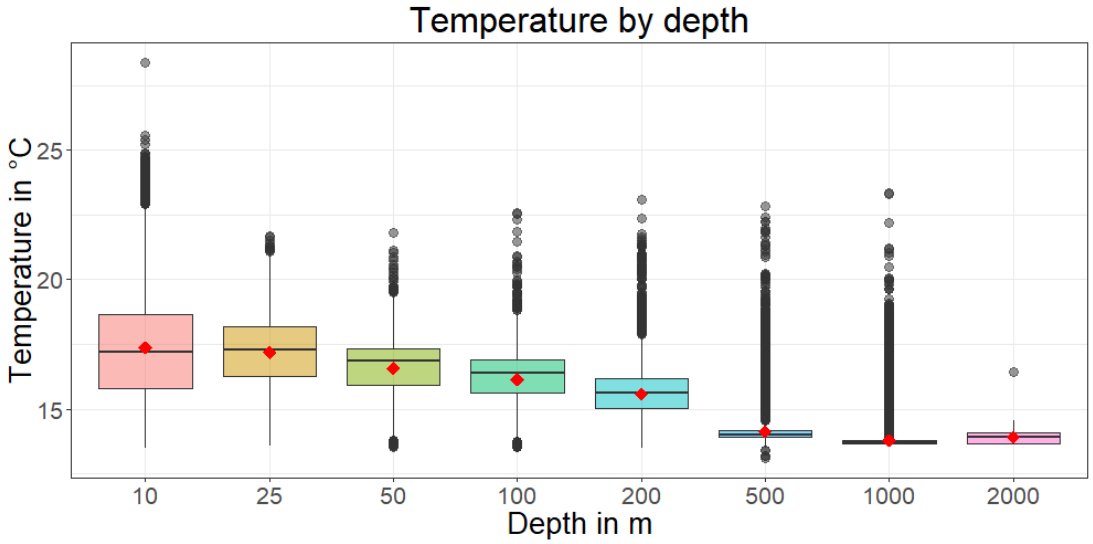

Figure 88 Spring SWT boxplot per depth

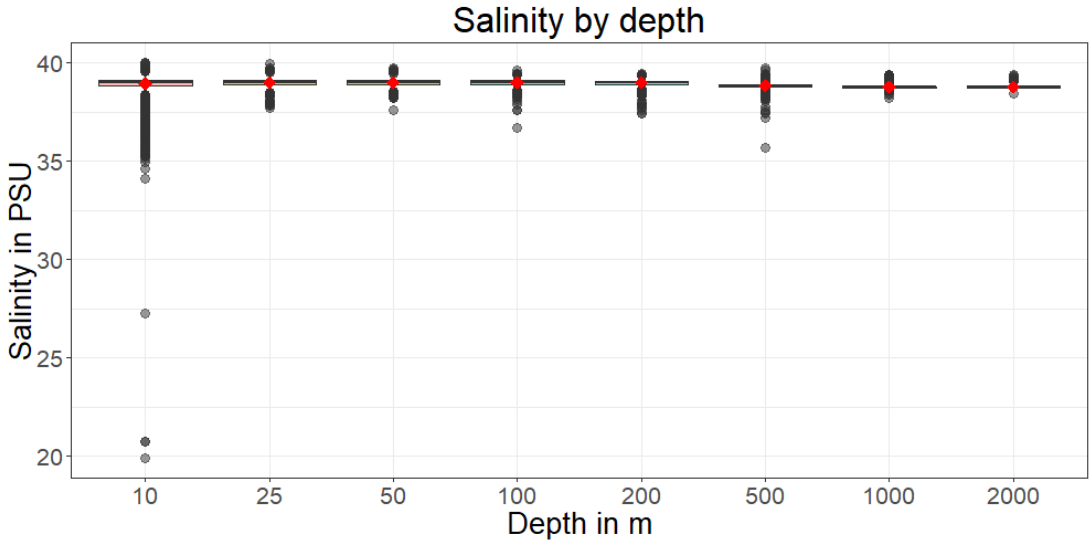

Figure 89 Spring SWS boxplot per depth

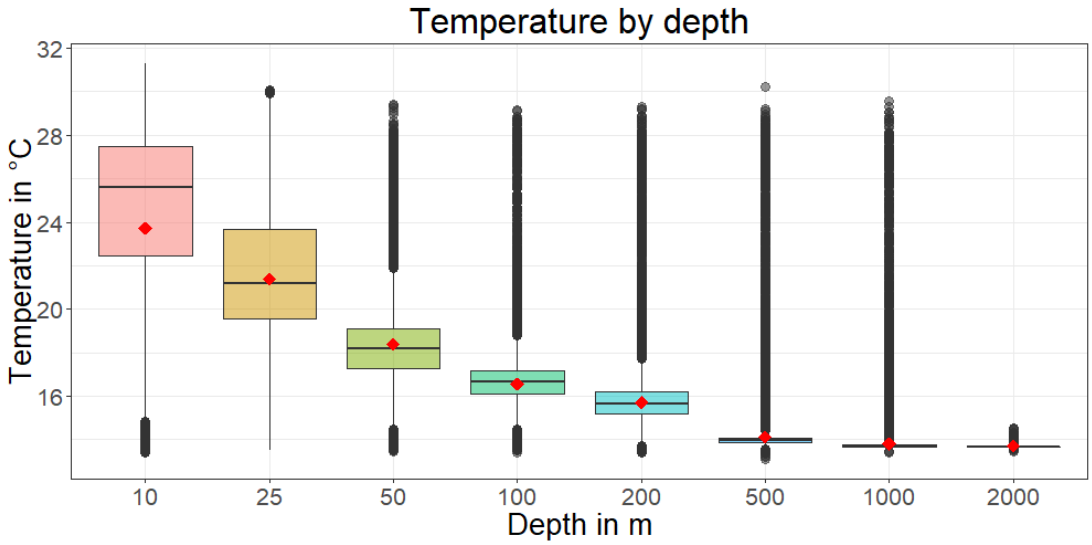

Figure 90 Summer SWT boxplot per depth

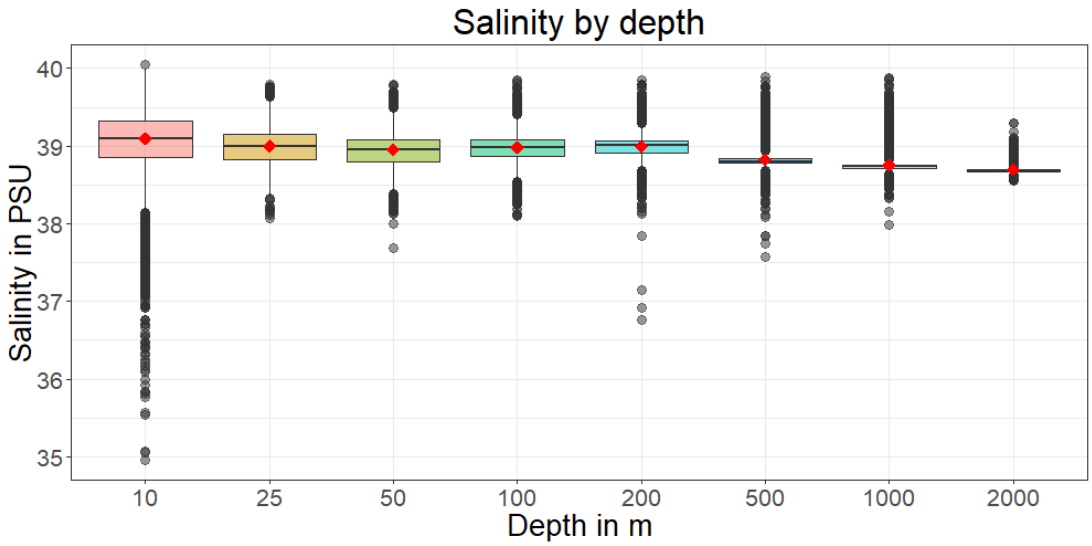

Figure 91 Summer SWS boxplot per depth

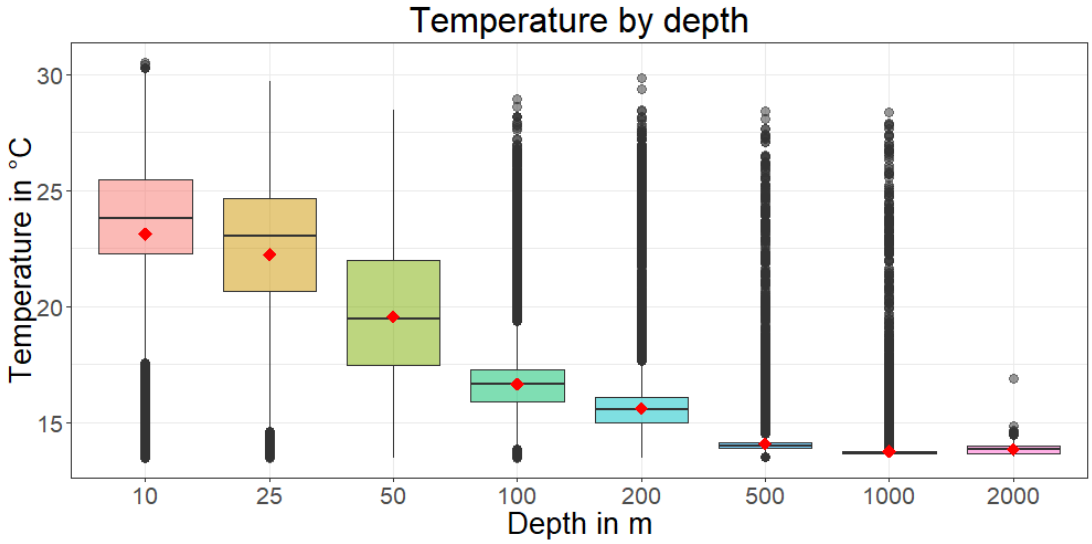

Figure 92 Fall SWT boxplot per depth

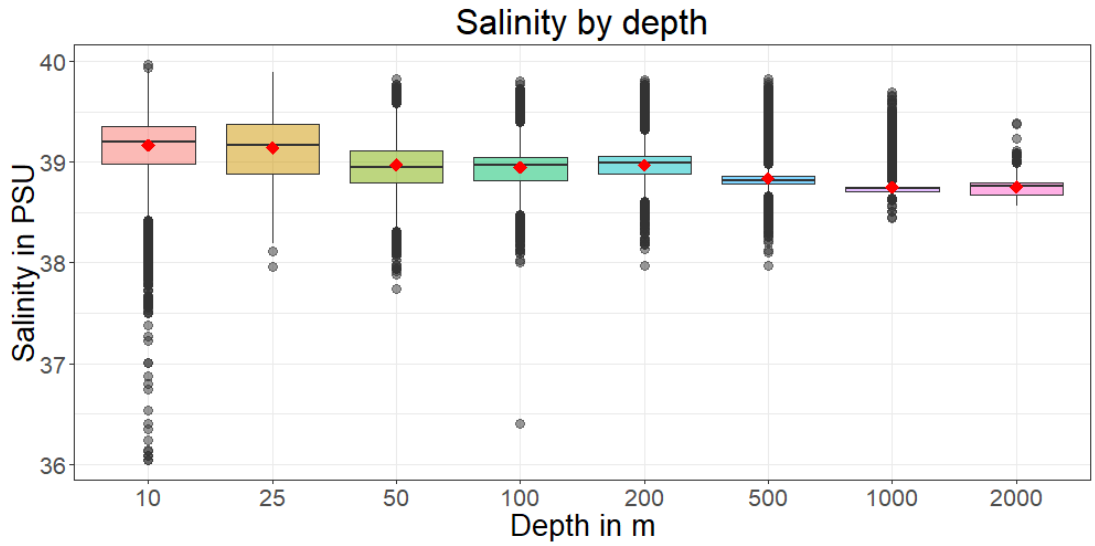

Figure 93 Fall SWS boxplot per depth

The boxplots show interestingly higher SWT values at 25m and 50m in winter (Figure 84) compared to the surface, most likely a result of the faster cooling due to the interaction with the colder atmospheric temperature in winter. SWT otherwise follows the expected pattern of dropping the deeper we go. Due to the nature of SWS, noticing minute changes is difficult, but during the transitional seasons of summer and winter, there is more variability compared to the relatively stable results obtained in spring.

During the computing process, some aspects of the data became apparent, making it impossible to do regression analysis using exogenous (i.e. predicted) variables for SWT and SWS. The way the data is sampled creates clusters that are densely condensed both in time and space compared to the total area we are working with. This clustering results in very similar groups of values, especially for SWS. Moreover, due to the nature of beta distribution using all the available data combined with the property mentioned above makes the regression not converge during computation resulting in a crash. We needed to take only a portion of the data available at all depth ranges analysed to look at the results, and we noticed an increase in conversion rates if the total number of data is higher, yet even at the maximum sample size selected, 15,000, the model does not converge for around 50% of the regression attempts. By extension, as predicted, if SWS values cannot be

obtained, it is not possible to acquire lognormal regression results for SWT. All the factors mentioned above give us a clear picture that we have data that is ill-suited, meaning that the sampling process is exceptionally uneven. We had identified this phenomenon while examining our sub-regions and confirmed in our attempt to conduct a regression analysis using exogenous variables taking advantage of the beta and lognormal models.

Fortunately, due to the size of our dataset, the distributions can both be taken as normal meaning that we can attempt a linear regression. We first did a regression analysis using empirical SWT and SWS values. Using ordinary least squared method, we can obtain predicted SWT and SWS values to mitigate the endogeneity and accomplish and exogenous linear regression by replacing SWT and SWS values with the predicted ones. We compare the evolution of SWT for latitude, longitude and depth for SWT in Table 35 while Table 36 summarises the results for latitude, longitude and depth for SWS.

Seasonal Temperature	Latitude	Longitude	10m	25m	50m	100m	200m	500m	1000m	2000m
Winter	+	-	-	+	+	-	-	-	-	-
Spring	+	-	-	-	-	-	-	-	-	-
Summer	+	-	-	-	-	-	-	-	-	-
Fall	+	-	-	-	-	-	-	-	-	-

Table 35 Linear regression for SWT using empirical data in LS from 1960 to 2017

Per our knowledge, LS becomes warmer as longitude increases, meaning we go further east which is not the case for our results. Meanwhile, higher latitude results in lower SWT values, which is equivalent to going east. These are in direct opposition of your knowledge of the area and are likely the result of our the two spatial variables do not take into account depth. The deeper we go, the more SWT drops except for winter, which is most likely the result of the interaction between the sea surface and the cooler atmosphere, leaving the intermediary region between 25m and 50m at a higher SWT than the rest of the water mass.

Season Salinity	Latitude	Longitude	10m	25m	50m	100m	200m	500m	1000m	2000m
Winter	+	+	+	+	+	-	-	-	-	-
Spring	-	+	+	+	+	+	+	-	-	-
Summer	+	+	+	-	-	-	-	-	-	-
Fall	+	+	+	-	-	-	-	-	-	-

Table 36 Linear regression for SWS using empirical data in LS from 1960 to 2017

SWS increases as we go further north except for spring when most of the LS show similar temperature values as seen in our climatological maps in Section 5.1.2. An interesting point is the higher values for SWS as we go east, which was an expected result. The latitude does not account for depth, so this might be the result of interactions in LIW and EMDW. The sinking of the LSW and MAW to form the LIW during the colder winter and spring seasons explains the higher SWS in 25m to 200m range.

Using our predicted values to eliminate endogeneity, we obtained the following results for our linear regression analysis using predicted SWT and SWS. The results are summarised in Table 37 and 38.

Seasonal Temperature	Latitude	Longitude	Predicted SWS
Winter	+	-	+
Spring	+	-	+
Summer	+	-	+
Fall	-	-	-

Table 37 Exogenous seasonal linear regression for SWT using predicted SWS in LS from 1960 to 2017

Except for fall, the latitude corresponds to those found in the second-stage linear regression with an increase in temperature when moving eastward. In the case of the fall seasons, the higher average temperature during this period across the entire LS renders the impact of latitude less significant. Longitude shows the same result as first stage regression. Higher predicted SWS, most likely resulting from more significant evaporation, can be directly linked to SWT.

Seasonal Salinity	Latitude	Longitude	Predicted SWT
Winter	-	+	+
Spring	-	+	+
Summer	+	+	+
Fall	+	+	+

Table 38 Exogenous seasonal linear regression for SWS using predicted SWT in LS from 1960 to 2017

As we go east, SWS increases during summer and fall as expected, during spring and winter SWS normalises across the LS as shown in our climatological maps in Section 5.1.2. Going north SWS increases, and it should be noted that the regression is for all data points and not only the surface, so further study is required to give a conclusive explanation to this phenomenon. It might be due to the properties of the LIW and EMDW, but this is only a speculative hypothesis. Increased predicted SWT automatically results in higher SWS, which is entirely within our expectations, knowing that evaporation plays a part in the SWS.

CHAPTER 7

THESIS CONCLUSION

This thesis investigated the in-situ data available in LS between 1960 and 2017, for a total number of 81,317 stations and 10,590,891 individual entries. We gave a three-dimensional spatial definition for the LS and sub-regions accompanied by their distinctive quality and significance to the larger Mediterranean Sea. The traditional methods for both in-situ and remote data collection are described to establish the origin of our data and the distribution infrastructure available to researchers. The "Mediterranean Sea - Temperature and Salinity Historical Data Collection SeaDataCloud V1" aggregated dataset is presented, and we elaborated upon the taken steps to transform it into an appropriate format allowing a better descriptive analysis. QC procedures and international standards for data quality and health followed for are summarised.

The boundaries of our sub-regions are delimited with climatological maps for SWT and SWS obtained in ODV with DIVA algorithm using our primary dataset and supported by isothermal SST temperature maps employing WOA18 data for LS. Moreover, the resulting maps provided more insights into the water properties of the region, demonstrating certain distinct constants of the EM such as the markedly cooler RG in almost all months and the west-east gradient of SWT and SWS. Clustering using the CLARA algorithm is applied to justify our study area by comparing the clusters with the selected sub-basins spatial coordinates, further demonstrating common seawater properties shared regionally at the sea surface and the amorphous shape of the sub-regions. There are overlaps between LB, CND and CB, an expected outcome considering their adjacent locations.

We examined the histograms for the three time ranges to determine the peak points in data collection activities. Certain events are noticeable by sudden drops, such as the Cyprus conflict in 1974, or increase as in the case of the POEM and GOIN research projects between 1985 and 1995. The ratio of missing data before and after 1980 shows a significant difference, rising from 0% to 7% for SWT and 7% to 27% for SWS. The absent entries are completed applying chained equation, and the resulting analysis did not demonstrate any significant differences, even in the case of SWS at 27%, through descriptive analysis except for smoother plots. Comparing the monthly mean SWT and SWS values prior and post 1980 it is discernible that average values are higher in the later period, sometimes as much as 5°C difference in peak SWT in August at the surface layer. The lower mean values get drowned in the combined 1960-2017 dataset, representing less than 1% of the total volume of data.

According to our descriptive analysis, the most studied region is LS, followed by RG. Meanwhile, the least explored areas are the CB and CND. The CB and LB show consistently higher SWT, especially at the surface layers with substantial seasonal variability and overall higher SWS compared to LS. On the other hand, the RG in almost all seasons is considerably colder than LS and displays presumably the EMT phenomenon. Across the board, SWT normalises at the 500m mark for all sub-regions and no longer show any seasonality. In all regions at a glance, the yearly plots seem to indicate an upward trend in both SWT and SWS. The distribution pattern of the data for SWT and SWS obtained using density plots is bimodal at the surface before taking a mounded appearance around 200m to 500m. SWS density is also bimodal at the 2000m layer, most likely an outcome of the EMT creating denser waters resulting in a bias in the density plot.

Cullen & Frey plots are used to identify the most fitting theoretical distribution models are performed. Also, empirical and theoretical CDF plots are created to visualise potential distribution models. Moreover, AD test supported by AIC measurements to determine the robustness of our theoretical model selections are computed. We identified lognormal distribution as the most significantly compliant with the empirical distribution of SWT data. We concluded that the beta distribution

is the best fit for SWS at the surface layers, but once we descend into the lower layers, the distribution becomes non-parametric, indicating that further analysis should be conducted in those depths. SWT and SWS are identified as definitely non-monotonic comparing our theoretical results with the empirical density plots rather than monotonic at all depth levels.

Furthermore, we applied a regression analysis to our dataset. Bearing in mind that SWT follows a lognormal distribution and SWS a beta distribution, regression using the two methods were attempted. To eliminate bias, predicted values were used for SWT and SWS. The analysis showcased that our data were ill-suited due to the distribution bias, with the sampling of the seawater resulting in clusters of very similar data preventing the conversion of the regression analysis, especially concerning SWS. It should be noted that increasing the number of tested values at each layer increase the probability of conversion slightly, but the limit was approximately 50% at 15,000 entries per depth level. Fortunately, the size of the data allowed us to treat it as if it follows a normal distribution. Once again, to prevent bias due to the similar values, which are consequences of temporally sparse and spatially limited sampling pattern, predicted SWT and SWS were used instead of the empirical observations to reduce bias. The results were within our expectation except for SWT decreasing the further east we moved, potentially an outcome of the fact that the analysis does not account for the depth indicating that the LIW and EMDW might have variable SWT at deeper layers compared to the assumed more homogenous distribution and require further study, it can also be the result of the more numerous data points in the lower layers.

In the future, we suggest that additional investigations should be conducted based on our descriptive statistical analysis and regression analysis to forecast and model the evolution of SWT and SWS in the region. The expected changes in the freshwater input due to the GERD on the Nile and increased water use in the rivers flowing to CB will most likely result in a change in the water properties and the ecosystem of the EM and by extension the entire Mediterranean Sea. Moreover, the controversial Akkuyu Nuclear Power Plant project presents unforeseen threats for the region. The

lack of data in particular sub-regions, such as CB and CND and the clustered nature of the data which is spatially restricted and temporally sparse, indicate the necessity for additional scientific expeditions from research institutions to accurately document and predict the upcoming changes in the physical properties of LS. Additionally, other variables than SWT and SWS should be studied and quantified for a better picture of the region. Such an undertaking requires the parties having a stake in the region to look past their differences to achieve sustainable development in this coveted and troubled geography.

REFERENCES

[1] Lima, F. P., & Wethey, D. S. (2012). Three decades of high-resolution coastal sea surface temperatures reveal more than warming. *Nature communications*, *3*, 704. DOI: 10.1038/ncomms1713

[2] Pachauri, R. K., Allen, M. R., Barros, V. R., Broome, J., Cramer, W., Christ, R., ... & Dubash, N. K. (2014). *Climate change 2014: synthesis report. Contribution of Working Groups I, II and III to the fifth assessment report of the Intergovernmental Panel on Climate Change* (p. 151). Ipcc.

[3] Change, I. C. (2013). The Physical Science Basis. Contribution of Working Group I to the Fifth Assessment Report of the Intergovernmental Panel on Climate Change. 2013. *There is no corresponding record for this reference.[Google Scholar]*, 33-118. DOI: 10.1017/CBO9781107415324

[4] Oliver, E. C., Donat, M. G., Burrows, M. T., Moore, P. J., Smale, D. A., Alexander, L. V., ... & Holbrook, N. J. (2018). Longer and more frequent marine heatwaves over the past century. *Nature communications*, *9*(1), 1324. DOI: 10.1038/s41467-018-03732-9

[5] Robinson, A. R., Leslie, W. G., Theocharis, A., & Lascaratos, A. (2001). Mediterranean sea circulation. *Ocean currents*, *1*, 19. DOI: 10.1006/rwos.2001.0376

[6] Rohling, E. J., & Bryden, H. L. (1992). Man-induced salinity and temperature increases in Western Mediterranean Deep Water. *Journal of Geophysical Research: Oceans*, *97*(C7), 11191-11198. DOI: 10.1029/92JC00767

[7] Giorgi, F. (2006). Climate change hot-spots. *Geophysical research letters*, *33*(8). DOI: 10.1029/2006GL025734

[8] Bethoux, J. P. (1979). Budgets of the Mediterranean Sea- Their dependance on the local climate and on the characteristics of the Atlantic waters. *Oceanologica acta*, *2*, 157-163.

[9] Bryden, H. L., & Kinder, T. H. (1991). Steady two-layer exchange through the Strait of Gibraltar. *Deep Sea Research Part A. Oceanographic Research Papers*, *38*, S445-S463. DOI: 10.1016/S0198-0149(12)80020-3

[10] Bunker, A. F., Charnock, H., & Goldsmith, R. A. (1982). A note on the heat balance of the Mediterranean and Red Seas. *J. Mar. Res*, *40*, 73-84.

[11] Lejeusne, C., Chevaldonné, P., Pergent-Martini, C., Boudouresque, C. F., & Pérez, T. (2010). Climate change effects on a miniature ocean: the highly diverse, highly impacted Mediterranean Sea. *Trends in ecology & evolution*, *25*(4), 250-260. DOI: 10.1016/j.tree.2009.10.009

[12] Lozier, M. S., Owens, W. B., & Curry, R. G. (1995). The climatology of the North Atlantic. *Progress in Oceanography*, *36*(1), 1-44.

[13] Béthoux, J. P., Gentili, B., & Tailliez, D. (1998). Warming and freshwater budget change in the Mediterranean since the 1940s, their possible relation to the greenhouse effect. *Geophysical Research Letters*, *25*(7), 1023-1026.

[14] Rahmstorf, S. (1998). Influence of Mediterranean outflow on climate. *Eos, Transactions American Geophysical Union*, *79*(24), 281-282.

[15] Raitsos, D. E., Beaugrand, G., Georgopoulos, D., Zenetos, A., Pancucci-Papadopoulou, A. M., Theocharis, A., & Papathanassiou, E. (2010). Global climate change amplifies the entry of tropical species into the Eastern Mediterranean Sea. *Limnology and Oceanography*, *55*(4), 1478-1484.

[16] Schmidt, C., Morard, R., Almogi-Labin, A., Weinmann, A. E., Titelboim, D., Abramovich, S., & Kucera, M. (2015). Recent invasion of the symbiont-bearing foraminifera Pararotalia into the Eastern Mediterranean facilitated by the ongoing warming trend. *PLoS One*, *10*(8), e0132917.

[17] Myers, N., Mittermeier, R. A., Mittermeier, C. G., Da Fonseca, G. A., & Kent, J. (2000). Biodiversity hotspots for conservation priorities. *Nature*, *403*(6772), 853. DOI: 10.1038/35002501

[18] Tanhua, T., Hainbucher, D., Schroeder, K., Cardin, V., Álvarez, M., & Civitarese, G. (2013). The Mediterranean Sea system: a review and an introduction to the special issue. *Ocean Science*, *9*(5), 789-803. DOI: 10.5194/os-9-789-2013

[19] Gertman, I., & Hecht, A. (2002). Annual and long-term changes in the salinity and the temperature of the waters of the South-eastern Levantine Basin. *CIESM Work Ser*, *16*.

[20] European Marine Spatial Platform, https://www.msp-platform.eu/sea-basins/east-mediterranean (Last Accessed 06/06/2019)

[21] Bean, G., & Mitchell, S. (2015, December 22). Cilicia. *Oxford Classical Dictionary*. Retrieved 15 Jul. 2019, from https://oxfordre.com/classics/view/10.1093/acrefore/9780199381135.001.0001/acrefore-9780199381135-e-1572 DOI: 10.1093/acrefore/9780199381135.013.1572

[22] Özsoy, E., & Sözer, A. (2006). Forecasting circulation in the Cilician Basin of the Levantine Sea. *Ocean Science Discussions*, *3*(5), 1481-1514.

[23] Robinson, A. R., Malanotte-Rizzoli, P., Hecht, A., Michelato, A., Roether, W., Theocharis, A., ... & Bishop, J. (1992). General circulation of the Eastern Mediterranean. *Earth-Science Reviews*, *32*(4), 285-309. DOI: 10.1016/0012-8252(92)90002-B

[24] Özsoy, E., Hecht, A., Ünlüata, Ü., Brenner, S., Sur, H. I., Bishop, J., ... & Oğuz, T. (1993). A synthesis of the Levantine Basin circulation and hydrography, 1985–1990. *Deep sea research part II: topical studies in oceanography*, *40*(6), 1075-1119. DOI: 10.1016/0967-0645(93)90063-S

[25] Lehner, B., Verdin, K., & Jarvis, A. (2008). New global hydrography derived from spaceborne elevation data. *Eos, Transactions American Geophysical Union*, *89*(10), 93-94. DOI: 10.1029/2008EO100001

[26] Bonacci, O. (2002). From conflict to co-operation in international water resources management: challenges and opportunities. *Hrvatska Vodoprivreda*, *11*(121-122), 20-21.

[27] Hamza, W., Ennet, P., Tamsalu, R., & Zalesny, V. (2003). The 3D physical-biological model study in the Egyptian Mediterranean coastal sea. *Aquatic Ecology*, *37*(3), 307-324. DOI: 10.1023/A:1025836929341

[28] Pinardi, N., Arneri, E., Crise, A., Ravaioli, M., & Zavatarelli, M. (2006). The physical, sedimentary and ecological structure and variability of shelf areas in the Mediterranean sea (27). *The sea*, *14*, 1243-330.

[29] Struglia, M. V., Mariotti, A., & Filograsso, A. (2004). River discharge into the Mediterranean Sea: climatology and aspects of the observed variability. *Journal of Climate*, *17*(24), 4740-4751. DOI: 10.1175/JCLI-3225.1

[30] Aydın, C., Güven, O., Salihoğlu, B., & Kıdeyş, A. E. (2016). The influence of land use on coastal litter: An approach to identify abundance and sources in the coastal area of Cilician Basin, Turkey. *Turkish Journal of Fisheries and Aquatic Sciences*, *16*(1), 029-039. DOI: 10.4194/1303-2712-v16_1_04

[31] Schenk, C. J., Kirschbaum, M. A., Charpentier, R. R., Klett, T. R., Brownfield, M. E., Pitman, J. K., ... & Tennyson, M. E. (2010). Assessment of undiscovered oil and gas resources of the Levant Basin Province, Eastern Mediterranean. *US Geological Survey Fact Sheet*, *3014*(4).

[32] Bornstein, R. (2018). EASTERN MEDITERRANEAN REGIONAL DYNAMICS: CONFLICTS AND OPPORTUNITIES FOR CONFLICT RESOLUTION SUPPORT.

[33] Zhukov, Y. M. (2013). Trouble in the eastern Mediterranean Sea: The coming dash for gas. *Foreign Affairs*.

[34] Sharaf El Din, S. H. (1977). Effect of the Aswan High Dam on the Nile flood and on the estuarine and coastal circulation pattern along the Mediterranean Egyptian coast. *Limnology and Oceanography*, *22*(2), 194-207. DOI: 10.4319/lo.1977.22.2.0194

[35] Darwish, K., Smith, S. E., Torab, M., Monsef, H., & Hussein, O. (2016). Geomorphological changes along the Nile Delta coastline between 1945 and 2015 detected using satellite remote sensing and GIS. *Journal of Coastal Research*, *33*(4), 786-794. DOI: 10.2112/JCOASTRES-D-16-00056.1

[36] Nixon, S. W. (2004). The Artificial Nile: the Aswan High Dam blocked and diverted nutrients and destroyed a Mediterranean fishery, but human activities may have revived it. *American Scientist*, *92*(2), 158-165.

[37] Nixon, S. W. (2003). Replacing the Nile: are anthropogenic nutrients providing the fertility once brought to the Mediterranean by a great river?. *AMBIO: A journal of the human environment*, *32*(1), 30-40. DOI: 10.1579/0044-7447-32.1.30

[38] Ethiopia – News, Research and Analysis – The Conversation .... http://theconversation.com/nz/topics/ethiopia-2730 (Last Accessed 16/07/2019)

[39] Milliff, R. F., & Robinson, A. R. (1992). Structure and dynamics of the Rhodes gyre system and dynamical interpolation for estimates of the mesoscale variability. *Journal of Physical Oceanography*, *22*(4), 317-337. DOI: 10.1016/0012-8252(92)90002-B

[40] Notarbartolo di Sciara, G., & Bearzi, G. (2010). National Strategy and Action Plan for the conservation of cetaceans in Greece, 2010-2015. *Initiative for the Conservation of Cetaceans in Greece, Athens*. DOI: 10.13140/RG.2.2.36302.97600

[41] Lascaratos, A., Williams, R. G., & Tragou, E. (1993). A mixed-layer study of the formation of Levantine Intermediate Water. *Journal of Geophysical Research: Oceans*, *98*(C8), 14739-14749. DOI 10.1029/93JC00912

[42] Lascaratos, A., & Nittis, K. (1998). A high-resolution three-dimensional numerical study of intermediate water formation in the Levantine Sea. *Journal of Geophysical Research: Oceans*, *103*(C9), 18497-18511. DOI: 10.1029/98JC01196

[43] Marullo, S., Napolitano, E., Santoleri, R., Manca, B., & Evans, R. (2003). Variability of rhodes and Ierapetra gyres during Levantine intermediate water experiment: Observations and model results. *Journal of Geophysical Research: Oceans*, *108*(C9). DOI: 10.1029/2002JC001393

[44] Schlitzer, R., Ocean Data View, odv.awi.de, 2018, Last Accessed (06/06/2019)

[45] Rayner, N. A., Brohan, P., Parker, D. E., Folland, C. K., Kennedy, J. J., Vanicek, M., ... & Tett, S. F. B. (2006). Improved analyses of changes and uncertainties in sea surface temperature measured in situ since the mid-nineteenth century: The HadSST2 dataset. *Journal of Climate*, *19*(3), 446-469. DOI: 10.1175/JCLI3637.1

[46] Bahamon, N., Aguzzi, J., Bernardello, R., Ahumada-Sempoal, M. A., Puigdefabregas, J., Cateura, J., ... & Cruzado, A. (2011). The new pelagic Operational Observatory of the Catalan Sea (OOCS) for the multisensor coordinated measurement of atmospheric and oceanographic conditions. *Sensors*, *11*(12), 11251-11272. DOI: 10.3390/s111211251

[47] Isa, K., & Arshad, M. R. (2015). Experimental analysis of homeostatic-inspired motion controller for a hybrid-driven autonomous underwater glider. *Jurnal Teknologi*, *74*(9). DOI: 10.11113/jt.v74.4808

[48] SeaDataCloud,. https://www.seadatanet.org/, Last Accessed (07/06/2019)

[49] Sextant catalogue that contains the dataset “Mediterranean Sea - Temperature and salinity Historical Data Collection SeaDataCloud V1”,

https://sextant.ifremer.fr/eng/Donnees/Catalogue#/metadata/2698a37e-c78b-4f78-be0b-ec536c4cb4b3, Last Accessed (06/06/2019)

[50] SeaDataNet Data Quality Control Procedures V2.0 https://www.seadatanet.org/content/download/596/3118/file/SeaDataNet_QC_procedures_V2_%28May_2010%29.pdf?version=1, Last Accessed (07/06/2019)

[51] Wijffels, S. E., Willis, J., Domingues, C. M., Barker, P., White, N. J., Gronell, A., ... & Church, J. A. (2008). Changing expendable bathythermograph fall rates and their impact on estimates of thermosteric sea level rise. *Journal of Climate*, *21*(21), 5657-5672. DOI: 10.1175/2008JCLI2290.1

[52] National Oceanic and Atmospheric Administration XBT correction, https://www.nodc.noaa.gov/OC5/SELECT/dbsearch/xbt_bias_info.html (Last Accessed 10/06/2019)

[53] Iona, A., Theodorou, A., Watelet, S., Troupin, C., Beckers, J. M., & Simoncelli, S. (2018). Mediterranean Sea Hydrographic Atlas: towards optimal data analysis by including time-dependent statistical parameters. *Earth System Science Data*. DOI: 10.5194/essd-2018-9

[54] Mikhaĭlov, N. N., Levitus, S., & Tatusko, R. (2002). Russian marine expeditionary investigations of the world ocean.

[55] Ovchinnikov, I. M. (1966). CIRCULATION IN SURFACE AND INTERMEDIATE LAYERSOF MEDITERRANEAN. *OCEANOLOGY-USSR*, *6*(1), 48-+.

[56] Nielsen, J. N. (1912). *Hydrography of the Mediterranean and adjacent waters*.

[57] Ovchinnikov, I. M., & Plakhin, E. (1976). Hydrology of the Mediterranean Sea. *Gidrometeoizdat, Leningrad(USSR), 1976, 375*.

[58] Hecht, A., & Gertman, I. (2001). Physical features of the eastern Mediterranean resulting from the integration of POEM data with Russian Mediterranean cruises.

Deep Sea Research Part I: Oceanographic Research Papers, *48*(8), 1847-1876. DOI: 10.1016/S0967-0637(00)00113-8

[59] Özsoy, E., Hecht, A., & Ünlüata, Ü. (1989). Circulation and hydrography of the Levantine Basin. Results of POEM coordinated experiments 1985–1986. *Progress in Oceanography*, *22*(2), 125-170. DOI: 10.1016/0079-6611(89)90004-9

[60] Özsoy, E., Hecht, A., Ünlüata, Ü., Brenner, S., Oğuz, T., Bishop, J., ... & Rozentraub, Z. (1991). A review of the Levantine Basin circulation and its variability during 1985–1988. *Dynamics of Atmospheres and Oceans*, *15*(3-5), 421-456. DOI: 10.1016/0377-0265(91)90027-D

[61] MALANOTTE, P. (1988). Large-scale properties. *Oceanol. Acta*, *11*(4), 323-335.

[62] Robinson, A. R., Golnaraghi, M., Leslie, W. G., Artegiani, A., Hecht, A., Lazzoni, E., ... & Ünlüata, Ü. (1991). The eastern Mediterranean general circulation: features, structure and variability. *Dynamics of Atmospheres and Oceans*, *15*(3-5), 215-240. DOI: 10.1016/0377-0265(91)90021-7

[63] Malanotte-Rizzoli, P., Manca, B. B., d'Alcalà, M. R., Theocharis, A., Bergamasco, A., Bregant, D., ... & Sansone, E. (1997). A synthesis of the Ionian Sea hydrography, circulation and water mass pathways during POEM-Phase I. *Progress in Oceanography*, *39*(3), 153-204. DOI: 10.1016/S0079-6611(97)00013-X

[64] Klein, B., Roether, W., Manca, B. B., Bregant, D., Beitzel, V., Kovacevic, V., & Luchetta, A. (1999). The large deep water transient in the Eastern Mediterranean. *Deep Sea Research Part I: Oceanographic Research Papers*, *46*(3), 371-414. DOI: 10.1016/S0967-0637(98)00075-2

[65] Lascaratos, A., Roether, W., Nittis, K., & Klein, B. (1999). Recent changes in deep water formation and spreading in the eastern Mediterranean Sea: a review. *Progress in oceanography*, *44*(1-3), 5-36. DOI: 10.1016/S0079-6611(99)00019-1

[66] Malanotte-Rizzoli, P., Manca, B. B., d'Alcala, M. R., Theocharis, A., Brenner, S., Budillon, G., & Ozsoy, E. (1999). The Eastern Mediterranean in the 80s and in the 90s: the big transition in the intermediate and deep circulations. *Dynamics of Atmospheres and Oceans*, *29*(2-4), 365-395. DOI: 10.1007/978-94-011-4796-5_1

[67] Roether, W., Manca, B. B., Klein, B., Bregant, D., Georgopoulos, D., Beitzel, V., ... & Luchetta, A. (1996). Recent changes in eastern Mediterranean deep waters. *Science*, *271*(5247), 333-335.

[68] Nof, D. (1979). On man-induced variations in the circulation of the Mediterranean Sea. *Tellus*, *31*(6), 558-564.

[69] Lacombe, H., Tchernia, P., & Gamberoni, L. (1985). Variable bottom water in the western Mediterranean basin. *Progress in Oceanography*, *14*, 319-338.

[70] Skliris, N., & Lascaratos, A. (2004). Impacts of the Nile River damming on the thermohaline circulation and water mass characteristics of the Mediterranean Sea. *Journal of Marine Systems*, *52*(1-4), 121-143.

[71] Levitus, S. (2007). Global Oceanographic Data Archeology and Rescue (GODAR) Project.

[72] Maillard, C., Balopoulos, E., Giorgetti, A., Fichaut, M., Iona, A., Larour, M., ... & Sanchez-Cabeza, J. A. (2002). An integrated system for managing multidisciplinary oceanographic data collected in the Mediterranean Sea during the basin-scale research project EU/MAST-MATER (1996–2000). *Journal of Marine Systems*, *33*, 523-538. DOI: 10.1016/S0924-7963(02)00074-X

[73] Jourdan, D., Balopoulos, E., Garcia-Fernandez, M. J., & Maillard, C. (1998). Objective analysis of temperature and salinity historical data set over the Mediterranean Basin. In *IEEE Oceanic Engineering Society. OCEANS'98. Conference Proceedings (Cat. No. 98CH36259)* (Vol. 1, pp. 82-87). IEEE. DOI: 10.1109/OCEANS.1998.725649

[74] Skliris, N., Sofianos, S., Gkanasos, A., Mantziafou, A., Vervatis, V., Axaopoulos, P., & Lascaratos, A. (2012). Decadal scale variability of sea surface temperature in the Mediterranean Sea in relation to atmospheric variability. *Ocean Dynamics*, *62*(1), 13-30. DOI: 10.1007/s10236-011-0493-5

[75] Zveryaev, I. I. (2015). Seasonal differences in intraseasonal and interannual variability of M editerranean S ea surface temperature. *Journal of Geophysical Research: Oceans*, *120*(4), 2813-2825. DOI: 10.1002/2014JC010387

[76] Macias, Diego M., Elisa Garcia-Gorriz, and Adolf Stips. "Productivity changes in the Mediterranean Sea for the twenty-first century in response to changes in the regional atmospheric forcing." *Frontiers in Marine Science* 2 (2015): 79.

[77] Pastor, F., Valiente, J. A., & Palau, J. L. (2019). Sea surface temperature in the Mediterranean: Trends and spatial patterns (1982–2016). In *Meteorology and Climatology of the Mediterranean and Black Seas* (pp. 297-309). Birkhäuser, Cham. DOI: 10.1007/978-3-030-11958-4_18

[78] Shaltout, M., & Omstedt, A. (2014). Recent sea surface temperature trends and future scenarios for the Mediterranean Sea. *Oceanologia*, *56*(3), 411-443. DOI: 10.5697/oc.56-3.411

[79] Gandin, L. S. (1963). Objective analysis of meteorological field. *Gidrometeorologicheskoe Izdate'stvo*, *286*. DOI: 10.1002/qj.49709239320

[80] Wahba, G., & Wendelberger, J. (1980). Some new mathematical methods for variational objective analysis using splines and cross validation. *Monthly weather review*, *108*(8), 1122-1143. DOI: 10.1175/1520-0493(1980)108<1122:SNMMFV>2.0.CO;2

[81] Brasseur, P., Beckers, J. M., Brankart, J. M., & Schoenauen, R. (1996). Seasonal temperature and salinity fields in the Mediterranean Sea: Climatological analyses of a historical data set. *Deep Sea Research Part I: Oceanographic Research Papers*, *43*(2), 159-192. DOI: 10.1016/0967-0637(96)00012-X

[82] Troupin, C., Ouberdous, M., Sirjacobs, D., Alvera-Azcárate, A., Barth, A., Toussaint, M. E., & Beckers, J. M. (2013). DIVA User Guide. GeoHydrodynamics and Environment Research, Department of Astrophysics. *Geophysics, University of Liège, Belgium, 199pp*.

[83] Rousseeuw, P. J., & Kaufman, L. (1990). Finding groups in data. *Hoboken: Wiley Online Library*.

[84] Wilkinson, Leland. "The grammar of graphics." *Handbook of Computational Statistics*. Springer, Berlin, Heidelberg, 2012. 375-414. DOI: 10.1007/0-387-28695-0

APPENDIX A

DENSITY PLOTS

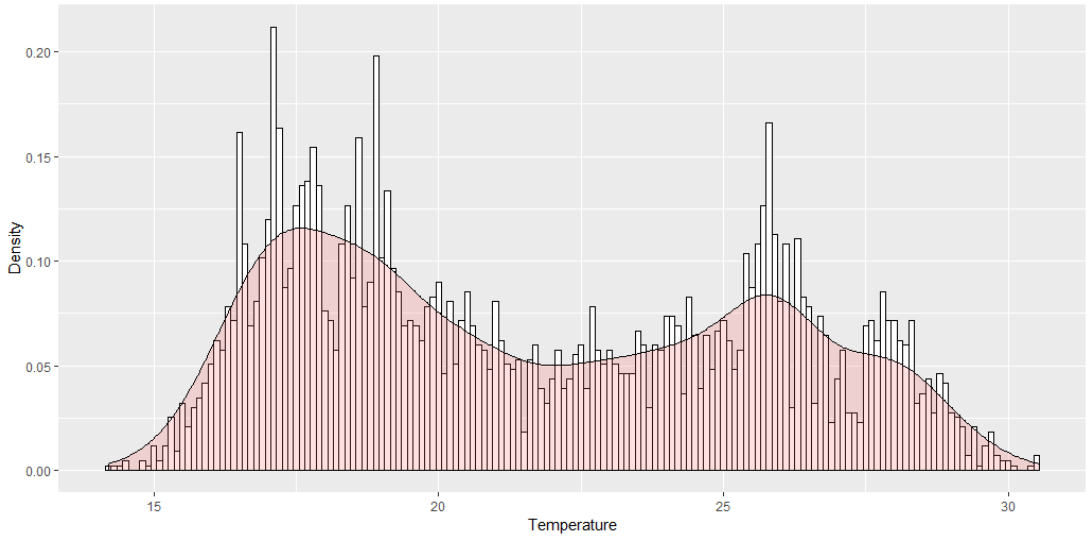

Appendix A 1 Temperature 10m Density, 1960-1980

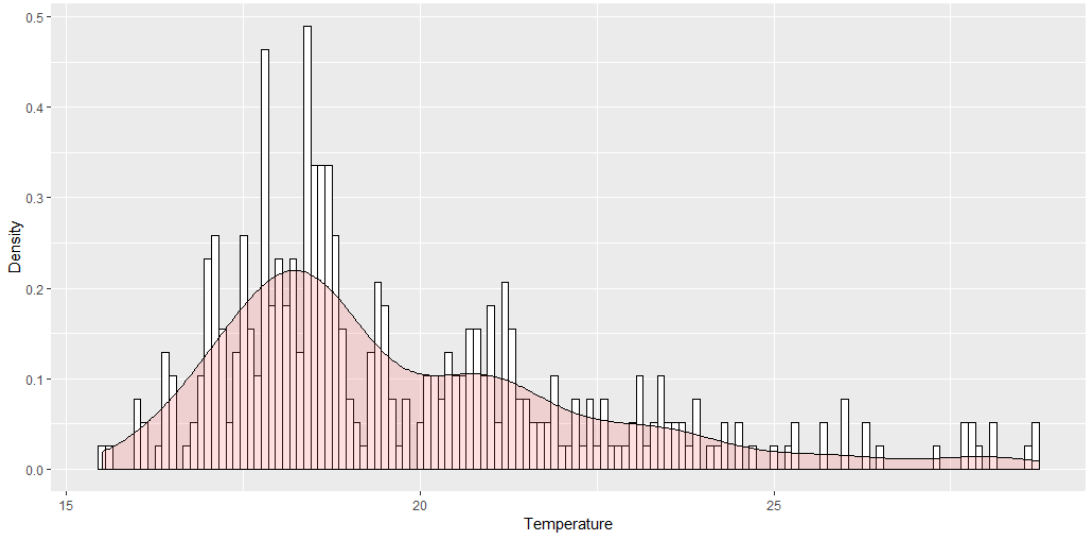

Appendix A 2 Temperature 25m Density, 1960-1980

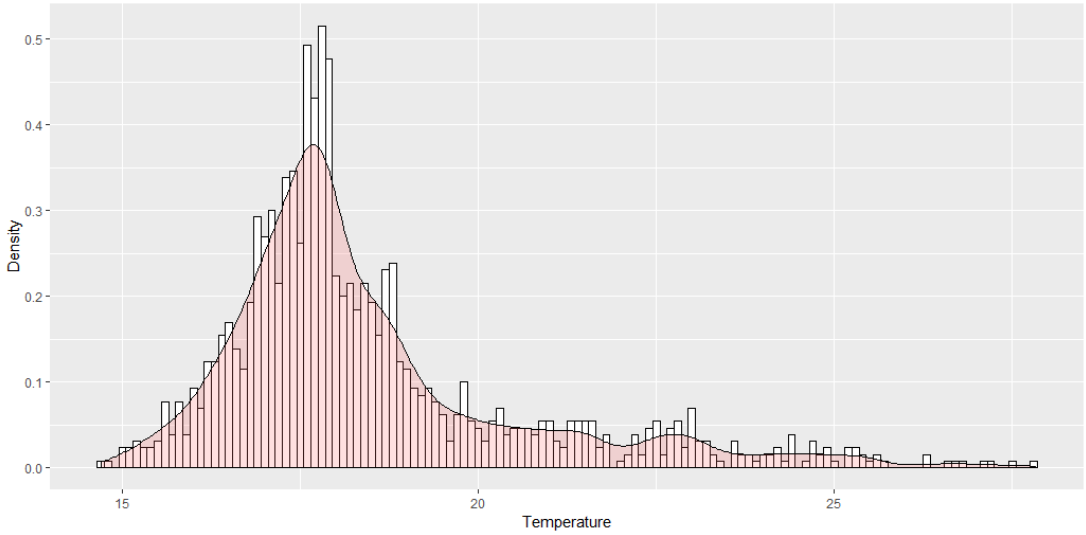

Appendix A 3 Temperature 50m Density, 1960-1980

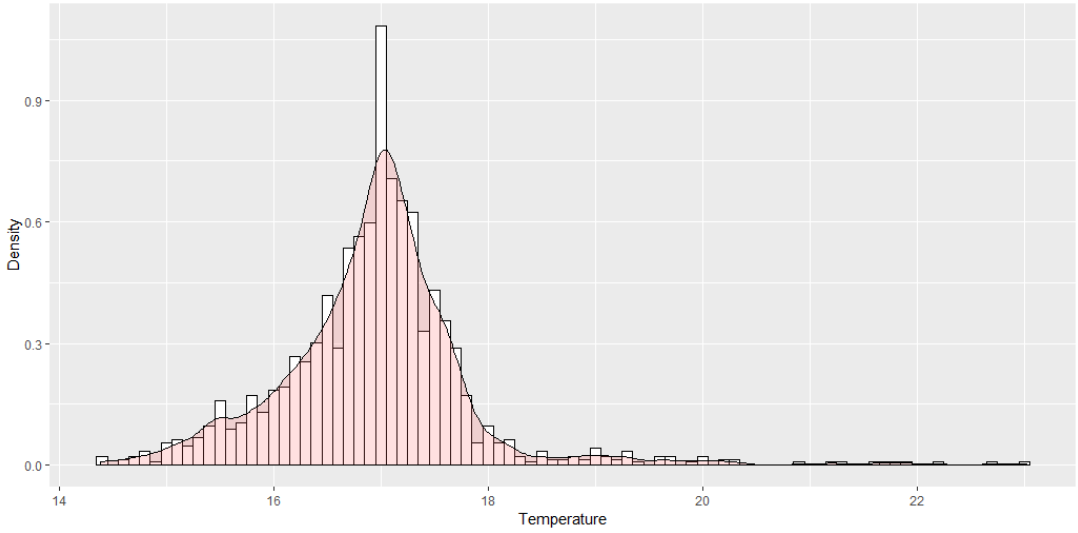

Appendix A 4 Temperature 100m Density, 1960-1980

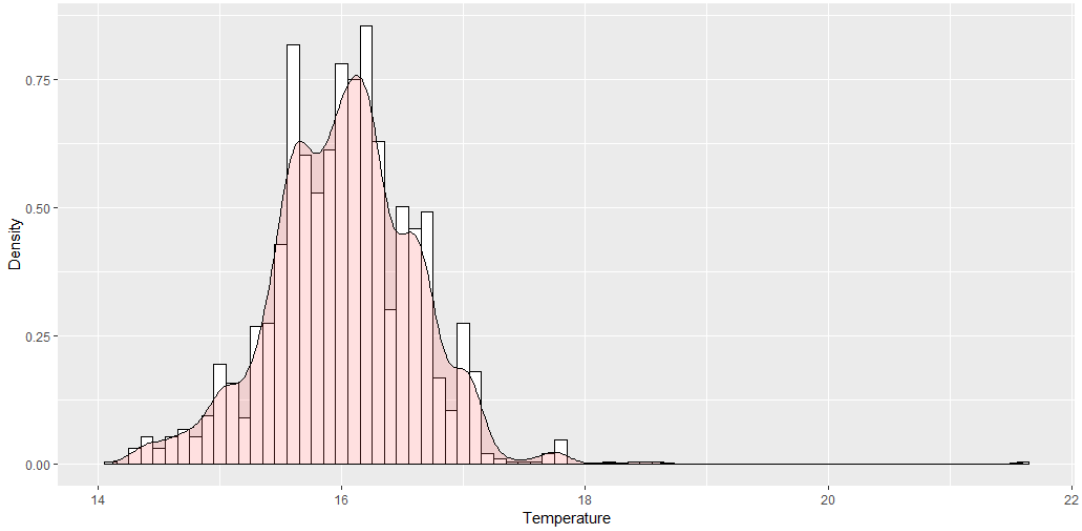

Appendix A 5 Temperature 200m Density, 1960-1980

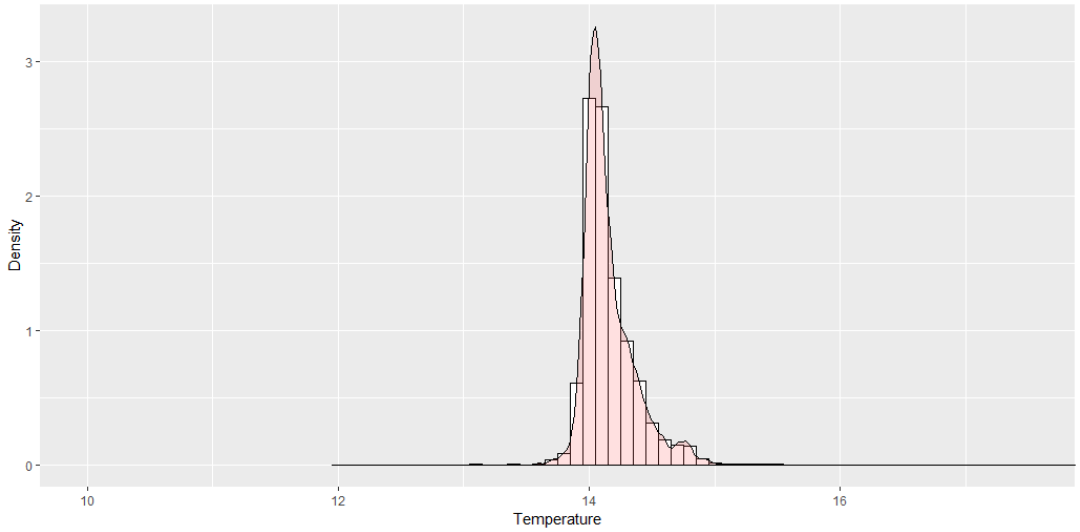

Appendix A 6 Temperature 500m Density, 1960-1980

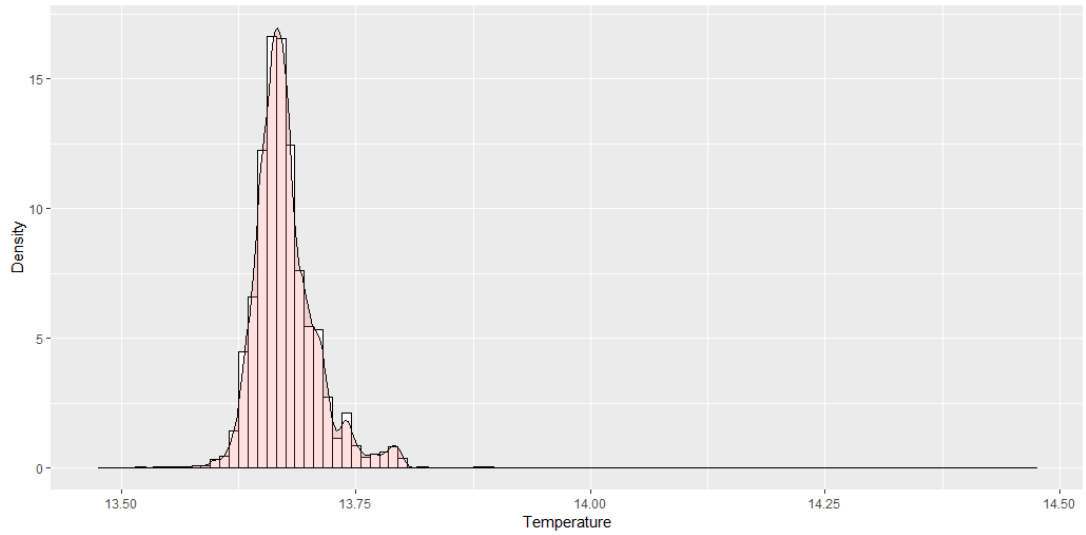

Appendix A 7 Temperature 1000m Density, 1960-1980

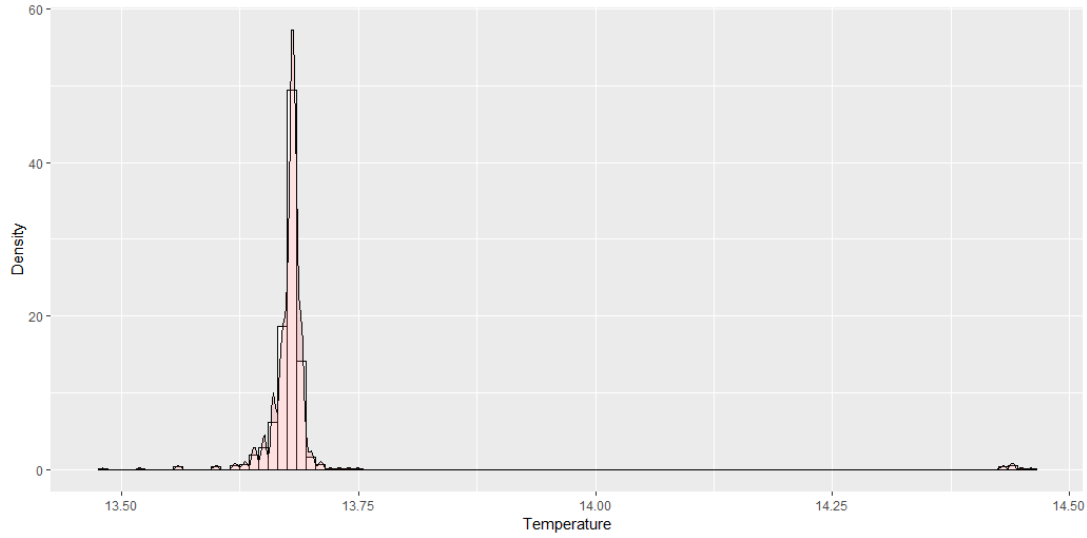

Appendix A 8 Temperature 2000m Density, 1960-1980

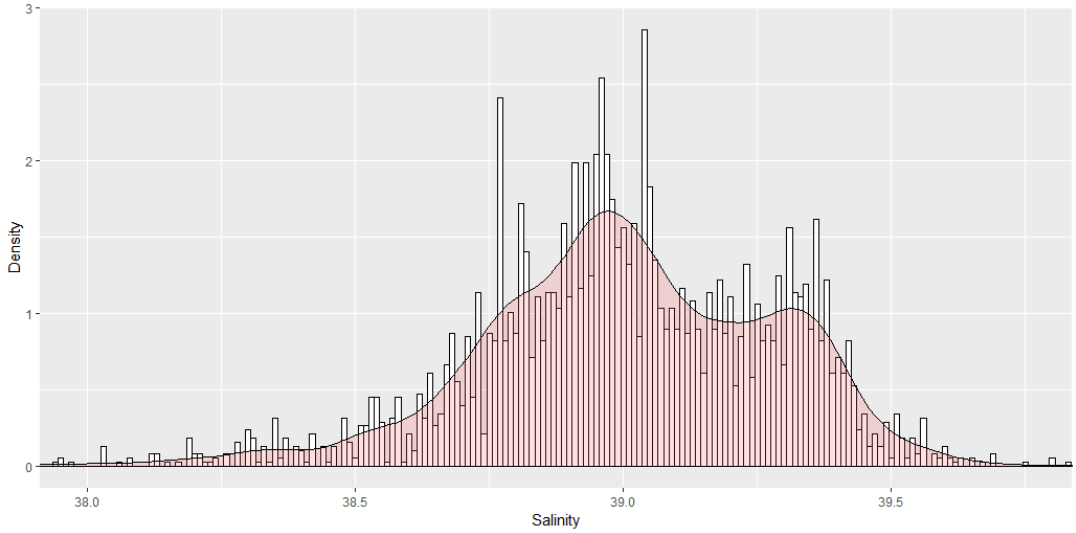

Appendix A 9 Salinity 10m Density, 1960-1980

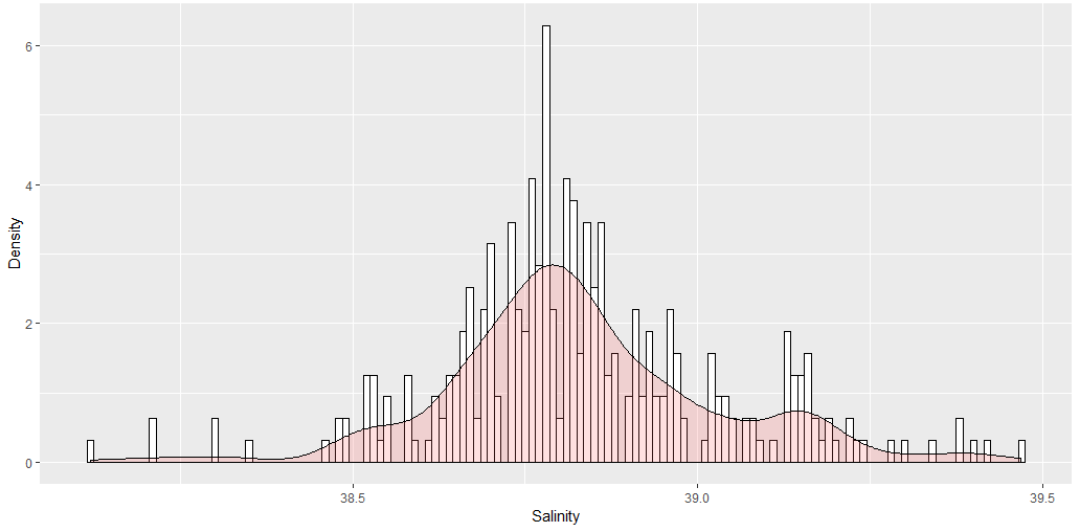

Appendix A 10 Salinity 25m Density, 1960-1980

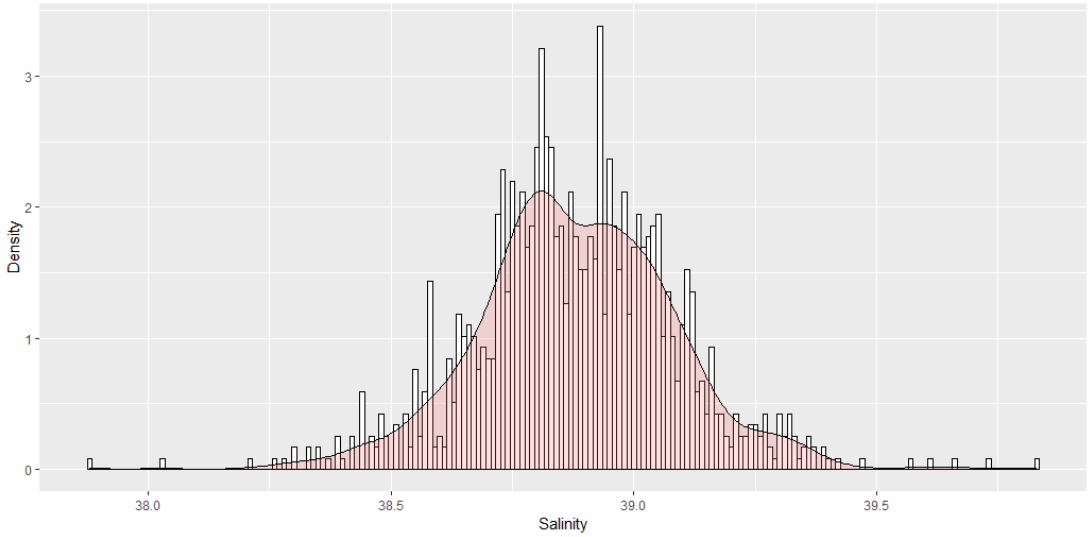

Appendix A 11 Salinity 50m Density, 1960-1980

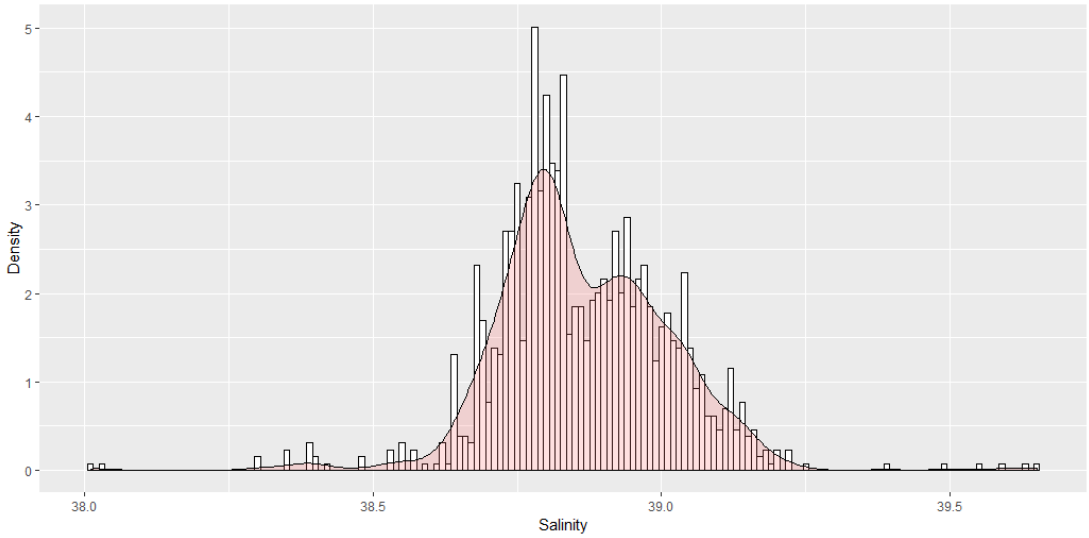

Appendix A 12 Salinity 100m Density, 1960-1980

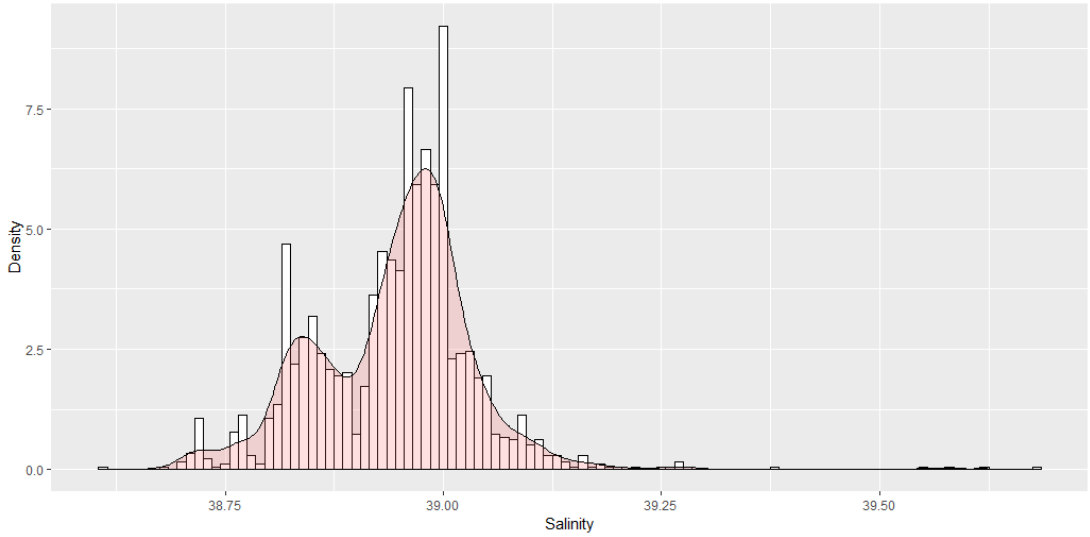

Appendix A 13 Salinity 200m Density, 1960-1980

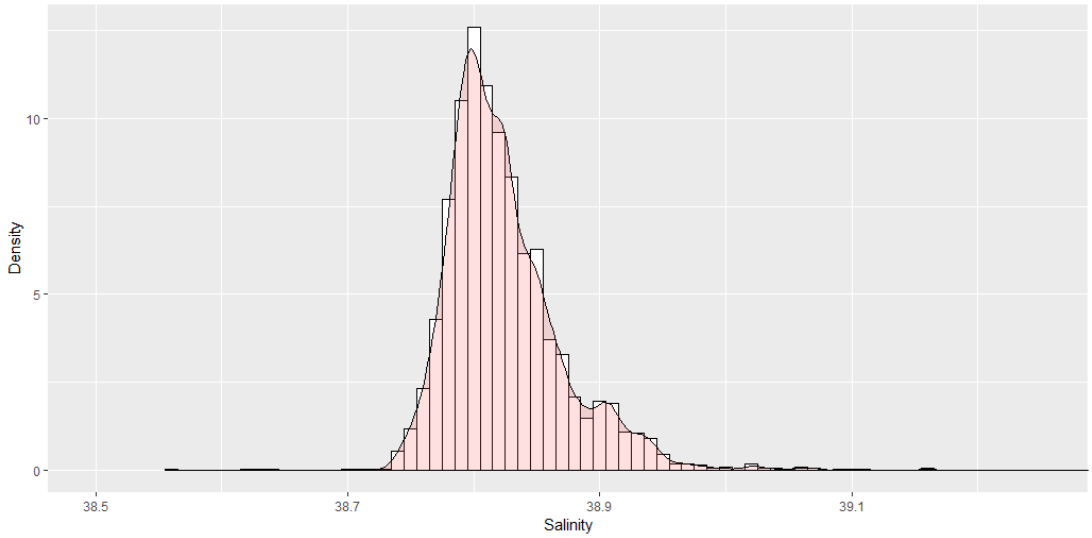

Appendix A 14 Salinity 500m Density, 1960-1980

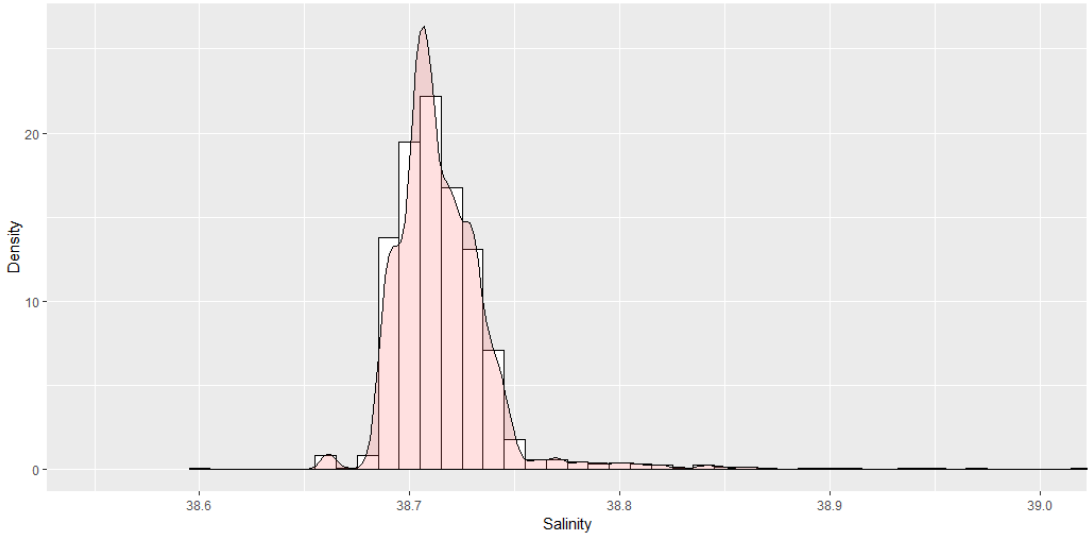

Appendix A 15 Salinity 1000m Density, 1960-1980

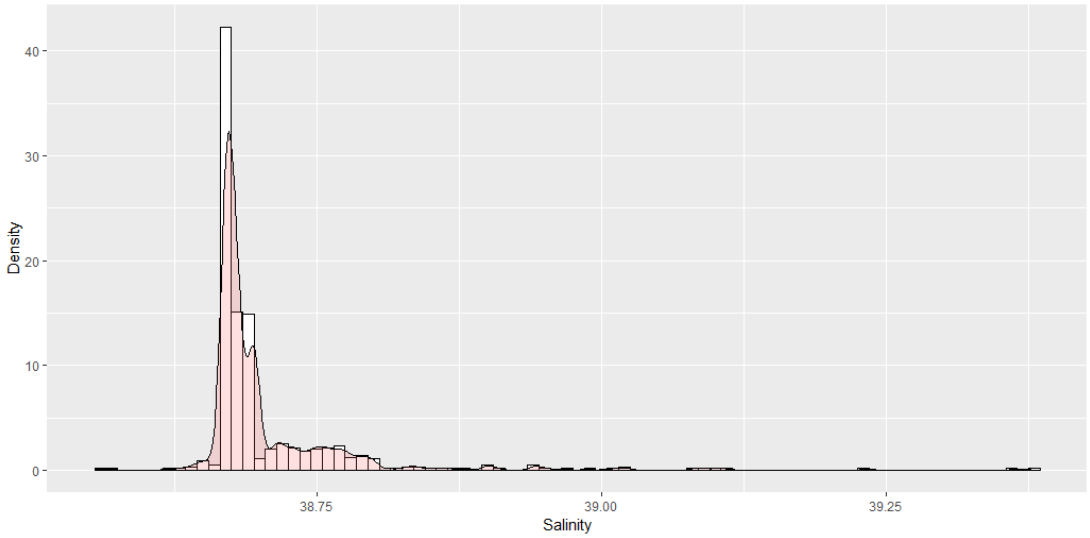

Appendix A 16 Salinity 2000m Density, 1960-1980

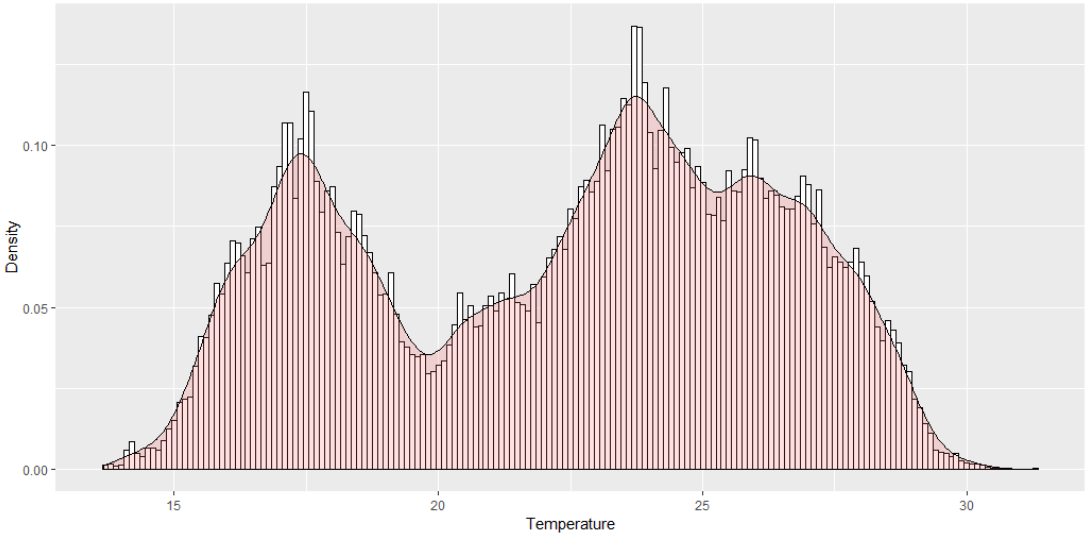

Appendix A 17 Temperature 10m Density, 1980-2017

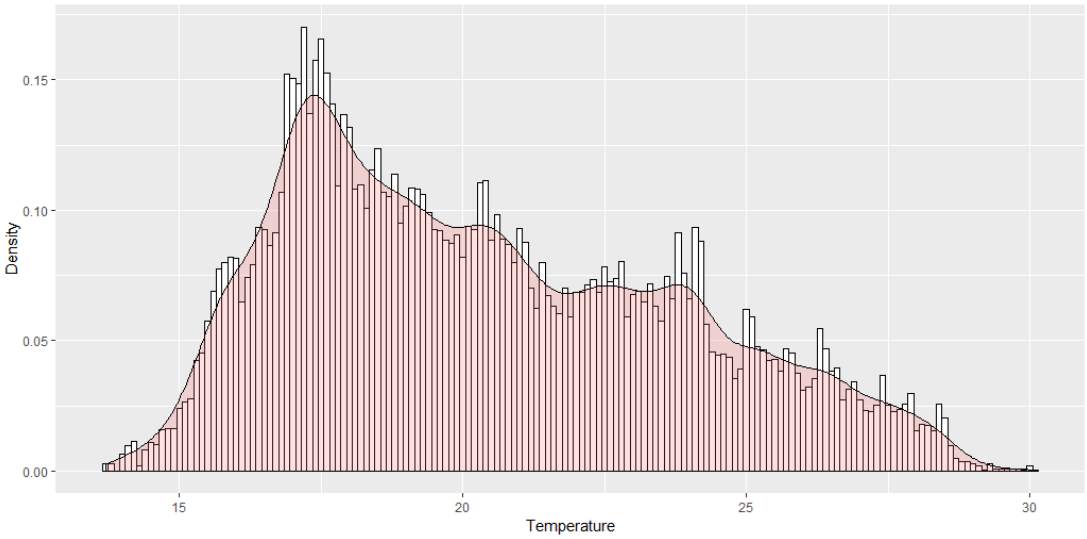

Appendix A 18 Temperature 25m Density, 1980-2017

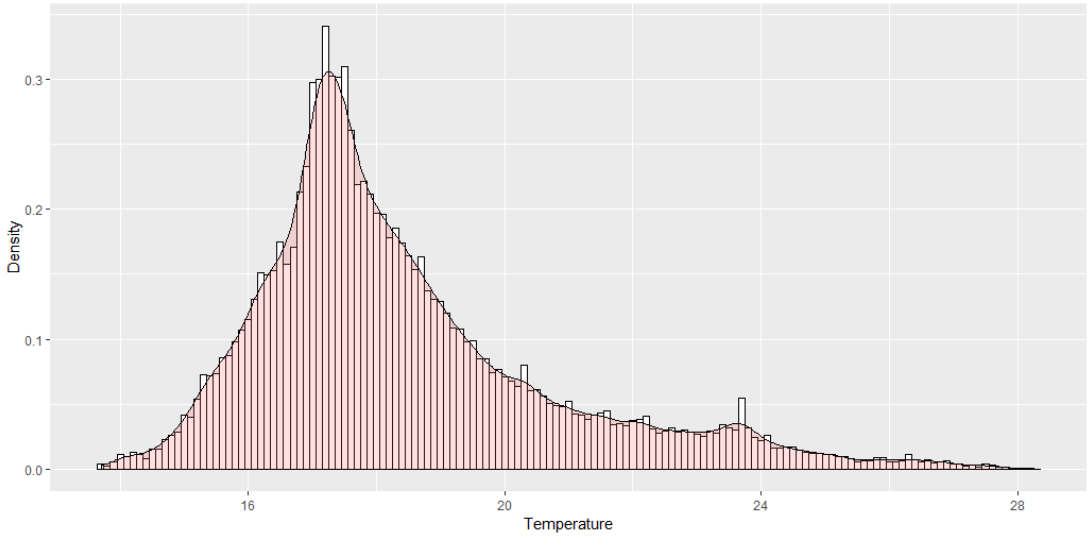

Appendix A 19 Temperature 50m Density, 1980-2017

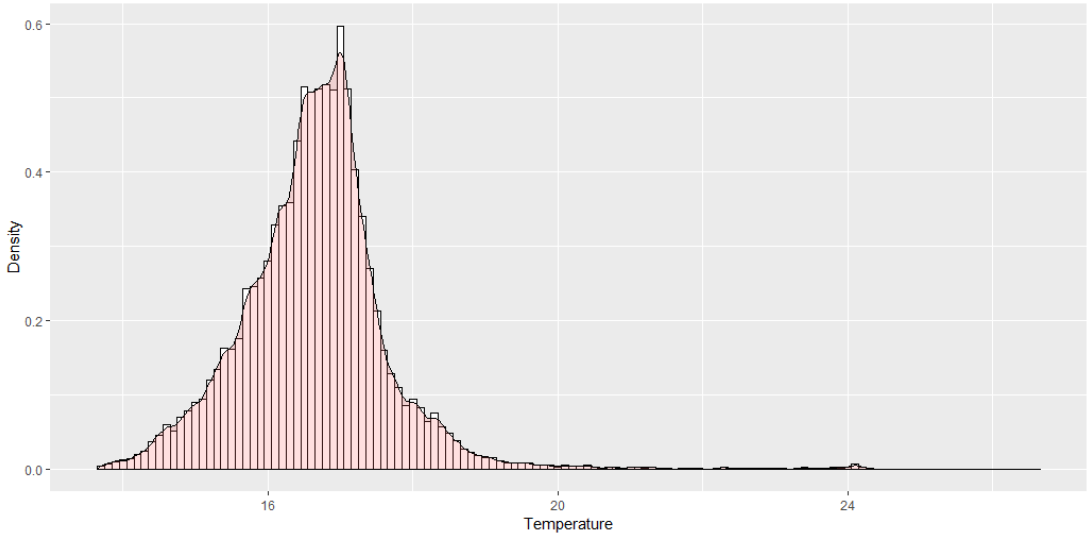

Appendix A 20 Temperature 100m Density, 1980-2017

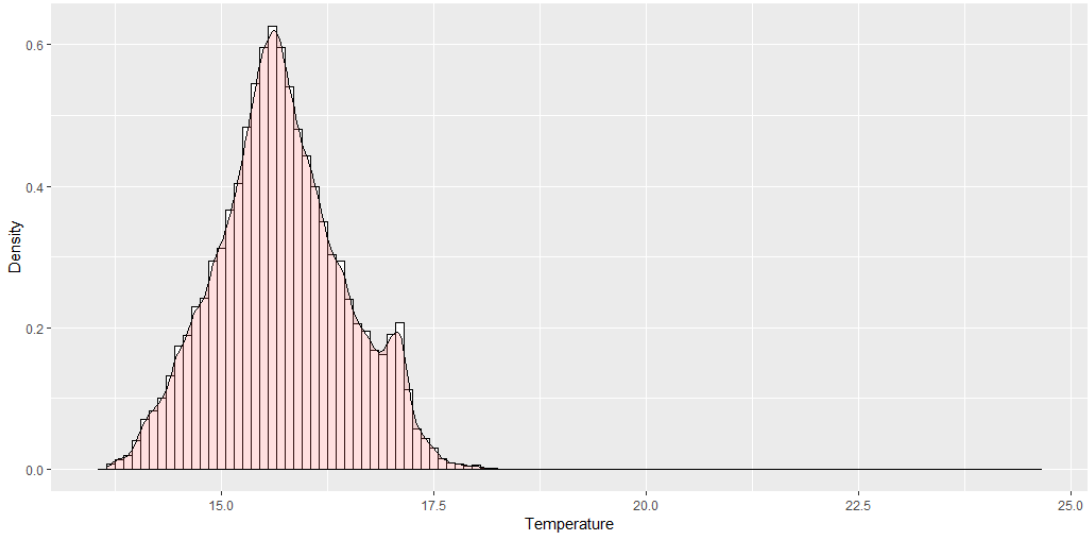

Appendix A 21 Temperature 200m Density, 1980-2017

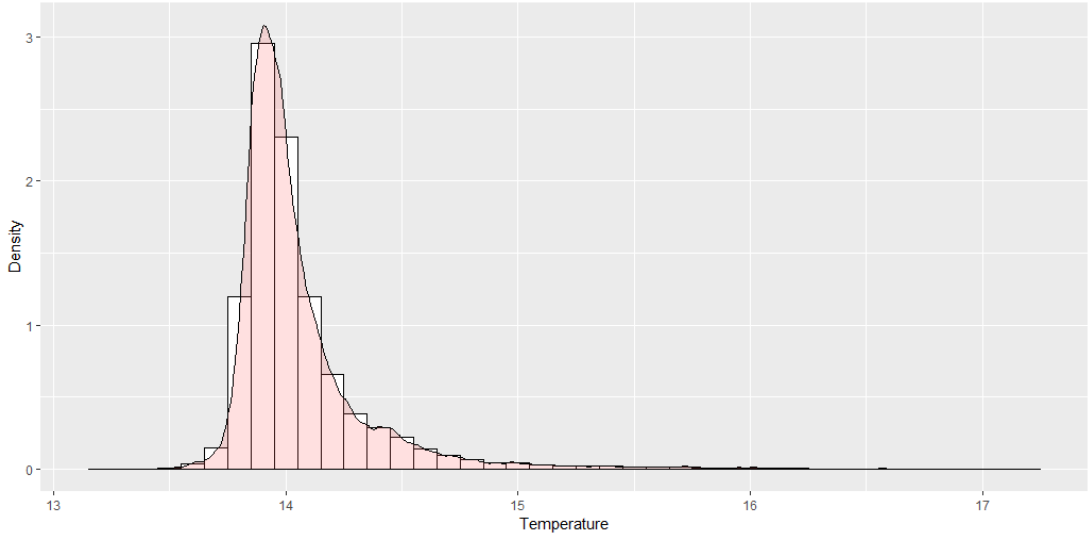

Appendix A 22 Temperature 500m Density, 1980-2017

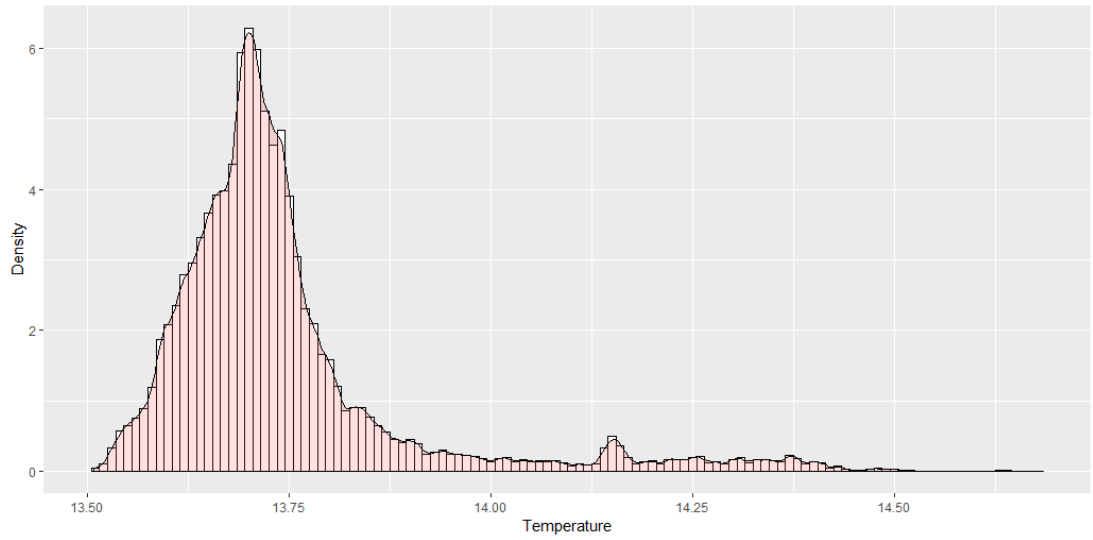

Appendix A 23 Temperature 1000m Density, 1980-2017

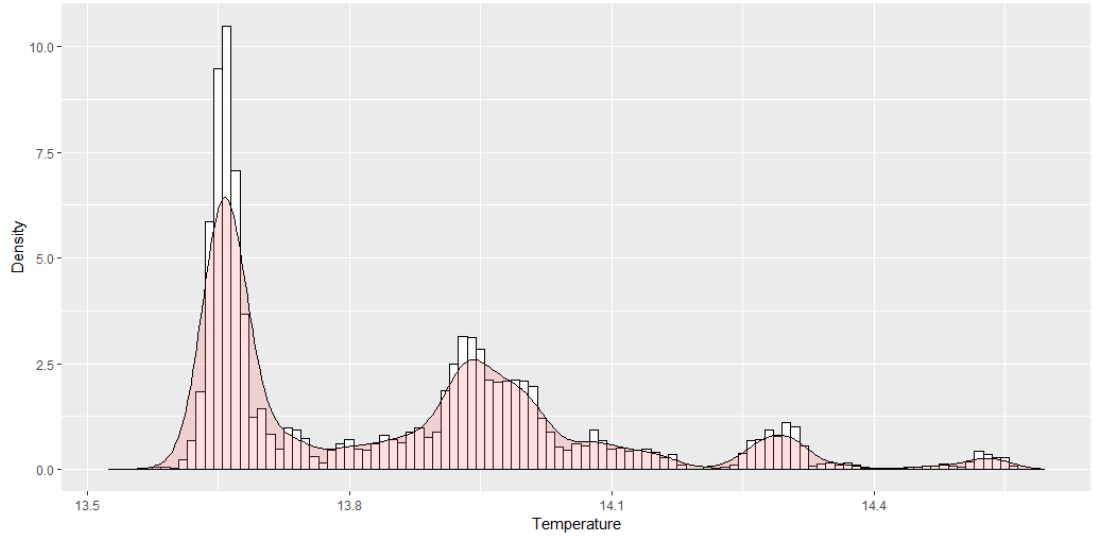

Appendix A 24 Temperature 2000m Density, 1980-2017

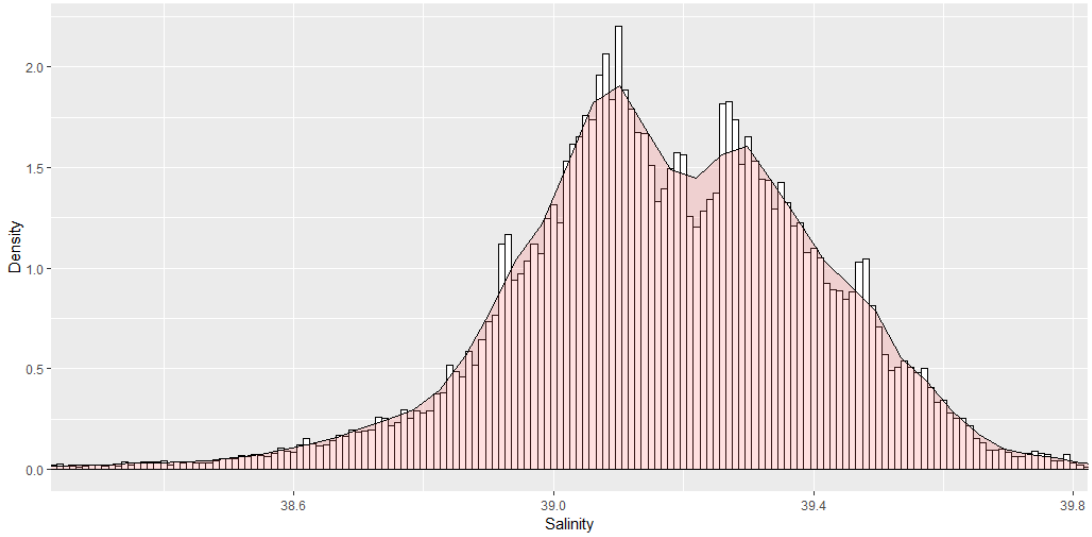

Appendix A 25 Salinity 10m Density, 1980-2017

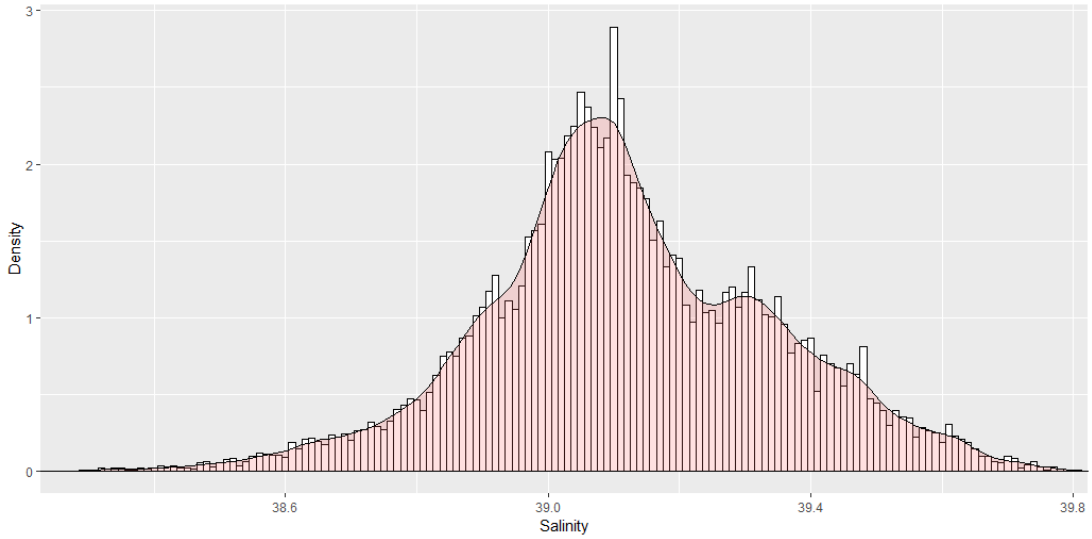

Appendix A 26 Salinity 25m Density, 1980-2017

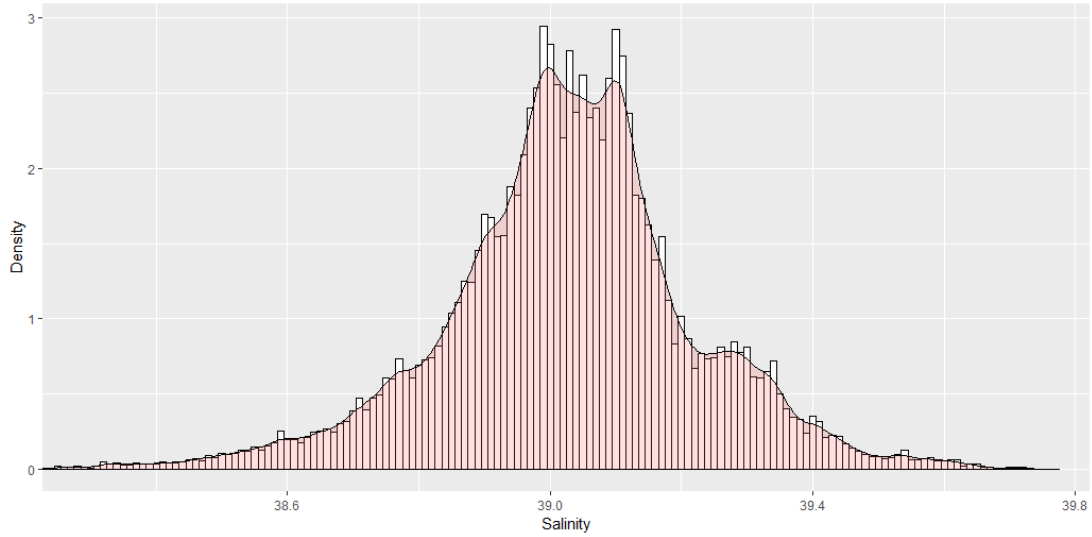

Appendix A 27 Salinity 50m Density, 1980-2017

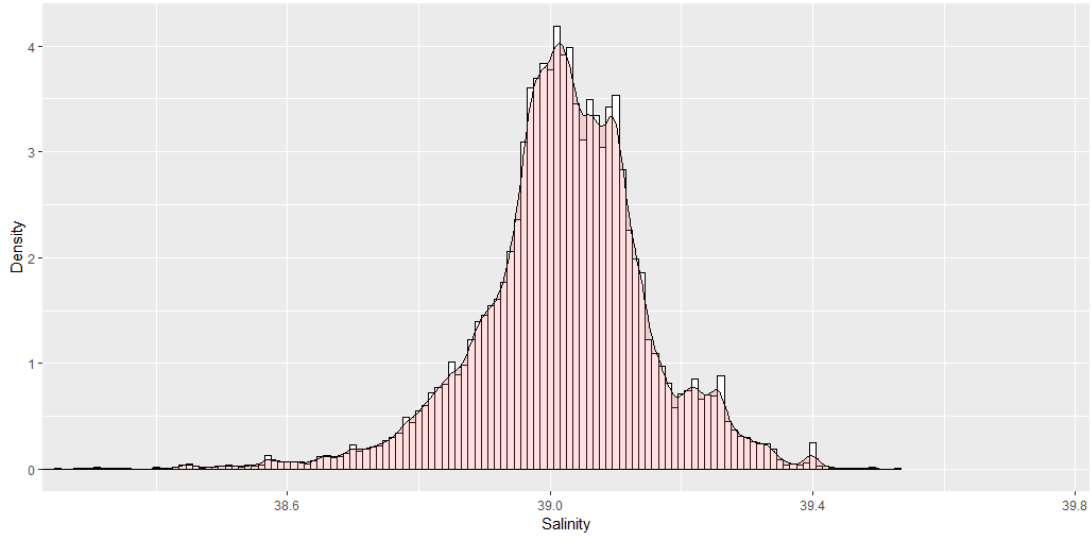

Appendix A 28 Salinity 100m Density, 1980-2017

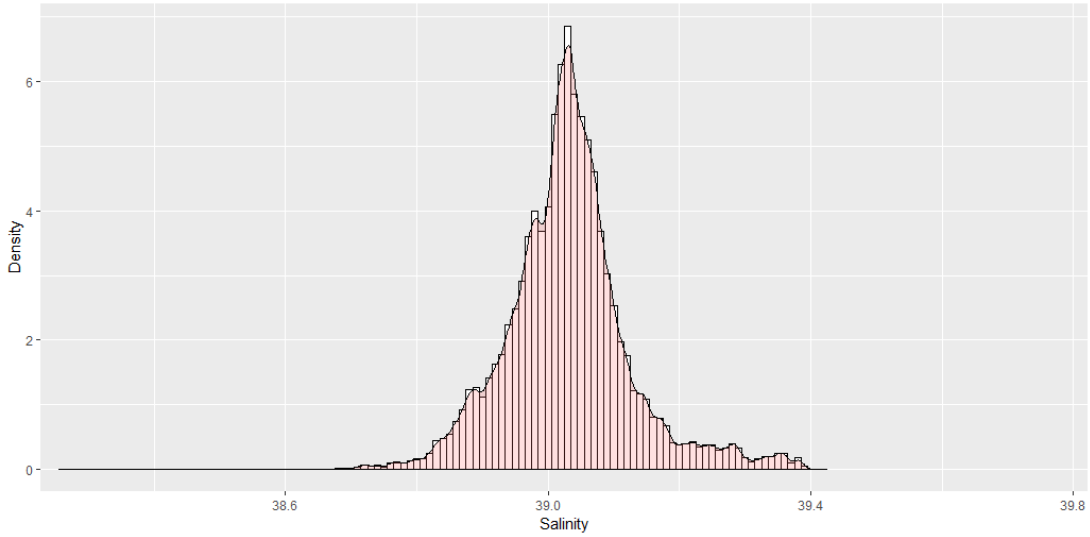

Appendix A 29 Salinity 200m Density, 1980-2017

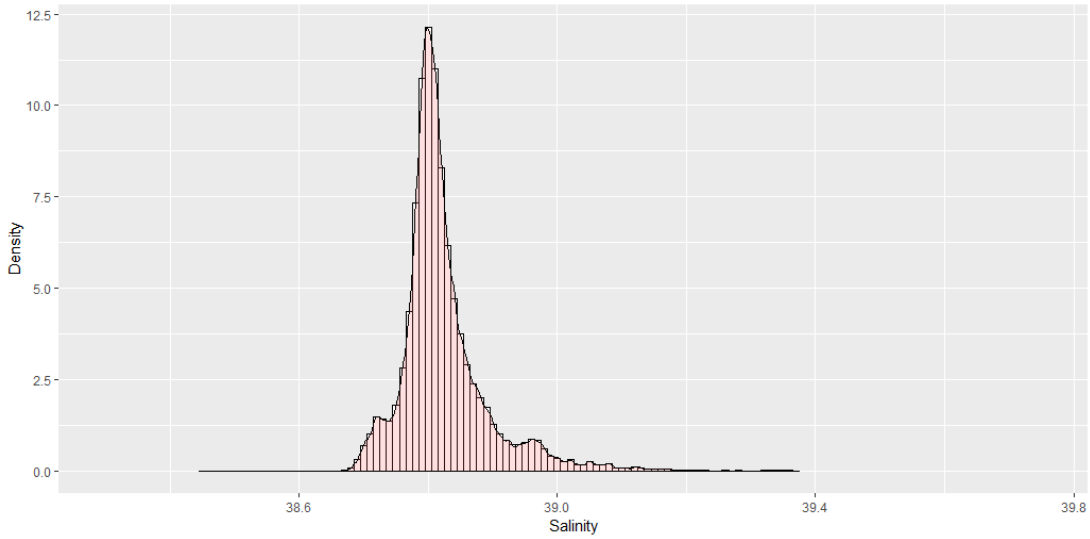

Appendix A 30 Salinity 500m Density, 1980-2017

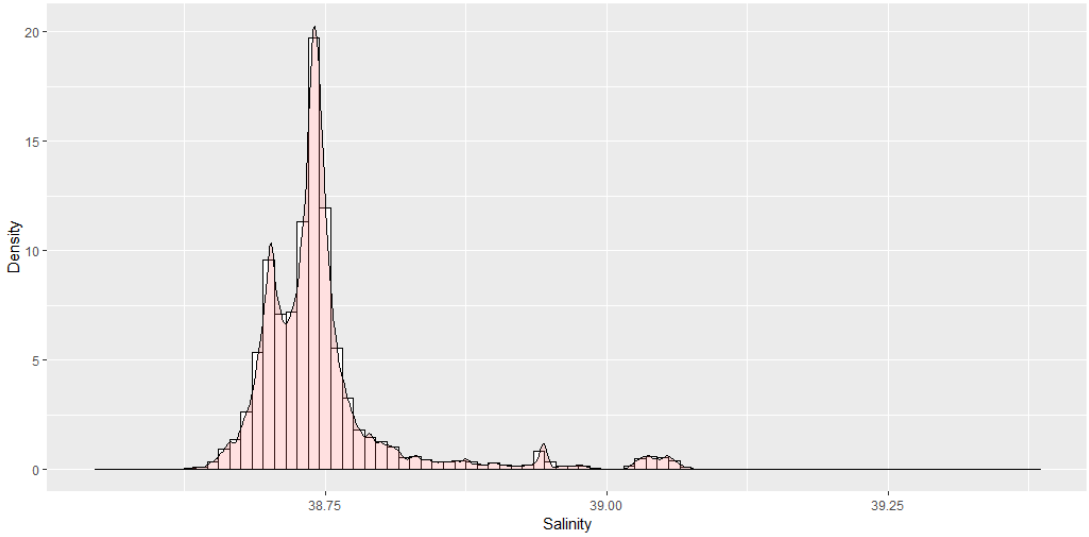

Appendix A 31 Salinity 1000m Density, 1980-2017

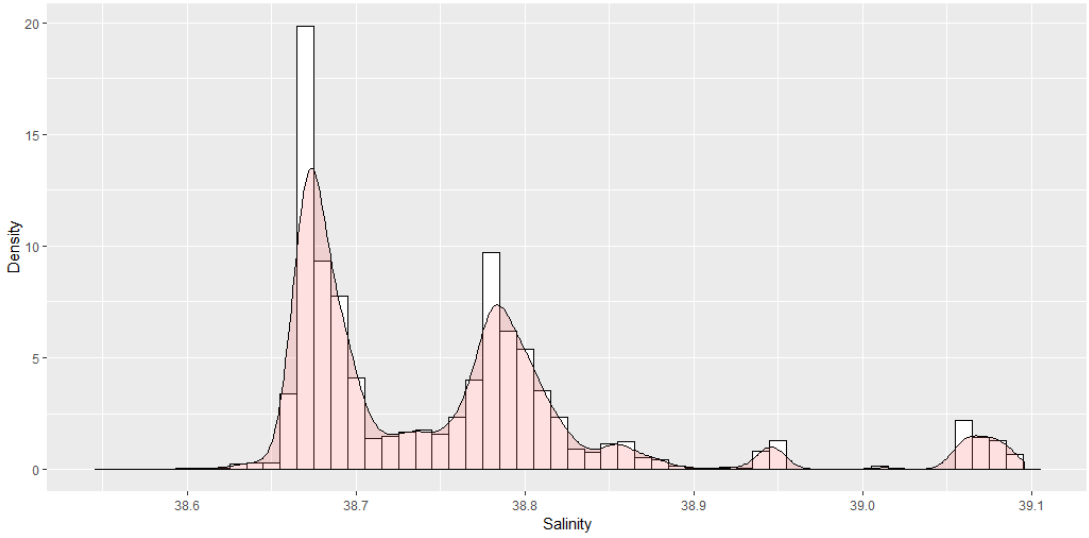

Appendix A 32 Salinity 2000m Density, 1980-2017

Appendix B

Isotherm Temperature Maps

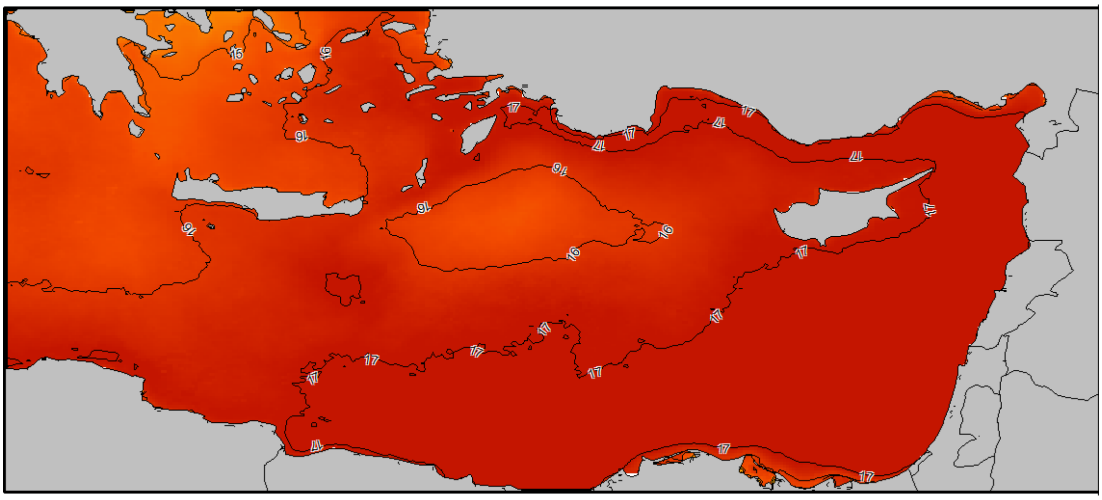

Appendix B 1 Sea Surface Temperature and resulting Isotherms according to the data provided by the WOA18, January

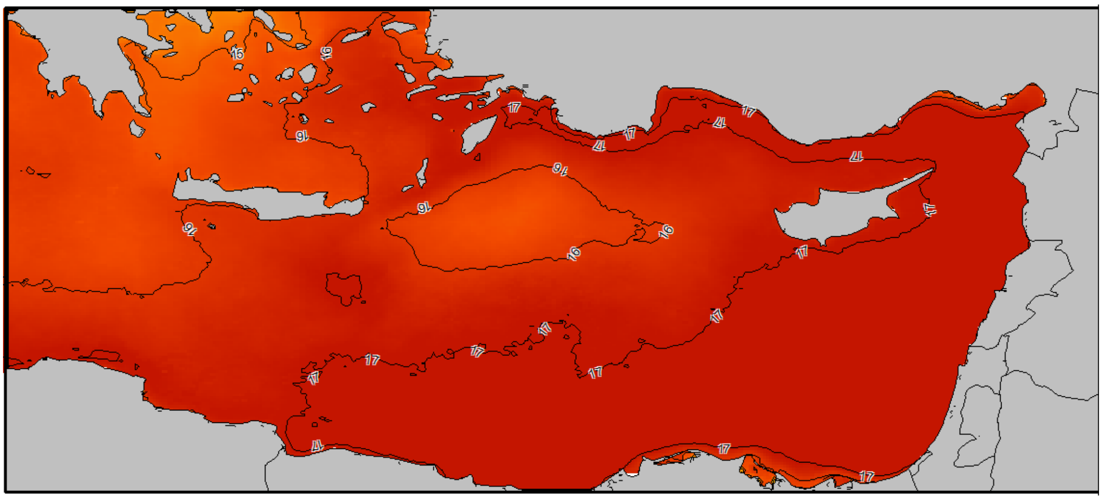

Appendix B 2 Sea Surface Temperature and resulting Isotherms according to the data provided by the WOA18, February

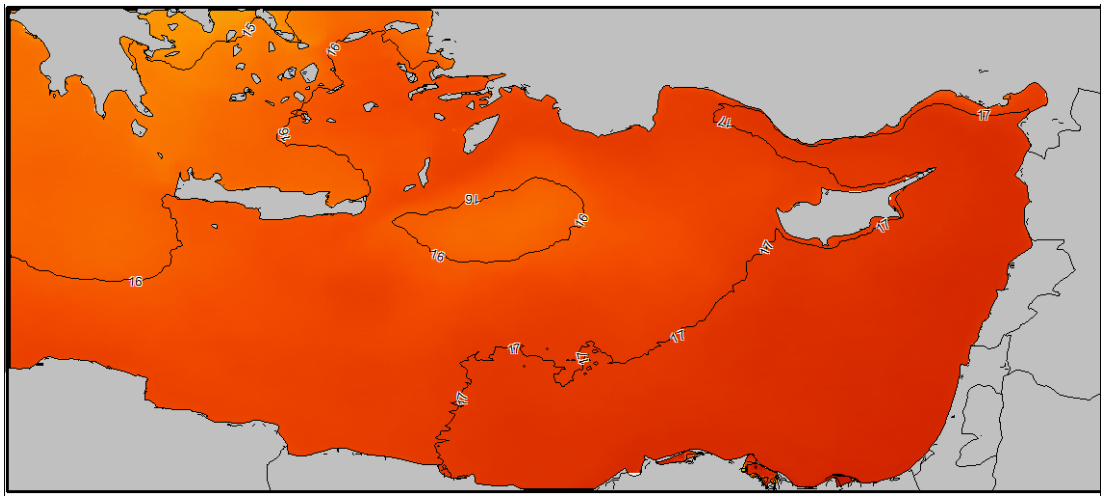

Appendix B 3 Sea Surface Temperature and resulting Isotherms according to the data provided by the WOA18, March

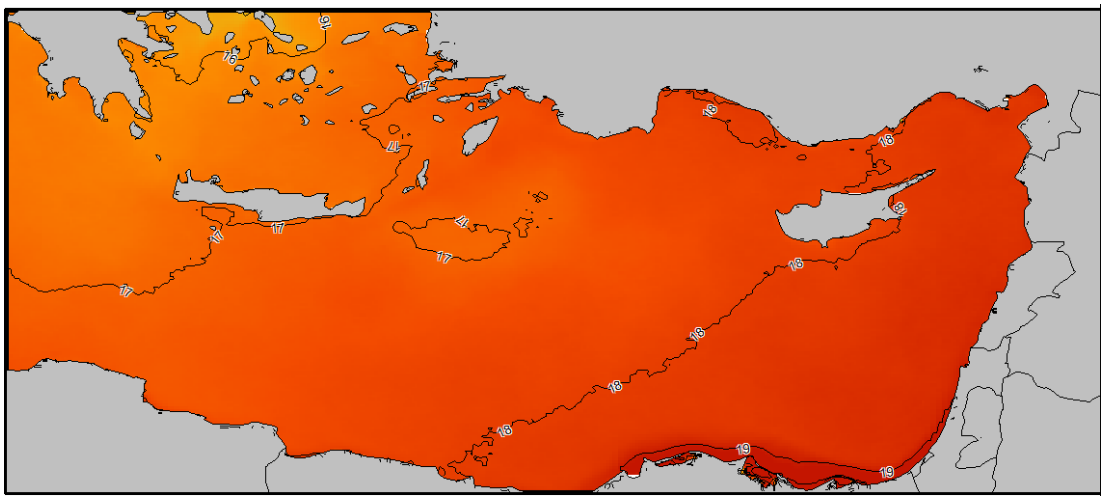

Appendix B 4 Sea Surface Temperature and resulting Isotherms according to the data provided by the WOA18, April

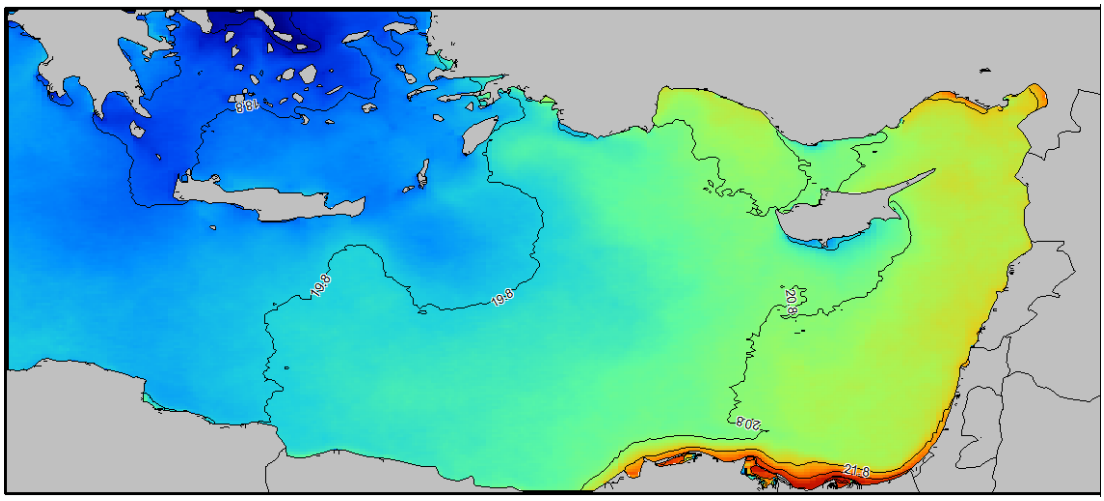

Appendix B 5 Sea Surface Temperature and resulting Isotherms according to the data provided by the WOA18, May

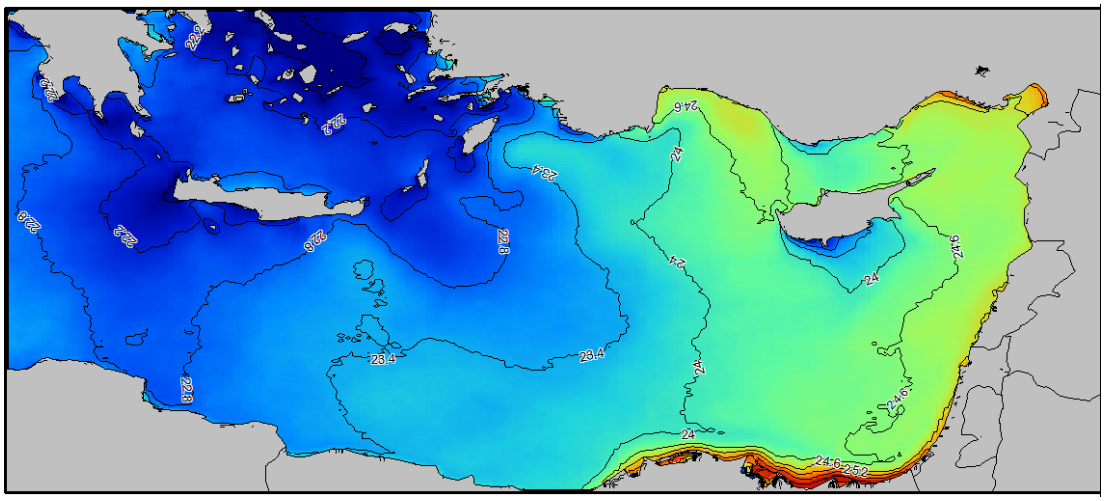

Appendix B 6 Sea Surface Temperature and resulting Isotherms according to the data provided by the WOA18, June

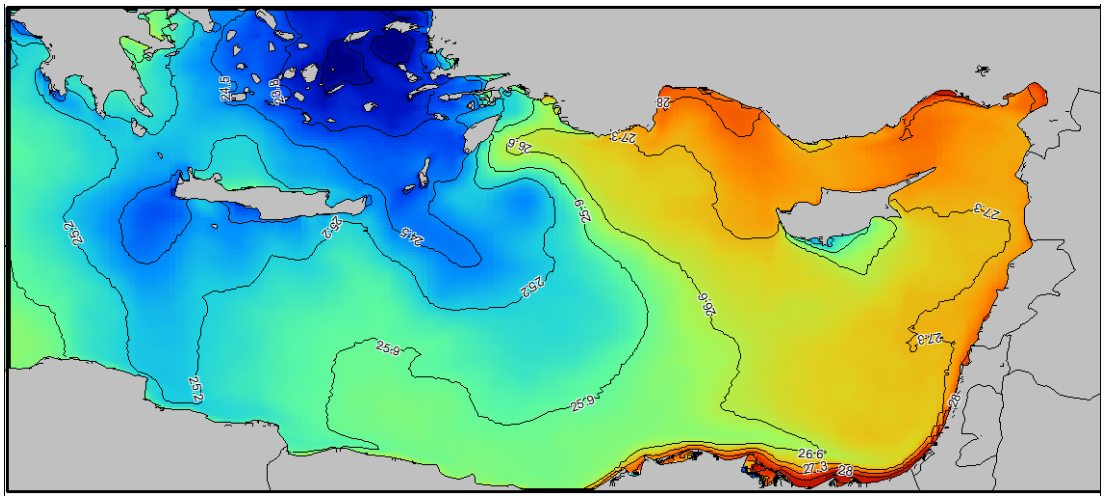

Appendix B 7 Sea Surface Temperature and resulting Isotherms according to the data provided by the WOA18, July

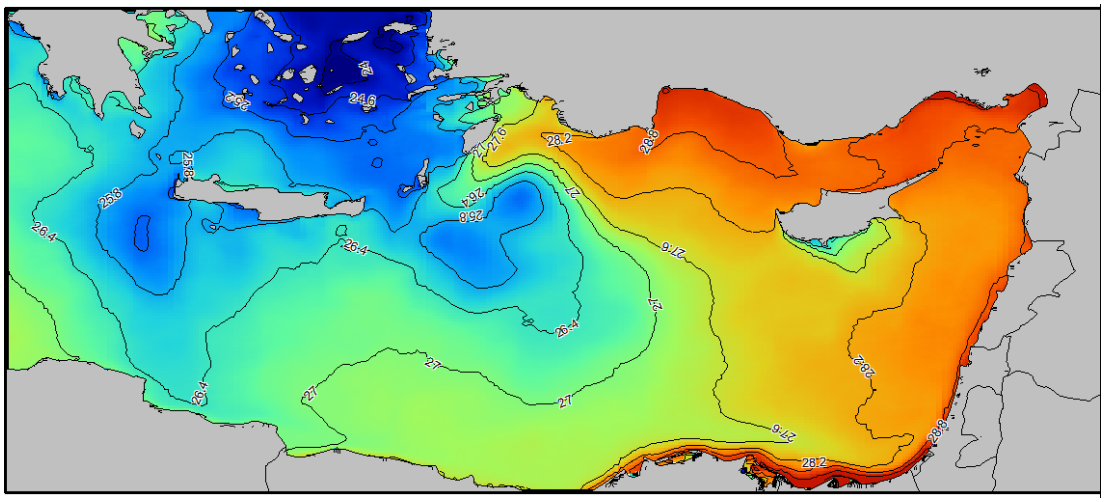

Appendix B 8 Sea Surface Temperature and resulting Isotherms according to the data provided by the WOA18, August

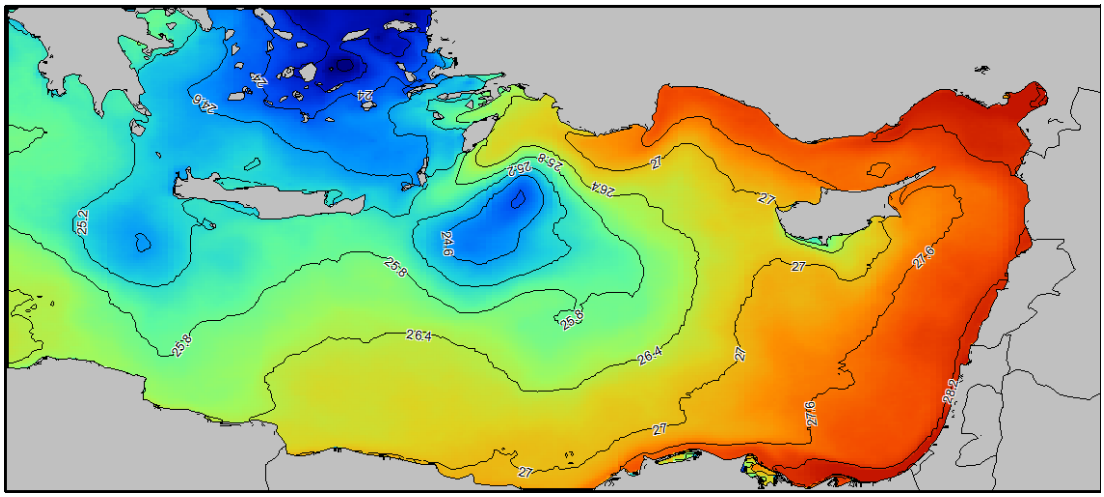

Appendix B 9 Sea Surface Temperature and resulting Isotherms according to the data provided by the WOA18, September

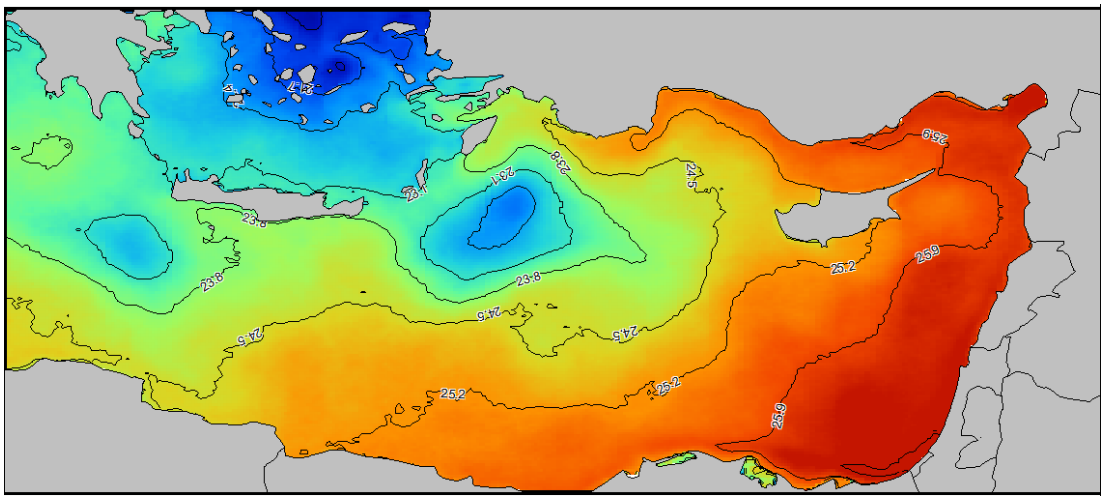

Appendix B 10 Sea Surface Temperature and resulting Isotherms according to the data provided by the WOA18, October

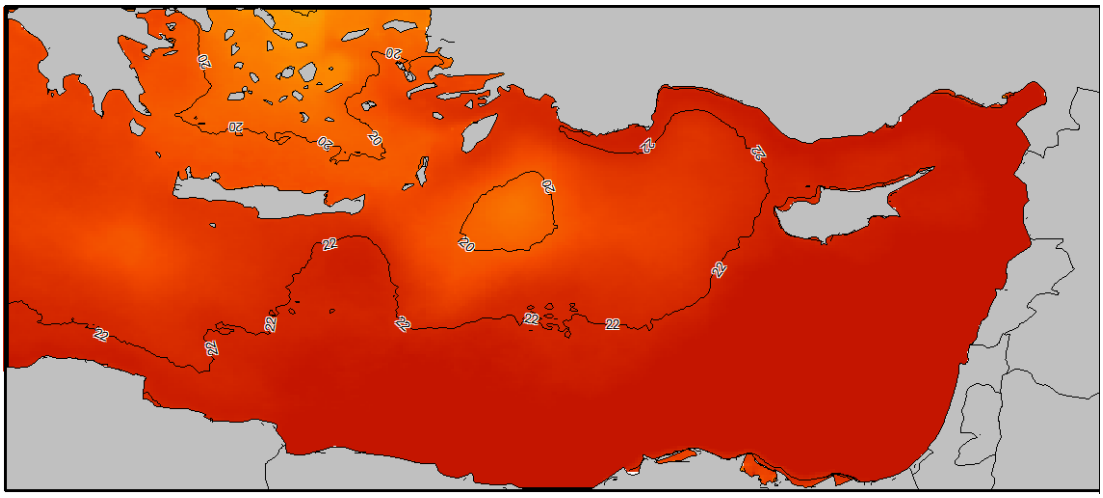

Appendix B 11 Sea Surface Temperature and resulting Isotherms according to the data provided by the WOA18, November

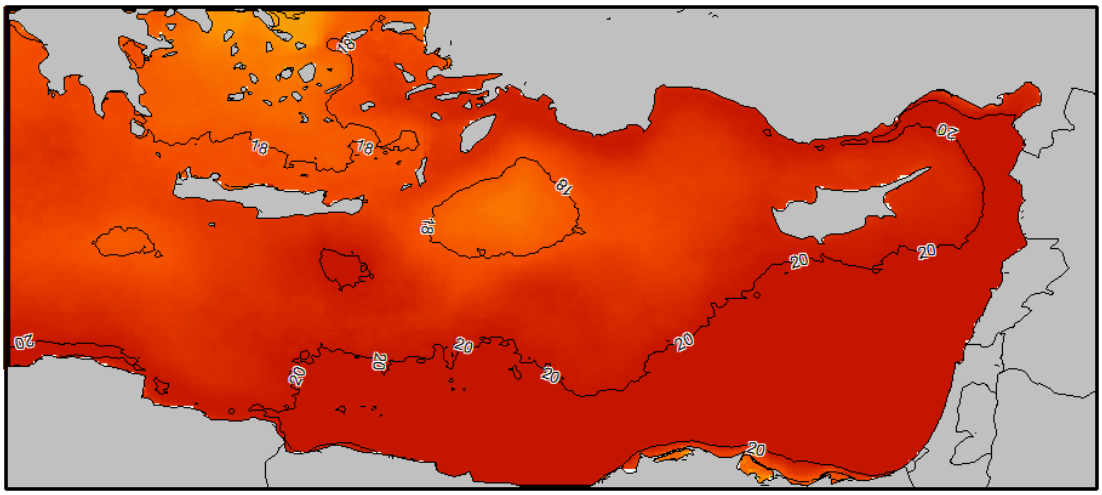

Appendix B 12 Sea Surface Temperature and resulting Isotherms according to the data provided by the WOA18, December

APPENDIX C

YEARLY PLOTS

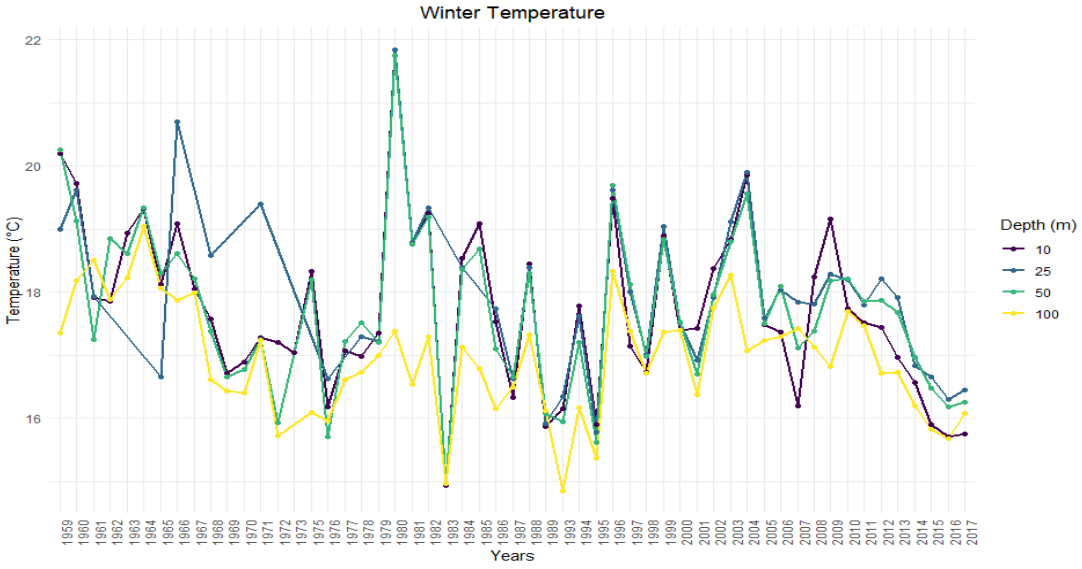

Appendix C 1 Annual winter temperature means in the surface to the 100m range, the Levantine Sea from 1960 to 2017

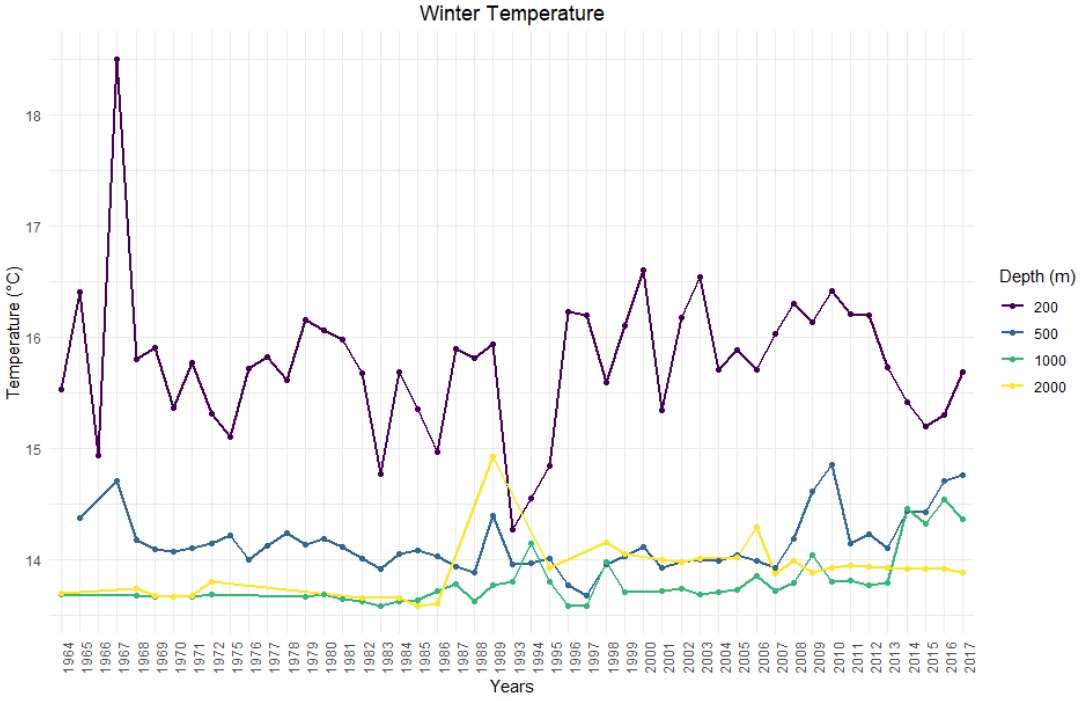

Appendix C 2 Annual winter temperature means in the 200m to the 2000m range, the Levantine Sea from 1960 to 2017

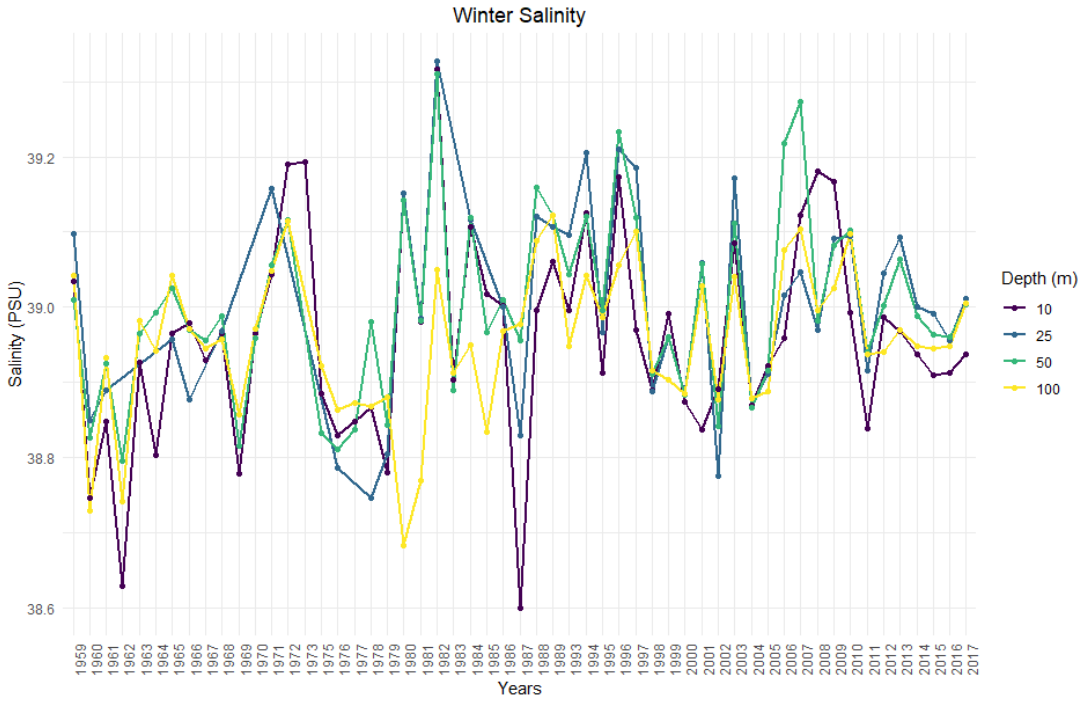

Appendix C 3 Annual winter salinity means in the surface to the 100m range, the Levantine Sea from 1960 to 2017

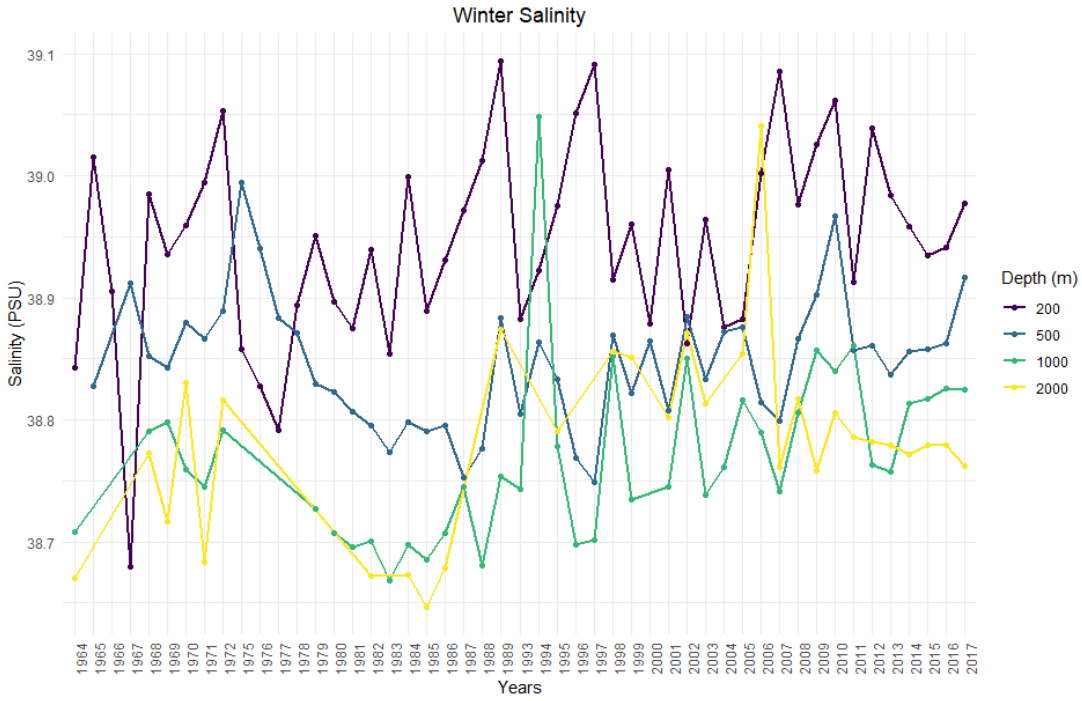

Appendix C 4 Annual winter salinity means in the 200m to the 2000m range, the Levantine Sea from 1960 to 2017

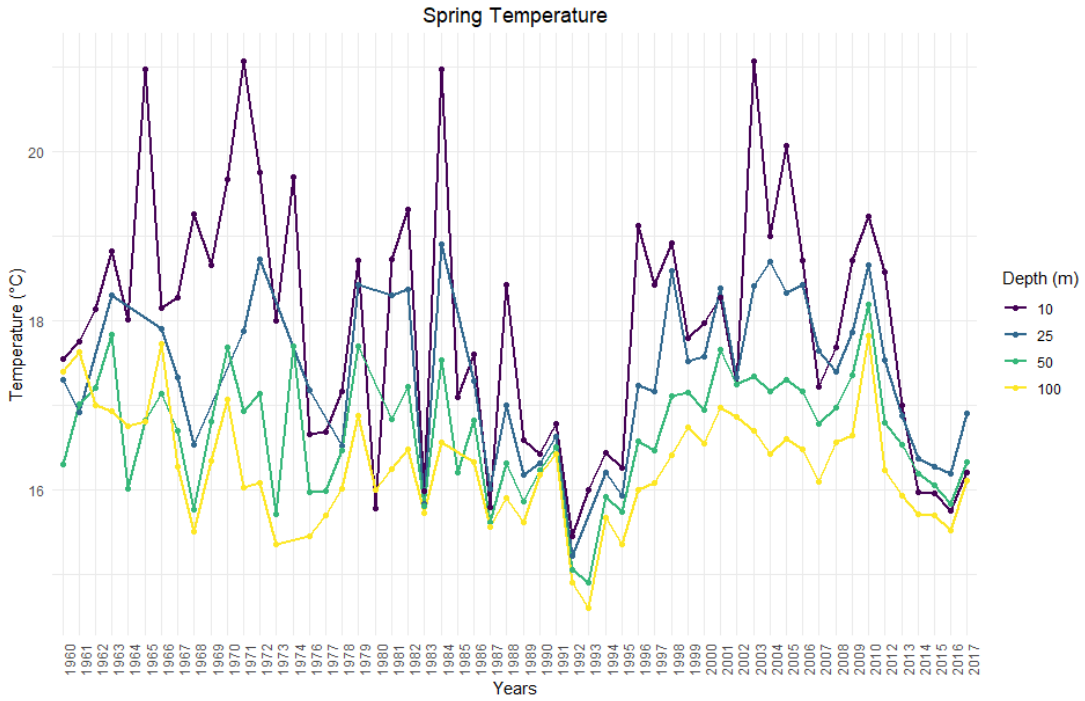

Appendix C 5 Annual spring temperature means in the surface to the 100m range, the Levantine Sea from 1960 to 2017

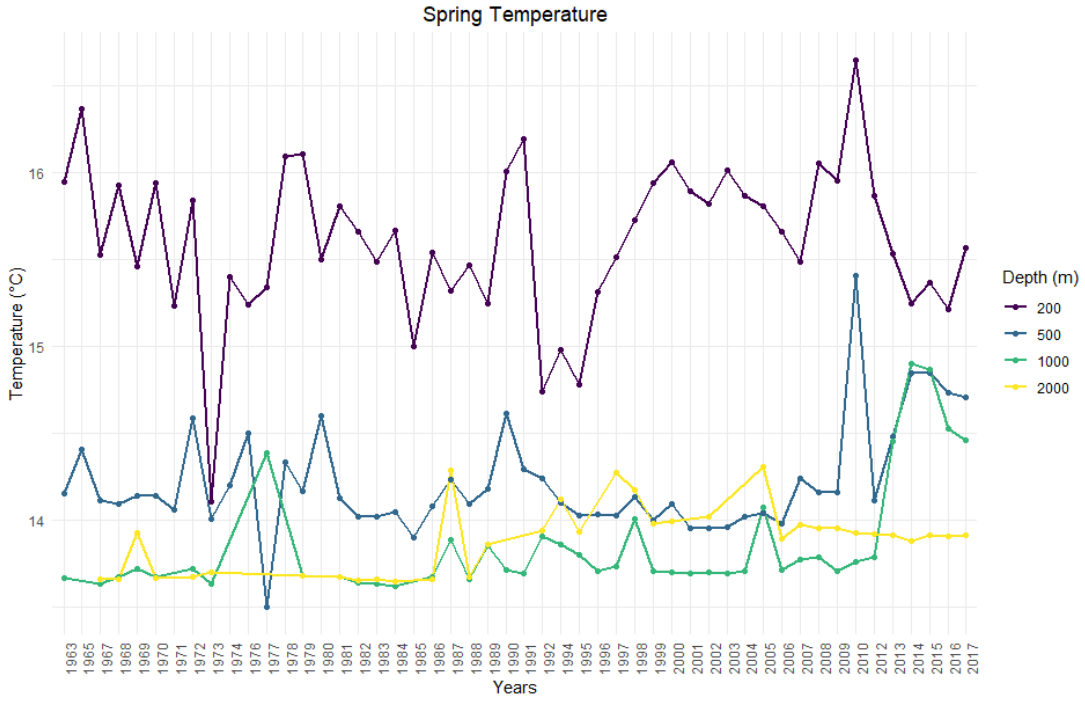

Appendix C 6 Annual spring temperature means in the 200m to the 2000m range, the Levantine Sea from 1960 to 2017

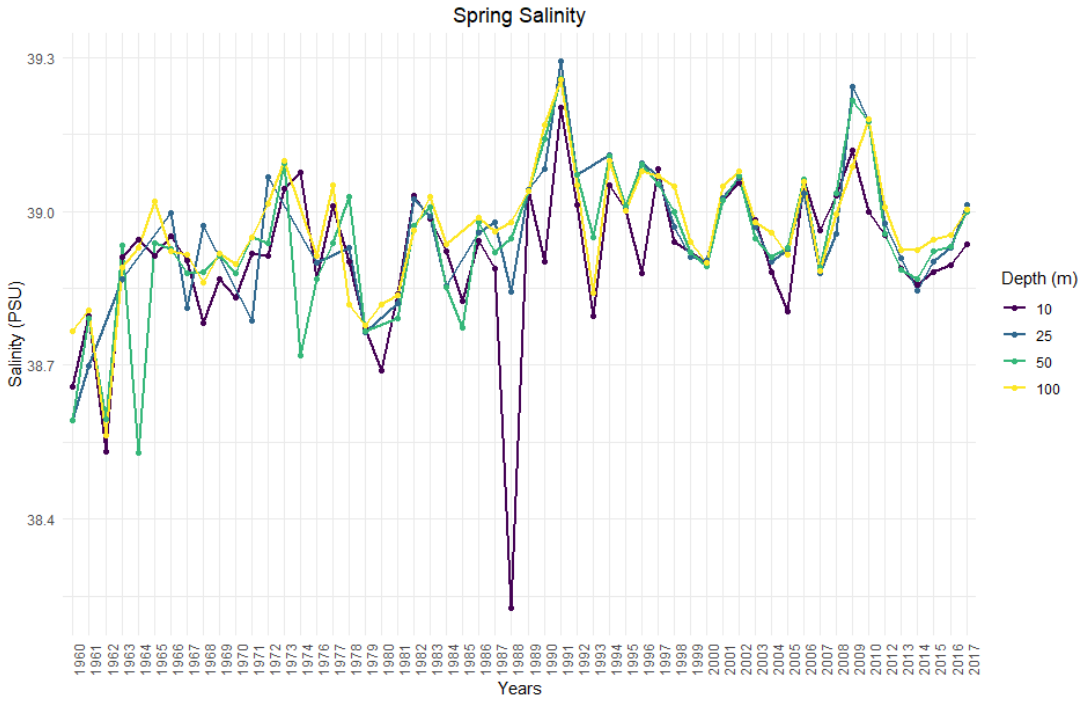

Appendix C 7 Annual spring salinity means in the surface to the 100m range, the Levantine Sea from 1960 to 2017

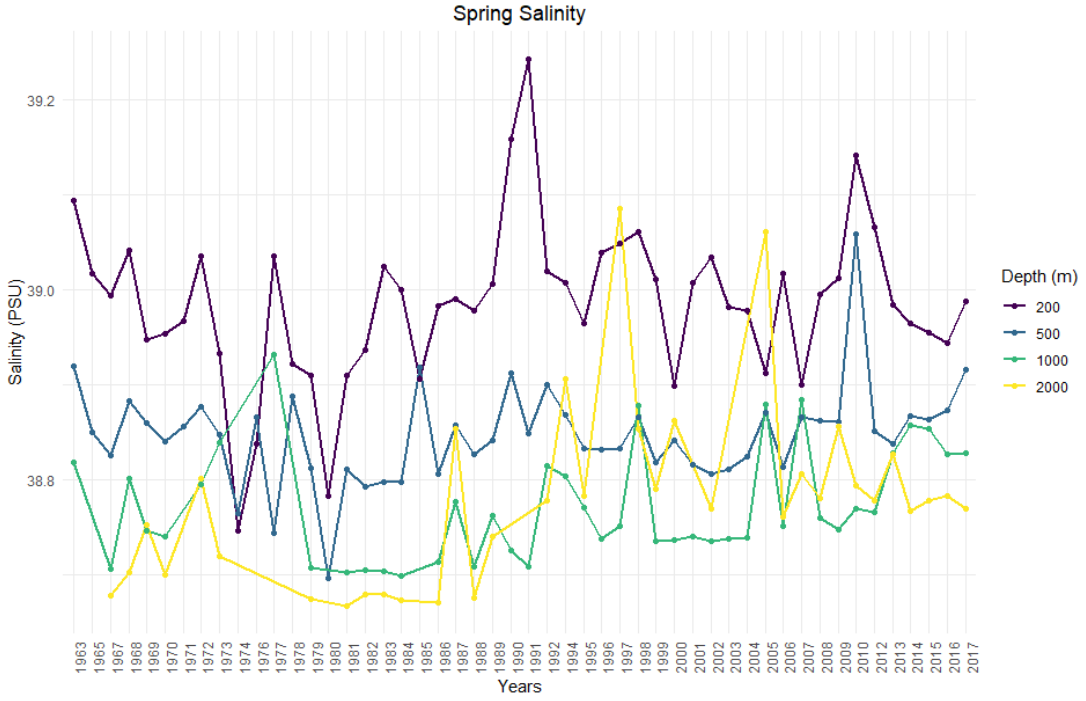

Appendix C 8 Annual spring salinity means in the 200m to the 2000m range, the Levantine Sea from 1960 to 2017

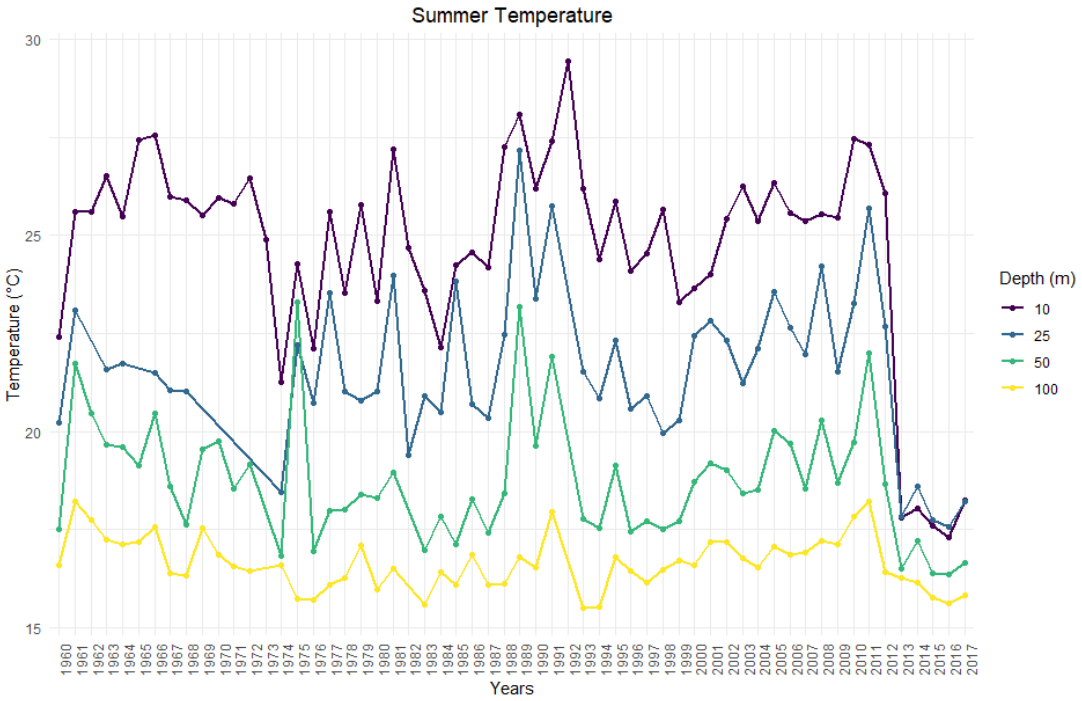

Appendix C 9 Annual summer temperature means in the surface to the 100m range, the Levantine Sea from 1960 to 2017

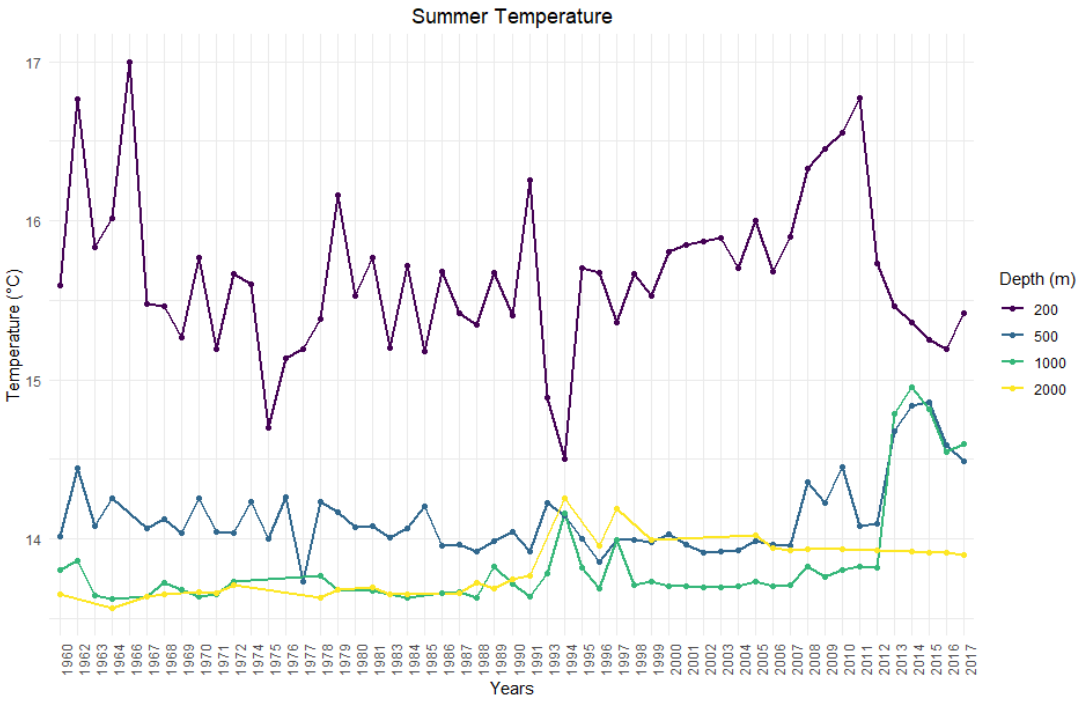

Appendix C 10 Annual summer temperature means in the 200m to the 2000m range, the Levantine Sea from 1960 to 2017

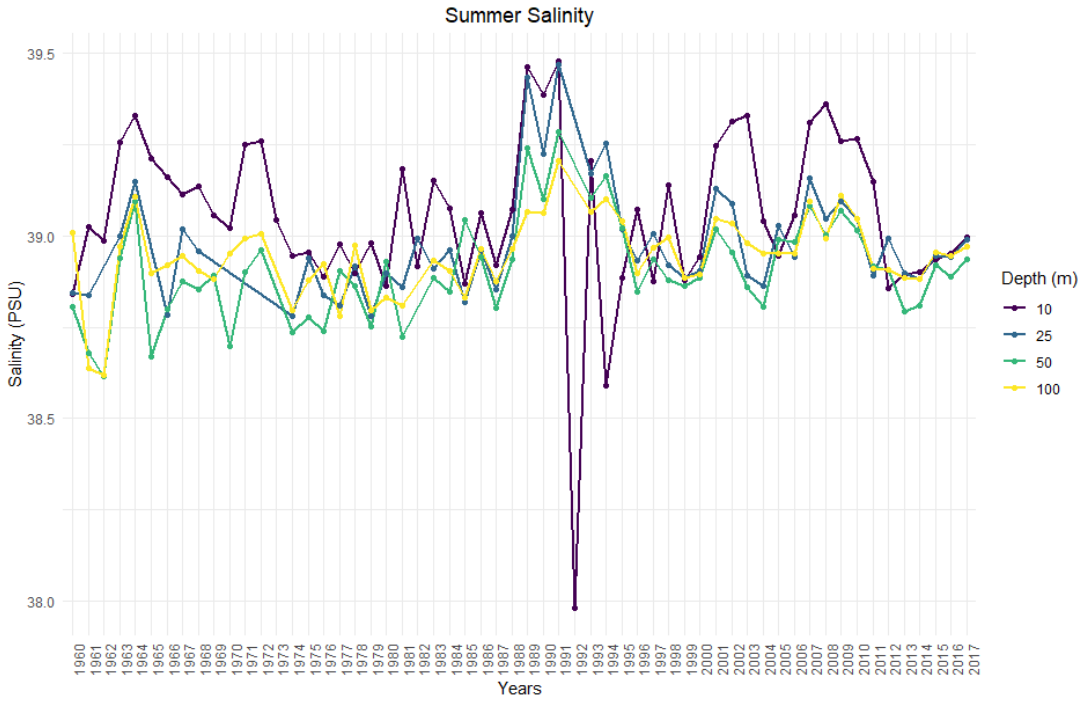

Appendix C 11 Annual summer salinity means in the surface to the 100m range, the Levantine Sea from 1960 to 2017

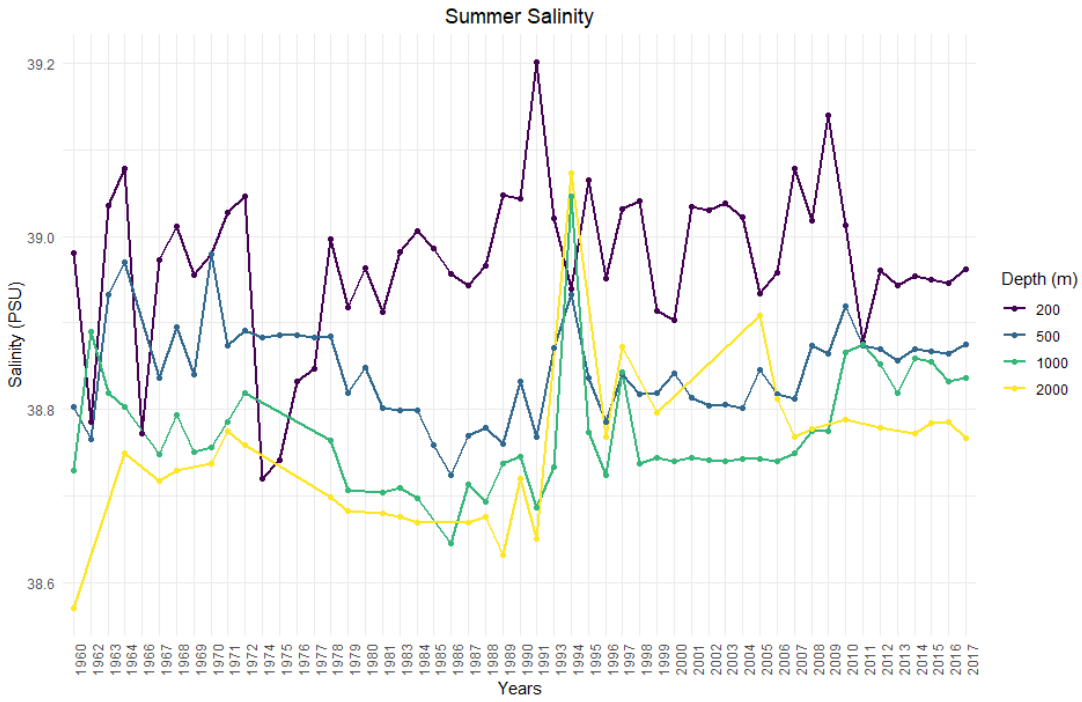

Appendix C 12 Annual summer salinity means in the 200m to the 2000m range, the Levantine Sea from 1960 to 2017

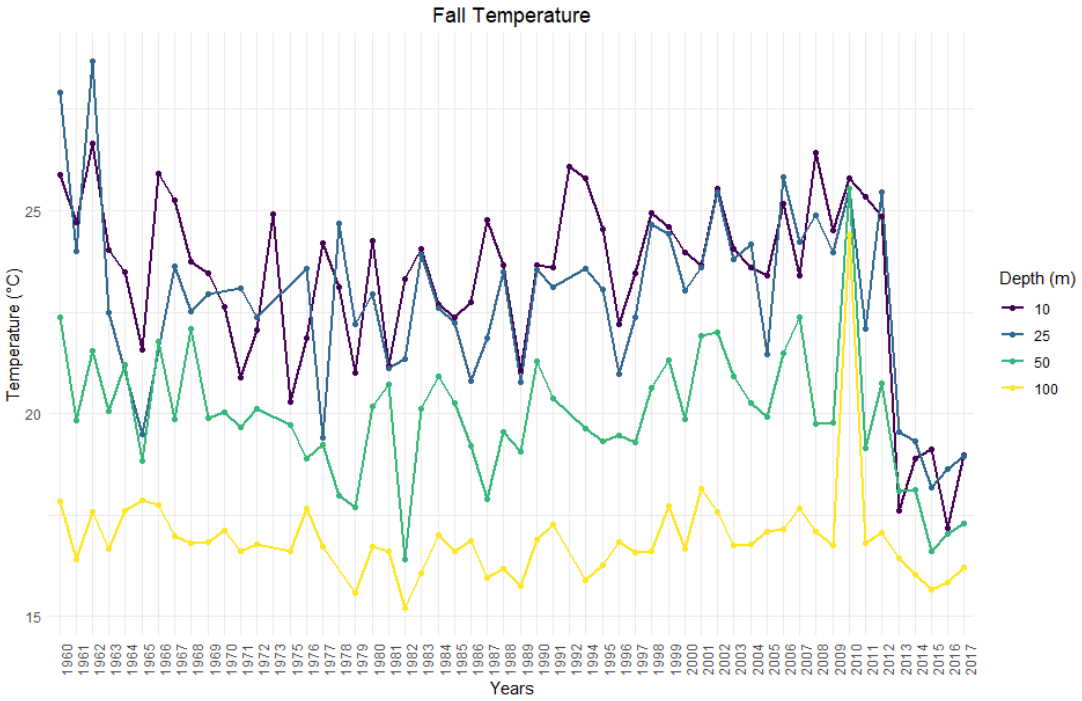

Appendix C 13 Annual fall temperature means in the surface to the 100m range, the Levantine Sea from 1960 to 2017

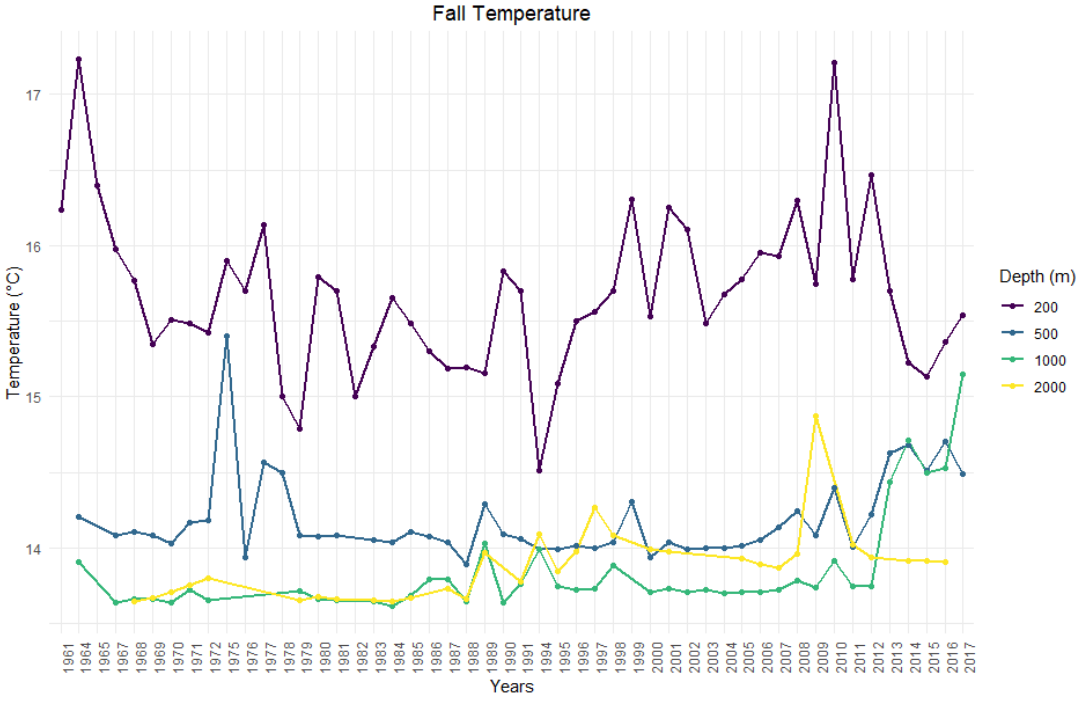

Appendix C 14 Annual fall temperature means in the 200m to the 2000m range, the Levantine Sea from 1960 to 2017

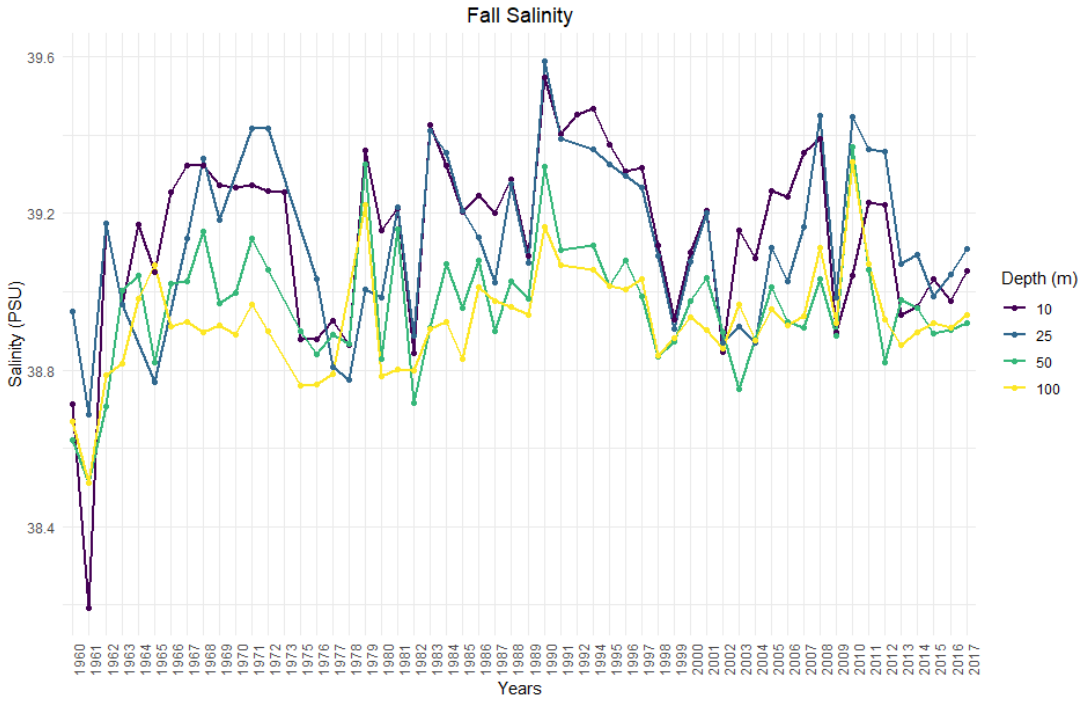

Appendix C 15 Annual fall salinity means in the surface to the 100m range, the Levantine Sea from 1960 to 2017

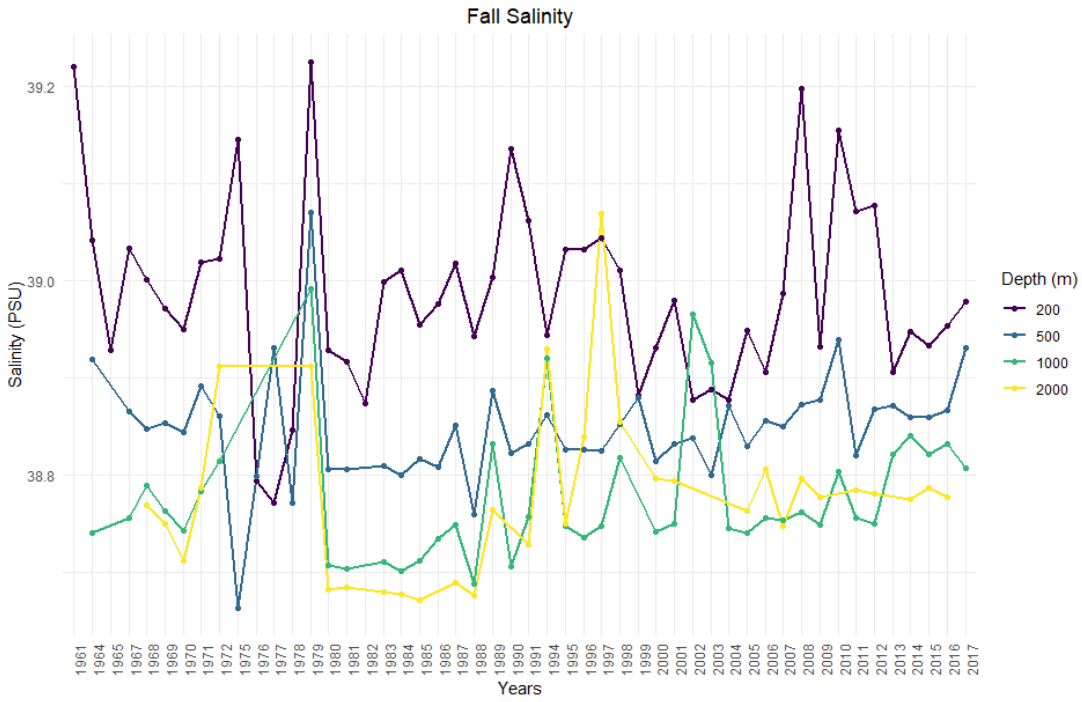

Appendix C 16 Annual fall salinity means in the 200m to the 2000m range, the Levantine Sea from 1960 to 2017

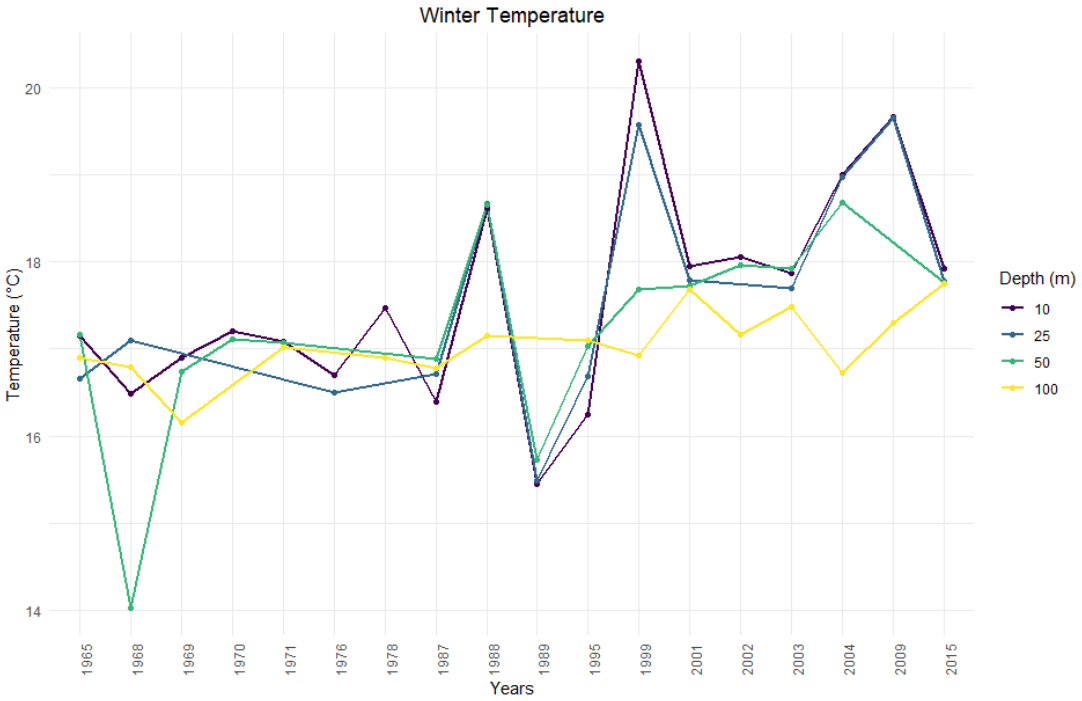

Appendix C 17 Annual winter temperature means in the surface to the 100m range, the Cilician Basin from 1960 to 2017

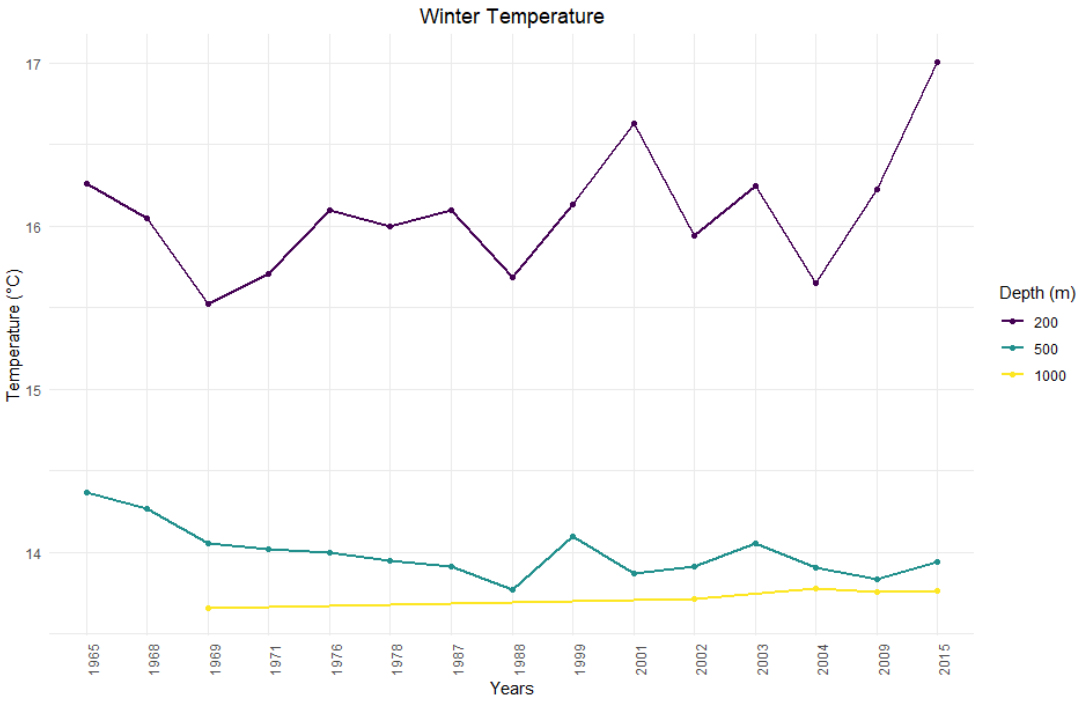

Appendix C 18 Annual winter temperature means in the 200m to the 1000m range, the Cilician Basin from 1960 to 2017

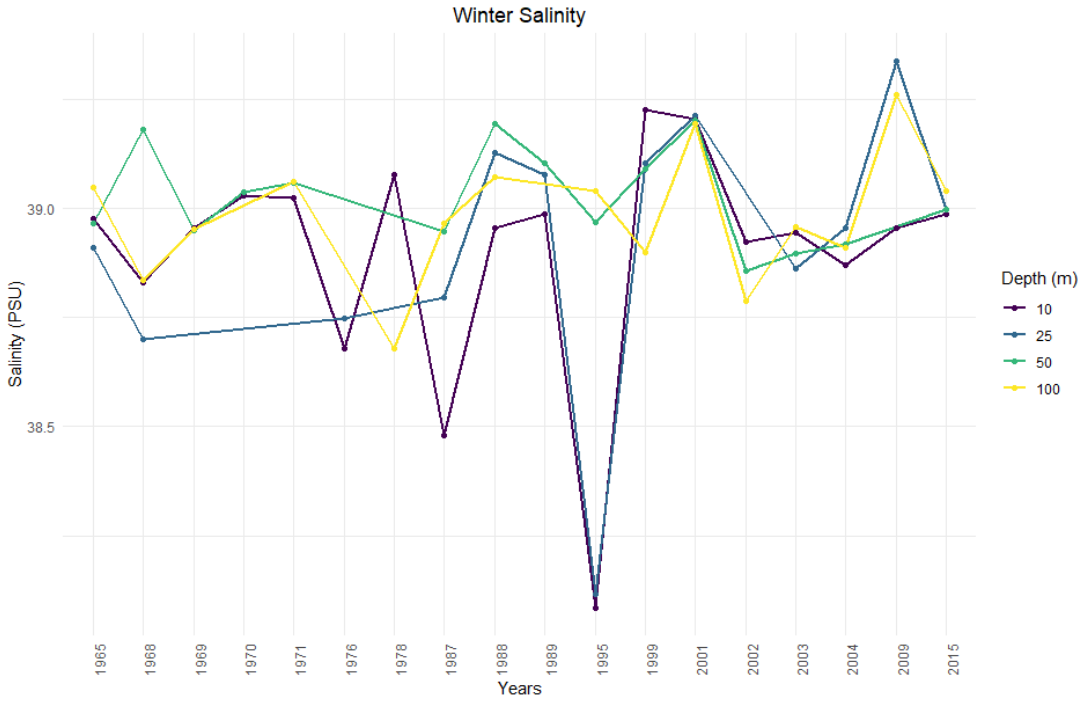

Appendix C 19 Annual winter salinity means in the surface to the 100m range, the Cilician Basin from 1960 to 2017

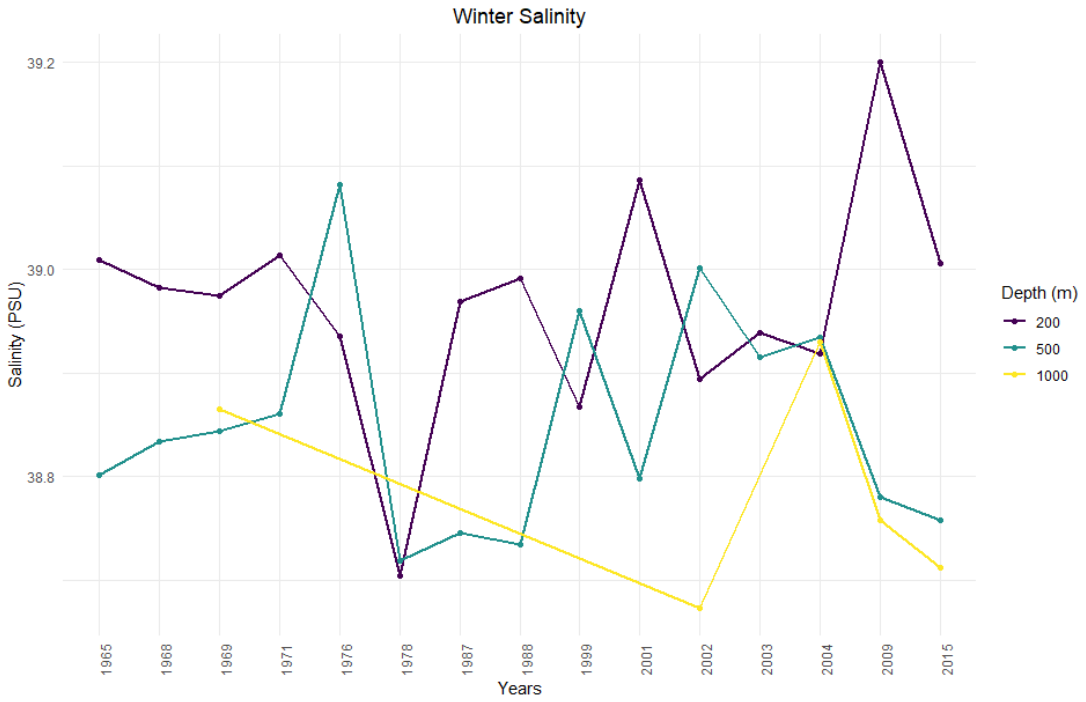

Appendix C 20 Annual winter salinity means in the 200m to the 1000m range, the Cilician Basin from 1960 to 2017

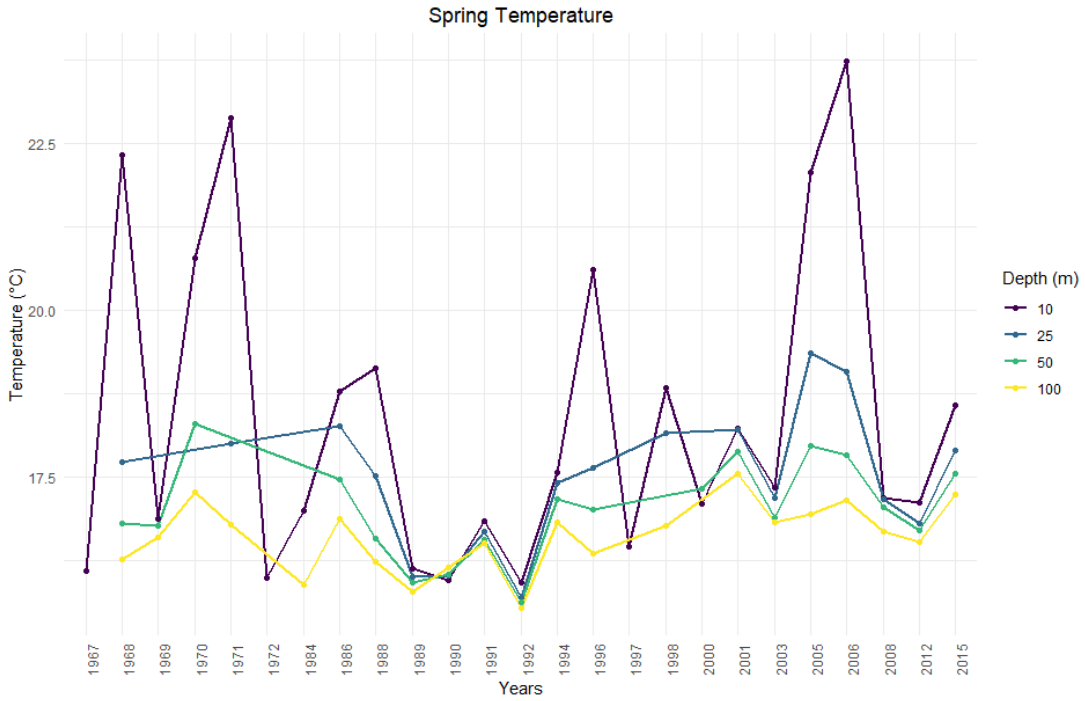

Appendix C 21 Annual spring temperature means in the surface to the 100m range, the Cilician Basin from 1960 to 2017

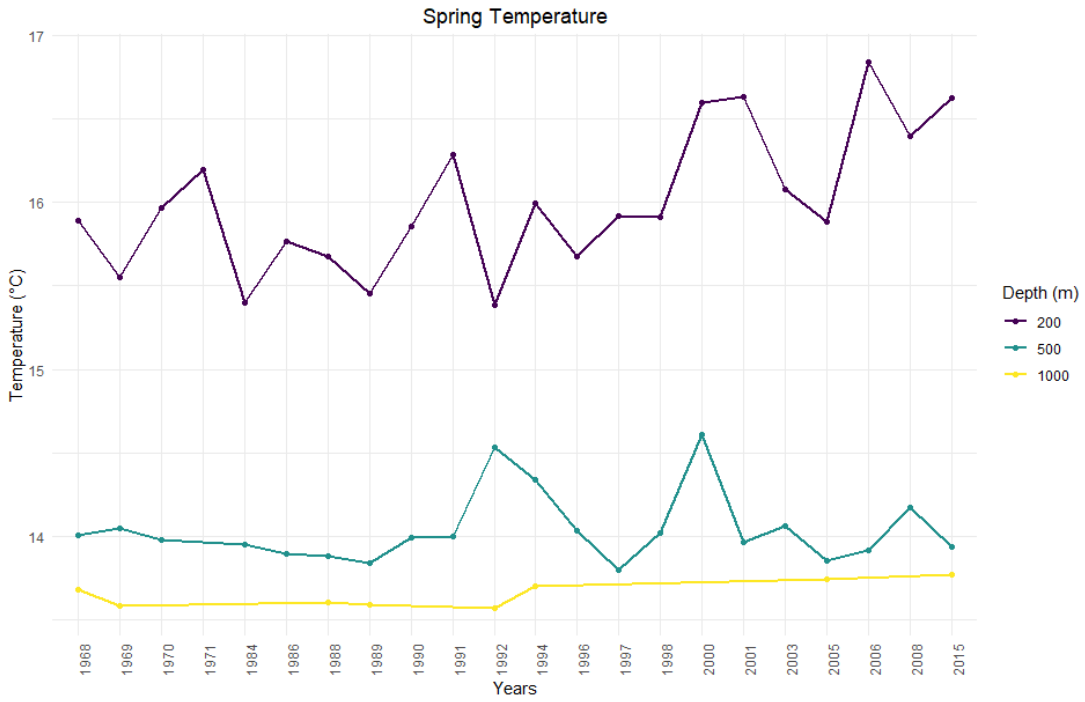

Appendix C 22 Annual spring temperature means in the 200m to the 1000m range, the Cilician Basin from 1960 to 2017

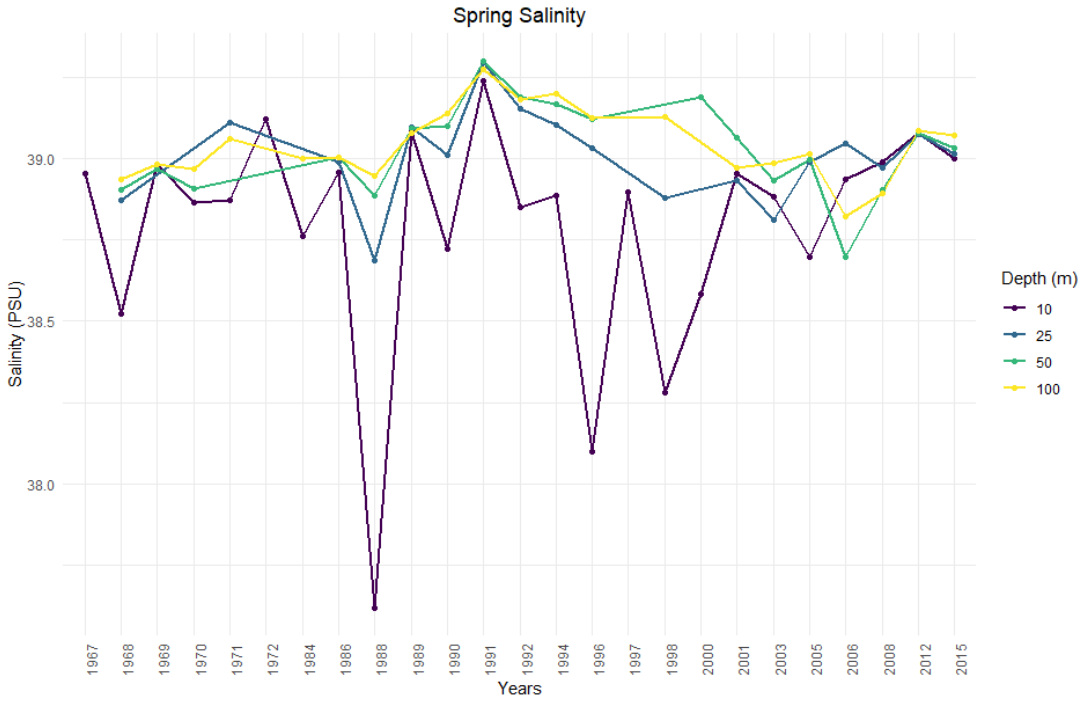

Appendix C 23 Annual spring salinity means in the surface to the 100m range, the Cilician Basin from 1960 to 2017

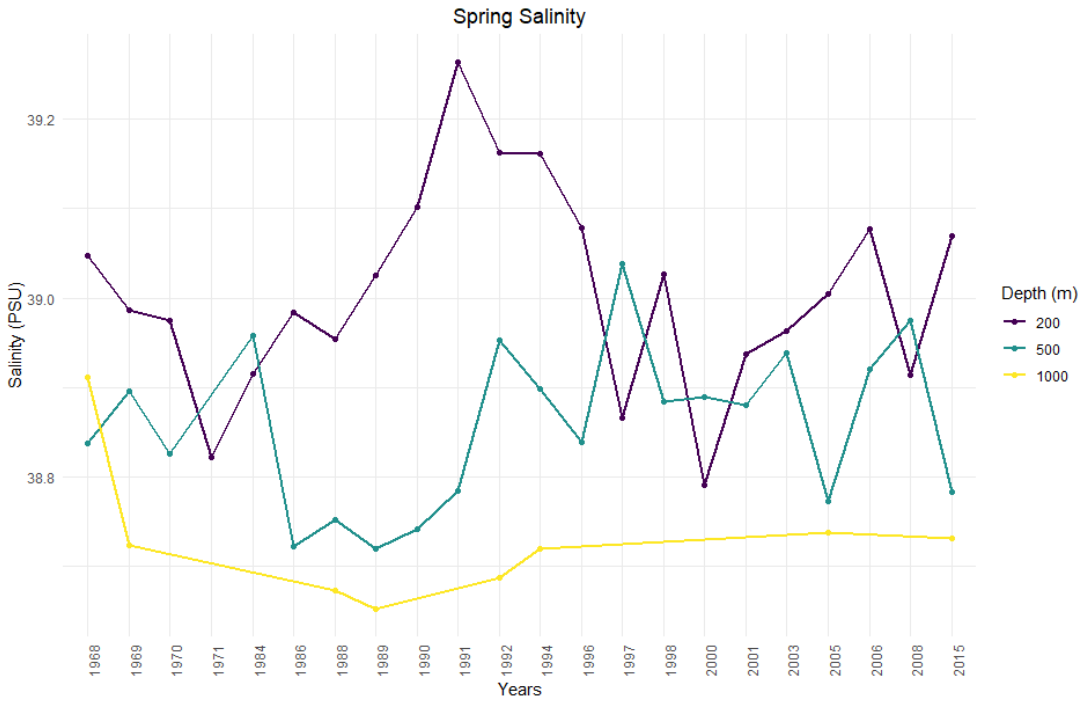

Appendix C 24 Annual spring salinity means in the 200m to the 1000m range, the Cilician Basin from 1960 to 2017

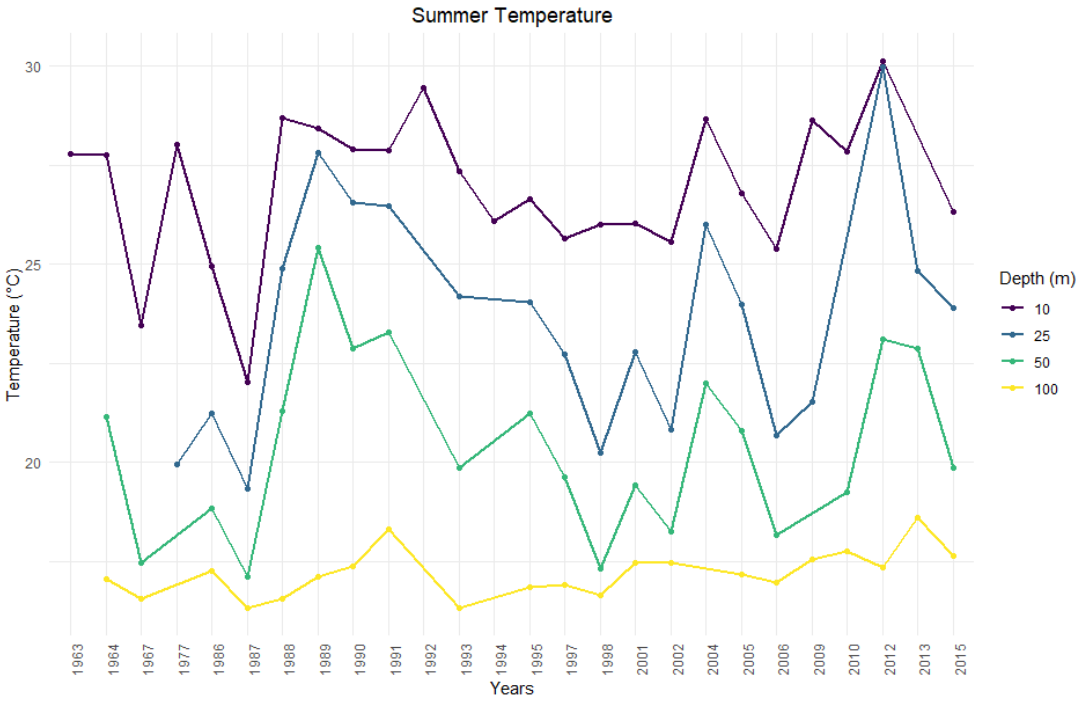

Appendix C 25 Annual summer temperature means in the surface to the 100m range, the Cilician Basin from 1960 to 2017

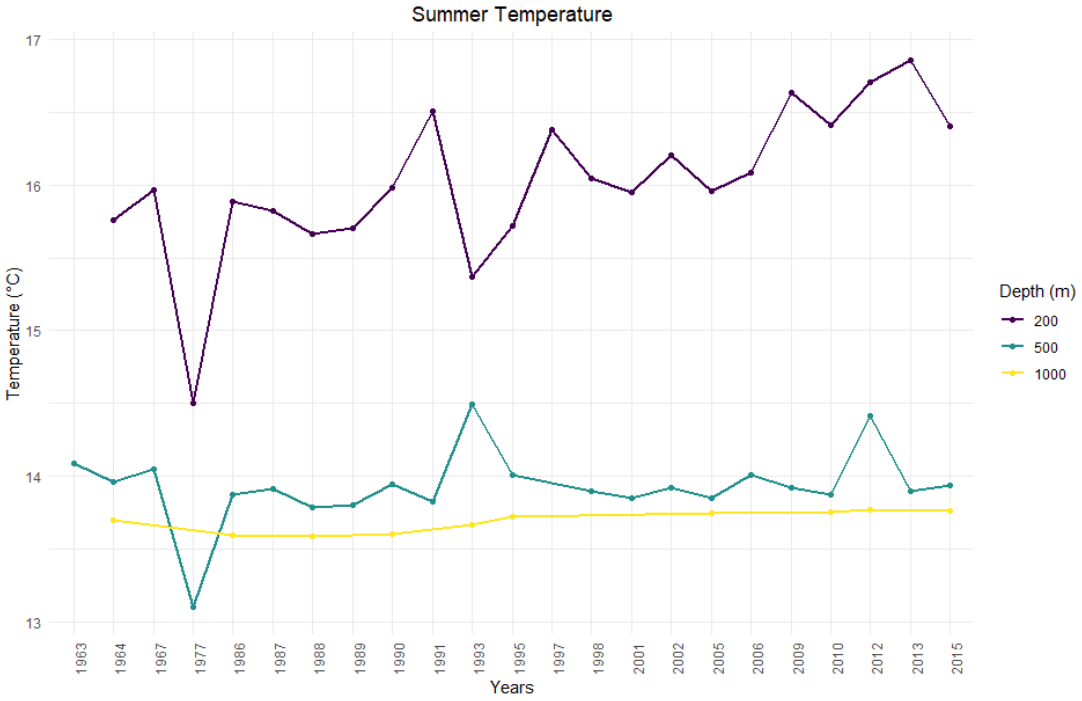

Appendix C 26 Annual summer temperature means in the 200m to the 1000m range, the Cilician Basin from 1960 to 2017

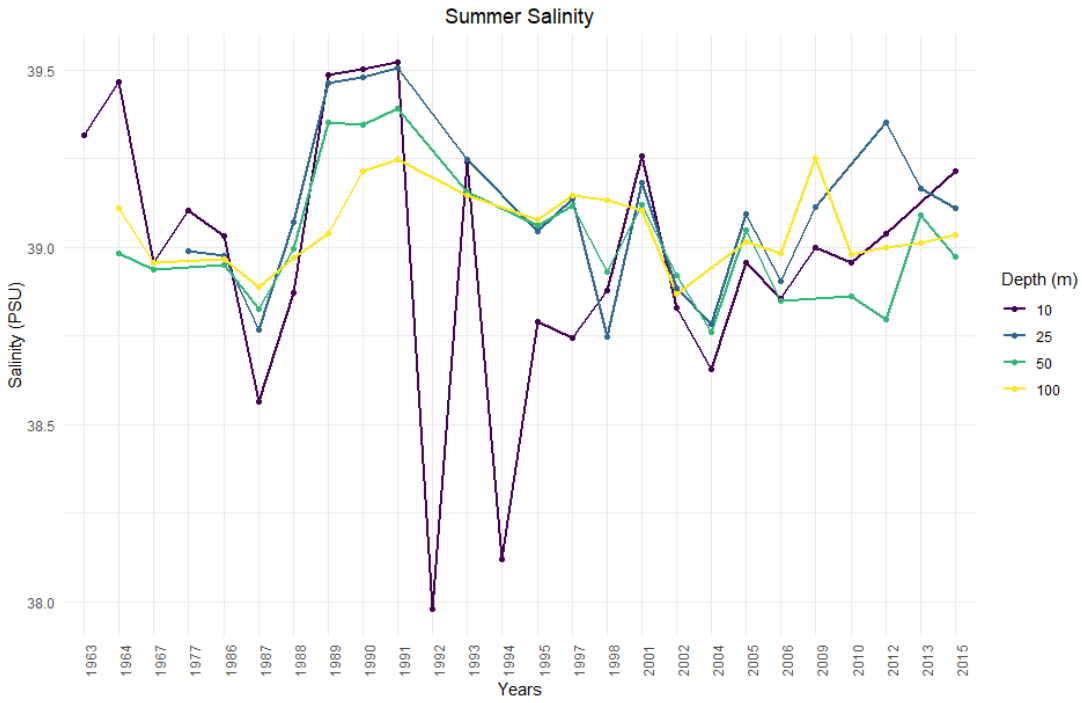

Appendix C 27 Annual summer salinity means in the surface to the 100m range, the Cilician Basin from 1960 to 2017

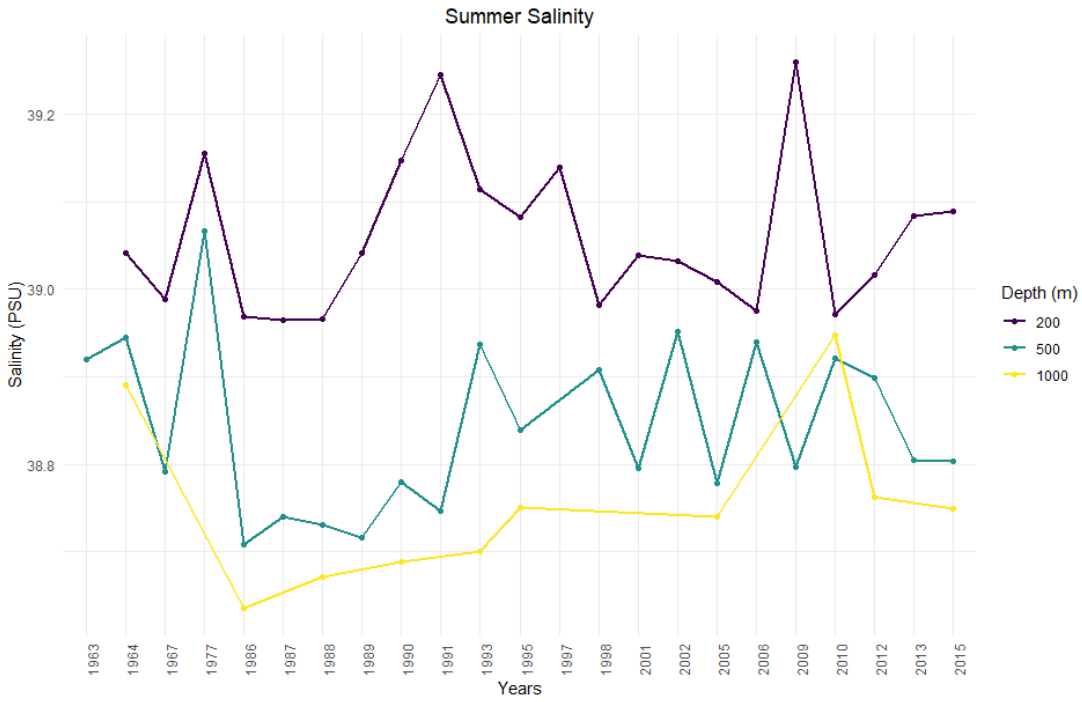

Appendix C 28 Annual summer salinity means in the 200m to the 1000m range, the Cilician Basin from 1960 to 2017

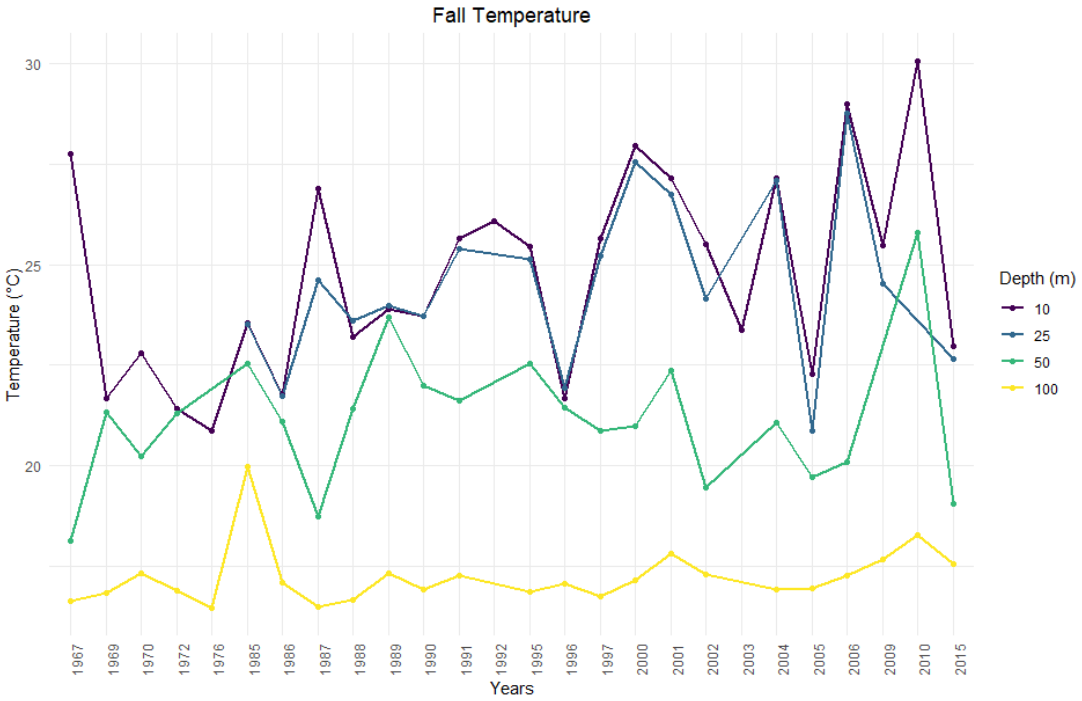

Appendix C 29 Annual fall temperature means in the surface to the 100m range, the Cilician Basin from 1960 to 2017

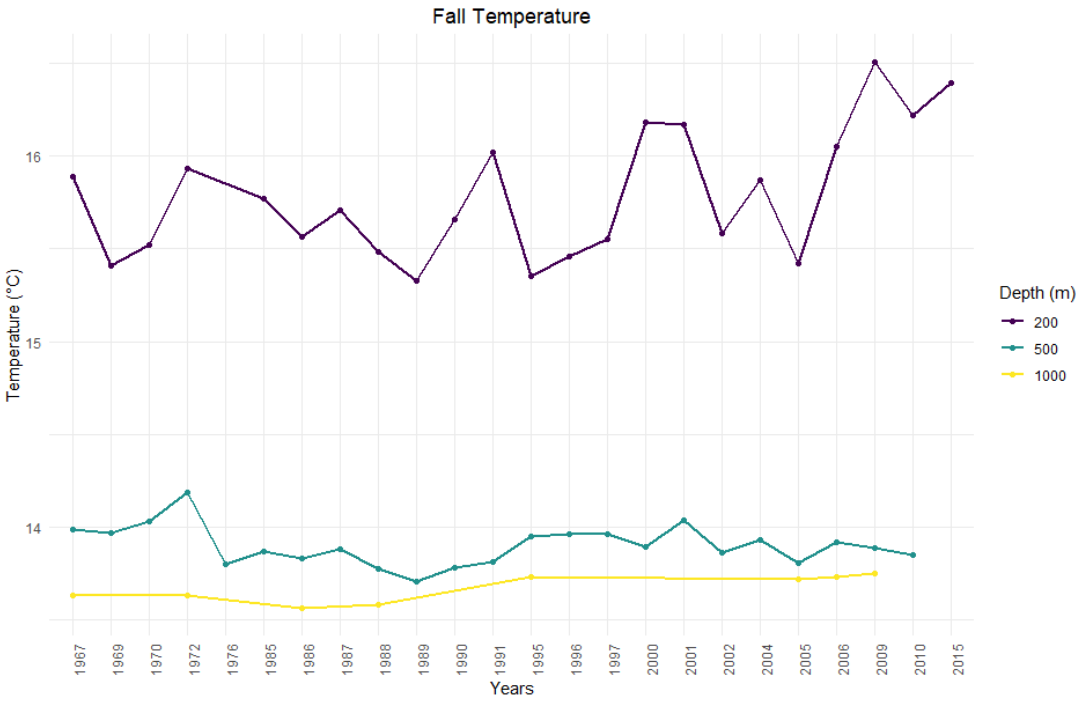

Appendix C 30 Annual fall temperature means in the 200m to the 1000m range, the Cilician Basin from 1960 to 2017

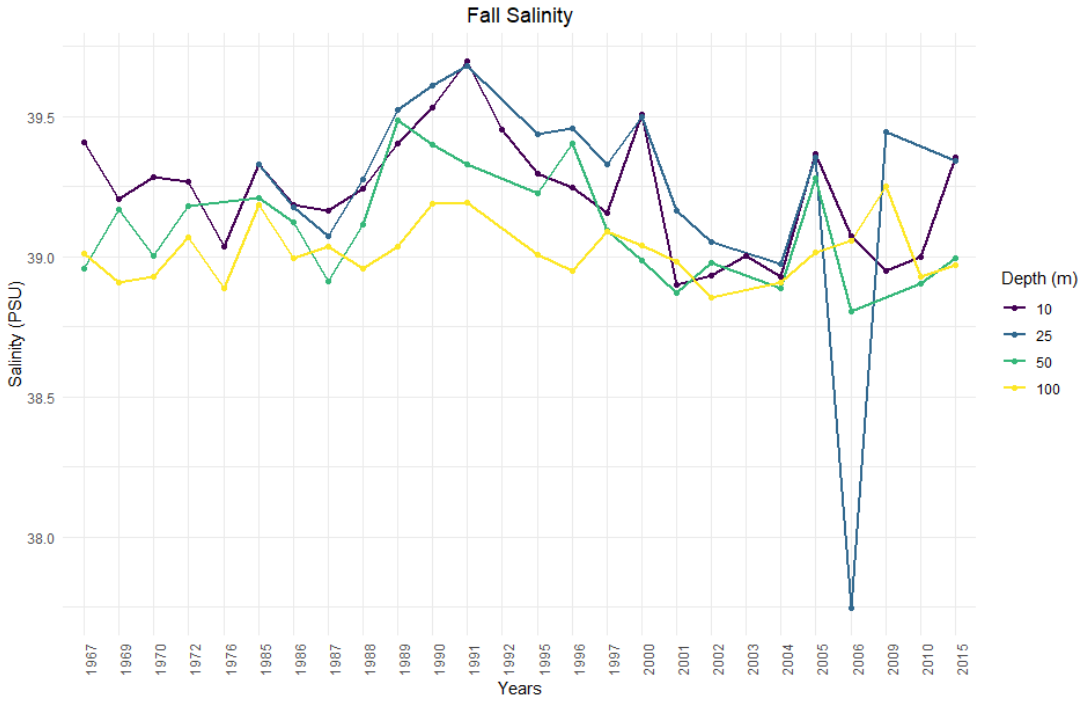

Appendix C 31 Annual fall salinity means in the surface to the 100m range, the Cilician Basin from 1960 to 2017

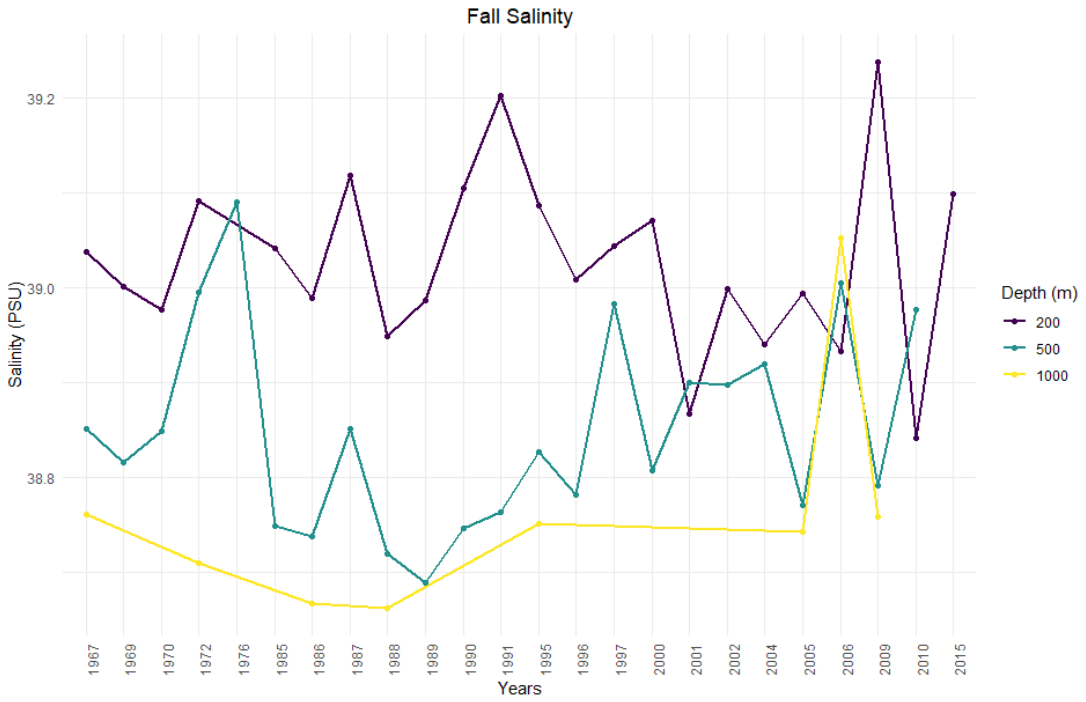

Appendix C 32 Annual fall salinity means in the 200m to the 1000m range, the Cilician Basin from 1960 to 2017

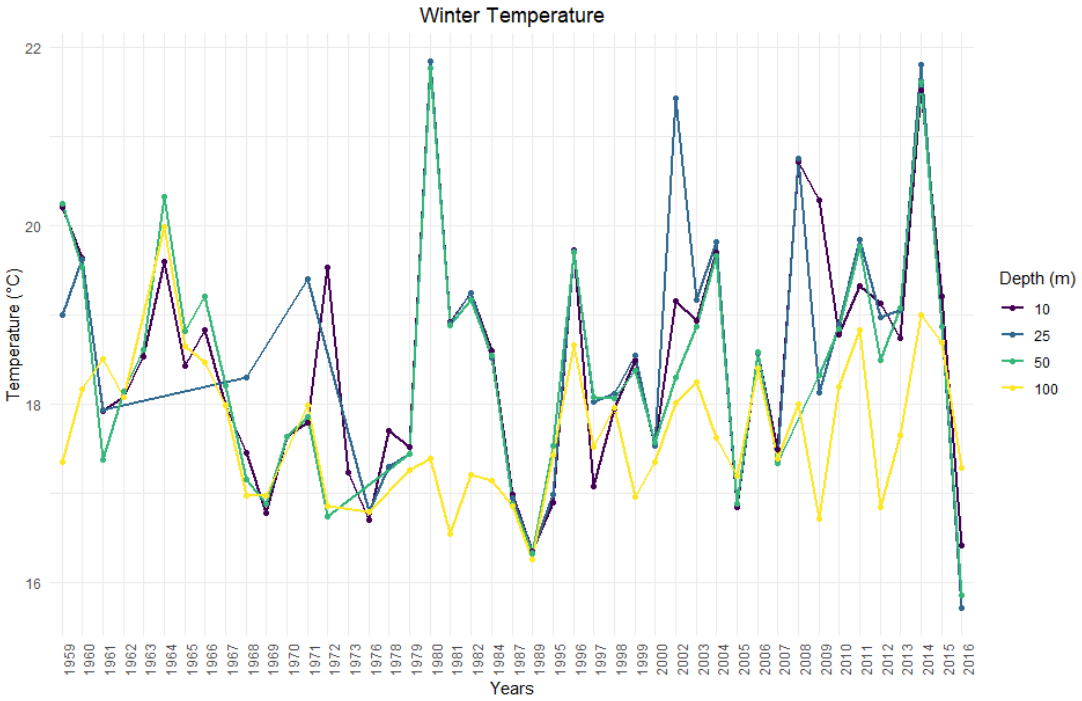

Appendix C 33 Annual winter temperature means in the surface to the 100m range, the Levantine Basin from 1960 to 2017

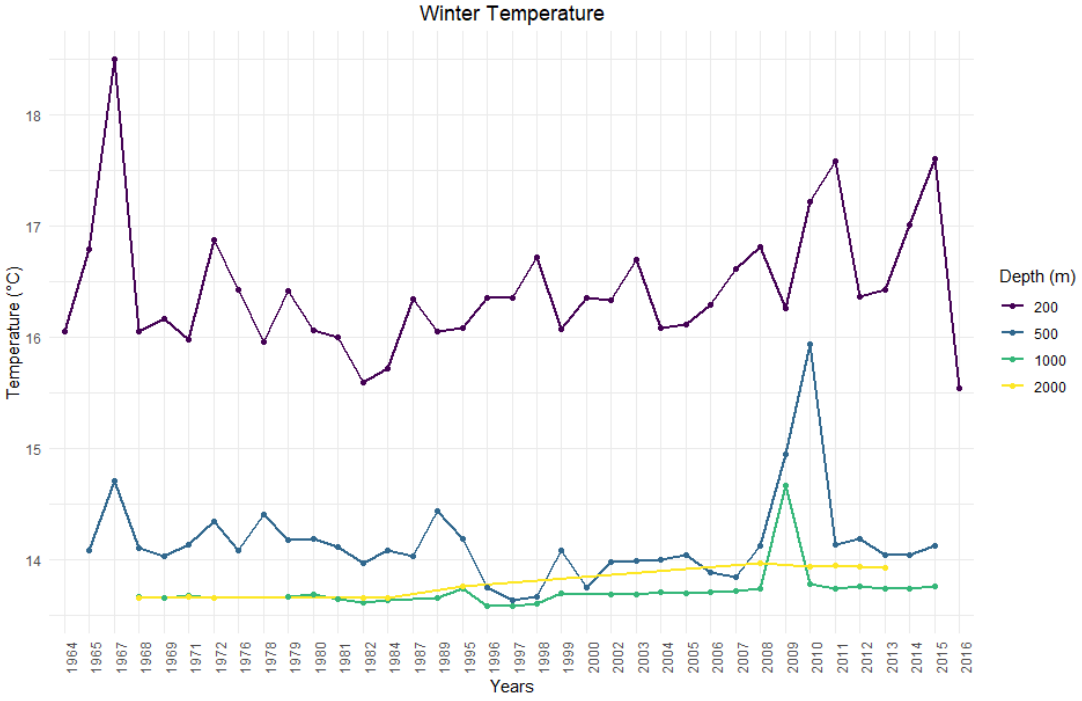

Appendix C 34 Annual winter temperature means in the 200m to the 2000m range, the Levantine Basin from 1960 to 2017

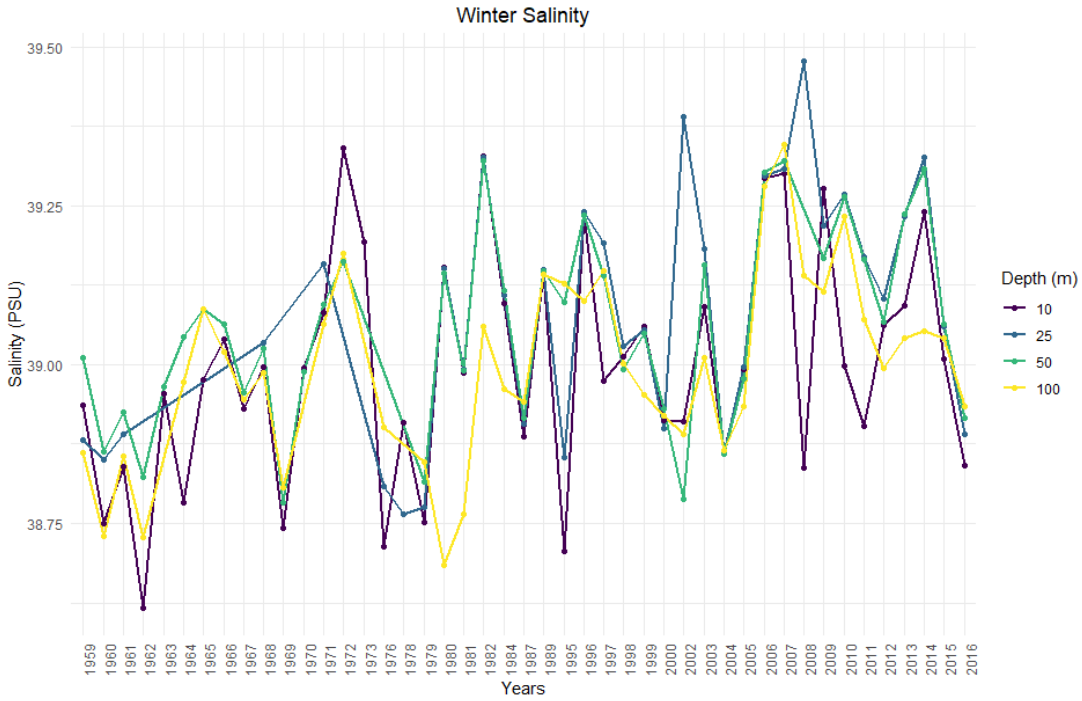

Appendix C 35 Annual winter salinity means in the surface to the 100m range, the Levantine Basin from 1960 to 2017

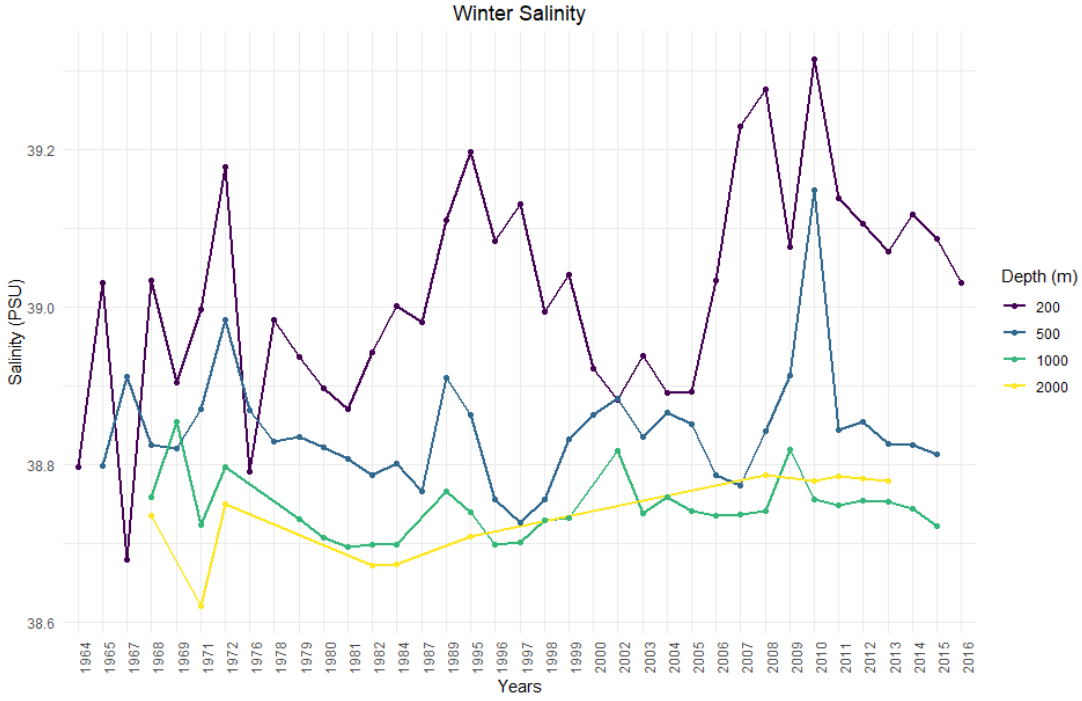

Appendix C 36 Annual winter salinity means for in the 200m to the 2000m range, the Levantine Basin from 1960 to 2017

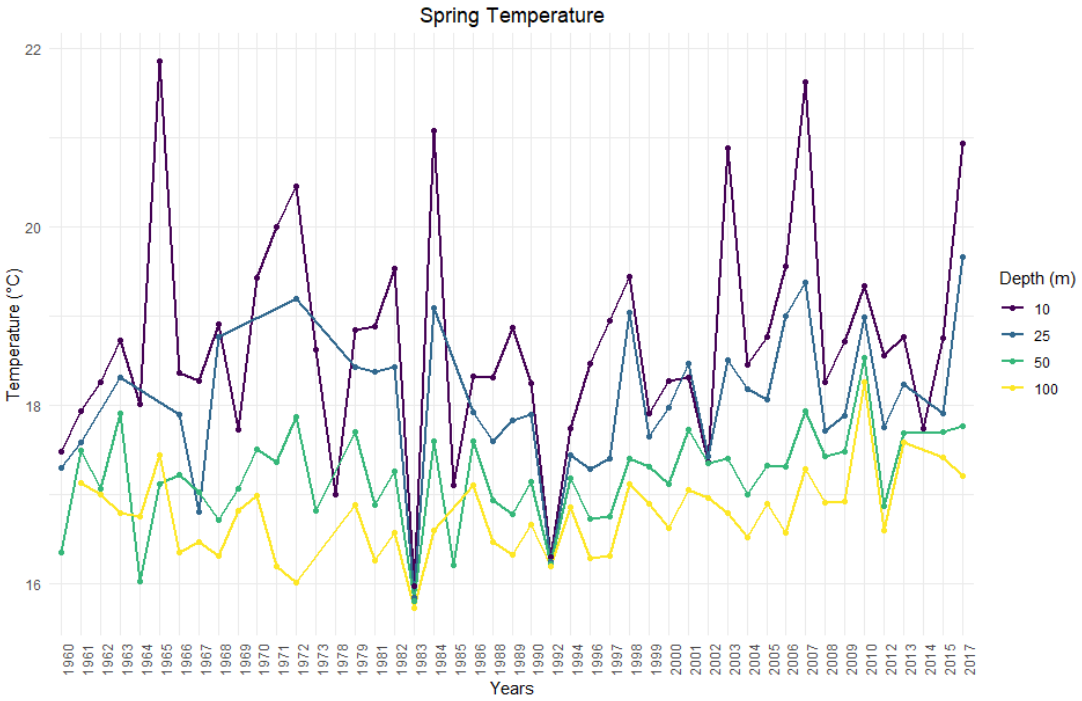

Appendix C 37 Annual spring temperature means in the surface to the 100m range, the Levantine Basin from 1960 to 2017

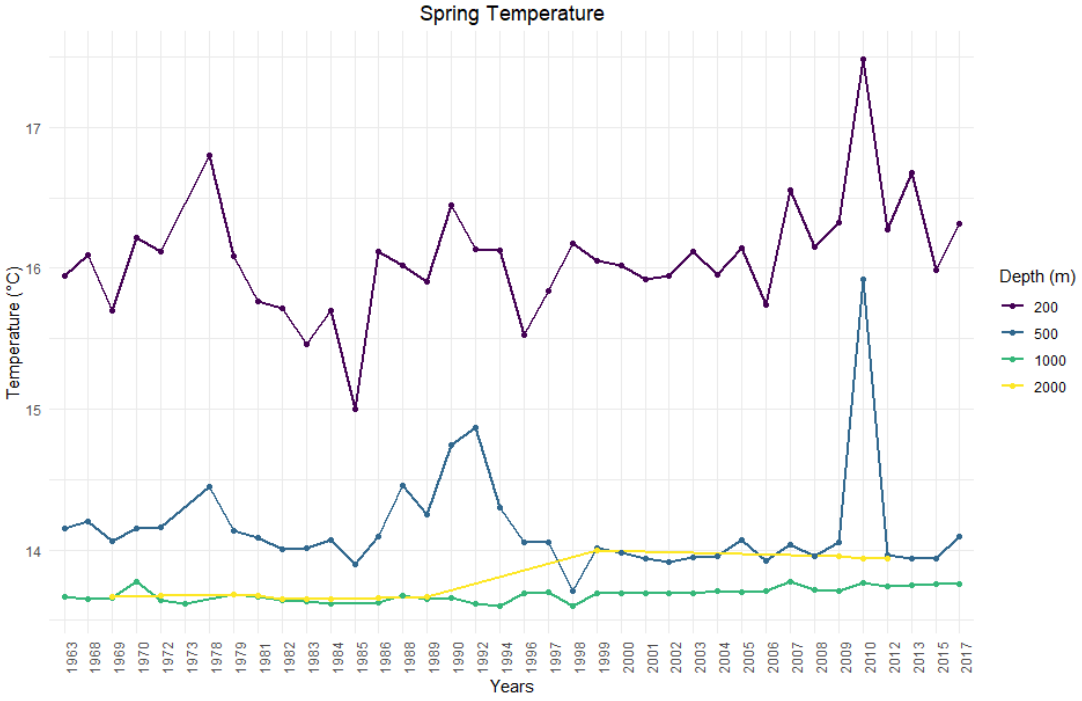

Appendix C 38 Annual spring temperature means in the 200m to the 2000m range, the Levantine Basin from 1960 to 2017

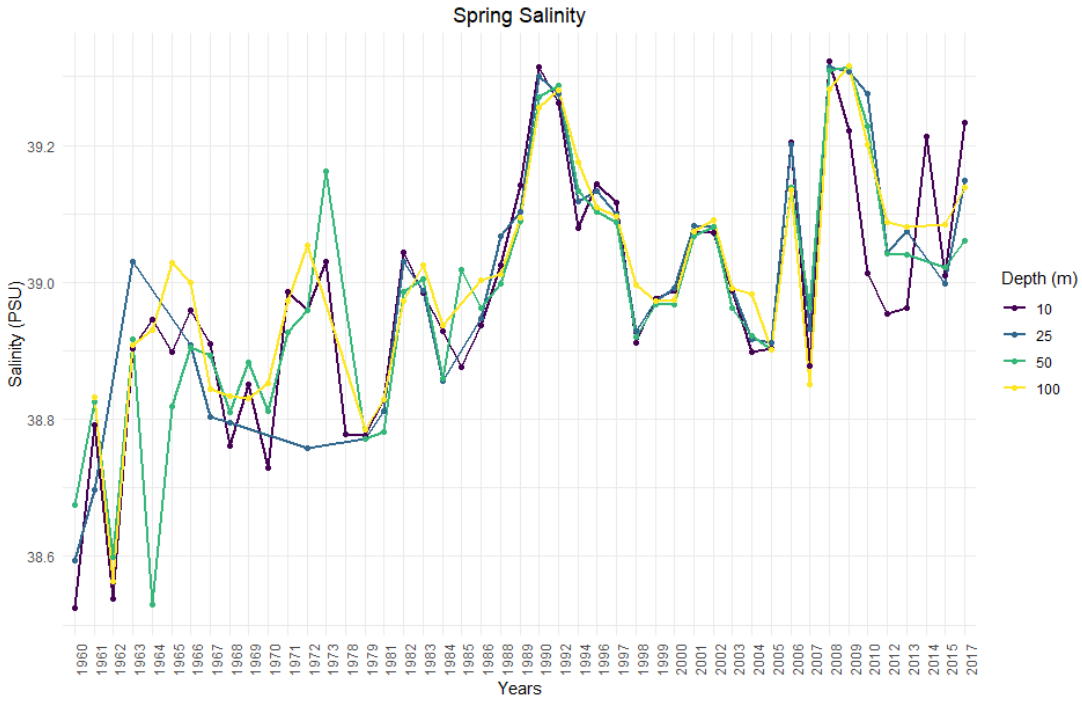

Appendix C 39 Annual spring salinity means in the surface to the 100m range, the Levantine Basin from 1960 to 2017

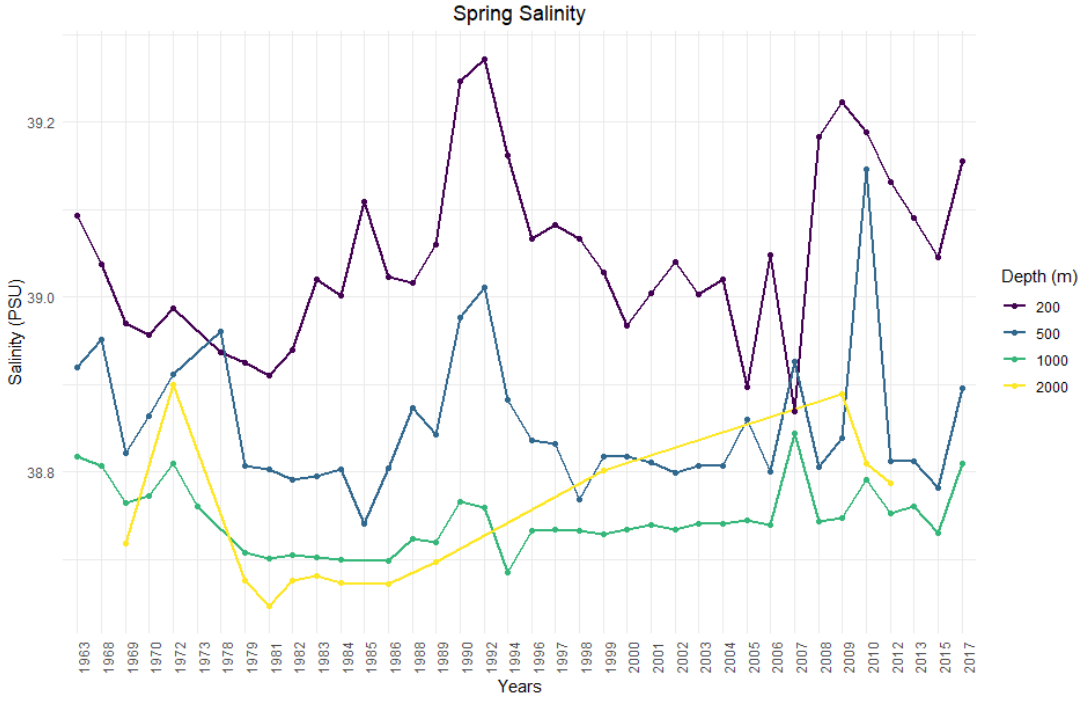

Appendix C 40 Annual spring salinity means in the 200m to the 2000m range, the Levantine Basin from 1960 to 2017

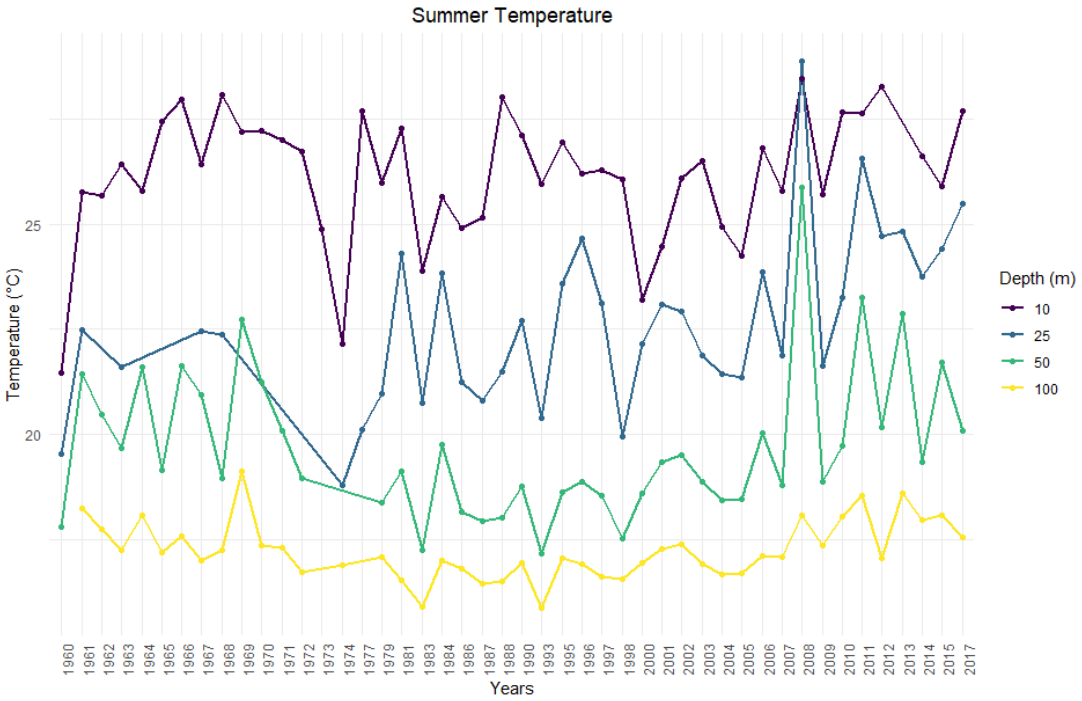

Appendix C 41 Annual summer temperature means in the surface to the 100m range, the Levantine Basin from 1960 to 2017

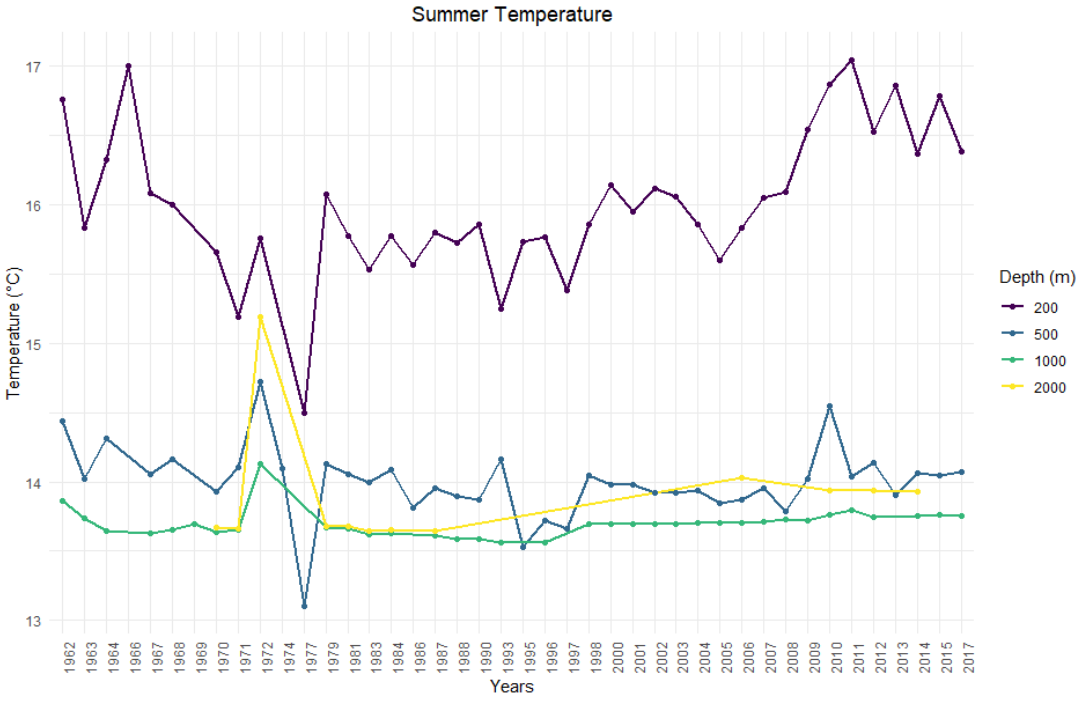

Appendix C 42 Annual summer temperature means in the 200m to the 2000m range, the Levantine Basin from 1960 to 2017

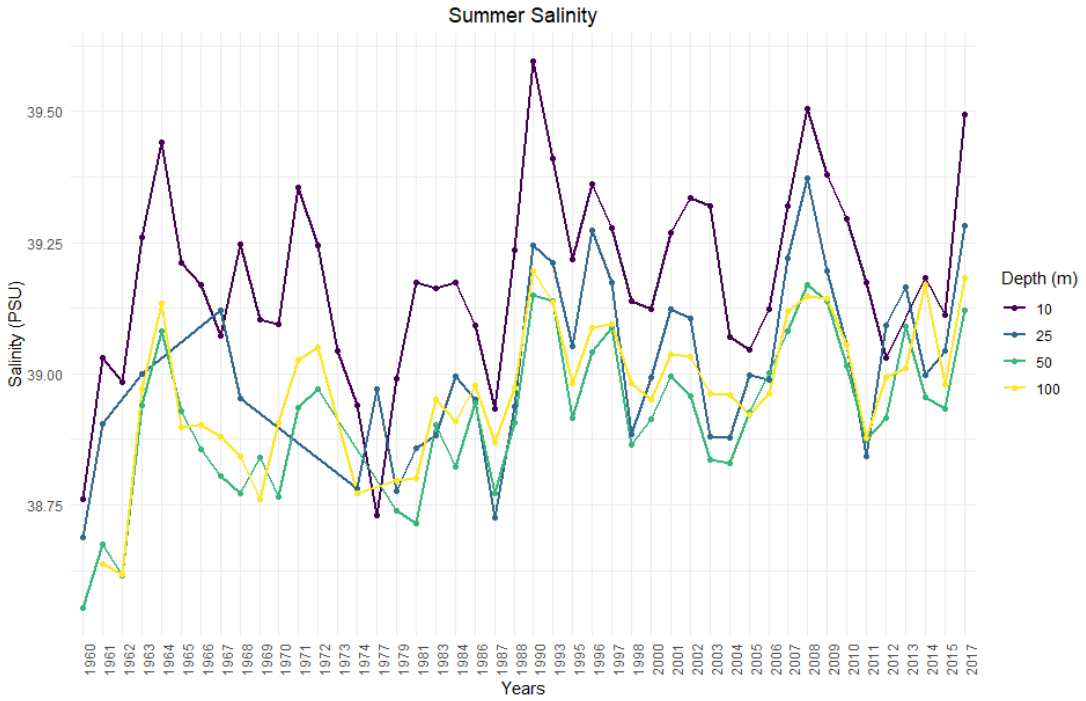

Appendix C 43 Annual summer salinity means in the surface to the 100m range, the Levantine Basin from 1960 to 2017

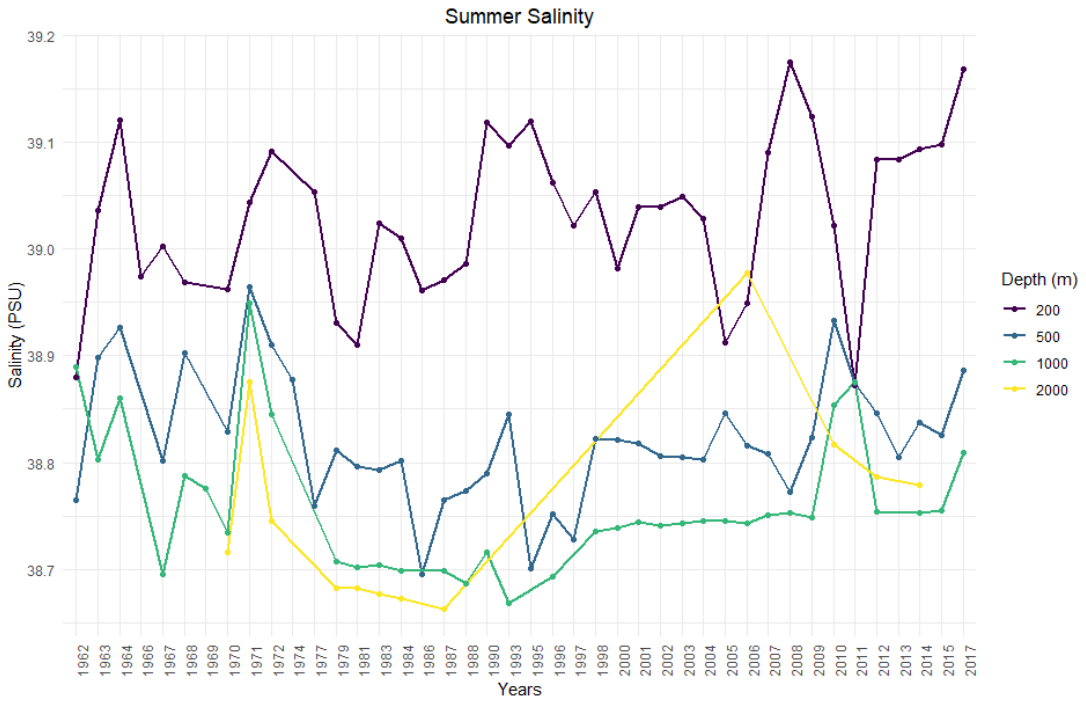

Appendix C 44 Annual summer salinity means in the 200m to the 2000m range, the Levantine Basin from 1960 to 2017

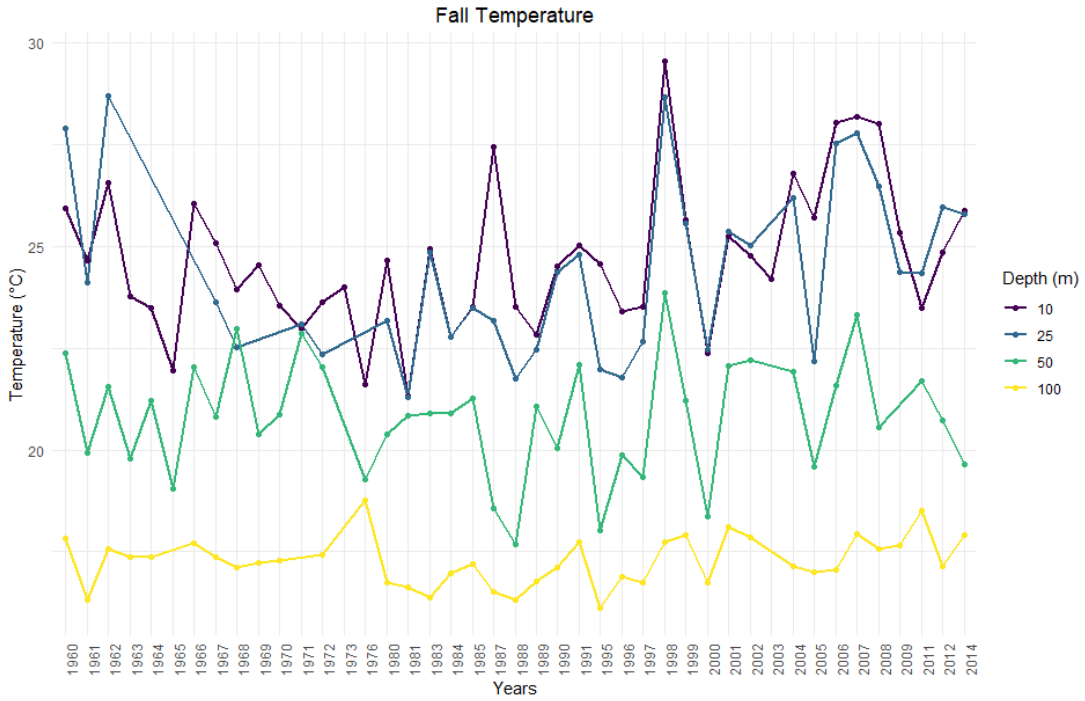

Appendix C 45 Annual fall temperature means in the surface to the 100m range, the Levantine Basin from 1960 to 2017

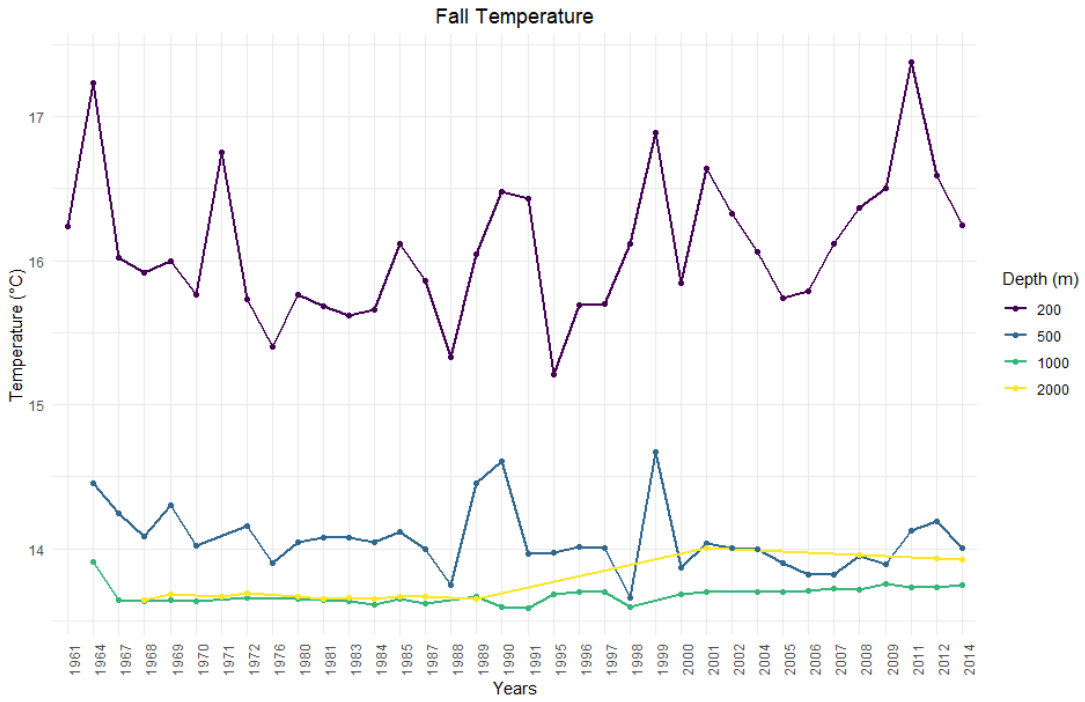

Appendix C 46 Annual fall temperature means in the 200m to the 2000m range, the Levantine Basin from 1960 to 2017

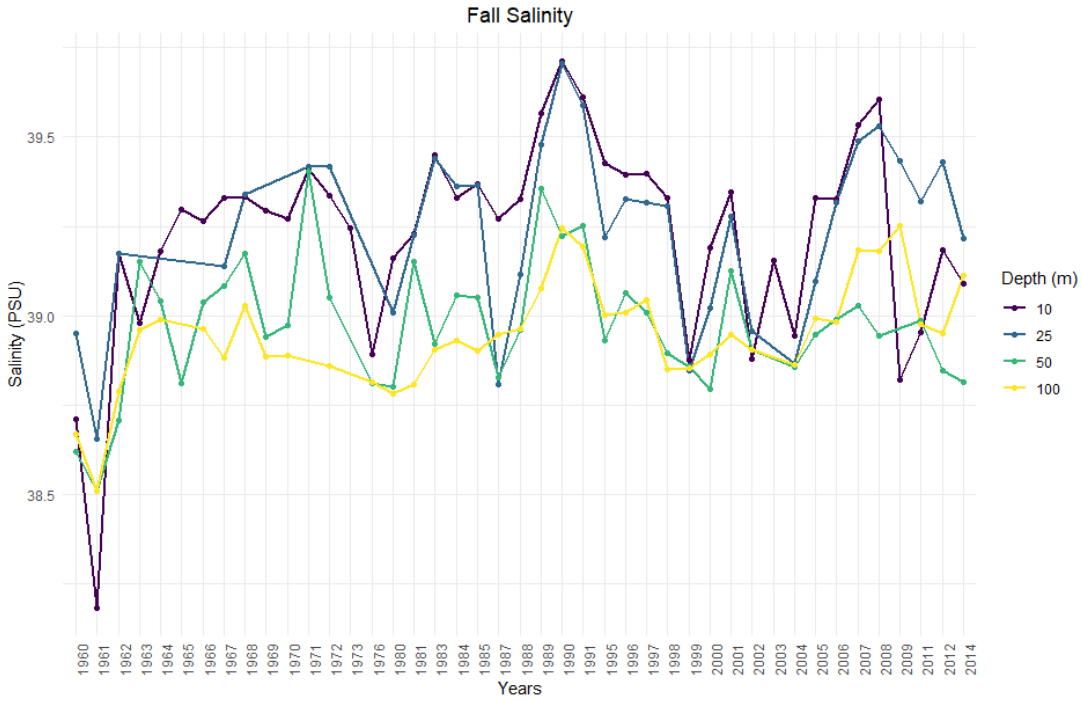

Appendix C 47 Annual fall salinity means in the surface to the 100m range, the Levantine Basin from 1960 to 2017

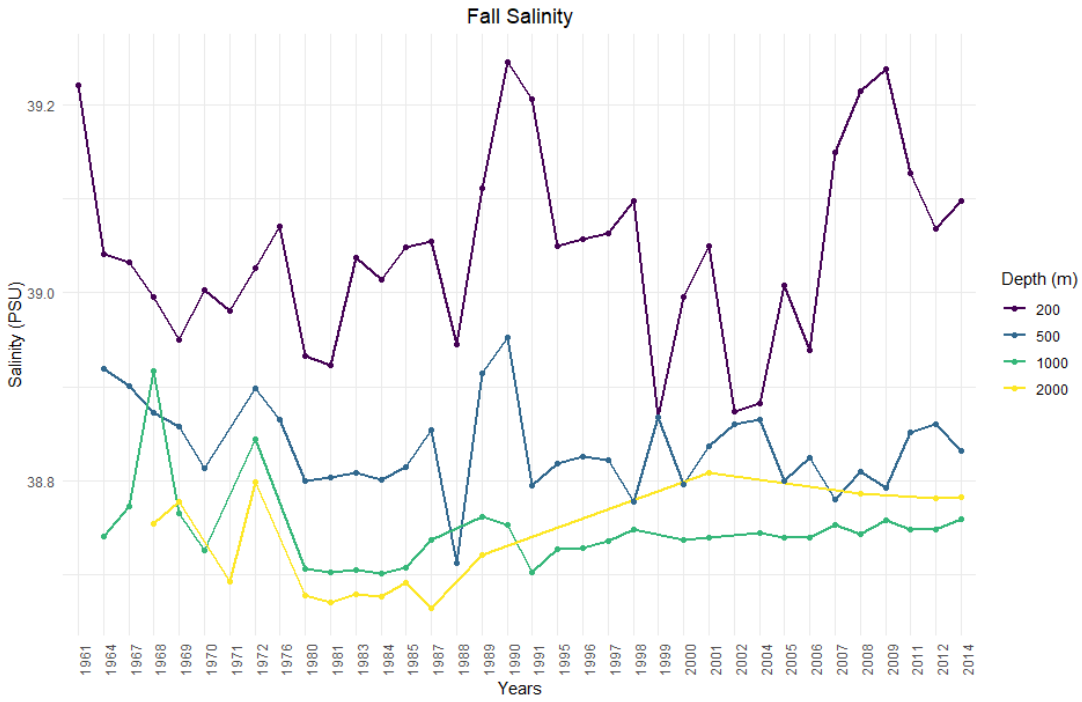

Appendix C 48 Annual fall salinity means in the 200m to the 2000m range, the Levantine Basin from 1960 to 2017

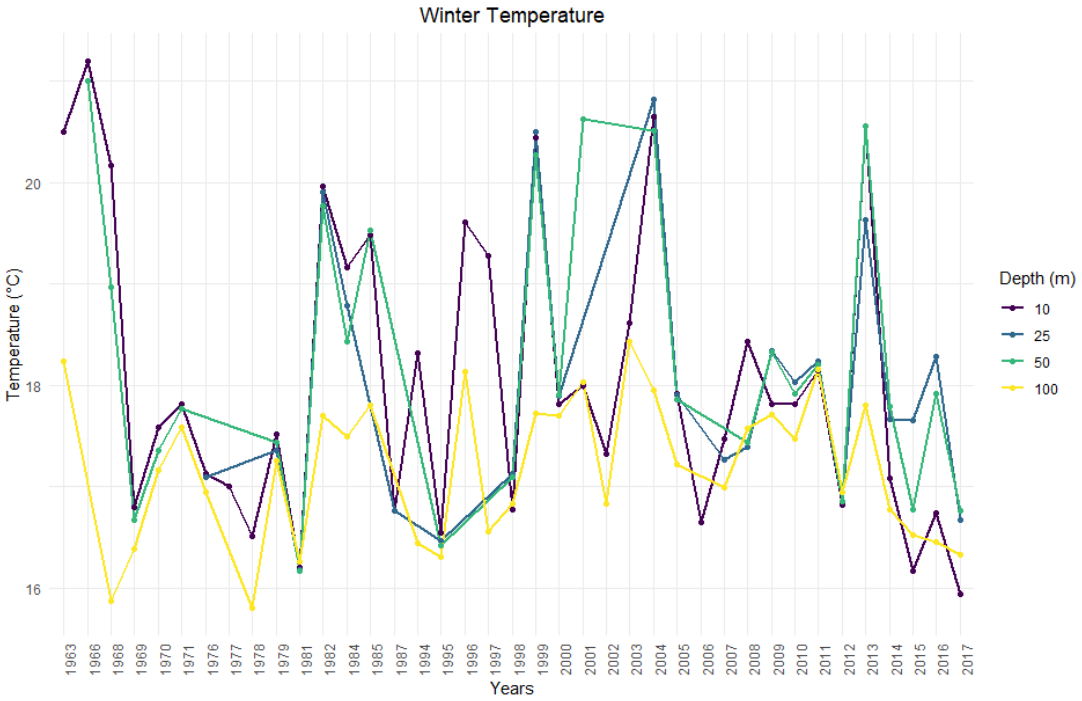

Appendix C 49 Annual winter temperature means in the surface to the 100m range, the Coastal Nile Delta from 1960 to 2017

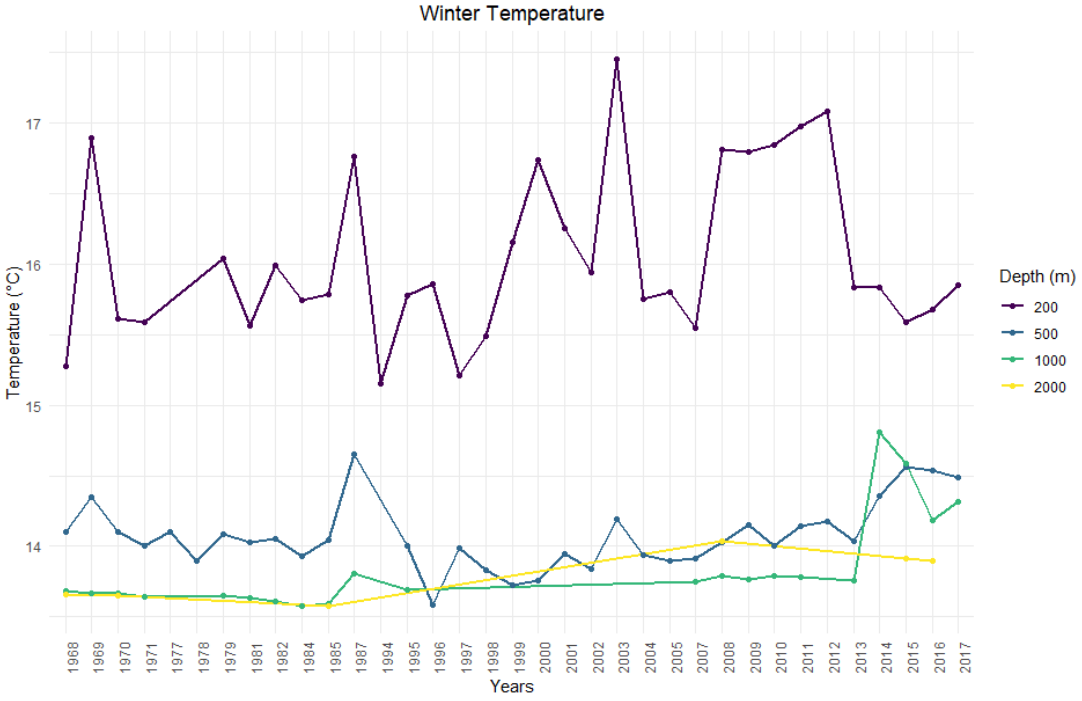

Appendix C 50 Annual winter temperature means in the 200m to the 2000m range, the Coastal Nile Delta from 1960 to 2017

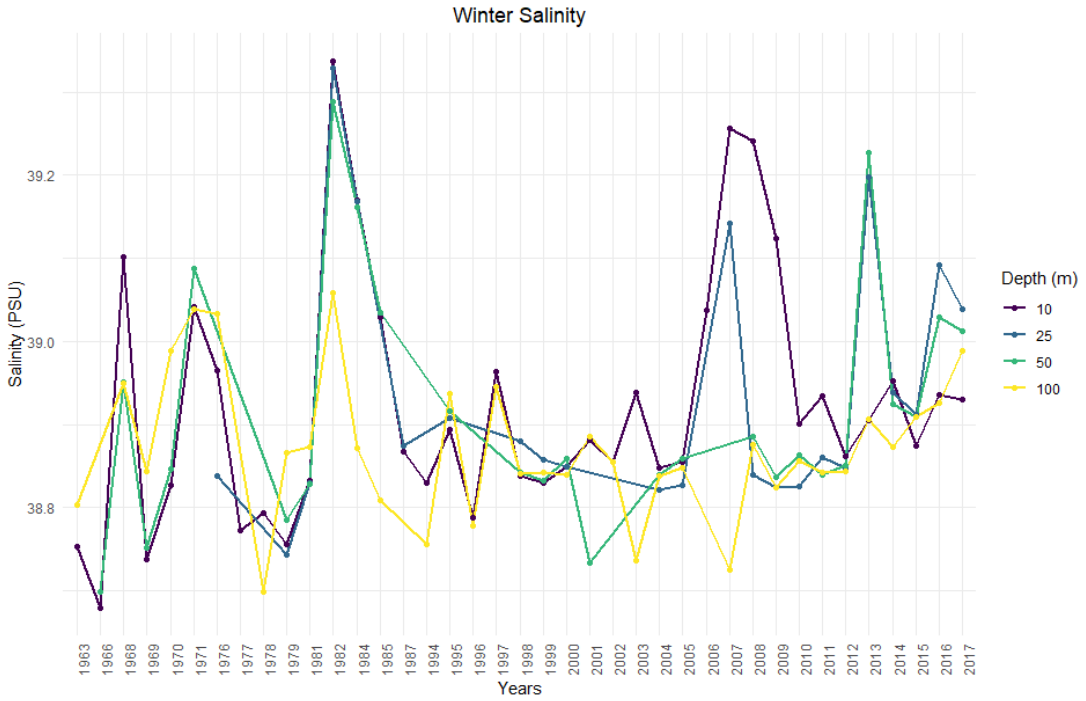

Appendix C 51 Annual winter salinity means in the surface to the 100m range, the Coastal Nile Delta from 1960 to 2017

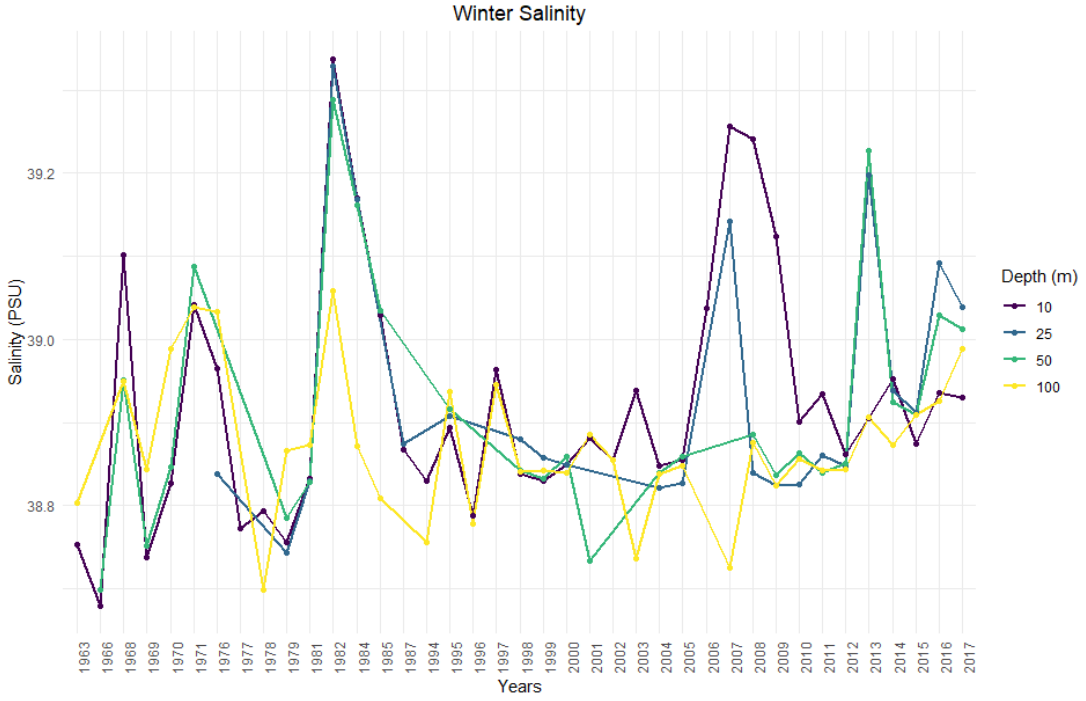

Appendix C 52 Annual winter salinity means in the 200m to the 2000m range, the Coastal Nile Delta from 1960 to 2017

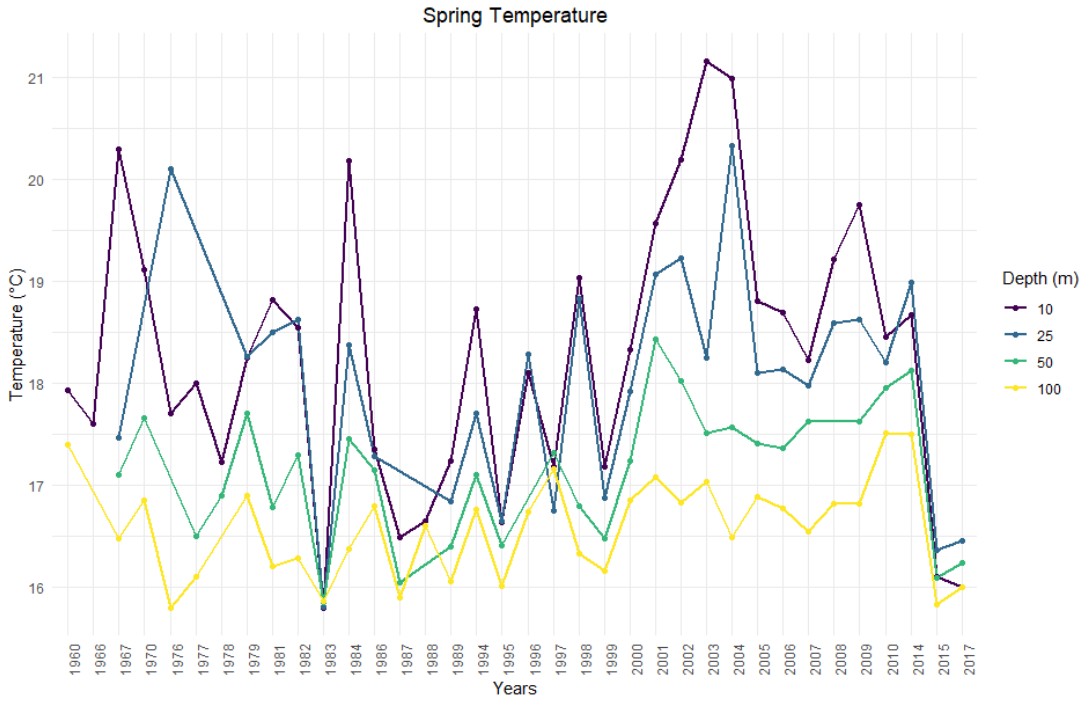

Appendix C 53 Annual spring temperature means in the surface to the 100m range, the Coastal Nile Delta from 1960 to 2017

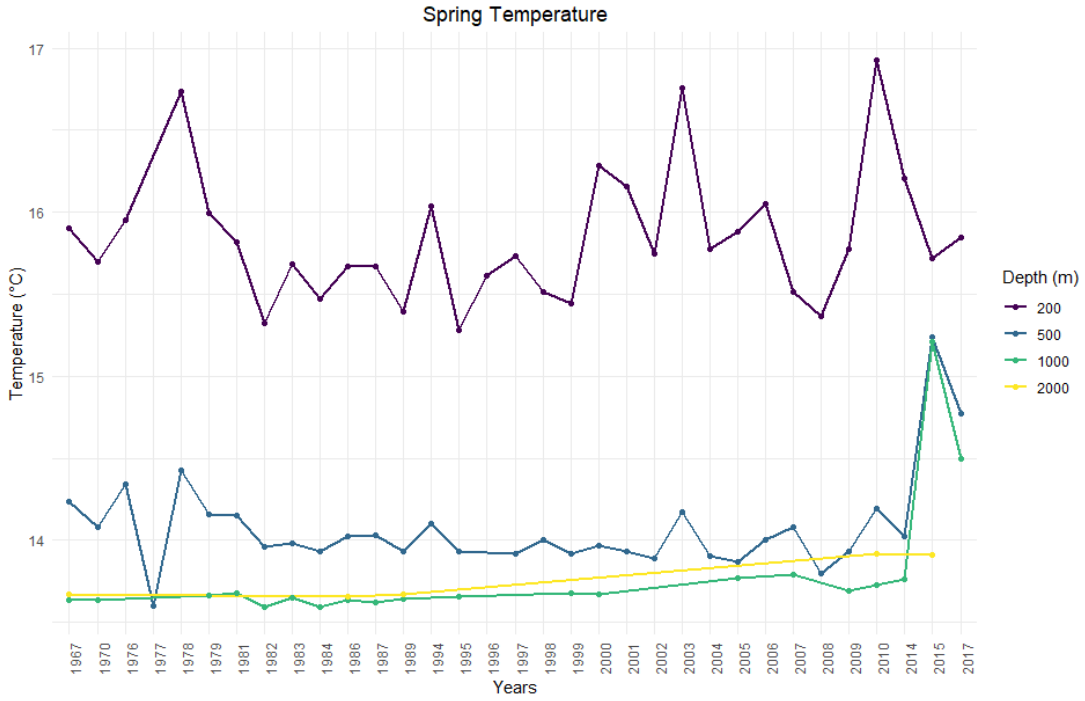

Appendix C 54 Annual spring temperature means in the 200m to the 2000m range, the Coastal Nile Delta from 1960 to 2017

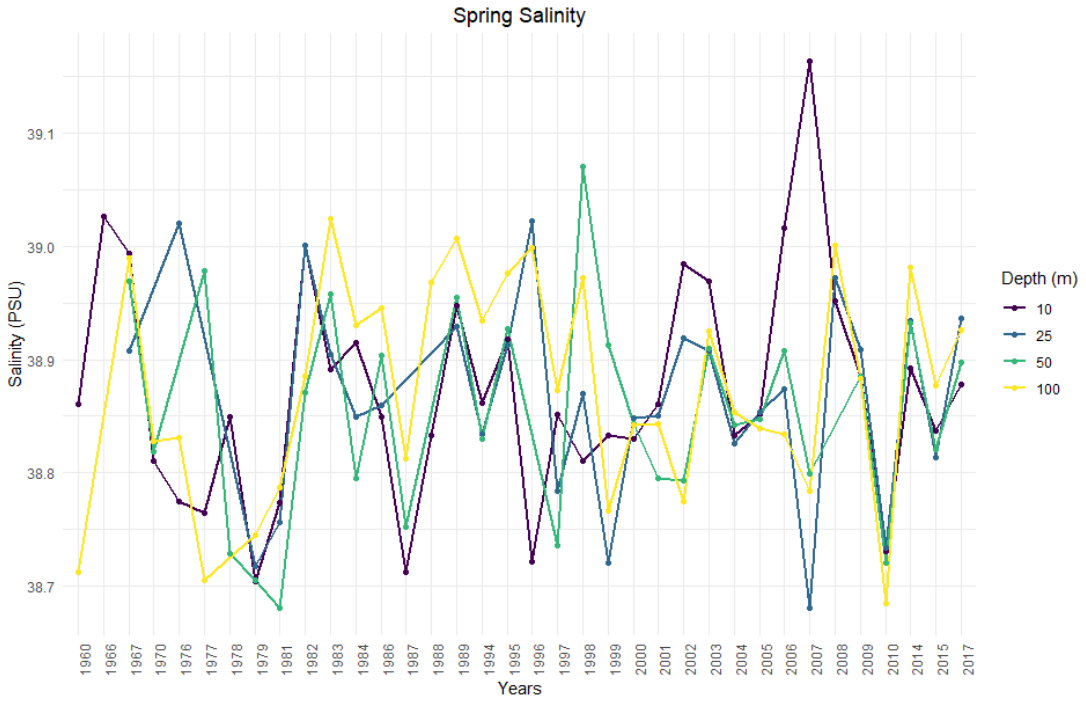

Appendix C 55 Annual spring salinity means in the surface to the 100m range, the Coastal Nile Delta from 1960 to 2017

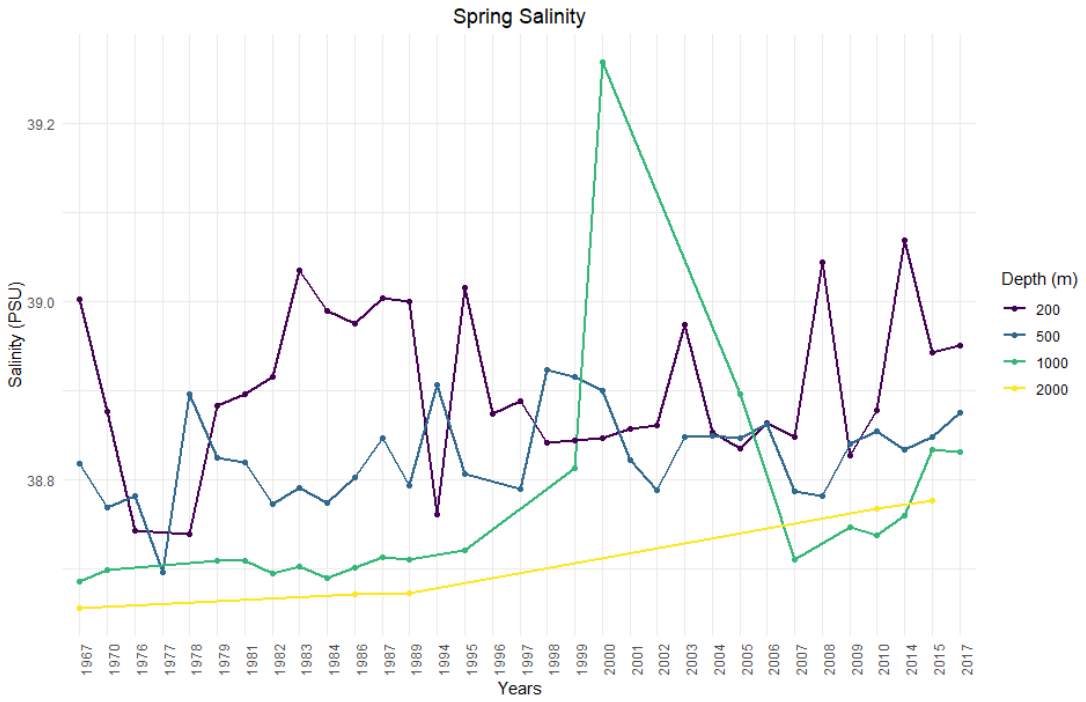

Appendix C 56 Annual spring salinity means in the 200m to the 2000m range, the Coastal Nile Delta from 1960 to 2017

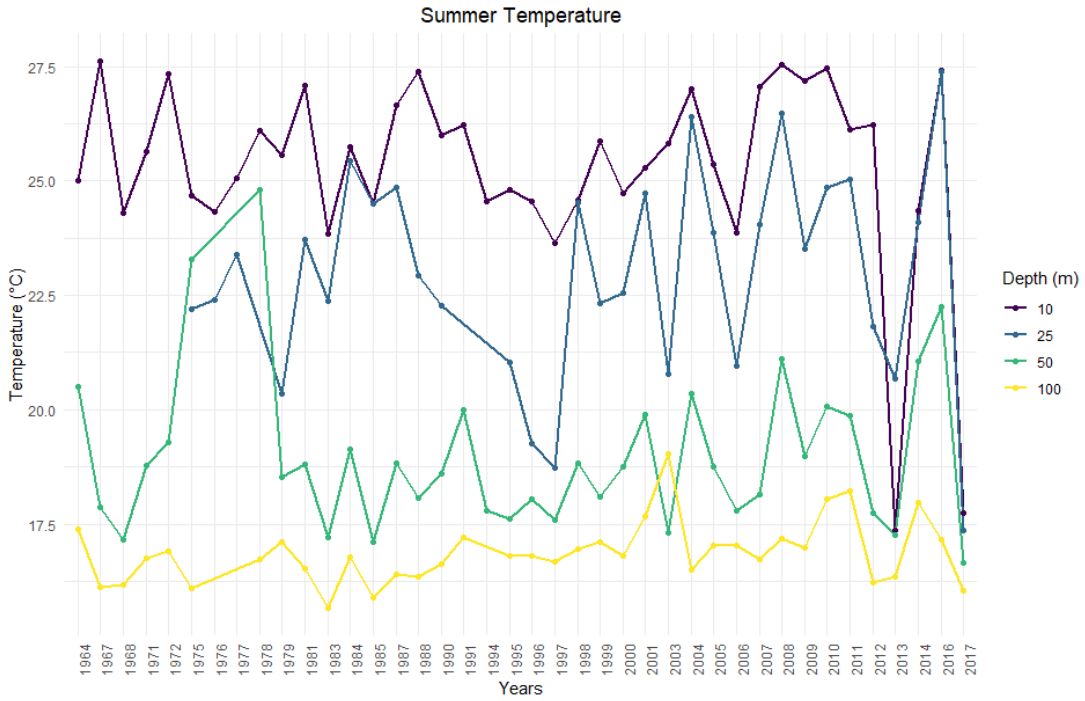

Appendix C 57 Annual summer temperature means in the surface to the 100m range, the Coastal Nile Delta from 1960 to 2017

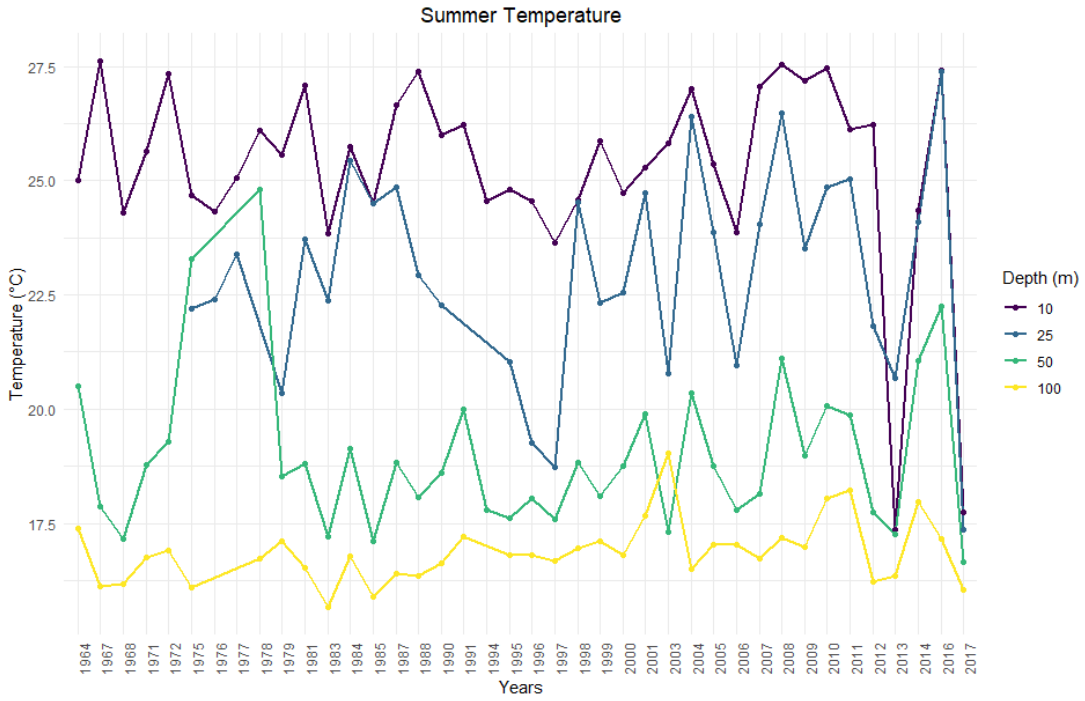

Appendix C 58 Annual summer temperature means in the 200m to the 2000m range, the Coastal Nile Delta from 1960 to 2017

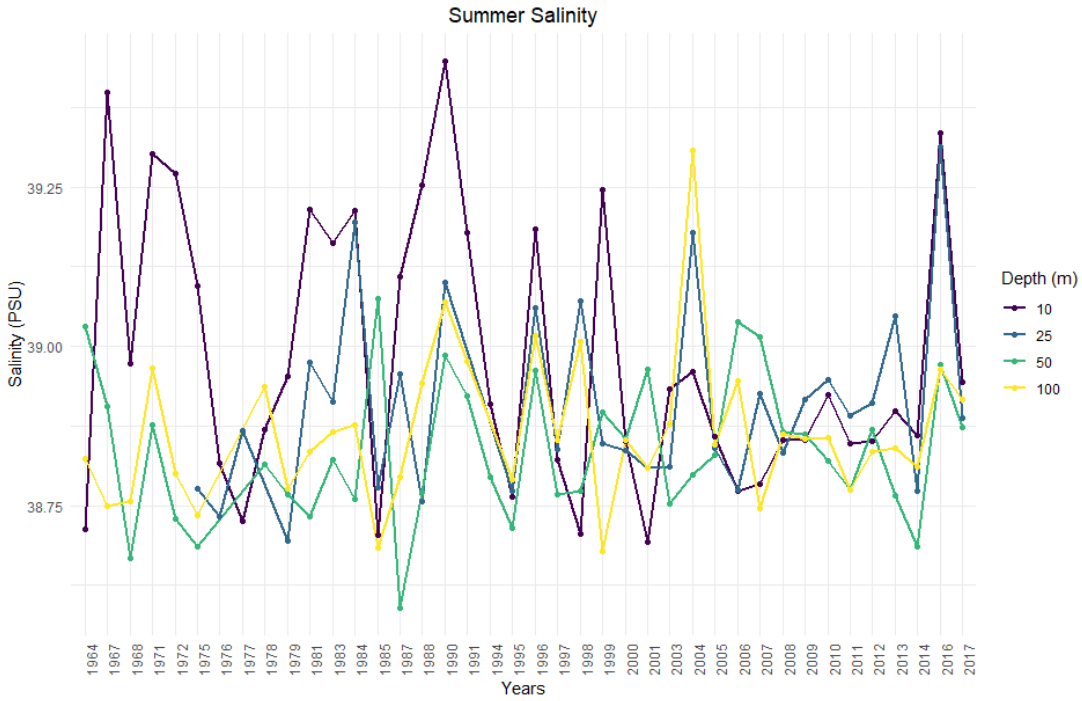

Appendix C 59 Annual summer salinity means in the surface to the 100m range, the Coastal Nile Delta from 1960 to 2017

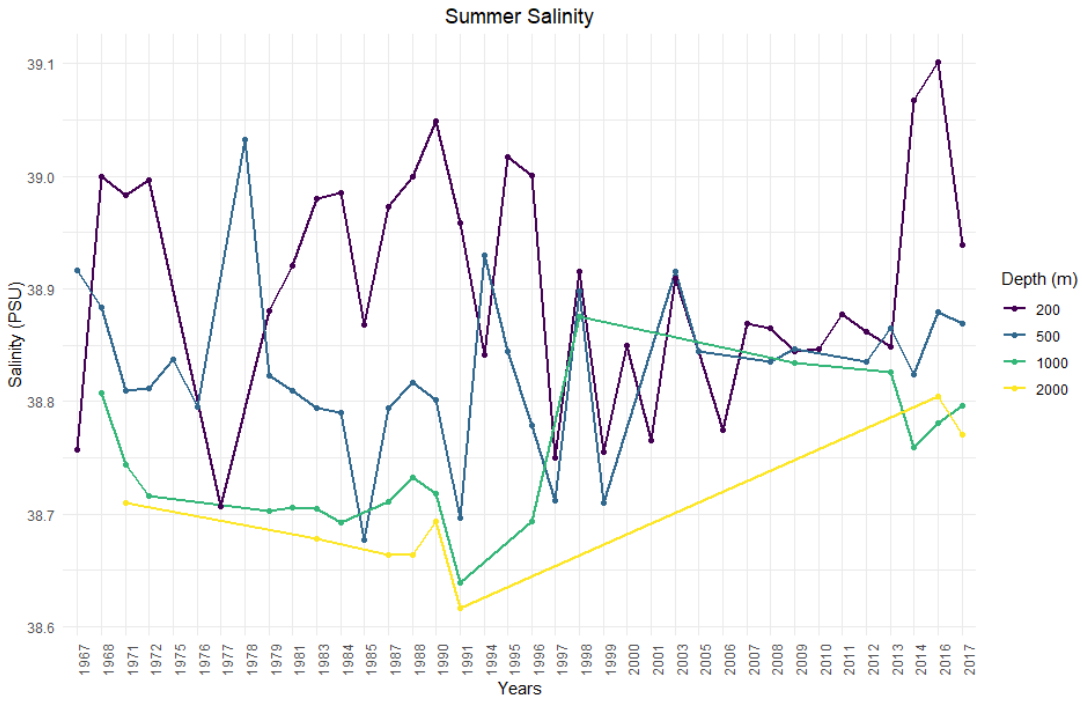

Appendix C 60 Annual summer salinity means in the 200m to the 2000m range, the Coastal Nile Delta from 1960 to 2017

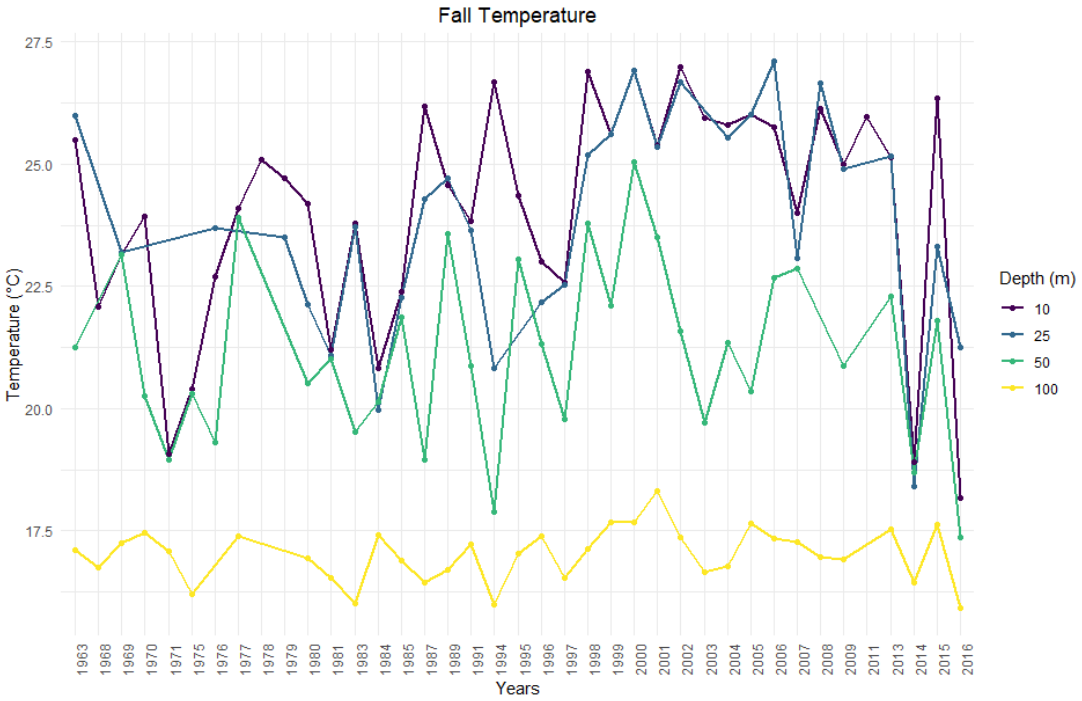

Appendix C 61 Annual fall temperature means in the surface to the 100m range, the Coastal Nile Delta from 1960 to 2017

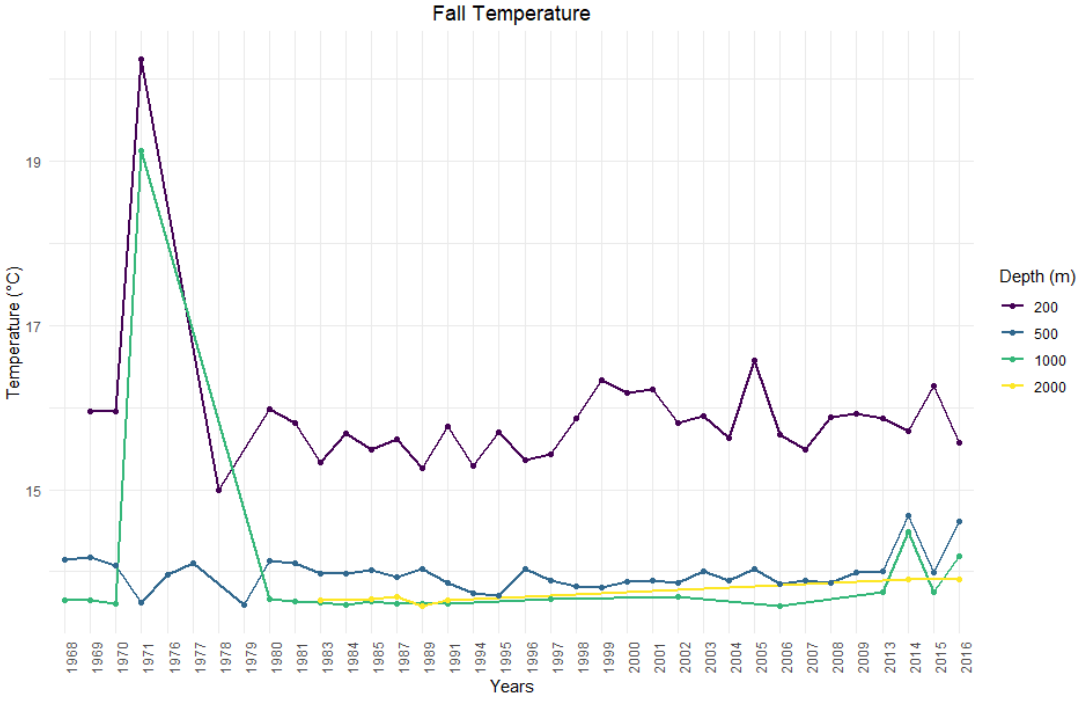

Appendix C 62 Annual fall temperature means in the 200m to the 2000m range, the Coastal Nile Delta from 1960 to 2017

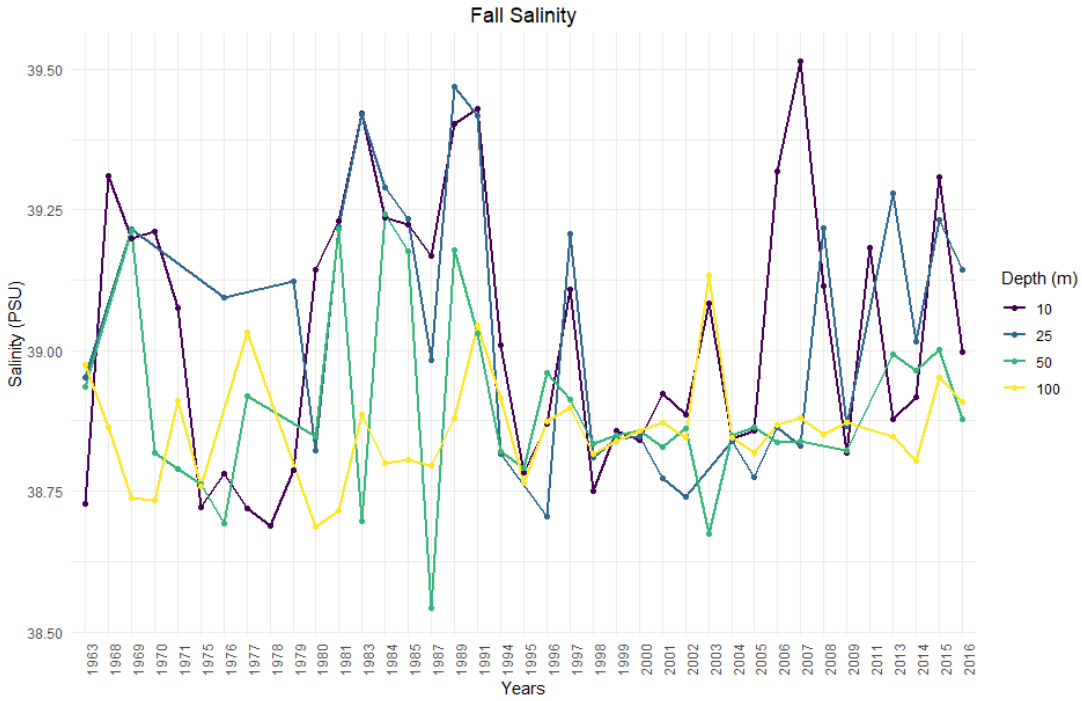

Appendix C 63 Annual fall salinity means in the surface to the 100m range, the Coastal Nile Delta from 1960 to 2017

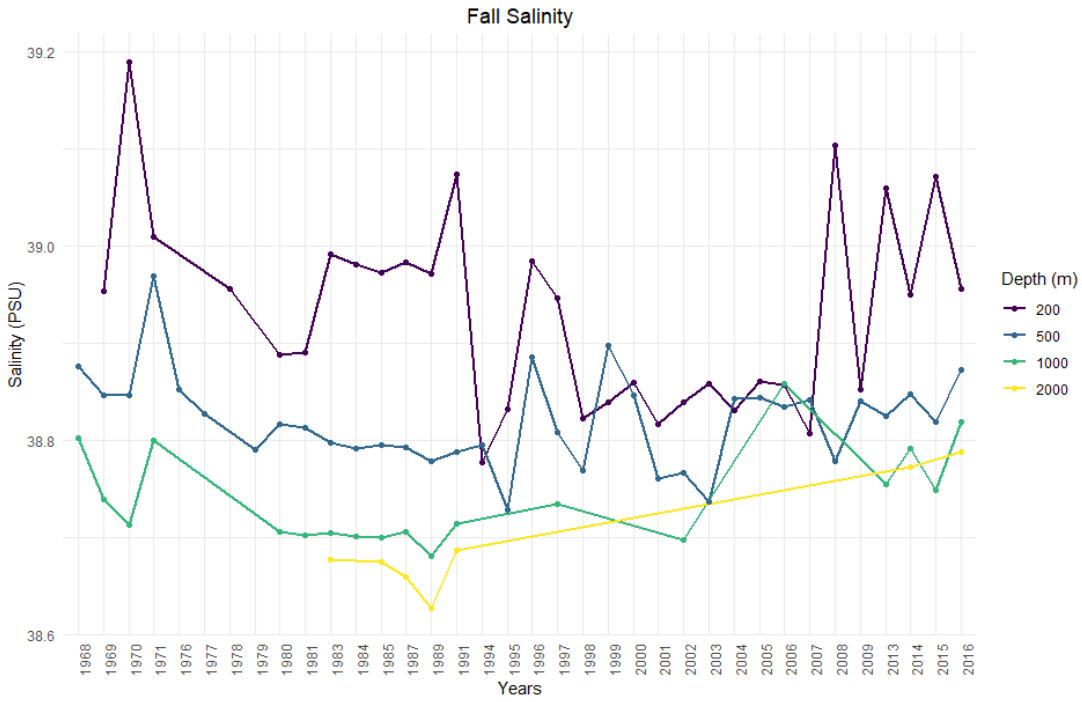

Appendix C 64 Annual fall salinity means in the 200m to the 2000m range, the Coastal Nile Delta from 1960 to 2017

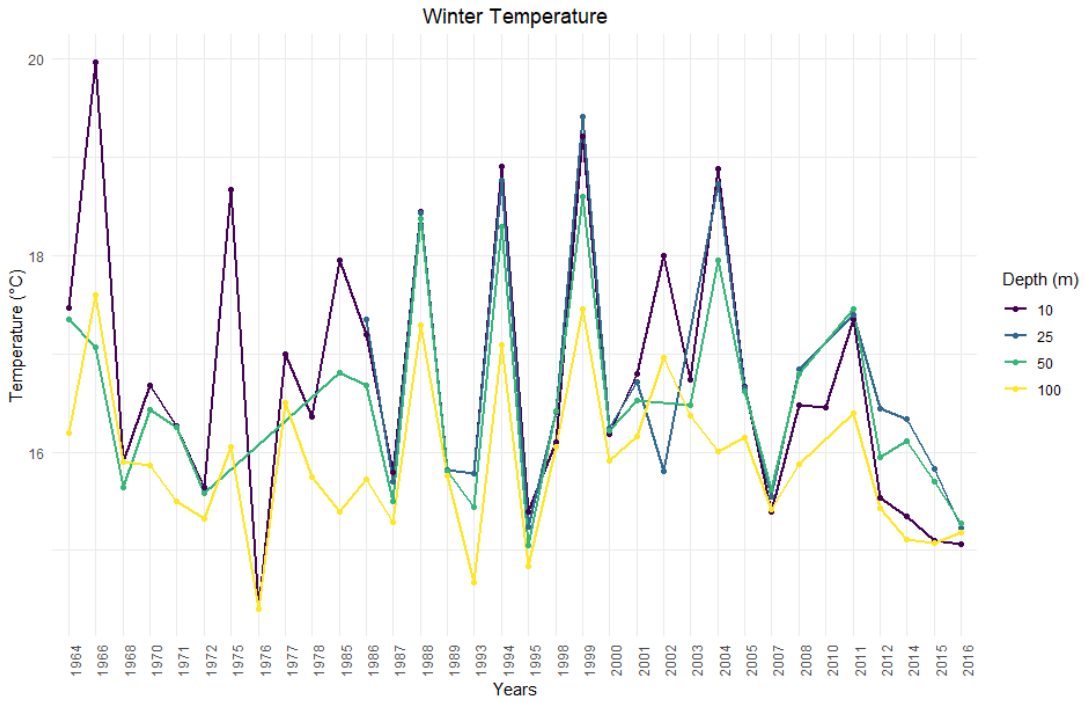

Appendix C 65 Annual winter temperature means in the surface to the 100m range, the Rhodes Gyre from 1960 to 2017

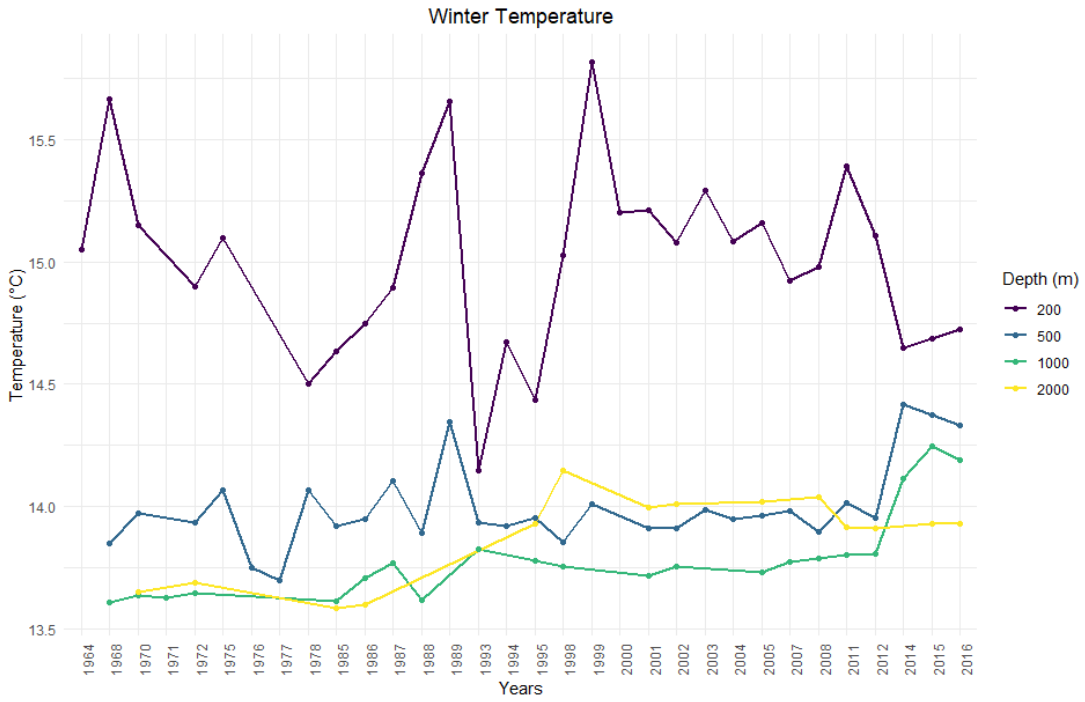

Appendix C 66 Annual winter temperature means in the 200m to the 2000m range, the Rhodes Gyre from 1960 to 2017

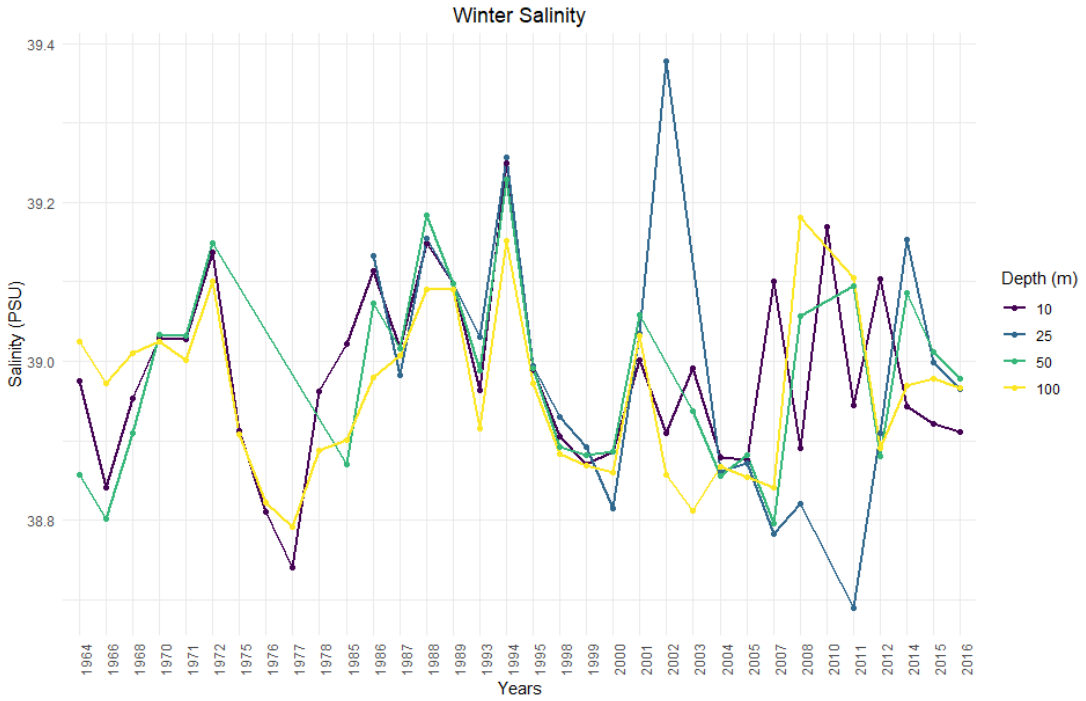

Appendix C 67 Annual winter salinity means in the surface to the 100m range, the Rhodes Gyre from 1960 to 2017

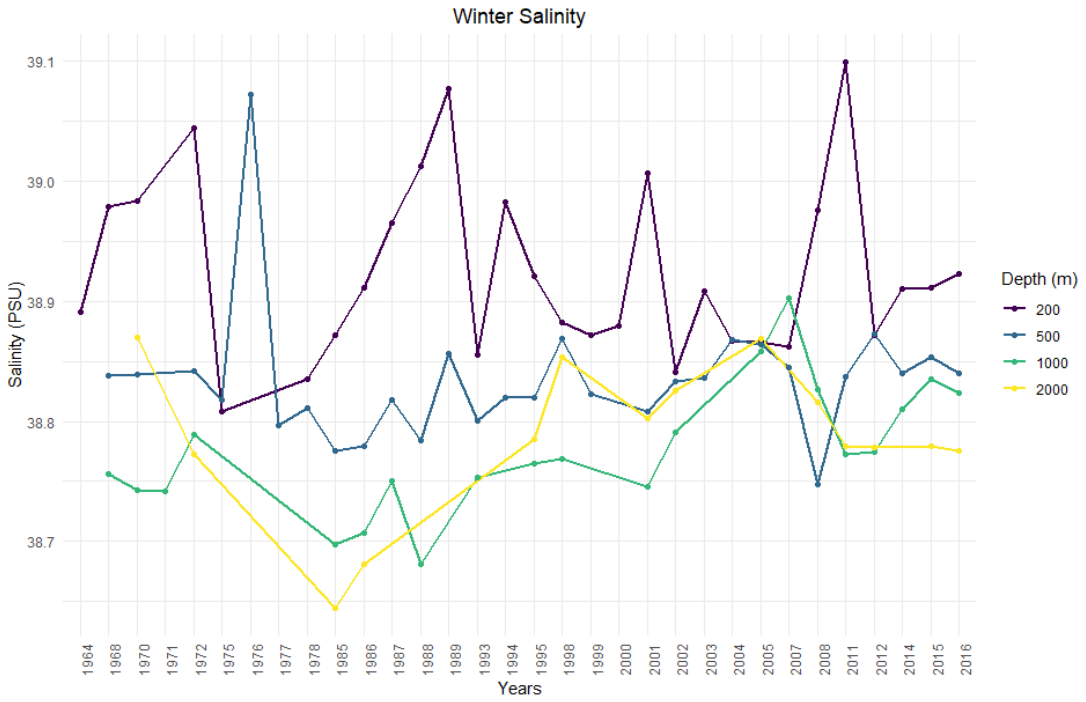

Appendix C 68 Annual winter salinity means for the 200m to the 2000m range, the Rhodes Gyre from 1960 to 2017

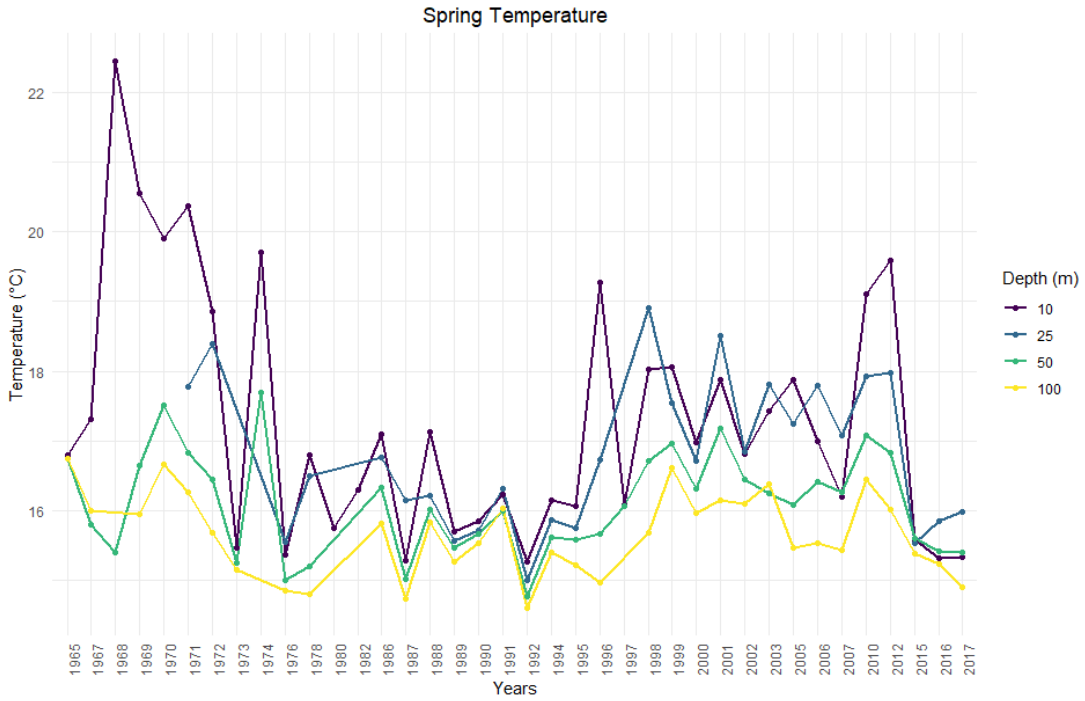

Appendix C 69 Annual spring temperature means in the surface to the 100m range, the Rhodes Gyre from 1960 to 2017

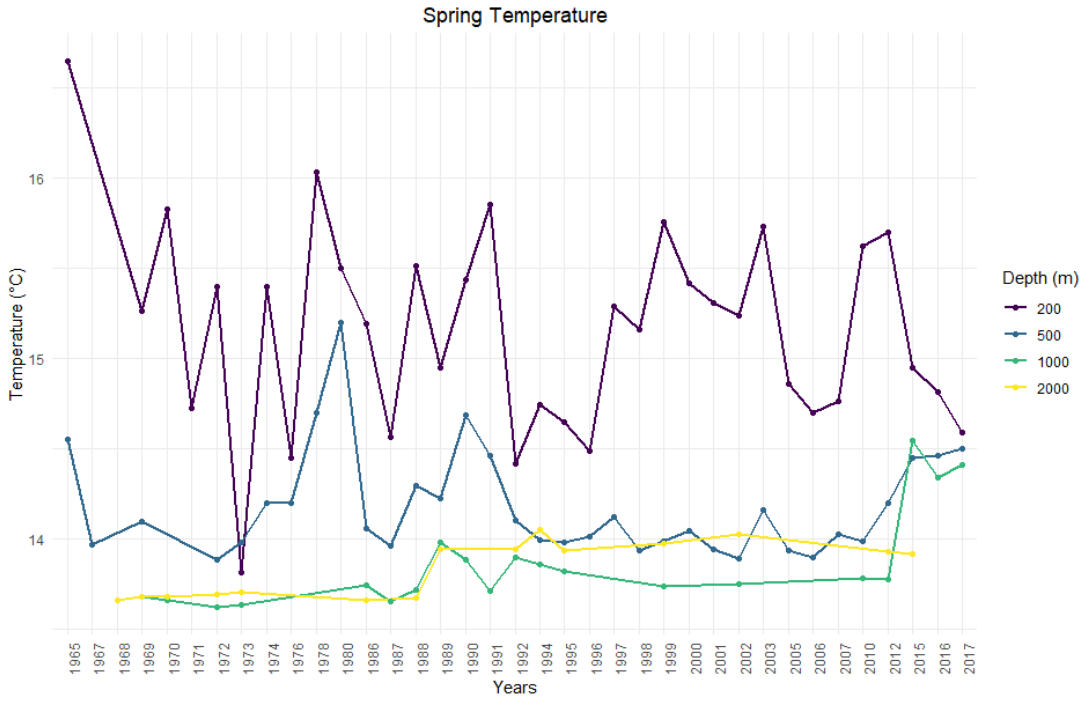

Appendix C 70 Annual spring temperature means in the 200m to the 2000m range, the Rhodes Gyre from 1960 to 2017

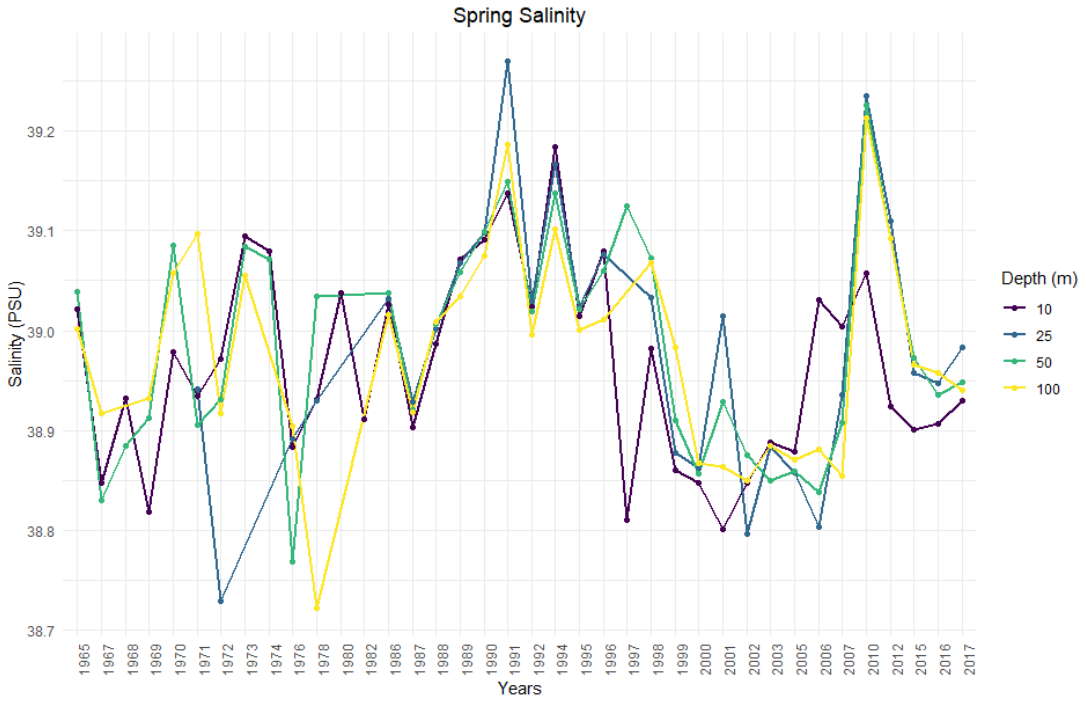

Appendix C 71 Annual spring salinity means in the surface to the 100m range, the Rhodes Gyre from 1960 to 2017

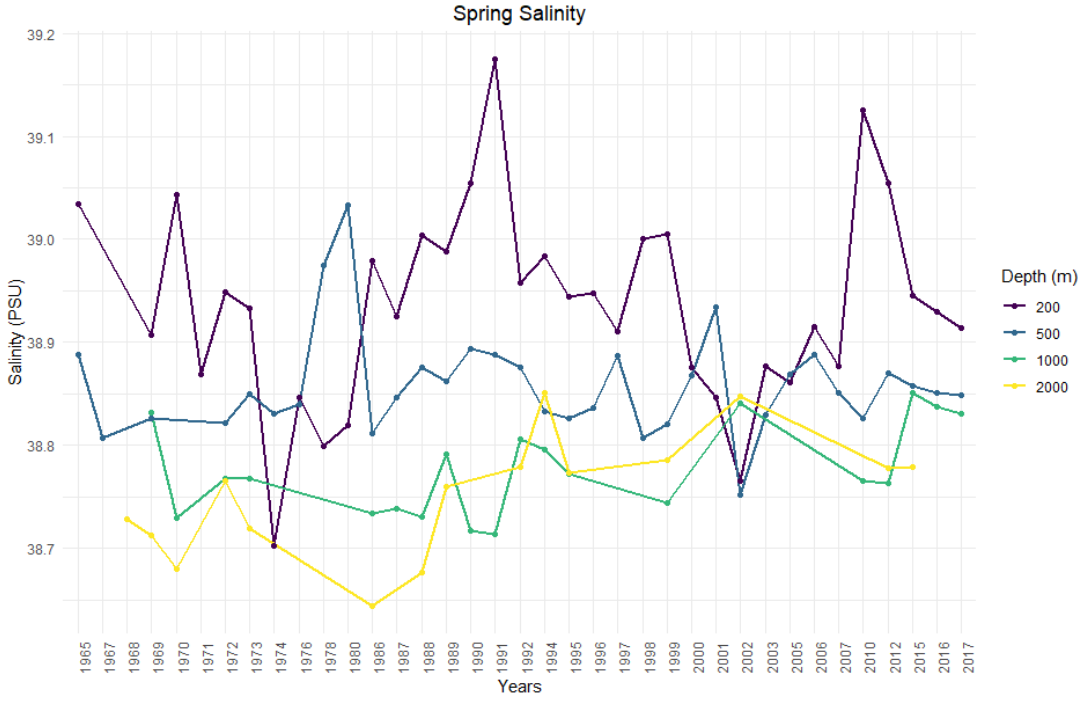

Appendix C 72 Annual spring salinity means in the 200m to the 2000m range, the Rhodes Gyre from 1960 to 2017

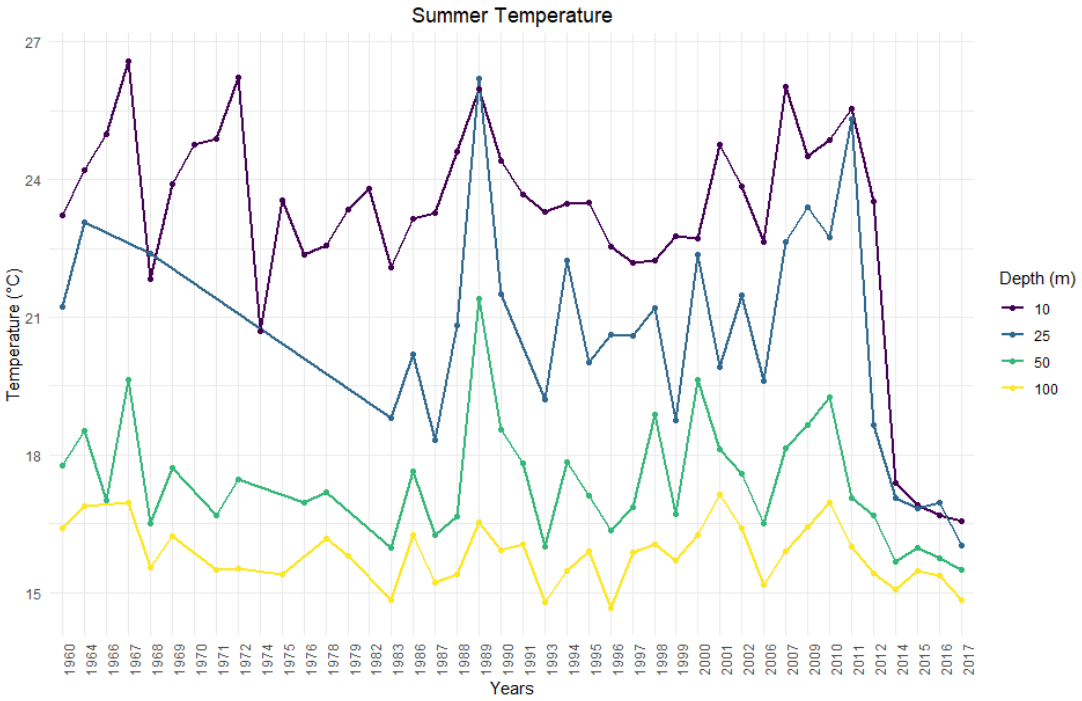

Appendix C 73 Annual summer temperature means in the surface to the 100m range, the Rhodes Gyre from 1960 to 2017

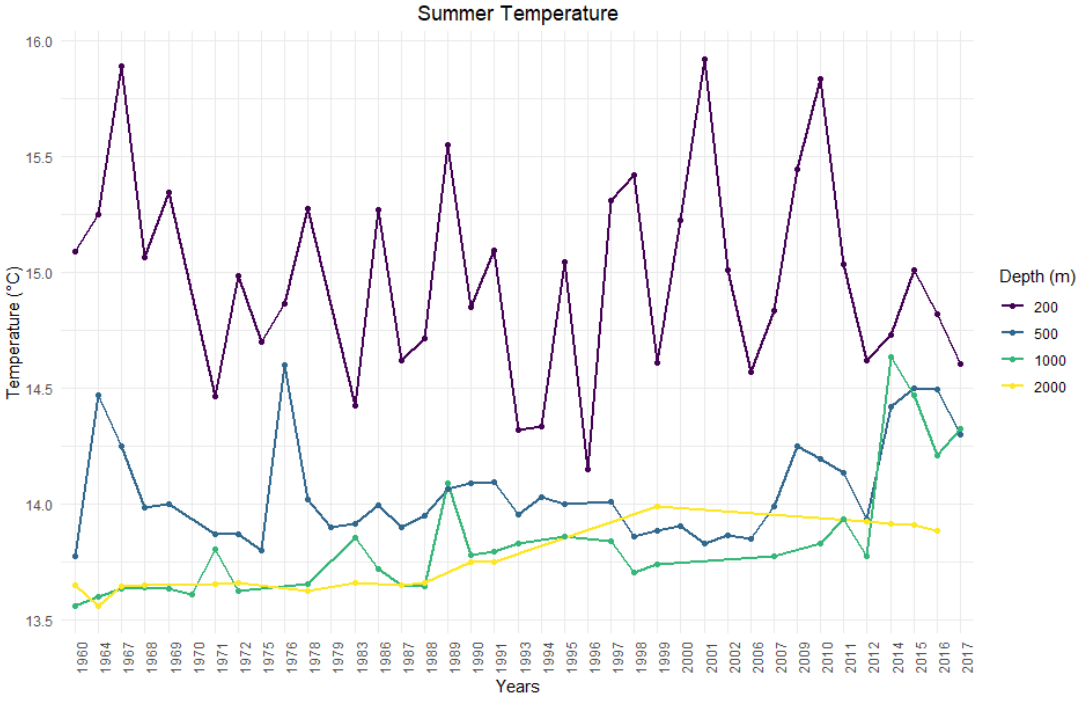

Appendix C 74 Annual summer temperature means in the 200m to the 2000m range, the Rhodes Gyre from 1960 to 2017

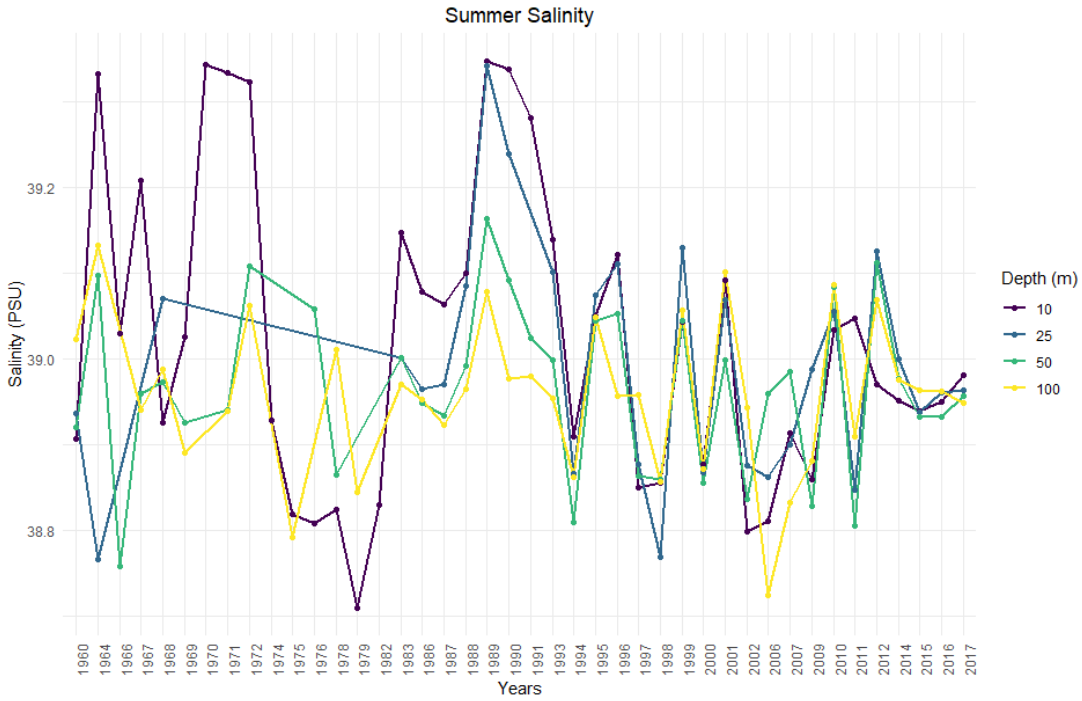

Appendix C 75 Annual summer salinity means in the surface to the 100m range, the Rhodes Gyre from 1960 to 2017

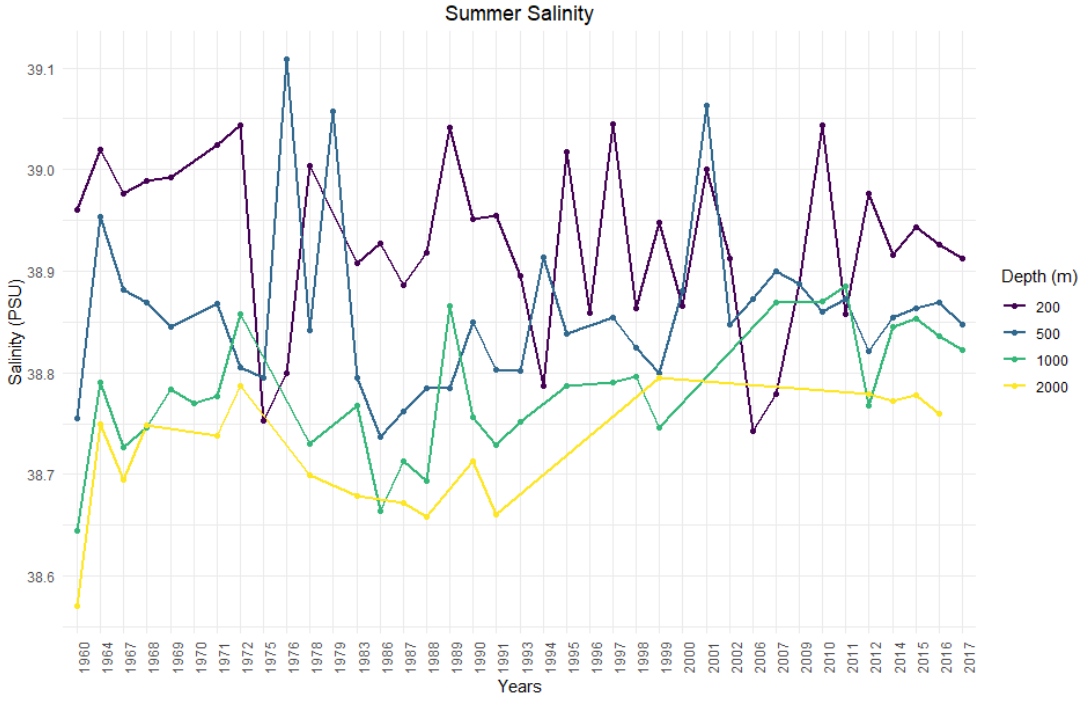

Appendix C 76 Annual summer salinity means in the 200m to the 2000m range, the Rhodes Gyre from 1960 to 2017

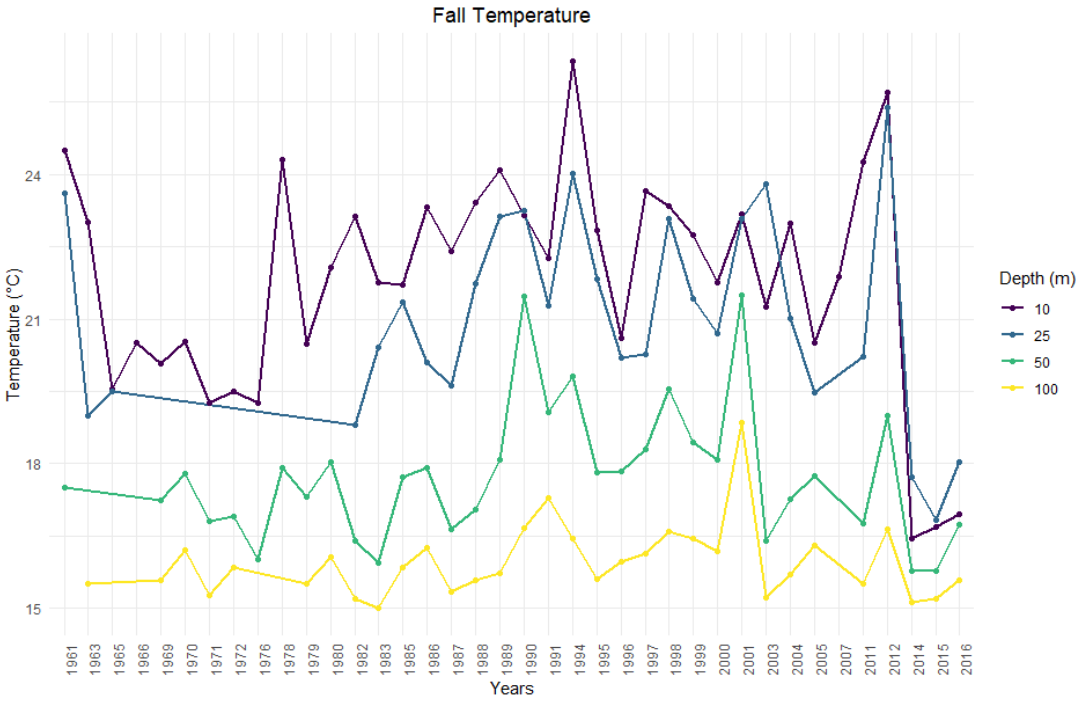

Appendix C 77 Annual fall temperature means in the surface to the 100m range, the Rhodes Gyre from 1960 to 2017

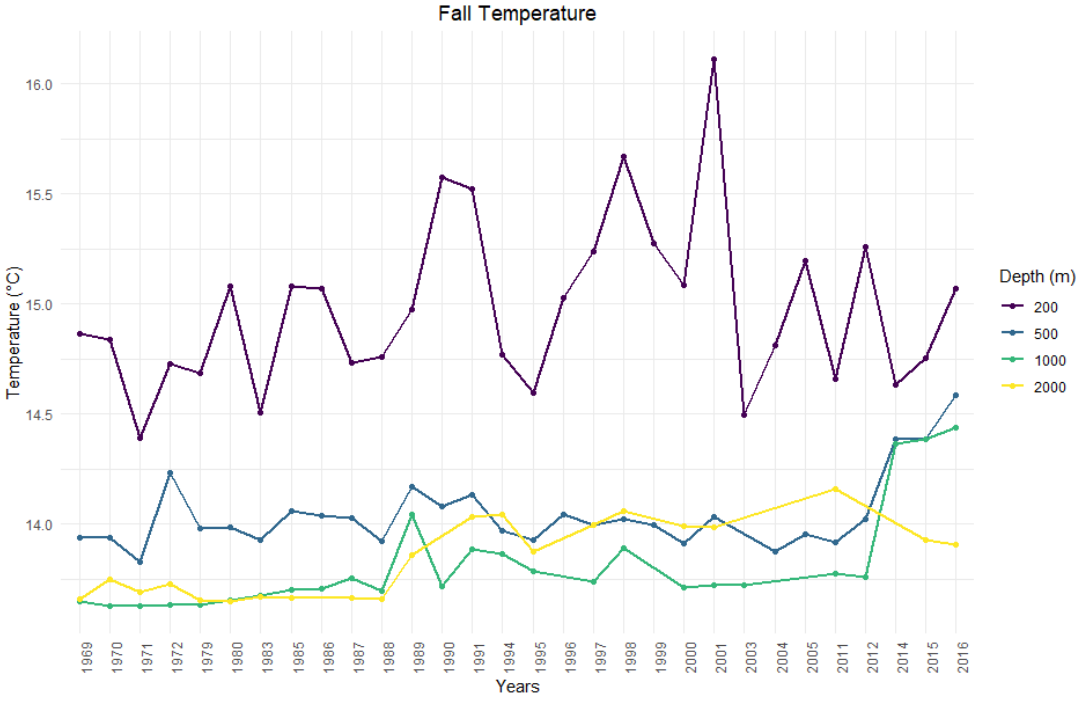

Appendix C 78 Annual fall temperature means in the 200m to the 2000m range, the Rhodes Gyre from 1960 to 2017

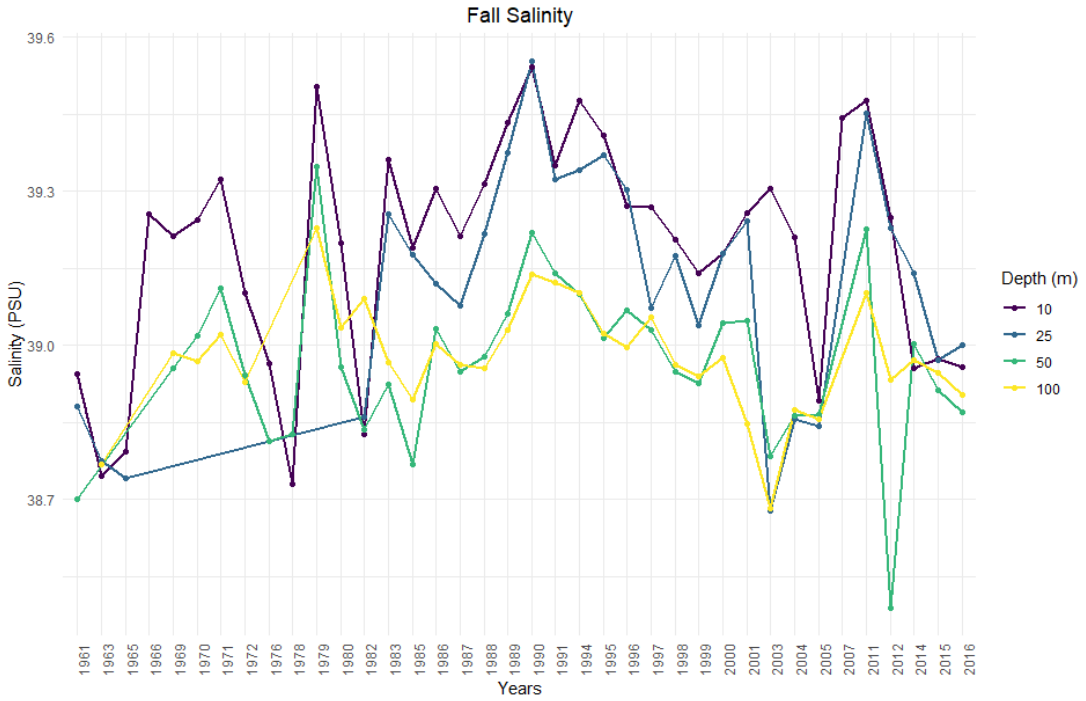

Appendix C 79 Annual fall salinity means in the surface to the 100m range, the Rhodes Gyre from 1960 to 2017

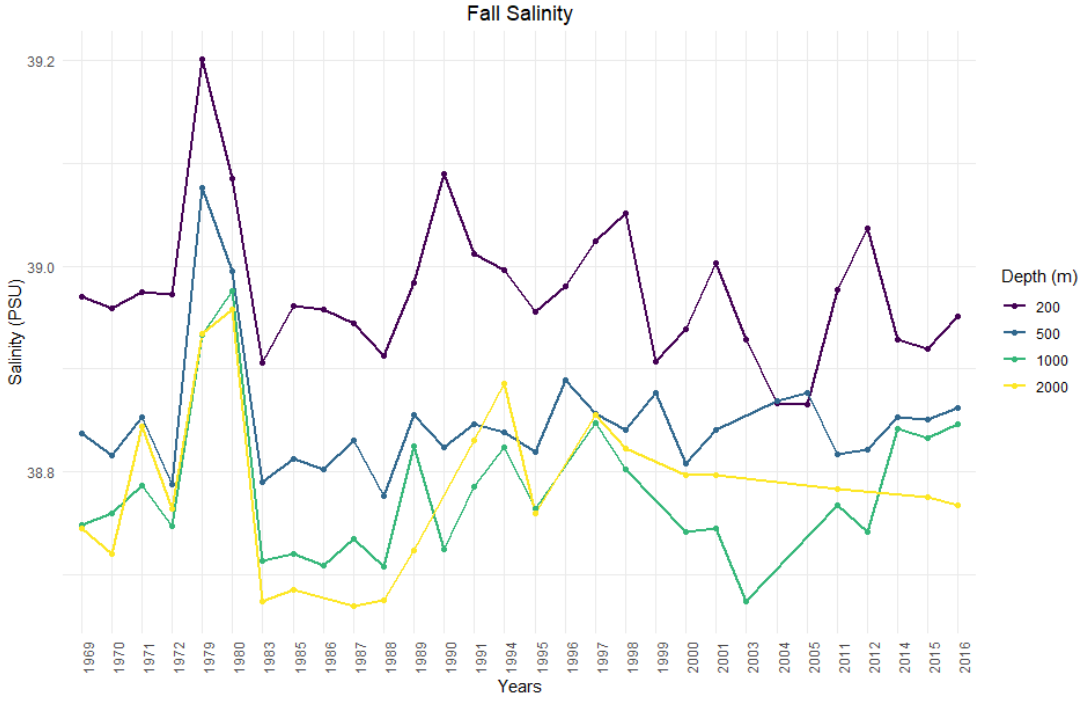

Appendix C 80 Annual fall salinity means in the 200m to the 2000m range, the Rhodes Gyre from 1960 to 2017

APPENDIX D

R & PACKAGES

The R Project for Statistical Computing (https://www.r-project.org/), abbreviated to R, is a powerful and flexible programming language and software for graphical and statistical computing based on the architecture and principles of the S language. The language is well-developed, high level, simple and effective with many of the core functionality expected from a user such as logical operators, conditionals, loops, and user-defined recursive functions and input and output facilities. Since its inception in 1993 and the first stable beta version in 2000, it has increased in popularity and ranks 22 in the TIOBE index (https://www.tiobe.com/tiobe-index/) at the time this passage is written. Despite its name, R is not a language for the sole purpose of statistical analysis but an environment where statistical techniques are implemented. It is open source and has excellent support from its community with constant new specialised libraries about different domains added to its repertoire. R is capable of handling and storing vast amounts of data and efficiently processes them without overflow issues. The software is especially suited for the calculations of arrays, in particular, matrices, with a special suit of operators dedicated to them.

A large amount of integrated collection of intermediate tools for data analysis makes the R software versatile, even without recourse to subject-specific packages. Another significant advantage of R is its capacity to produce plots worthy of publication both on-screen and as hard copies. The totalities of the descriptive and inferential statistical analysis of this work are computed in R and the various packages available on the Comprehensive R Archive Network (CRAN, https://cran.r-project.org/).

Packages

The following are the packages employed during our calculations listed to provide proper credit:

- dataMaid is a data cleaning extension to R, a necessary task before undertaking any data analysis takes place. It has been applied extensively to get an overview of the data at hand and to perform data cleaning for any suspicious outliers after QF check on ODV. Fortunately, from the resulting information, there is no instance that requires reporting, as the ODV software's selection tool and the work performed by its makers proved to be excellent, knowing that the only data used are the ones with a QF of 1 or 2, meaning "good" or "probably good".

- ggplot2 is the primary tool for data visualisation and is a well-known extension to the R working environment based on "The grammar of graphics" [84], and has been the go-to package for the community for the past ten years. Nearly every graph, plot and histogram in this work has been constructed using this package unless noted otherwise in its description.

- plyr is a simple package to break down large arrays into its various parts, apply individual function pieces and recombining the results and to obtain a summary of data groups in a resource-efficient fashion. The functions in the plyr package are as fast as or faster than the built-in equivalents of the R program. It is used in our study to write functions to treat the aggregated dataset.

- e1071 contains miscellaneous functions for various calculations such as fuzzy clustering, Fourier Transformation, shortest path computation, among others. Rather than the more complex functions, some of its basic applications such as kurtosis calculation are employed for creating plots and descriptive operations.

- fBasics is a collection of functions for explorative data analysis and the investigation of distributional properties, including parameter distribution and hypothesis testing. It also possesses various utility functions concerning data management and handling.

- xlsx package is a powerful tool for working, importing and exporting Excel files in R. In our case it is mainly used to export data analysis results into excel sheets for better visibility and storage of the descriptive results obtained during our calculations done mainly with the e1071 and fBasics packages.

- cluster, as its name implies, is a package that contains multiple methods for cluster analysis. It allows the user to create groups showing similar patterns in their data distribution and values to create sub-groups for a more in-depth analysis.

- VIM is a package for the visualisation and the imputation of missing values in a dataset. In our case, there are multiple entries with missing SWT and SWS values, although not to an extent prohibiting us from using an algorithm to input values derived from existing entries is unfeasible. Accordingly, the package is used extensively during our analysis.

- mice package is used concurrently with the VIM package to accomplish multivariate imputation for missing variables with chained equations as our dataset is multivariate. It keeps consistency in the imputation by means of passive imputation, allowing us to deal with the missing values in the dataset.

- fitdistrplus is used for its powerful parametric distribution functions, for Cullen and Frey graphs, empirical density plots, cumulative distribution analysis, theoretical density plots and comparison between empirical and projected distribution (Q-Q plot, P-P plot, CDF etc.).

APPENDIX E:

TEZ FOTOKOPI İZIN FORMU

PROGRAM

SEES ☐

PSIR ☐

ELT ☐

YAZARIN

Soyadı:
Adı:
Bölümü:

TEZİN ADI (İngilizce):

TEZİN TÜRÜ: Yüksek Lisans ☐ Doktora ☐

1. Tezimin tamamından kaynak gösterilmek şartıyla fotokopi alınabilir. ☐
2. Tezimin içindekiler sayfası, özet, indeks sayfalarından ve/veya bir bölümünden kaynak gösterilmek şartıyla fotokopi alınabilir. ☐
3. Tezimden bir bir (1) yıl süreyle fotokopi alınamaz. ☐

TEZİN KÜTÜPHANEYE TESLİM TARİHİ: